

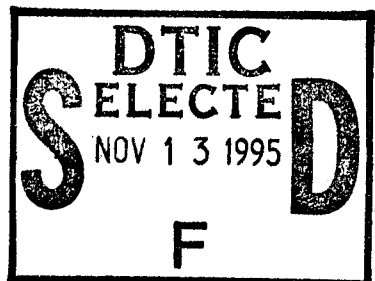
RL-TR-95-175, Vol V (of five)  
Final Technical Report  
September 1995



# HIGH-LEVEL ADAPTIVE SIGNAL PROCESSING ARCHITECTURE WITH APPLICATIONS TO RADAR NON- GAUSSIAN CLUTTER, A New Approach to Radar Detection based on the Partitioning and Statistical Characterization of the Surveillance Volume

University of Massachusetts at Amherst

Mohamed Adel Slamani (Syracuse University)



APPROVED FOR PUBLIC RELEASE; DISTRIBUTION UNLIMITED.

19951109 098

Copyright 1994 Mohamed Adel Slamani  
This material may be reproduced by or for the U.S. Government pursuant to the copyright license  
under clause at DFARS 252.227-7013 (1995).

DTIC QUALITY INSPECTED 5

Rome Laboratory  
Air Force Materiel Command  
Griffiss Air Force Base, New York

PII Redacted

This report has been reviewed by the Rome Laboratory Public Affairs Office (PA) and is releasable to the National Technical Information Service (NTIS). At NTIS it will be releasable to the general public, including foreign nations.

RL-TR-95-164, Vol V (of five), has been reviewed and is approved for publication.

APPROVED:



DR. VINCENT C. VANNICOLA  
Project Engineer

FOR THE COMMANDER:



DONALD W. HANSON  
Director of Surveillance & Photonics

If your address has changed or if you wish to be removed from the Rome Laboratory mailing list, or if the addressee is no longer employed by your organization, please notify RL ( OCSS ) Griffiss AFB NY 13441. This will assist us in maintaining a current mailing list.

Do not return copies of this report unless contractual obligations or notices on a specific document require that it be returned.

# REPORT DOCUMENTATION PAGE

Form Approved  
OMB No. 0704-0188

Public reporting burden for this collection of information is estimated to average 1 hour per response, including the time for reviewing instructions, searching existing data sources, gathering and maintaining the data needed, and completing and reviewing the collection of information. Send comments regarding this burden estimate or any other aspect of this collection of information, including suggestions for reducing this burden, to Washington Headquarters Services, Directorate for Information Operations and Reports, 1215 Jefferson Davis Highway, Suite 1204, Arlington, VA 22202-4302, and to the Office of Management and Budget, Paperwork Reduction Project (0704-0188), Washington, DC 20503.

1. AGENCY USE ONLY (Leave Blank)		2. REPORT DATE September 1995	3. REPORT TYPE AND DATES COVERED Final Apr 91 - Jun 94
4. TITLE AND SUBTITLE HIGH-LEVEL ADAPTIVE SIGNAL PROCESSING ARCHITECTURE WITH APPLICATIONS TO RADAR NON-GAUSSIAN CLUTTER , A New Approach to Radar Detection based on the (see reverse)		5. FUNDING NUMBERS C - F30602-91-C-0038 PE - 62702F PR - 4506 TA - 11 WU - 1B	
6. AUTHOR(S) Mohamed Adel Slamani (Syracuse University)			
7. PERFORMING ORGANIZATION NAME(S) AND ADDRESS(ES) University of Massachusetts at Amherst Department of Computer Science Lederle Graduate Research Center Amherst MA 01003		8. PERFORMING ORGANIZATION REPORT NUMBER N/A	
9. SPONSORING/MONITORING AGENCY NAME(S) AND ADDRESS(ES) Rome Laboratory (OCSS) 26 Electronic Pky Griffiss AFB NY 13441-4514		10. SPONSORING/MONITORING AGENCY REPORT NUMBER RL-TR-95-164, Vol V (of five)	
11. SUPPLEMENTARY NOTES Rome Laboratory Project Engineer: Dr. Vincent C. Vannicola/OCSS/(315) 330-2861			
12a. DISTRIBUTION/AVAILABILITY STATEMENT Approved for public release; distribution unlimited.		12b. DISTRIBUTION CODE	
13. ABSTRACT (Maximum 200 words) We describe the accomplishments of a collaborative effort carried out by a team of researchers from the University of Massachusetts at Amherst (headed by V. Lesser), Boston University (headed by H. Nawab), and Syracuse University (headed by D. Weiner) on the development of a high-level signal processing architecture called IPUS (Integrated Processing and Understanding of Signals). Based on the IPUS generic testbed architecture and "radar and sound understanding" (RESUN) architectures, we have been able to transfer IPUS technology from a LISP environment to a C++ environment for use in an IPUS Radar Clutter Analysis Testbed. Though not as well-developed as the sound understanding application because of its newness, this radar testbed has still clearly demonstrated the potential of IPUS-like technologies for CFAR processing of radar returns. There has also been significant development of knowledge for weak signal detection. This knowledge has involved the application of the Ozturk algorithm to hypothesize the distribution of data in a clutter patch based on a small amount of data. Also, techniques have been developed for partitioning the radar surveillance volume into background noise and clutter patches, for weak signal detection in K-distributed clutter, and the efficient use of Rejection Theorem for Weibull clutter generation. Though the effort on the application of IPUS to communications was given less priority, we still did some interesting theoretical work on (see reverse)			
14. SUBJECT TERMS Radar, Signal processing, Artificial intelligence detection. Clutter, Non-Gaussian		15. NUMBER OF PAGES 270	16. PRICE CODE
17. SECURITY CLASSIFICATION OF REPORT UNCLASSIFIED	18. SECURITY CLASSIFICATION OF THIS PAGE UNCLASSIFIED	19. SECURITY CLASSIFICATION OF ABSTRACT UNCLASSIFIED	20. LIMITATION OF ABSTRACT III

4. (Cont'd)

Partitioning and Statistical Characterization of the Surveillance Volume

13. (Cont'd)

weak signal detection in communication systems subject to spherically invariant random processes (SIRP) interference.

Accesion For	
NTIS CRA&I	
DTIC TAB	
Unannounced	
Justification	
By	
Distribution /	
Availability Codes	
Dist	Avail and / or Special
A-1	

## Abstract

In signal processing applications it is common to assume Gaussian statistics in the design of optimal signal processors. However, non-Gaussian processes do arise in many situations. For example, measurements reveal that radar clutter may be approximated by either Weibull, K-distributed, Lognormal, or Gaussian distributions depending upon the scenario. When the possibility of a non-Gaussian problem is encountered, the question as to which probability distributions should be utilized in a specific situation for modeling the data needs to be answered.

In practice, the underlying probability distributions are not known a priori. Consequently, an assessment must be made by monitoring the environment. Another consideration is that radar detection problems can usually be divided into strong, intermediate, and weak signal cases. Hence, the system that monitors a radar environment must be able to subdivide the surveillance volume into weak background noise and clutter patches in addition to approximating the underlying probability distributions for each patch. This is in contrast to current practice where a single robust detector, usually based on the Gaussian assumption, is employed.

The objective of this work is to develop techniques that monitor the environment and select the appropriate detector for processing the data.

The main contributions are: (1) an image processing technique is devised which enables partitioning of the surveillance volume into background noise and clutter patches, (2) the Ozturk algorithm is used to identify suitable approximations to the probability density function for each clutter patch, and (3) rules to be used with an expert system shell under development at the University of Massachusetts and Boston University are formulated for monitoring the environment and selecting the appropriate detector for processing the data.

Computer simulated examples demonstrate the effectiveness by which the approach proposed in this work is able to partition the surveillance volume and approximate the probability distributions within homogeneous regions.

## Acknowledgment

I wish to express my very special appreciation to my advisor Professor Donald D. Weiner for the guidance he provided during this research. His interest, advice, and effort were essential for the completion of this thesis.

This work was supported by Rome Laboratory U.S. Air Force, under contract number UM915025/28140. Thanks are due to Lisa Slaski and Vince Vannicola of Rome Laboratory for their constructive suggestions. I also gratefully acknowledge Dr. Vic Lesser of the University of Massachusetts and Hamid Nawab of Boston University for familiarizing me with the IPUS program.

Finally, thanks are also due to Dr. P. Varshney, the dissertation reader, Dr. H. Wang, and Dr. C. Isik with whom I had many helpful discussions.

I am extremely grateful to my entire family for the continuous support they have given me, for the values they have taught me, and for the sacrifices they have made for the sake of my education. I dedicate this dissertation to my mother and father and to my two brothers Ahmed and Mounir.

A special dedication goes to my mother who traveled from Algeria to be with me during the last months of my Ph.D. program so that I could devote full attention to my dissertation work.

## Table of Contents

Introduction	1
Chapter I: Radar Detection with A Priori Statistical Knowledge of the Environment	3
I.1 - Introduction	3
I.2 - Spherically Invariant Random Vector	5
I.2.1 - Definitions	5
I.2.2 - Properties of SIRVs	7
I.3 - Locally Optimum Detector	8
Chapter II: Signal Understanding and Detection Using a Feedforward Expert System	12
II.1 - Introduction	12
II.2 - Classification of the Test Cells	13
II.2.1 - Mapping of the Space	13
II.2.2 - Indexing of the Cells	14
II.3 - Target Detection	15
Chapter III: Signal Understanding and Detection Using a Feedback Expert System	21
III.1 - Introduction	21
III.2 - IPUS Architecture	24
III.2.1 - Introduction	24
III.2.2 - Discrepancy Detection	28
III.2.3 - Diagnosis and Reprocessing	29
III.2.4 - Interpretation Process	30
III.2.5 - Sources of Uncertainty (SOUs) and RESUN	30
III.3 - Application of IPUS to Radar Signal Understanding	34
Chapter IV: Description of the Proposed Radar Signal Processing System	36
IV.1 - Data Collection and Preprocessing	36
IV.2 - Mapping	43

<b>Chapter V: Mapping Procedure</b>	<b>46</b>
<b>V.1 - Introduction</b>	<b>46</b>
<b>V.2 - Observations on BN and CL Cells</b>	<b>48</b>
<b>V.2.1 - Observations on BN Cells</b>	<b>48</b>
<b>V.2.2 - Observations on CL Cells</b>	<b>49</b>
<b>V.3 - Mapping Procedure</b>	<b>50</b>
<b>V.3.1 - Separation of CL Patches from BN</b>	<b>50</b>
<b>V.3.1.1 - Thresholding and Quantization</b>	<b>50</b>
<b>V.3.1.2 - Correction</b>	<b>52</b>
<b>V.3.1.3 - Assessment</b>	<b>56</b>
<b>V.3.1.4 - Smoothing</b>	<b>57</b>
<b>V.3.2 - Detection of Clutter Patch Edges and Edge Enhancement</b>	<b>57</b>
<b>V.3.2.1 - Detection of Clutter Patch Edges</b>	<b>57</b>
<b>V.3.2.2 - Enhancement of Clutter Patch Edges</b>	<b>61</b>
<b>V.3.3 - Conclusion</b>	<b>62</b>
<b>V.4 - Examples of the Mapping Procedure</b>	<b>62</b>
<b>V.4.1 - Introduction</b>	<b>62</b>
<b>V.4.2 - Examples</b>	<b>64</b>
<b>V.4.2.1 - Example 1</b>	<b>64</b>
<b>V.4.2.2 - Example 2</b>	<b>74</b>
<b>V.4.2.3 - Example 3</b>	<b>84</b>
<b>V.5 - Convergence of the Mapping Procedure</b>	<b>94</b>
<b>V.5.1 - Introduction</b>	<b>94</b>
<b>V.5.2 - Separation Between BN and CL Patches</b>	<b>97</b>
<b>V.6 - Extension of the Mapping Procedure to R/A/D Cells</b>	<b>109</b>
<b>V.7 - Conclusion</b>	<b>111</b>
<b>Chapter VI: Indexing Procedure</b>	<b>112</b>
<b>VI.1 - Introduction</b>	<b>112</b>
<b>VI.2 - Assessment Stage</b>	<b>113</b>
<b>VI.2.1 - Identification of the BN Region and CL Patches</b>	<b>113</b>
<b>VI.2.2 - Computation of CNRs</b>	<b>116</b>
<b>VI.2.3 - Classification of CL Patches</b>	<b>116</b>

VI.3 - CL Subpatch Investigation Stage	117
VI.4 - PDF Approximation of WSC CL Patches	118
VI.4.1 - Test Cell Selection	118
VI.4.2 - PDF Approximation	121
VI.4.2.1 - Introduction to Ozturk Algorithm	122
VI.4.2.2 - Goodness of Fit Test	122
VI.4.2.3 - Approximation Chart Mode	124
VI.4.3 - PDF Approximation Metric	124
VI.4.4 - Outliers	126
VI.4.5 - PDF Approximation Strategy	131
VI.5 - Examples	132
VI.5.1 - Example 1	132
VI.5.2 - Example 2	141
VI.5.3 - Example 3	146
VI.6 - Extension of the Indexing Procedure to R/A/D Cells	152
VI.7 - Conclusion	153
Chapter VII: Application of IPUS to the Radar Detection Problem	155
VII.1 - Summary of IPUS Concepts	155
VII.2 - Role of IPUS in the Mapping Procedure	156
VII.2.1 - IPUS Stages Included in the Mapping Procedure	156
VII.2.1.1 - SPA and SPA Instance	156
VII.2.1.2 - Observations on Setting of the Control Parameters	157
VII.2.1.3 - Resolution of Discrepancies	161
VII.3 - Examples	170
VII.3.1 - Example 1	171
VII.3.2 - Example 2	172
VII.3.3 - Example 3	173
VII.4 - Role of IPUS in the Indexing Procedure	174
VII.4.1 - IPUS Stages Included in the Assessment Stage	174
VII.4.2 - IPUS Stages Included in the CL Subpatch Investigation Stage	174

VII.4.2.1 - SPA and SPA Instance	174
VII.4.2.2 - Observations on the Setting of the Control Parameters	175
VII.4.2.3 - Resolution of Discrepancies	175
VII.4.3 - Examples	179
VII.4.3.1 - Example 1	179
VII.4.3.2 - Example 2	182
VII.4.3.3 - Example 3	184
VII.4.4 - IPUS Stages Included in the PDF Approximation Stage	188
VII.4.4.1 - Step 6 of the PDF Approximation Strategy	188
VII.4.4.2 - SPA and SPA Instance	193
VII.4.4.3 - Resolution of Discrepancies	194
VII.5 - Examples	200
VII.5.1 - Example 1	201
VII.5.2 - Example 2	210
VII.5.3 - Example 3	223
VII.6 - Conclusion	234
Chapter VIII: Conclusion	235
VIII.1 - Conclusion	235
VIII.2 - Future Research	235
References	238

## List of Figures

Figure I.3.1	- Power function for three different receivers	10
Figure I.3.2	- Illustration of non-optimality of LOD when $\theta > \theta_c$	11
Figure II.3.1	- Signal Understanding and Detection Using a Feed Forward Expert System (SUD/FFES)	17
Figure II.3.2	- Signal Processors and Interpreters in a SUD/FFES	18
Figure III.1.1	- Signal Understanding and Detection Using a Feed Back Expert System (SUD/FBES)	22
Figure III.1.2	- Signal Processing and Interpretation Blocks in a SUD/FBES	23
Figure IV.1.1	- Envelope of the Transmitted Signal	36
Figure IV.1.2	- Range Cells in a Constant Azimuth Beam	37
Figure IV.1.3	- Range Cells and Their Corresponding Time Bins	38
Figure IV.1.4	- Rectangular Format for Representing Cells at Different Ranges and Azimuth Angles	39
Figure IV.1.5	- Collection of Azimuth Cells for a Fixed Range	40
Figure IV.1.6	- Block Diagram of Data Preprocessing Stage	41
Figure IV.1.7	- Cubic Format for Representing Cells at Different Ranges, Azimuth Angles, and Doppler Frequencies.	42
Figure IV.2.1	- Block Diagram of the Preprocessing and Mapping of Data	45
Figure V.1.1	- Block Diagram of Data Preprocessing Stage for P=1	46
Figure V.1.2	- Block Diagram of Preprocessing and mapping Stages for P=1	47
Figure V.2.1	- Example of a BN histogram	48
Figure V.2.2	- Concentration of large data in a scanned volume	49
Figure V.3.1	- Example of a Generated R/A Volume that is to be Separated by the Mapping Procedure	51
Figure V.3.2	- Example of a Quantized R/A Volume	52
Figure V.3.3	- 3x3 R/A Cells	53
Figure V.3.4	- Example of a "Corrected" R/A Volume	54
Figure V.3.5	- Example of the CCV Corresponding to the CQV of Fig. V.3.4	55
Figure V.3.6	- Example of the SV Corresponding to the CCV of Fig. V.3.5	58
Figure V.3.7	- Weighting Filter	59
Figure V.3.8	- Quantized Values of the 3x3 Array Corresponding to the $jk^{\text{th}}$ Cell	59

Figure V.3.9 - Example of Unsharp Masking Technique	61
Figure V.3.10 - Block Diagram of the Mapping Procedure	63
Figure V.4.1 - Boundaries of the CL Regions	66
Figure V.4.2 - 3-D Envelope Plot of the Surveillance Volume	66
Figure V.4.3 - Probability Density Functions and Histograms of the Background Noise and Clutter Patches	67
Figure V.4.4 - Contour plot of the Quantized Volume with BNQP=10%	68
Figure V.4.5 - Contour Plot of the First Correction Volume with NCQ=8	68
Figure V.4.6 - Contour Plot of the Second Correction Volume with NCC=1	69
Figure V.4.7 - Contour Plot of the Quantized Volume with BNQP=63.37%	70
Figure V.4.8 - Contour Plot of the First Correction Volume with NCQ=5	71
Figure V.4.9 - Contour Plot of the Second Correction Volume with NCC=3	71
Figure V.4.10 - Contour Plot of the Smoothed Volume with NS=7	73
Figure V.4.11 - Contour Plot of the Edge Enhanced Volume	73
Figure V.4.12 - Contour Plot of the Edge Selected Volume	74
Figure V.4.13 - Boundaries of the CL Regions	76
Figure V.4.14 - 3-D Envelope Plot of the Surveillance Volume	76
Figure V.4.15 - Probability Density Functions and Histograms of the Background Noise and Clutter Patches	77
Figure V.4.16 - Contour Plot of the Quantized Volume with BNQP=10%	78
Figure V.4.17 - Contour Plot of the First Correction Volume with NCQ=8	78
Figure V.4.18 - Contour Plot of the Second Correction Volume with NCC=1	79
Figure V.4.19 - Contour Plot of the Quantized Volume with BNQP=75.78%	81
Figure V.4.20 - Contour Plot of the First Correction Volume with NCQ=5	81
Figure V.4.21 - Contour Plot of the Second Correction Volume with NCC=1	82
Figure V.4.22 - Contour Plot of the Smoothed Volume with NS=7	82
Figure V.4.23 - Contour Plot of the Edge Enhanced Volume	83
Figure V.4.24 - Contour Plot of the Edge Detected Volume	83
Figure V.4.25 - Boundaries of the CL Regions	87
Figure V.4.26 - 3-D Envelope Plot of the Surveillance Volume	87
Figure V.4.27 - Probability Density Functions and Histograms of the Background Noise and Clutter Patches	88
Figure V.4.28 - Contour Plot of the Quantized Volume with BNQP=10%	89

Figure V.4.29 - Contour Plot of the First Correction Volume with NCQ=8	89
Figure V.4.30 - Contour Plot of the Second Correction Volume with NCC=1	90
Figure V.4.31 - Contour Plot of the Quantized Volume with BNQP=84.70%	91
Figure V.4.32 - Contour Plot of the First Correction Volume with NCQ=5	92
Figure V.4.33 - Contour Plot of the Second Correction Volume with NCC=3	92
Figure V.4.34 - Contour Plot of the Smoothed Volume with NS=7	93
Figure V.4.35 - Contour Plot of the Edge Enhanced Volume	93
Figure V.4.36 - Contour Plot of the Edge Detected Volume	94
Figure V.5.1 - Nonoverlapping PDFs of Two Distinct Regions	95
Figure V.5.2 - Overlapping PDFs of Two Distinct Regions with a Small Overlapping Area	96
Figure V.5.3 - Overlapping PDFs of Two Distinct Regions with a Big Overlapping Area	97
Figure V.5.4 - PDF of the Rayleigh Distributed Patch	98
Figure V.5.5 - Overlapping PDFs of BN Region and CL Patches	102
Figure V.5.6 - Region Histograms Corresponding to BNQP=10%, NCQ=8 and NCC=1	104-5
Figure V.5.7 - Region Histograms Corresponding to BNQP=10%, NCQ=8 and NCC=1	106-8
Figure V.6.1 - BN Declared Rows and their Corresponding BN Declared Planes	110
Figure VI.2.1 - Mask Used in Numbering	114
Figure VI.2.2 - Example of a Sharply Shaped Boundary	115
Figure VI.3.1 - Example a CL Patch Containing CL Subpatches	117
Figure VI.3.2 - Assessment Stage	119
Figure VI.3.3 - CL Subpatch Investigation Stage	119
Figure VI.3.4 - Assessment and CL Subpatch Investigation	120
Figure VI.4.1 - Goodness of Fit Test	123
Figure VI.4.2 - Approximation Chart	125
Figure VI.4.3 - Histogram of Set A	128
Figure VI.4.4 - Histogram of Set B	129
Figure VI.4.5 - Approximation Chart for the End Point of Set A	129
Figure VI.4.6 - Approximation Chart for the End Point of Set B	130

Figure VI.4.7 - Goodness of Fit Test for Set A	130
Figure VI.4.8 - Goodness of Fit Test for Set B	131
Figure VI.5.1 - Contour Plot of the Mapped Volume after Numbering	133
Figure VI.5.2 - Contour Plot of the Mapped Volume after Numbering	136
Figure VI.5.3 - Contour Plot of the Mapped Volume after Numbering	142
Figure VI.5.4 - Contour Plot of the Mapped Volume after Numbering	147
Figure VI.6.1 - Mask Used in Numbering the R/A/D Volume	153
Figure VII.2.1 - Plot of $BNCQP _{NCQ=8}$ - $BNCQP _{NCQ=7}$ Versus BNQP-BNQP <sub>t</sub> for Different Values of BNQP <sub>t</sub>	164
Figure VII.2.2 - Threshold Approximation Stage	165
Figure VII.2.3 - Threshold Fine-Tuning Stage	169
Figure VII.4.1 - Threshold Approximation Stage	176
Figure VII.4.2 - Threshold Fine-Tuning Stage	177
Figure VII.4.3 - PDF Approximation Stage	193
Figure VII.5.1 - Location of the Locus End Point for CL Patch A	204
Figure VII.5.2 - PDF Comparison for CL patch A	205
Figure VII.5.3 - Location of the Locus End Point for CL Patch B	205
Figure VII.5.4 - PDF Comparison for CL patch B	206
Figure VII.5.5 - Location of the Locus End Point for CL Patch C	206
Figure VII.5.6 - PDF Comparison for CL patch C	207
Figure VII.5.7 - Location of the Locus End Point for CL Patch D	207
Figure VII.5.8 - PDF Comparison for CL patch D	208
Figure VII.5.9 - Histogram and Best Approximating PDF for CL Patch A	208
Figure VII.5.10 - Histogram and Best Approximating PDF for CL Patch B	209
Figure VII.5.11 - Histogram and Best Approximating PDF for CL Patch C	209
Figure VII.5.12 - Histogram and Best Approximating PDF for CL Patch D	210
Figure VII.5.13 - Boundaries of the Scene Resulting from Step 6 of the PDF Approximation Stage	215
Figure VII.5.14 - Location of the Locus End Point for CL Patch A	217
Figure VII.5.15 - PDF Comparison for CL patch A	218
Figure VII.5.16 - Location of the Locus End Point for CL Patch B	218
Figure VII.5.17 - PDF Comparison for CL patch B	219

Figure VII.5.18 - Location of the Locus End Point for CL Patch C	219
Figure VII.5.19 - PDF Comparison for CL patch C	220
Figure VII.5.20 - Location of the Locus End Point for CL Patch D	220
Figure VII.5.21 - PDF Comparison for CL patch D	221
Figure VII.5.22 - Histogram and Best Approximating PDF for CL Patch A	221
Figure VII.5.23 - Histogram and Best Approximating PDF for CL Patch B	222
Figure VII.5.24 - Histogram and Best Approximating PDF for CL Patch C	222
Figure VII.5.25 - Histogram and Best Approximating PDF for CL Patch D	223
Figure VII.5.26 - Data Amplitude Histograms Including Additive BN Data for (a) CL Patch C and (b) CL Patch D	226
Figure VII.5.27 - Location of the Locus End Point for CL Patch A	228
Figure VII.5.28 - PDF Comparison for CL patch A	228
Figure VII.5.29 - Location of the Locus End Point for CL Patch B	229
Figure VII.5.30 - PDF Comparison for CL patch B	229
Figure VII.5.31 - Location of the Locus End Point for CL Patch C	230
Figure VII.5.32 - PDF Comparison for CL patch C	230
Figure VII.5.33 - Location of the Locus End Point for CL Patch D	231
Figure VII.5.34 - PDF Comparison for CL patch D	231
Figure VII.5.35 - Histogram and Best Approximating PDF for CL Patch A	232
Figure VII.5.36 - Histogram and Best Approximating PDF for CL Patch B	232
Figure VII.5.37 - Histogram and Best Approximating PDF for CL Patch C	233
Figure VII.5.38 - Histogram and Best Approximating PDF for CL Patch D	233

## List of Tables

Table II.3.1	- Functioning of the Signal Processing and Interpretation Blocks in a SUD/FFES	20
Table V.4.1	- CL Patch Parameters	65
Table V.4.2	- Settings of BNQP	70
Table V.4.3	- CL Patch Parameters after Assessment	72
Table V.4.4	- CL Patch Parameters	74
Table V.4.5	- Settings of BNQP	79
Table V.4.6	- CL Patch Parameters after Assessment	84
Table V.4.7	- CL Patch Parameters	84
Table V.4.8	- Settings of BNQP	86
Table V.4.9	- CL patch parameters after assessment	94
Table V.5.1	- BN Percentages and Threshold Values Corresponding to the Rayleigh Distributed BN	98
Table V.5.2	- BN Percentages of Example 3 of Section V.4.2.2	100
Table V.5.3	- CL-to-BN and BN-to-CL transitions in Example 3 of Section V.4.2.2	100
Table VI.2.1	- Classification of a CL Patch	116
Table VI.4.1	- PDF Approximation Metric for Different PDFs, $N_R=100$	127
Table VI.5.1	- CL Patch Parameters	132
Table VI.5.2	- Assessment Parameters	133
Table VI.5.3	- Mapping Procedure Applied to CL Patch 1	134
Table VI.5.4	- Mapping Procedure Applied to CL Patch 2	135
Table VI.5.5	- Mapping Procedure Applied to CL Patch 3	135
Table VI.5.6	- Assessment Parameters	137
Table VI.5.7	- PDF Approximation for CL Patch 1	138
Table VI.5.8	- PDF Approximation for CL Patch 2	139
Table VI.5.9	- PDF Approximation for CL Patch 3	140
Table VI.5.10	- PDF Approximation for CL Patch 4	140
Table VI.5.11	- CL Patch Parameters	141
Table VI.5.12	- Assessment Parameters	141
Table VI.5.13	- Mapping Procedure Applied to CL Patch 1	142

Table VI.5.14 - Mapping Procedure Applied to CL Patch 2	143
Table VI.5.15 - Mapping Procedure Applied to CL Patch 3	143
Table VI.5.16 - PDF Approximation for CL Patch 1	144
Table VI.5.17 - PDF Approximation for CL Patch 2	145
Table VI.5.18 - PDF Approximation for CL Patch 3	145
Table VI.5.19 - CL Patch Parameters	146
Table VI.5.20 - Assessment Parameters	146
Table VI.5.21 - Mapping Procedure Applied to CL Patch 1	147
Table VI.5.22 - Mapping Procedure Applied to CL Patch 2	148
Table VI.5.23 - Mapping Procedure Applied to CL Patch 3	148
Table VI.5.24 - PDF Approximation for CL Patch 1	149
Table VI.5.25 - PDF Approximation for CL Patch 2	150
Table VI.5.26 - PDF Approximation for CL Patch 3	151
Table VII.2.1 - Discrepancies in the Threshold Approximation Stage	166
Table VII.2.2 - Discrepancies in the Threshold Fine-Tuning Stage	170
Table VII.3.1 - Setting of BNQP in Both of the Threshold Approximation and Threshold Fine-tuning Stages	171
Table VII.3.2 - Setting of BNQP in Both of the Threshold Approximation and Threshold Fine-tuning Stages	172
Table VII.3.3 - Setting of BNQP in Both of the Threshold Approximation and Threshold Fine-tuning Stages	173
Table VII.4.1 - Discrepancies in the Threshold Approximation Stage	178
Table VII.4.2 - Discrepancies in the Threshold Fine-Tuning Stage	178
Table VII.4.3 - Setting of PLQP in Both of the Threshold Approximation and Threshold Fine-tuning Stages	179
Table VII.4.4 - Setting of PLQP in Both of the Threshold Approximation and Threshold Fine-tuning Stages	180
Table VII.4.5 - Setting of BNQP in Both of the Threshold Approximation and Threshold Fine-tuning Stages	181
Table VII.4.6 - Setting of PLQP in Both of the Threshold Approximation and Threshold Fine-tuning Stages	182
Table VII.4.7 - Setting of PLQP in Both of the Threshold Approximation and Threshold Fine-tuning Stages	183

Table VII.4.8 - Setting of BNQP in Both of the Threshold Approximation and Threshold Fine-tuning Stages	184
Table VII.4.9 - Setting of PLQP in Both of the Threshold Approximation and Threshold Fine-tuning Stages	185
Table VII.4.10 - Setting of PLQP in Both of the Threshold Approximation and Threshold Fine-tuning Stages	186
Table VII.4.11 - Setting of PLQP in Both of the Threshold Approximation and Threshold Fine-tuning Stages	187
Table VII.4.12 - Minor Axis Length for Different PDFs, $N_R=100$	190
Table VII.4.13 - Distance Between Every Two Test Cells for the Example of Table VI.5.9	192
Table VII.4.14 - Exclusion Table for the Example of Table VI.5.9	192
Table VII.4.15 - Discrepancies in the PDF Approximation of a Test Cell Stage	195
Table VII.4.16 - Exclusion Table for Cells a, b, c, d, and e	197
Table VII.4.17 - Exclusion Table When b and c are Interchanged	197
Table VII.4.18 - Exclusion Table When f, g, and h are Added	197
Table VII.4.19 - Exclusion Table When f, g, and h Are Added	198
Table VII.4.20 - Discrepancies in the PDF Approximation of a CL Patch	199
Table VII.5.1 - Average PDF(s) for CL Patch 1	201
Table VII.5.2 - Average PDF(s) for CL Patch 2	202
Table VII.5.3 - Average PDF(s) for CL Patch 3	202
Table VII.5.4 - Average PDF(s) for CL Patch 4	202
Table VII.5.5 - Assessment Parameters of the Mapping and Indexing Stages	202
Table VII.5.6 - Accurate Approximation of Underlying CL patch PDFs	204
Table VII.5.7 - Average PDF(s) for CL Patch 1	211
Table VII.5.8 - Average PDF(s) for CL Patch 2	211
Table VII.5.9 - Average PDF(s) for CL Patch 3	211
Table VII.5.10 - Exclusion Table for the Example of Table VI.5.17	212
Table VII.5.11 - PDF approximation for Test Cells No. 96, 115, and 134 of the Example of Section VI.5.2, CL Patch 2	212
Table VII.5.12 - Exclusion Table for the Example of Tables VI.5.17 and VII.5.11	213

Table VII.5.13 - Average PDF(s) for CL Patch 2 Using Test Cells Numbered 1 and 77	215
Table VII.5.14 - Average PDF(s) for CL Patch 4 Using Cells Numbered 154, 231, and 308	215
Table VII.5.15 - Assessment Parameters of the Mapping and Indexing Stages	215
Table VII.5.16 - Accurate Approximation of Underlying CL patch PDFs	217
Table VII.5.17 - Average PDF(s) for CL Patch 1	224
Table VII.5.18 - Average PDF(s) for CL Patch 2	225
Table VII.5.19 - Average PDF(s) for CL Patch 3	225
Table VII.5.20 - Assessment Parameters of the Mapping and Indexing Stages	225
Table VII.5.21 - Accurate Approximation of Underlying CL patch PDFs	227

## Glossary

### Chapter I

LRT	Likelihood Ratio Test
PDF	Probability Density Function
PFA	Probability of False Alarm
$(H_1, H_0)$	Binary Hypothesis
SIRP	Spherically Invariant Random Process
SIRV	Spherically Invariant Random Vector
LOD	Locally Optimum Detector
PD	Probability of Detection

### Chapter II

GLRT	Generalized Likelihood Ratio Test
SUD/FFES	Signal Understanding and Detection Using a Feed-Forward Expert System
WSUD/FFES	Weak Signal Understanding and Detection Using a Feed-Forward Expert System
SP	Signal Processor
SI	Signal Interpreter
SSC	Strong Signal Case
ISC	Intermediate Signal Case
WSC	Weak Signal Case

### Chapter III

SUD/FBES	Signal Understanding and Detection Using a Feed-Back Expert System
IPUS	Integrated Processing and Understanding of Signals
SPA	Signal Processing Algorithm

KS	Knowledge Source
SOU	Sources of Uncertainty
RESUN	Resolving Sources of Uncertainty

## Chapter IV

PRI	Pulse Repetition Interval
PRF	Pulse Repetition Frequency
$\tau_d$	Round Trip Delay
R	Range
A	Azimuth
D	Doppler
c	Velocity of Propagation of the Electromagnetic Wave
FFT	Fast Fourier Transform
BN	Background Noise
CL	Clutter

## Chapter V

CNR	Clutter-to-Noise Ratio
NCQ	Neighboring Cells in the Quantized Volume
NCC	Neighboring Cells in the First Corrected Volume
QV	Quantized Volume
CQV	Corrected-Quantized Volume (First Corrected Volume)
CCV	Corrected-Corrected Volume (Second Corrected Volume)
BNQP	Percentage of BN cells in the Quantized Volume
BNCQP	Percentage of BN cells in the Corrected-Quantized Volume
BNCCP	Percentage of BN cells in the Corrected-Corrected Volume
SV	Smoothed Volume
NS	Neighboring Cells in the Smoothed Volume
CLE	CL Edge
$(BN \rightarrow CL)_{1,2}$	Percentage of the total number of cells in the surveillance

	volume that were below the threshold but are reclassified as CL cells after the first and second correction stages, respectively
$(CL \rightarrow BN)_{1,2}$	Percentage of the total number of cells in the surveillance volume that were above the threshold but are reclassified as BN cells after the first and second correction stages, respectively
G	Unique number assigned to a CL patch
H	Minimum positive number assigned to the neighboring cells
$N_R$	Number of reference cells. For the null hypothesis
W	Weibull distribution
L	Lognormal distribution
K	K distribution

## Chapter VI

PLQP	Percentage of cells the subpatch with the lowest power among the possible subpatches of a CL patch in the Quantized Volume
PLCQP	Percentage of cells the subpatch with the lowest power among the possible subpatches of a CL patch in the Corrected-Quantized Volume
PLCCP	Percentage of cells the subpatch with the lowest power among the possible subpatches of a CL patch in the Corrected-Corrected Volume
$N_T$	Number of test cells to be selected in a clutter patch test cells

## Chapter VII

$BNQP_t$	True value for the fraction of BN cells in the generated scene
$PLQP_t$	True value for PLQP

## Introduction

In signal processing applications it is common to assume a Gaussian problem in the design of optimal signal processors. However, non-Gaussian processes do arise in many situations. For example, measurements reveal that radar clutter may be approximated by either Weibull, K-distributed, Lognormal, or Gaussian distributions depending upon the scenario [4]-[10]. When the possibility of a non-Gaussian problem is encountered, the question as to which probability distributions should be utilized in a specific situation for modeling the data needs to be answered.

In practice, the underlying probability distributions are not known a priori. Consequently, an assessment must be made by monitoring the environment. Another consideration is that radar detection problems can usually be divided into strong, intermediate, and weak signal cases. Hence, the system that monitors a radar environment must be able to subdivide the surveillance volume into background noise and clutter patches in addition to approximating the underlying probability distributions for each patch. This is in contrast to current practice where a single robust detector, usually based on the Gaussian assumption, is employed.

The objective of this work is to develop techniques that monitor the environment and select the appropriate detector for processing the data.

The main contributions are: (1) an image processing technique is devised which enables partitioning of the surveillance volume into background noise and clutter patches, (2) a new algorithm, developed by Dr. Ozturk while he was a Visiting Professor at Syracuse University, [27]-[29], is used to identify suitable approximations to the probability density function for each clutter patch, and (3) rules to be used with the expert system, Integrated Processing and Understanding of Sig-

nals (IPUS), [20]-[22], are formulated for monitoring the environment and selecting the appropriate detector for processing the data.

This dissertation is organized as follows: Chapter I discusses some of the difficulties that arise in the classical radar detection problem. Their solution is proposed in Chapter II which uses an expert system with feed-forward processing. In Chapter III an improved solution is presented using feed-back processing. The general radar detection problem is described in Chapter IV and a mapping procedure is introduced to separate between background noise and clutter patches. In Chapter V an image processing technique is developed for the mapping procedure. Next, an indexing procedure is developed in Chapter VI to enable the investigation of clutter subpatches and the approximation of probability distributions for each clutter patch. Finally, expert system rules are developed in Chapter VII to enable the system to control both the mapping and indexing stages. Conclusions and suggestions for future research are given in Chapter VIII.

# Chapter I

## Radar Detection with A Priori Statistical Knowledge

### of the Environment

#### I.1 - Introduction

The optimal radar detection problem consists of collecting a set of  $N$  samples  $r_0, r_1, \dots, r_{N-1}$  from a given cell in the space, processing the data by a Neyman-Pearson receiver which takes the form of a likelihood ratio test (LRT) [1] and deciding for that cell whether or not a target is present. Let  $\mathbf{r}$  denote the vector formed by the  $N$  samples:  $\mathbf{r} = [r_0, r_1, \dots, r_{N-1}]^T$ . The LRT compares a statistic to a fixed threshold,  $\eta$ . The statistic consists of the ratio between the joint probability density function (PDF),  $p_r(\mathbf{R} | H_1)$ , of the  $N$  samples given that a target is present and the joint PDF,  $p_r(\mathbf{R} | H_0)$ , of the  $N$  samples given that no target is present.  $H_1$  and  $H_0$  denote the hypotheses that a target is present and absent, respectively. This ratio is called the likelihood ratio (LR). The threshold,  $\eta$ , is determined by constraining the false alarm probability (PFA) to a specified value.

The binary hypotheses ( $H_1, H_0$ ) are defined such that, under hypothesis  $H_1$ , the  $k^{\text{th}}$  collected sample,  $r_k$ ,  $k=0, 1, \dots, N-1$ , is composed of a target signal sample,  $s_k$ , plus an additive disturbance sample,  $d_k$ . Under hypothesis  $H_0$ , the  $k^{\text{th}}$  sample,  $r_k$ ,  $k=0, 1, \dots, N-1$ , consists only of the disturbance sample  $d_k$ . Hence,

$$r_k = \begin{cases} s_k + d_k & ; H_1 \\ d_k & ; H_0 \end{cases} \quad k=0, 1, \dots, N-1. \quad (\text{I.1-1})$$

In general, the disturbance sample  $d_k$  consists of a clutter sample,  $c_k$ , plus a background noise sample,  $n_k$ .

The LRT then takes the form

$$1 = \frac{p_r((R)|H_1)}{p_r((R)|H_0)} \stackrel{H_1}{>} \stackrel{H_0}{<} \eta. \quad (I.1-2)$$

For  $1 > \eta$ ,  $H_1$  is decided. Otherwise,  $H_0$  is decided.

Assuming that the samples are statistically independent, the joint PDF  $p_r((R)|H_i)$ ;  $i=0,1$ , is nothing but the product of the  $N$  marginal PDFs of the samples. Specifically,

$$p_r((R)|H_i) = \prod_{k=0}^{N-1} p_{r_k}(R_k|H_i) \quad ; i=0,1. \quad (I.1-3)$$

The LRT is then readily implemented provided the marginal PDFs are known.

In practice, the real data may be correlated in time making invalid the statistical independence assumption. Unless the joint PDFs of the correlated samples are assumed to be Gaussian, it is not commonly known how to specify the joint PDFs  $p_r((R)|H_i)$ ;  $i=0,1$ . Thus, many engineers invoke the Gaussian assumption even when it is known to be non-applicable. It is for this reason that most radars today are Gaussian receivers (i.e., they process the data using the LRT based on the joint Gaussian PDF). When the target signal,  $s_k$ , cannot be filtered from the disturbance,  $d_k$ , by means of spatial and/or temporal processing and  $d_k$  is much larger than  $s_k$ ,  $k=0,1,\dots,N-1$ , then  $r_k$  approximately equals  $d_k$  under both hypotheses and high precision is needed to evaluate the LRT because  $p_r(R|H_1)$  becomes approximately equal to  $p_r(R|H_0)$ . Specifically,

$$1 = \frac{p_r(R|H_1)}{p_r(R|H_0)} \approx 1 \quad (I.1-4)$$

and the statistic,  $I$ , becomes insensitive to the received data.

Recent work reported by Rangaswamy et al. [2] shows that it is possible to model  $N$  correlated non-Gaussian random samples as samples from a spherically invariant random process (SIRP). The vector  $r$  of the  $N$  samples is said to be a spherically invariant random vector (SIRV). More details about SIRVs are presented in Section I.2.

In addition, the work done by Chakravathi et al. [3] shows for the non-Gaussian weak signal case (i.e., the average power of  $s_k$  is much less than that of  $d_k$ ,  $k=0,1,\dots,N-1$ ) that the use of a locally optimum detector (LOD) provides improved performance over direct application of the Gaussian LRT. LODs are introduced in Section I.3.

## **I.2 - Spherically Invariant Random Vector (SIRV) [11] [2]**

Many investigators [4], [5], [6], [7] have reported experimental measurements for which the clutter probability density function has an extended tail. The extended tail gives rise to spiky clutter and relatively large probabilities of false alarm. The Gaussian model for the clutter fails to predict this behavior. Non-Gaussian models for the univariate (marginal) clutter PDF have been proposed. Commonly reported marginal non-Gaussian PDFs for the clutter are Weibull [4], log-normal [8],[9] and K-distributed [5], [6] and [10].

Usually, radars process  $N$  pulses at a time. A complete statistical characterization of the clutter requires the specification of the joint probability density function (PDF) of the  $N$  samples. The theory of spherically invariant random processes (SIRPs) provides a powerful mechanism for obtaining the joint PDF of the  $N$  correlated non-Gaussian random variables.

### **I.2.1 - Definitions**

A spherically invariant random vector (SIRV) is a random vector whose

PDF is uniquely determined by the specification of a mean vector, a covariance matrix and a characteristic first order PDF. The PDF of a random vector is defined to be the joint PDF of the components of the random vector.

A spherically invariant random process (SIRP) is a random process such that every random vector obtained by sampling this process is a SIRV.

The work of Kingman [12] and Yao [13] gave rise to a representation theorem, valid for all SIRVs. This is summarized below. Let  $\mathbf{z} = [z_1, z_2, \dots, z_N]^T$  denote a real zero mean Gaussian random vector with covariance matrix  $M$ . Let  $s$  denote a non-negative random variable with PDF  $f_s(s)$ . It is assumed that  $s$  is independent of  $\mathbf{z}$ . The representation theorem states that  $\mathbf{x}$  is an SIRV if and only if it can be expressed in the form  $\mathbf{x} = \mathbf{z}s$ . In particular the PDF of  $\mathbf{x}$  is given by

$$f_{\mathbf{x}}(\mathbf{x}) = (2\pi)^{-N/2} |M|^{-1/2} \int_0^{\infty} s^{-N} \exp\left(-\frac{\mathbf{x}^T M^{-1} \mathbf{x}}{2s^2}\right) f_s(s) ds \quad (I.2-1)$$

where  $|M|$  denotes the determinant of the covariance matrix  $M$ . Let  $P = \mathbf{x}^T M^{-1} \mathbf{x}$ . Then Eq. (I.2-1) can be written as

$$f_{\mathbf{x}}(\mathbf{x}) = (2\pi)^{-N/2} |M|^{-1/2} h_N(P) \quad (I.2-2)$$

where

$$h_N(P) = \int_0^{\infty} s^{-N} \exp\left(-\frac{P}{2s^2}\right) f_s(s) ds . \quad (I.2-3)$$

Note that  $f_s(s)$  is defined to be the characteristic PDF of the SIRV.

### I.2.2 - Properties of SIRVs [2], [14], [15], [16]

Several properties of SIRVs are stated below:

- It has been pointed out in [15] that when  $f_s(S) = \delta(S - 1)$ , where  $\delta(\cdot)$  is the unit impulse function, the resulting  $h_N(P)$  is the familiar multivariate Gaussian PDF.
- Differentiation of Eq. (I.2-3) with respect to the argument gives [16]

$$h_{N+2}(w) = -2 \frac{dh_N(w)}{dw} . \quad (I-2.4)$$

In Eq. (I.2-4) the argument has been replaced by  $w$  because the quadratic form  $p$  depends on  $N$  and, therefore, cannot be used in the equality. Eq. (I.2-4) provides a mechanism to relate the functional forms of the higher order PDFs with those of the lower order. Starting with  $N=1$  and using Eq.(I-2.4) repeatedly gives

$$h_{2N+1}(w) = (-2)^N \frac{d^N h_1(w)}{dw^N} . \quad (I-2.5)$$

Starting with  $N=2$ ,

$$h_{2N+2}(w) = (-2)^N \frac{d^N h_2(w)}{dw^N} . \quad (I-2.6)$$

It is, therefore, possible to construct all higher order PDFs for odd values of  $N$  and even values of  $N$ , starting from  $h_1(w)$  and  $h_2(w)$ , respectively.

- The PDF of a SIRV is a function of a non-negative quadratic form. The PDF is uniquely determined by specification of a mean vector, a covariance matrix and characteristic first order PDF.
- A SIRV is invariant under a linear transformation. More precisely, if  $\mathbf{x}$  is a SIRV with characteristic PDF  $f_s(S)$ , then  $\mathbf{y} = \mathbf{Ax} + \mathbf{B}$ , where  $\mathbf{A}$  is a matrix and  $\mathbf{B}$  is a

vector, is a SIRV with the same characteristic PDF as  $\mathbf{x}$ .

- $h_1(p)$  is related to the marginal (first order) PDF of  $x_k$ . This can be seen very easily by letting  $N=1$  in Eq. (I.2-2). More precisely,

$$f_{x_k}(X_k) = \frac{1}{\sqrt{2\pi\sigma_k^2}} h_1(P) ; k=0,1,2,\dots,N-1 \quad (I.2-7)$$

where  $P = \frac{x_k^2}{\sigma_k^2}$  and  $\sigma_k^2$  denotes the variance of  $x_k$ .

- Two of the possible techniques for obtaining the PDF of a SIRV are:

(1)- If the characteristic PDF of the SIRV is readily available, then evaluate  $h_N(P)$  directly from Eq.(I.2-3). Complete the characterization by specifying the mean vector and covariance matrix of the SIRV.

(2)- If the characteristic PDF of the SIRV is not readily available, but the marginal PDF is known, first obtain  $h_1(P)$  from the marginal PDF using Eq.(I.2-7). Then obtain  $f_s(S)$  by solving the integral equation in Eq.(I.2-3) with  $N=1$ . Next use  $f_s(S)$  in Eq.(I.2-3) for desired  $N$  to obtain  $h_N(P)$ . Finally, specify the mean vector and covariance matrix of the SIRV.

In the work that follows SIRP's will be used to model correlated non-Gaussian disturbances (i.e, clutter plus noise).

### I.3 - Locally Optimum Detector [17]

Assume that the received target signals have a very small unknown amplitude  $\theta$ , so that

$$\text{Under } H_1 \quad \mathbf{r} = \theta \mathbf{s} + \mathbf{d}$$

(I.3-1)

$$\text{Under } H_0 \quad \mathbf{r} = \mathbf{d}.$$

A Taylor series expansion of the numerator of the LR results in [17]

$$\frac{p_r(R|H_1)}{p_r(R|H_0)} = 1 + \theta \frac{\frac{d}{d\theta} p_r(R|H_1) \Big|_{\theta=0}}{p_r(R|H_0)} + \frac{\theta^2}{2} \frac{\frac{d^2}{d\theta^2} p_r(R|H_1) \Big|_{\theta=0}}{p_r(R|H_0)} + \dots \quad (I.3-2)$$

The LRT consists of comparing the LR to a threshold  $\eta$ . For the case where  $\theta$  is very small, it is assumed that the terms involving  $\theta^2, \theta^3, \dots$  are negligible with high probability. Ignoring these terms, the LRT simplifies to

$$1 + \theta \frac{\frac{d}{d\theta} p_r(R|H_1) \Big|_{\theta=0}}{p_r(R|H_0)} \begin{matrix} H_1 \\ > \\ H_0 \end{matrix} \quad \begin{matrix} < \\ \eta \end{matrix} \quad (I.3-3)$$

$$v = \frac{\frac{d}{d\theta} p_r(R|H_1) \Big|_{\theta=0}}{p_r(R|H_0)} \begin{matrix} H_1 \\ > \\ H_0 \end{matrix} \quad \begin{matrix} < \\ \frac{\eta - 1}{\theta} = \gamma \end{matrix} \quad (I.3-4)$$

The receiver which performs the above test is referred to as the locally optimum detector (LOD). Because the probability of detection (PD) and the probability of false alarm (PFA) are given by

$$PD = \int_{\gamma}^{\infty} p_v(v|H_1) dv \quad (I.3-5)$$

$$PFA = \int_{\gamma}^{\infty} p_v(v|H_0) dv \quad (I.3-6)$$

and because  $p_v(v|H_1)$  approaches  $p_v(v|H_0)$  as  $\theta$  goes to zero, it follows that  $PD=PFA$  when  $\theta=0$ . The power function of a receiver is defined as the curve relating  $PD$  and  $\theta$ . Under a fixed  $PFA$  constraint, a typical power function curve is shown in Fig. I.3.1

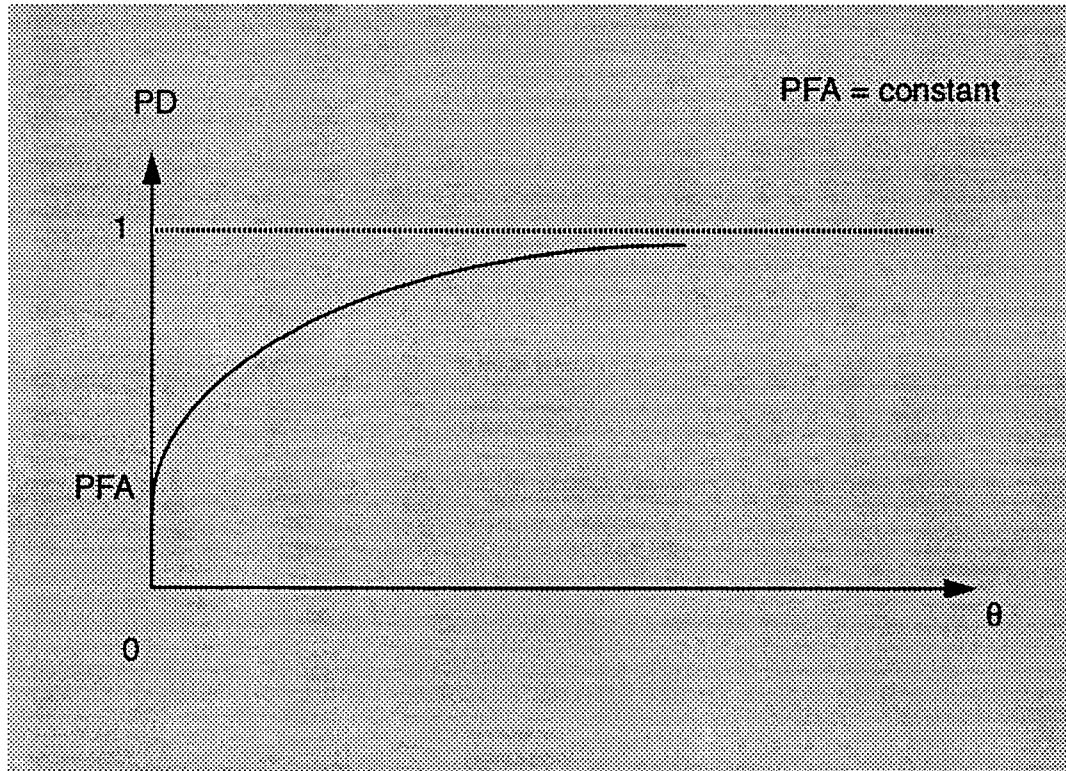


Figure I.3.1 - Power Function for Three Different Receivers

ent receivers. An alternative approach to the weak signal detection problem (i.e.,  $\theta \ll 1$ ) is to find that receiver which maximizes the slope of the power function at  $\theta=0$ . Solution of this optimization problem results in the same ratio test as given by Eq. (I.3-4). Consequently, the LOD is identical to that receiver which maximizes the slope of the power function at  $\theta=0$ . As a result, the LOD will maximize  $PD$  for  $\theta$  sufficiently small. However, other receivers may yield larger values of  $PD$  when  $\theta$  becomes large. As shown in Fig. I.3.2, for  $\theta > \theta_c$  another receiver is shown to outperform the LOD.

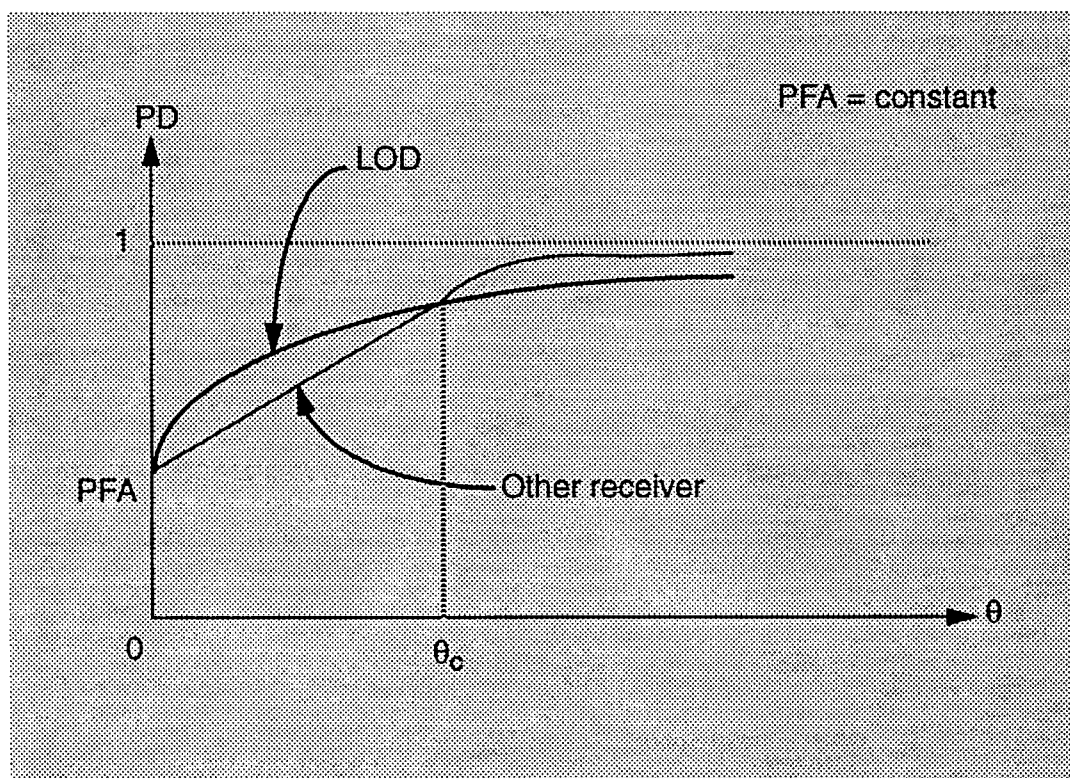


Figure I.3.2 - Illustration of Non-optimality of LOD when  $\theta > \theta_c$

## Chapter II

### Signal Understanding and Detection Using a Feedforward Expert System (SUD/FFES)

#### **II.1 - Introduction**

The use of SIRPs in the implementation of LRTs and LODs for the radar detection problem allows us to derive algorithms for performing both strong and weak signal detection in a non-Gaussian environment. Classical detection assumes a priori knowledge of the joint PDF underlying the received data. In practice, received data can come from a clear region, where background noise alone is present, or from a clutter region, where returns are due to reflections from such objects as ground, sea, buildings, birds,...etc. as well as background noise. When a desired target return is from a clear region and the background noise is sufficiently small, the signal-to-noise ratio will be large and the strong signal detector (i.e, the LRT) should be used. However, if a desired target return is from a clutter region, two situations can exist. When the desired target can be filtered from the clutter (CL) by means of space-time processing and the background noise (BN) is sufficiently small, the signal to noise ratio will be large and a strong signal detector should again be used. When the desired target cannot be filtered from the clutter by means of space-time processing and the clutter return is much larger then the desired target return, then a weak signal detector (i.e, LOD) should be used. Use of the LOD in a strong signal situation can result in a severe loss in performance. Hence, it is necessary for the receiver to determine whether a strong or weak signal situation exists.

All of this suggests use of an expert system in the radar detection problem for **1)** monitoring the environment and **2)** selecting the appropriate detector for processing the data. This is in contrast to current practice where a single robust detector, usually based on the Gaussian assumption, is employed. In addition, depending on statistical changes in the environment over time and space, the expert

system enables the receiver to adapt so as to achieve close to optimal performance. The goal of this study is to explore how an expert system can be used to develop an adaptive radar receiver which is able to outperform traditional radars with respect to high subclutter visibility. The focus of the study deals with the detection of weak targets that cannot be filtered from the clutter by means of space-time processing. For this purpose, it is convenient to divide the problem into two steps. The first step involves classification of the cells to be tested while the second has to do with determining whether or not a target is present in the test cell. The two steps are discussed in more detail in the following sections.

## **II.2 - Classification of the Test Cells**

Classification of the test cells involves two steps: mapping of the space and indexing of the cells.

### **II.2.1 - Mapping of the Space**

In this research, the term, space, is used in its most general context. In practice, an effort is made to filter the desired target return from the clutter to the extent possible. This is accomplished by performing space-time processing on the received data. In particular, given  $N$  temporal samples and  $M$  spatial samples from a single range ring, spatial and temporal spectra are generated by performing a linear transformation on the  $NM$  samples. When the random processes are modeled as SIRPs, the space-time processing will not change the nature of the random processes since a linear transformation of an SIRP results in an SIRP of the same type. For example, if the underlying samples are modeled as Weibull, the transformed samples will also be Weibull. The spatial spectra contain angle of arrival information while the temporal spectra contain Doppler information. Consequently, the space of interest consists of range/angle of arrival/Doppler cells. It is in this general context that we refer to space and cells.

The mapping of the space can be done in two different ways: First, a clutter

map of the entire space can be generated by assigning a scan of the radar receiver for this purpose. The clutter map will indicate a priori those locations which are likely to consist of clear regions (where background noise alone is present) and clutter patches. Another way, is to do a real time assessment of a test cell. In other words, the question of whether the test cell is in a clear region or in a clutter patch is determined in real time during the scan.

### **II.2.2 - Indexing of the Cells**

In the regions where clutter patches are present, a sufficient number of reference cells near the test cell must be chosen so that the number of samples from the reference cells (approximately 100 if using Ozturk's algorithm [26], [27]) are adequate for approximating the body of the joint PDF to be used in characterizing the disturbance of the test cell. It should be recognized that a clutter patch could be non-homogeneous. If so, it may be necessary to subdivide the clutter patch into subpatches. The samples from each subpatch would be approximated by a different joint PDF.

An important point is that knowledge of the body of the joint PDF describing the disturbance is usually insufficient for determining the threshold of the radar receiver. In this research our focus is on the weak signal detection problem. As pointed out earlier, the appropriate processor for this problem is the LOD. For the LOD, Chakravathi and Weiner [3] have conjectured that the body of the PDF for the disturbance may be sufficient for determining the tail of the PDF for the LOD statistic. The body of the joint PDF describing the disturbance could then be sufficient for determining the threshold of the LOD. This is significant because only around 100 reference cells are needed when Ozturk's identification algorithm is used.

A set of descriptors need to be allocated for each cell. This allocation is referred to as cell indexing. The first item that needs to be determined is whether the detection problem for the test cell should be classified as strong signal detection,

weak signal detection, or an intermediate case which falls between strong and weak signal detection. For the case of strong signal detection, the conventional radar receiver is adequate. For weak signal detection, the LOD should be used. For the intermediate case, it is proposed to use Wang's processor [19] based on the generalized likelihood ratio test (GLRT).

In all three cases, it is necessary to use reference cells to estimate information needed for implementation of the processor. This assumes that the disturbance is homogeneous such that reference cells neighboring the test cell are representative of the test cell. However, a test cell may be near the edge of a clutter patch or subpatch. Its location relative to these edges should be known so that reference cells are selected which are truly representative of the test cell.

For weak signal detection, the LOD differs from one joint PDF to another. Hence, it is necessary to know the type of random process (e.g., Gaussian, K-distributed, Weibull, etc.) associated with the disturbance in the region where the test cell is located. In practice, Ozturk's algorithm may indicate that several different PDF's are suitable for approximating a particular disturbance. When this is the case, it may be desirable to implement several LOD's and fuse the results. Hence, descriptors should be allocated to each cell for describing one or more joint PDF's in terms of their type, scale, location and shape parameters.

### **II.3 - Target Detection**

As mentioned previously, the type of detector depends upon whether the detection problem has been classified as a strong signal case (SSC), weak signal case (WSC), or intermediate signal case (ISC). Once the type of detector has been selected, parameters for the sufficient statistic of the detector are determined from the cell descriptors. In addition, information from the cell descriptors is used to determine the threshold. When several detectors are employed simultaneously, as could arise in the weak signal case, a fusion algorithm is used to arrive at a global decision [31].

The above discussion provides the basis for signal understanding and detection using a feed forward expert system (SUD/FFES). A block diagram of the SUD/FFES is shown in Fig. II.3.1

The preprocessor collects data, performs classical space-time processing, and stores the resulting data. This data is then used by the mapping, indexing, and detection blocks which implement the two steps discussed previously. A more detailed block diagram is shown in Fig. II.3.2 where each block is subdivided into signal processing blocks and signal interpretation blocks. Because weak signal detection will be emphasized in this study, that portion dealing with weak signal detection is shown using solid lines while the remaining portions are enclosed by dashed lines. The solid line portion is referred to as weak signal understanding and detection using a feedforward expert system (WSUD/FFES). A more detailed discussion of each block is provided in Table II.3.1, and further more in Chapters IV to VII. Note that this is a feedforward system in the sense that the mapping, indexing, and detection are done sequentially with no feedback between these blocks.

Since the data collected from the environment is random, it is not possible to carry out an exact probability distribution identification using a reasonably small amount of data. Consequently, it is better to think about the probability distribution identification problem as an approximation problem where we hope to select PDFs and their parameters which result in good approximations to the underlying probability distributions.

Because the expert system of Fig. II.3.1 is feedforward, it does not allow for verification of the interpretations made by any of the signal interpretation blocks of Fig. II.3.2. Also, reprocessing of the data is not allowed by the feedforward configuration. The system discussed in the next chapter adds to the expert system the ability to reprocess data if discrepancies are found to exist at the output of any signal interpretation block. The concept of discrepancy analysis is discussed in the next chapter.

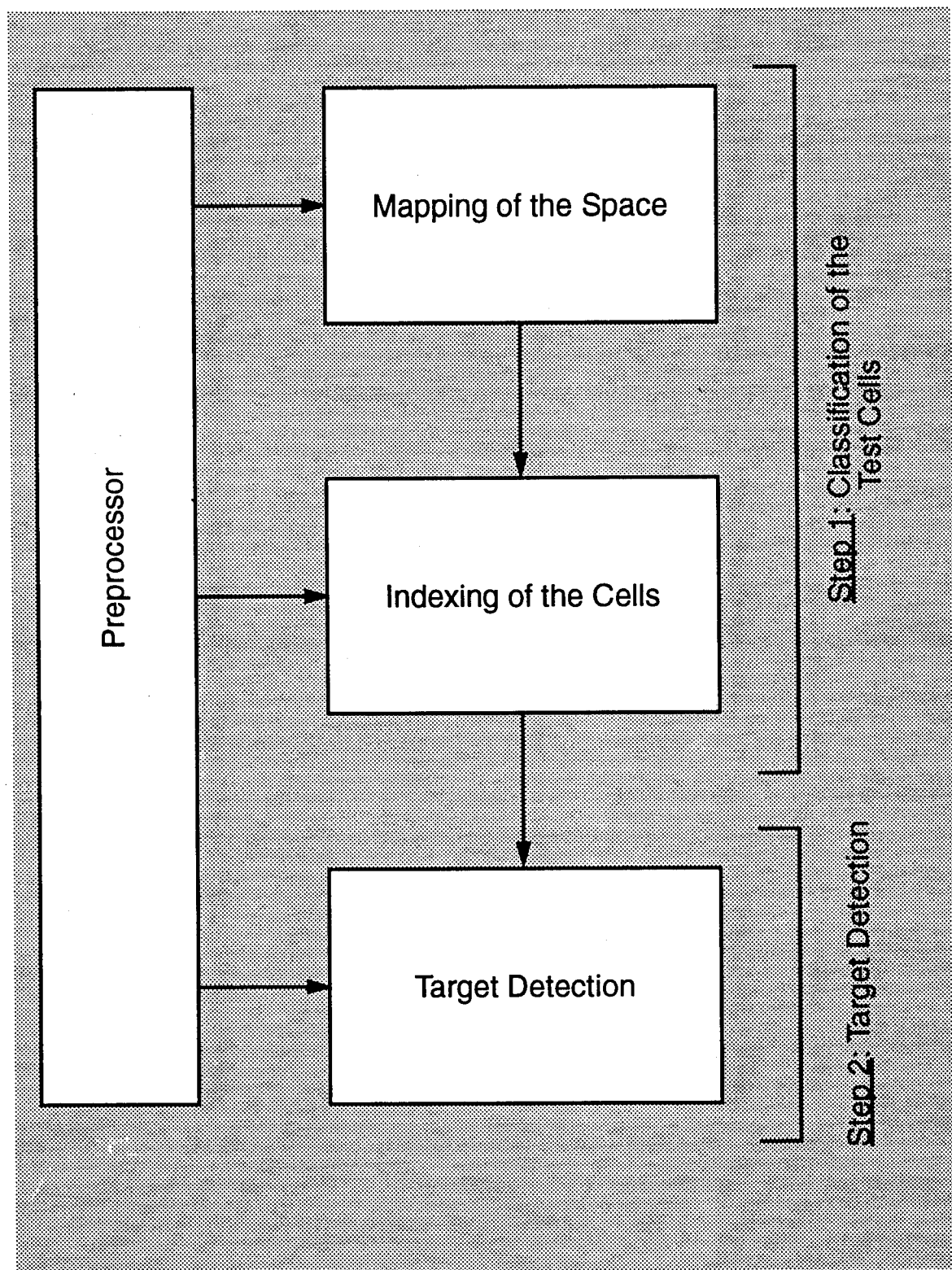


Figure II.3.1 - Signal Understanding and Detection Using a Feed Forward Expert System (SUD/FFES)

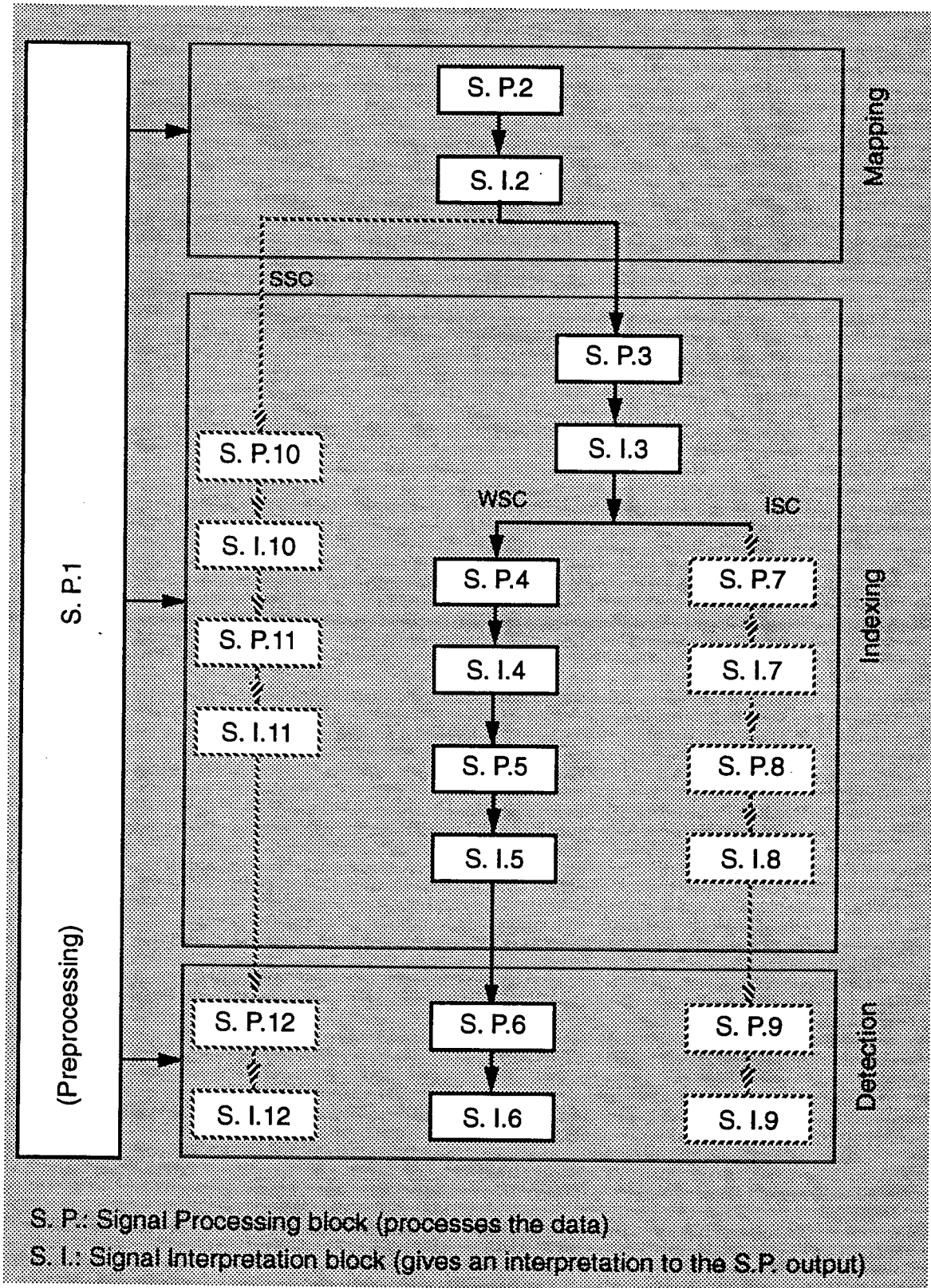


Figure II.3.2 - Signal Processing and Interpretation Blocks in a SUD/FFES

<i>Preprocessing</i>							
S. P. 1	<ul style="list-style-type: none"> <li>✓ Collects data.</li> <li>✓ Performs space-time processing for each range ring to produce a two-dimensional spectrum describing angle of arrival and Doppler frequency information.</li> </ul>						
<i>Mapping</i>							
S. P. 2	<ul style="list-style-type: none"> <li>✓ Uses spectral analysis and rank ordering or a thresholding technique to distinguish between clutter and background noise.</li> </ul>						
S. I. 2	<ul style="list-style-type: none"> <li>✓ Declares cells as BN (therefore SSC) or CL cells.</li> </ul>						
<i>Indexing</i>							
<b>SSC</b>	<p>S. P. 3</p> <ul style="list-style-type: none"> <li>✓ Uses rank ordering or thresholding technique to distinguish between WSC and ISC</li> </ul> <p>S. I. 3</p> <ul style="list-style-type: none"> <li>✓ Declares cells as WSC or ISC</li> </ul>						
	<table border="1" style="width: 100%; border-collapse: collapse;"> <thead> <tr> <th style="width: 50%;">WSC</th><th style="width: 50%;">ISC</th></tr> </thead> <tbody> <tr> <td>S. P. 10</td><td> <p>S. P. 4</p> <ul style="list-style-type: none"> <li>✓ For a given test cell assigns a homogeneous distance procedure to every pair of cells within a specified region of the space.</li> </ul> <p>S. I. 10</p> <ul style="list-style-type: none"> <li>✓ Chooses reference cells for the test cell based upon no. of reference cells required and the homogeneous distance procedure.</li> </ul> </td></tr> <tr> <td></td><td> <p>S. P. 7</p> <ul style="list-style-type: none"> <li>✓ For a given test cell assigns a homogeneous distance procedure to every pair of cells within a specified region of the space.</li> </ul> <p>S. I. 7</p> <ul style="list-style-type: none"> <li>✓ Chooses reference cells for the test cell based upon no. of reference cells required and the homogeneous distance procedure.</li> </ul> </td></tr> </tbody> </table>	WSC	ISC	S. P. 10	<p>S. P. 4</p> <ul style="list-style-type: none"> <li>✓ For a given test cell assigns a homogeneous distance procedure to every pair of cells within a specified region of the space.</li> </ul> <p>S. I. 10</p> <ul style="list-style-type: none"> <li>✓ Chooses reference cells for the test cell based upon no. of reference cells required and the homogeneous distance procedure.</li> </ul>		<p>S. P. 7</p> <ul style="list-style-type: none"> <li>✓ For a given test cell assigns a homogeneous distance procedure to every pair of cells within a specified region of the space.</li> </ul> <p>S. I. 7</p> <ul style="list-style-type: none"> <li>✓ Chooses reference cells for the test cell based upon no. of reference cells required and the homogeneous distance procedure.</li> </ul>
WSC	ISC						
S. P. 10	<p>S. P. 4</p> <ul style="list-style-type: none"> <li>✓ For a given test cell assigns a homogeneous distance procedure to every pair of cells within a specified region of the space.</li> </ul> <p>S. I. 10</p> <ul style="list-style-type: none"> <li>✓ Chooses reference cells for the test cell based upon no. of reference cells required and the homogeneous distance procedure.</li> </ul>						
	<p>S. P. 7</p> <ul style="list-style-type: none"> <li>✓ For a given test cell assigns a homogeneous distance procedure to every pair of cells within a specified region of the space.</li> </ul> <p>S. I. 7</p> <ul style="list-style-type: none"> <li>✓ Chooses reference cells for the test cell based upon no. of reference cells required and the homogeneous distance procedure.</li> </ul>						

Table II.3.1 - Caption to Appear in the Next Page

S. P. 11	S. P. 5	S. P. 8
✓ Estimates for each test cell the variance needed to determine threshold.	✓ Uses Ozturk's algorithm to determine the PDF (s) of the reference cells and the associated parameters (e.g. scale, location, shape, variance....).	✓ Estimates signal covariance matrix of the test cell using data from the reference cells.
S. I. 11	S. I. 5	S. I. 8
✓ Declares the cells from the clear region as SSC, stores the value of the variance for each cell (assuming white Gaussian background noise).	✓ Assigns one or more PDF (s) and their parameters to the test cell.	✓ Models data as having a jointly Gaussian PDF.
<i>Target Detection (SSC)</i>	<i>Target Detection (WSC)</i>	<i>Target Detection (ISC)</i>
S. P. 12	S. P. 6	S. P. 9
✓ Computes threshold and processes data from test cell using conventional radar (LRT).	✓ Computes threshold, processes data using one or more LODs, and fuses the results.	✓ Computes threshold and processes data using GLRT.
S. I. 12	S. I. 6	S. I. 9
✓ Target present or absent.	✓ Target present or absent.	✓ Target present or absent.

Table II.3.1 - Functioning of the Signal Processing and Interpretation Blocks in a SUD/FFES

## Chapter III

### Signal Understanding and Detection Using a Feedback Expert System (SUD/FBES)

#### III.1 - Introduction

To convert the feedforward system of the previous chapter to a feedback system, feedback is introduced within each block and to each previous block. This is shown in Figs. III.1.1 and III.1.2. We refer to such a system as signal understanding and detection using a feedback expert system (SUD/FBES). The expert system analyzes the output of each block and makes an assessment as to whether correct signal processing and understanding have taken place. The signal interpretation blocks of the feedforward system are augmented to carry out this task. Depending upon the assessment made, additional data and signal processing may be carried out.

The assessment procedure is indicated in Fig. III.1.1. by a block in the shape of a diamond which has one input and two outputs. The diamond input corresponds to the output of the block to be evaluated. If correct signal processing and understanding is believed to have taken place, the block under evaluation is allowed to communicate with the next block directly through the normal feedforward channel. Otherwise, additional data and signal processing are carried out under supervision of the expert system.

The feedback expert system to be used in this study is called IPUS [20] (Integrated Processing and Understanding of Signals). It is presently under development by V. Lesser and H. Nawab [21] and was successfully applied to a sound understanding problem [22]. In this study it is proposed to apply the IPUS expert system to the radar weak signal detection problem. In the following sections the theory of IPUS is introduced and examples for application of IPUS to the radar weak signal detection problem are discussed.

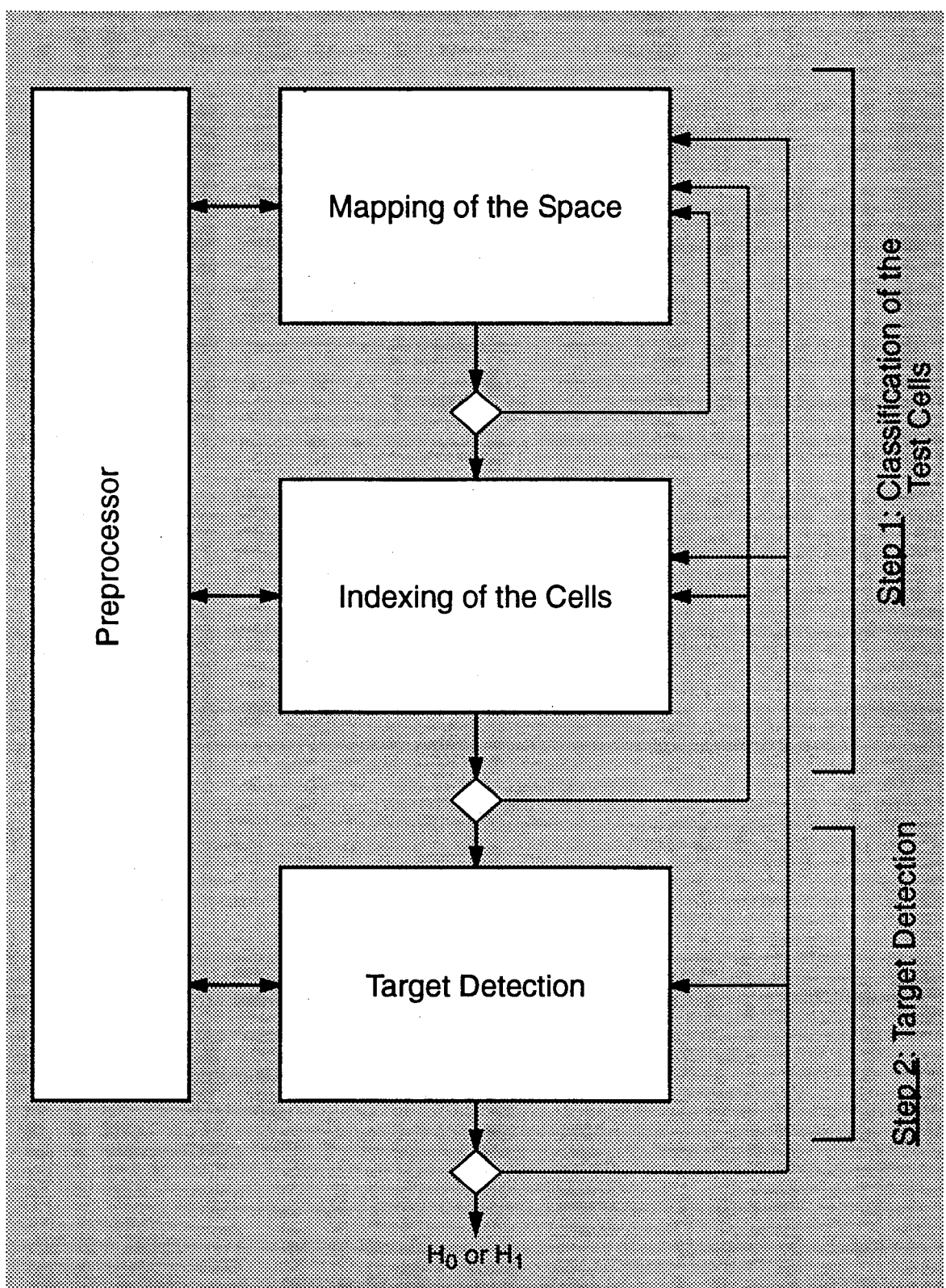


Figure III.1.1 - Signal Understanding and Detection Using a Feed Back Expert System (SUD/FBES)

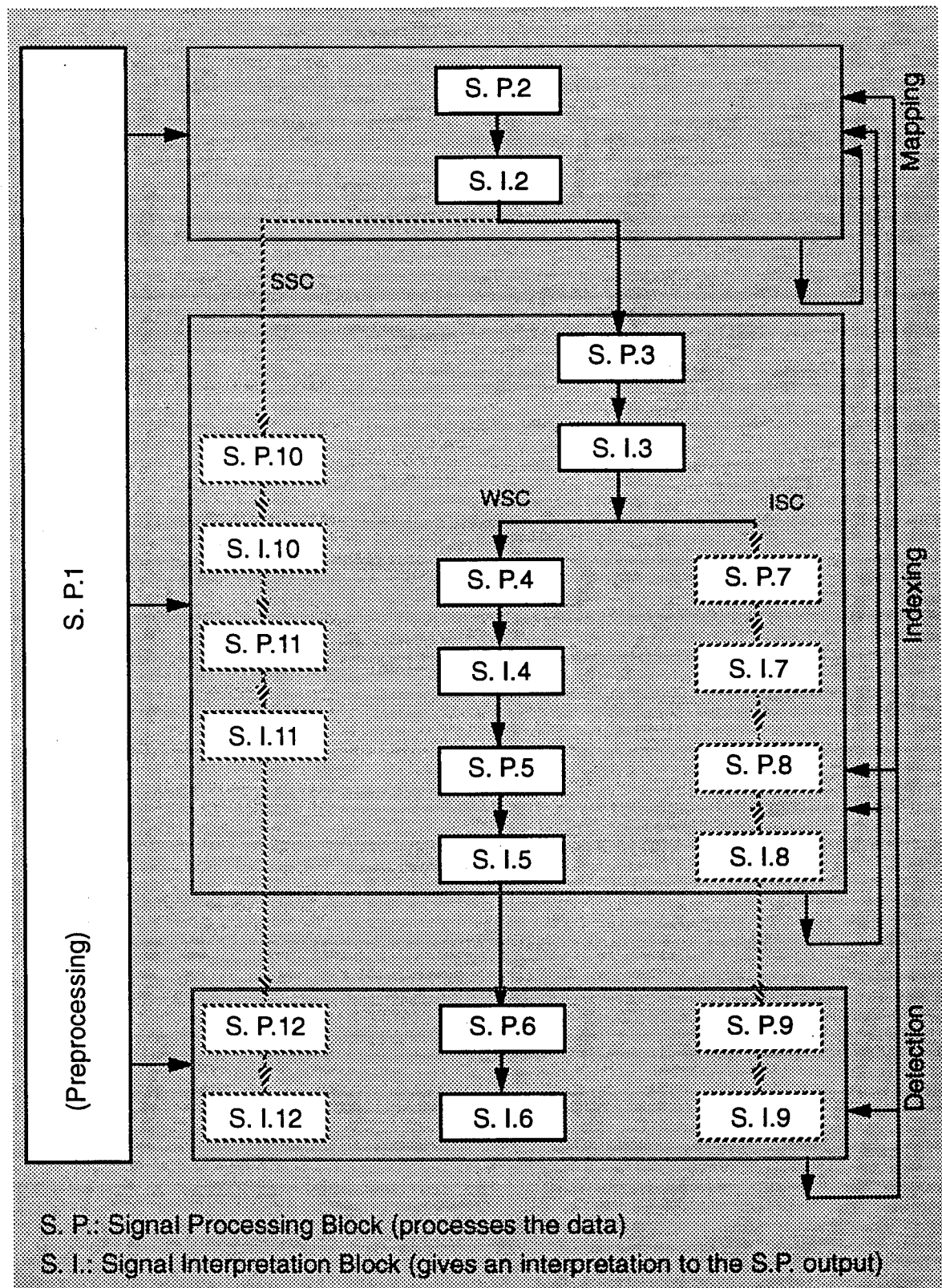


Figure III.1.2 - Signal Processing and Interpretation Blocks in a SUD/FBES

### **III.2 - IPUS Architecture [21]**

#### **III.2.1 - Introduction**

The IPUS architecture has evolved from research on the design of a sound understanding system [22]. The goal of such a system is to identify the origins of various sound sources (such as telephones, vacuum cleaners, crying infants, etc.). The complexity of the sound understanding problem arises because of two factors:

- a - The need to process a tremendous variety of signal types due to the situation dependent nature of the input. For example, not only may the input of a sound understanding system include different types of signals, such as narrow-band, impulsive, and harmonic signals, but may also include various combinations of these signals.
- b - The need to change processing goals in a context dependent way. For example, the goal of a signal understanding system might be to respond to either the sounds of an infant or a ringing telephone and to ignore other sound sources. If an infant sound is detected, the system would then ignore the telephone and would switch its main goal to determining whether the infant is laughing, crying or choking.

These two factors also arise in the radar detection problem. Specifically, complexity is encountered because of:

- a - The need to process a tremendous variety of signal types due to the situation dependent nature of the input. For example, the PDFs of the random received signals may be Gaussian, Weibull, K-distributed, etc., with various values for the scale, location, and shape parameters.
- b - The need to change processing goals in a context dependent

way. For example, the usual operational mode of a radar involves the processing of returns from clear regions which consist of strong signals embedded in a weak Gaussian background noise. If a return from a clutter region is determined, it must be decided whether either the intermediate or weak signal case exists. If the weak signal case is applicable, one or more LODs need to be selected.

In discussing the IPUS expert system, concepts are illustrated with examples taken from the radar detection problem.

In the radar detection problem considered in this research, it is assumed that the signal environment is unknown *a priori* even though mathematical models for various signals that can arise are assumed to be known. Once the environment has been determined, application of the appropriate signal detection algorithm (e.g., Gaussian receiver, LODs, GLRT) is straightforward. The difficult problem addressed by the IPUS architecture deals with the use of measured data to identify suitable mathematical models for approximating the various signals received from the unknown environment.

The algorithms employed in the IPUS architecture to identify the mathematical models for approximating the received signals are referred to as signal processing algorithms (SPA's).

Because of the two factors mentioned previously, it is very difficult, or even impossible, to design a single mathematically derived signal processing algorithm that can be applied to all possible input signals to produce the desired information for each input. To deal with such complexities, the approach taken in the IPUS architecture is for the signal understanding system to have access to a "data-base" of mathematically derived algorithms. For the radar detection problem, examples are the mean estimation algorithm, covariance matrix estimation algorithm, goodness of fit test algorithm, and the PDF approximation algorithm. This data base is indexed by the type of assumptions made about the input signal and the type of

output information desired in accordance with the current goals of the signal understanding system.

For example, it may be assumed that the input signal is Gaussian. A goodness of fit test algorithm would be applied to determine whether the data is statistically consistent with the Gaussian assumption. If the Gaussian assumption is not rejected, then the desired output information would be the sample mean vector and sample covariance matrix of the data.

The IPUS architecture utilizes the fact that signal processing theories often supply a system designer with a signal processing algorithm that has adjustable control parameters (sampling period of data samples, number and location of reference cells, etc.) SPA denotes a data base of SPA "instances", each instance corresponding to a particular set of fixed values for the control parameters. The IPUS architecture is designed to search for appropriate SPA instances to be utilized in particular situations in order to accurately model the unknown environment.

Two basic approaches for carrying out the signal processing are:

- a- Process the incoming signal with all the SPA-instances that are potentially relevant to the entire class of possible input signals in the application domain and then choose the output data that has the most consistent interpretation. This approach requires vast amounts of signal-processing output data to be examined by the higher level interpretation processes.
- b- Process the incoming signal with one or a small number of the possibly relevant SPA instances, then use some mechanism to recognize if incorrect processing has taken place. This is followed by determining the nature of the incorrect processing through a diagnostic reasoning process, and finally changing the parameter settings of the SPA with the aim of obtaining an SPA-instance which is

appropriate for the processing of the input signal. The SPA-instance with adjusted control parameter settings is then used to reprocess the input signal.

In order to select appropriate values for the SPA control parameters, the system must consider the current system goals as well as knowledge about certain characteristics of the particular input signal. This leads to the dilemma that choosing the appropriate control parameter values requires knowledge about the signal, but this knowledge can only be obtained by first processing the signal with an algorithm with appropriate control parameter setting. The IPUS architecture uses an iterative technique for converging to the appropriate control parameter values. The technique begins by using the best available guess for the SPA control parameters values. The SPA instance output is then analyzed through a discrepancy detection mechanism for indicating the presence of distorted SPA output data. A diagnosis is then performed for mapping the detected discrepancies to distortion hypotheses. A signal reprocessing phase then proposes a new set of values for the control parameters of the SPA with the aim of eliminating the hypothesized distortions. The SPA instance corresponding to the new control parameter values is then used to reprocess the input signal. The output from the reprocessing once again undergoes discrepancy detection and if necessary is followed by diagnosis, signal reprocessing planning, and further reprocessing of the input signal.

The signal data and the interpretation hypotheses derived from that data are stored on a blackboard with hierarchically organized information levels. The hypotheses on the blackboard fall into two basic categories: hypotheses posted to explain the signal data and hypotheses posted to specify expectations about the nature of the signal data. The inferencing on the blackboard is performed by different knowledge sources (KS's) for tasks such as discrepancy detection, diagnosis and reprocessing, and data interpretation. These tasks are presented in the

following sections.

### **III.2.2 - Discrepancy Detection**

Ideally, application of an SPA instance to input data results in undistorted output data. However, if the control parameters of the SPA instance are not appropriately chosen, distorted output data may result. The key to discrepancy detection is the ability to recognize and classify discrepancies due to distortion introduced by the SPA instance. Three types of discrepancies are possible:

1 - The first type of discrepancy is referred to as a violation. A violation occurs when the SPA output data implies the presence of a signal that is not a member of the allowable class of input signals. For example, disturbances arising from cells in the clear region are always modeled in this work as Gaussian processes because of the expectation that background noise is Gaussian. Suppose that the output data from an SPA instance implies that the disturbance from a cell in the clear region is non-Gaussian. This constitutes a violation type of discrepancy.

2 - The second type of discrepancy is referred to as a conflict. A conflict occurs when the current SPA output data is inconsistent with expectations arising from interpretations of past data. There are two types of conflicts depending on whether all, or only a portion, of the current SPA output data is inconsistent. For an example of the first type of conflict, suppose previous SPA output data arose from disturbances in the clear region while current SPA output data is arising from disturbances in a clutter patch. A conflict of the first type occurs if all of the current SPA output data, such as an increase in variance and non-Gaussianity of the data, conflict with previous interpretations from the clear region. For an example of the second type of conflict, suppose that previous SPA output data has resulted in the interpretation that the disturbance is from the clear region. This might be implied by the SPA output data indicating Gaussian statistics, zero mean, and a variance level in the range of the background noise. A conflict of the second type occurs when, even though Gaussian statistics are confirmed by the current SPA

output data, they also reveal that the mean is no longer zero and the variance level has increased significantly. This could happen if the disturbance is now coming from a Gaussian clutter patch where the data is highly correlated.

3 - The third type of discrepancy is referred to as a fault. A fault can also arise in two different ways. The first kind occurs when two or more different SPA's that are applied to the same data result in different output interpretations. The other kind occurs when two or more instances of a single SPA (i.e., the same SPA with different parameter values) result in different interpretations when applied to the same data. An example of the first kind of fault would be the situation where SPA # 1, a power level detector, indicates a power level consistent with the background noise while SPA # 2, Ozturk's distribution identification algorithm, indicates a non-Gaussian distribution. This is a fault because the background noise is assumed to be Gaussian. An example of the second kind of fault would be the situation where use of Ozturk's algorithm based on 50 and 100 samples from the same clutter patch results in a different interpretation.

### **III.2.3 - Diagnosis and Reprocessing**

When the signal being monitored does not satisfy the requirements of the SPA instance, the output of the SPA is distorted resulting in a discrepancy. Once a discrepancy has been detected, a diagnosis procedure is used to identify the distortion that may have led to the discrepancy. Knowing the distortion, then either the appropriate parameters of the same SPA can be adjusted or a different SPA chosen to reprocess the data. In a sense, the diagnosis procedure maps symptoms (discrepancies) to hypothesized underlying causes (distortions). For example, assume the sample mean of a clutter patch is repeatedly being evaluated by processing 50 samples at a time. Although, the first eight trials result in values close to zero, the ninth trial produces a large negative value for the mean. This represents a conflict of the first kind. The diagnosis procedure may surmise that the conflict may be due to the presence of one or more outliers. Consequently, the

reprocessing procedure concludes that the data from the ninth trial should be re-processed after removal of the outliers.

### **III.2.4 - Interpretation Process**

The interpretation process is a search through a space of sets of interpretation models for modeling signals. When a possible combinatorial explosion in interpretation models does not exist, the interpretation process may be viewed as just a straight forward classification process. Otherwise, the search must be carried out as a constructive problem solving process. The IPUS architecture employs the constructive problem solving approach which reduces to the classification approach in the absence of a combinatorial explosion.

Constructive problem solving techniques must be used when the set of possible solutions is too large to be enumerated. For example, although the set of PDF types is finite in the radar problem, there are an infinity of different PDF's possible because of the infinite number of values that can be assumed by the scale, location, and shape parameters. Consequently, constructive problem solving is needed to approximate the underlying probability distribution of the data.

### **III.2.5 - Sources of Uncertainty (SOUs) and RESUN**

At any stage in monitoring the environment, one can never be totally sure that various interpretations are correct. Sources of uncertainty (SOU) always exist with regard to whether the data was processed correctly and with regard to how much confidence should be placed in the interpretation. The objective of IPUS is to continue to reprocess data, as time permits, so as to reduce the SOUs. This reprocessing is continued until either the level of uncertainty has been reduced to some acceptable level or until all the time allotted for reprocessing has been utilized.

The process of reducing the SOUs can be viewed as a problem solving activity. At each stage of the IPUS architecture, it is necessary to identify the SOUs

associated with a particular output and to have a strategy for reprocessing the data so as to reduce the SOUs associated with a particular output in an efficient manner. The Resolving Sources of Uncertainty (RESUN) control [21] structure is used to direct the problem-solving procedure used to gather evidence in order to resolve particular SOUs in the interpretation hypotheses.

In this section we discuss the relationship between the mechanism in IPUS and the concept of SOUs utilized by the RESUN control structure. The basis for this relationship is largely empirical and is continually evolving. The current view of this relationship is described below:

### **1 - Violation-Type Discrepancies and SOUs**

A violation type discrepancy occurs when signal processing output data violates the a priori known characteristics of the entire class of possible input signals for the radar problem. For example, background noise is assumed to have zero mean. Assume that a signal has been interpreted as white and Gaussian and has a very small power level. In addition, the mean has been interpreted as being non-zero. Because of the non-zero mean, the signal cannot be classified as background noise. Also, because of the small power level, the signal cannot be classified as clutter. Clearly, a violation exists. The condition that has been violated is the zero-mean condition. There are various SOUs that could have caused this violation. For example,

- 1)** there could have been one or more outliers in the data,
- 2)** there may not have been an adequate number of samples processed,
- 3)** the random samples may not have been representative of the zero-mean signal,
- 4)** a desired target return could be contained in one or more of the reference cells.

For each of the above SOUs, respectively, one or more procedures exist for their

reduction. For example,

- 1) extreme values could be excised from the data,
- 2) the number of samples processed could be increased,
- 3) an entire set of new samples could be processed,
- 4) previously detected targets could be checked to determine whether one or more targets are likely to be present in one or more of the reference cells. If so, these cells should be eliminated as reference cells for the test cell of interest.

When a violation-type discrepancy is noted, the hypothesis that a violation exists is posted on the interpretation blackboard of the expert system. For each condition being violated and each SOU that could have caused the violation, an additional output data hypothesis is posted which describes the condition being violated and the SOU that could have caused the violation. SOUs that fail to produce some particular support evidence for a single input signal or fail to result in any valid explanation for a combination of input signals are classified as negative evidence SOUs. The hypothesis concerning the violation-type discrepancy and each of the additional hypotheses are then connected by a negative evidence link and are labeled **VIOLATION-NEGATIVE EVIDENCE SOU**. Further problem solving to reduce the SOU can then be carried out by reprocessing the underlying signal with different SPA instances.

## **2 - Conflict-type Discrepancies and SOUs**

After processing a certain quantity of data, various expectations relative to the data to be processed arise. Conflicts occur when these expectations are not met. If all the expectations are not met, the conflict is said to be of the first kind. If some expectations are met while others are not, the conflict is said to be of the second type.

We say that an unverified expectation hypothesis exists when there is a conflict of the first type. A **NO-SUPPORT SOU** label is attached to each unverified expectation hypothesis. For each expectation (i.e., component of the hypothesis)

not being met and for each SOU that might be responsible, an additional hypothesis is posted on the interpretation blackboard which describes the unsupported expectation and the corresponding SOU. The hypothesis concerning the conflict-type discrepancy and each of the additional hypotheses are connected by a link labeled **NO-SUPPORT SOU**. Further problem solving can then attempt to find SPA instances so as to produce output data that can support the expectation.

When there is a conflict of the second type, a partially verified expectation hypothesis is posted on the interpretation blackboard with a **PARTIAL-EVIDENCE SOU** label. As in the previous case, each unsupported expectation (i.e, inference or hypothesis component) is associated with a hypothesis, labeled **NO-SUPPORT SOU**, which describes the unsupported expectation and the corresponding SOU. The hypothesis labeled **PARTIAL-EVIDENCE SOU** can trigger further problem solving to find support for the lower component hypotheses labeled **NO-SUPPORT SOU**.

By way of example, assume that the previous ten test cells were classified as having been in the clear. Our expectation hypothesis, therefore, is that the eleventh test cell will also be in the clear. If the eleventh test cell fails the Gaussian, zero-mean, and small power level inferences, we have a conflict of the first type. On the other hand, if the Gaussian and zero-mean inferences are found to have support while the small power level inference is unsupported, we have a conflict of the second type. As discussed above, SOUs and corresponding linked hypotheses would be identified with each unsupported inference and additional signal processing would be carried out to reduce the level of SOUs as time permits.

### **3 - Fault-type Discrepancies and SOUs**

Fault-type discrepancies arise when two different signal processing algorithms or instances produce different output interpretations. In such a case, a

composite hypothesis is created which is a copy of the more reliable of the two data hypothesis (i.e., the two output interpretations). A link labeled with a **NEGATIVE-EVIDENCE SOU** connects the less reliable hypothesis to the composite hypothesis. Further problem solving attempts to remove the negative-evidence SOU by reprocessing the signal using different SPA instances for the less reliable SPA. Two outcomes are then possible. Either the negative evidence SOU is eliminated or it is replaced by another negative-evidence SOU. In the latter case, further problem solving can attempt to reprocess the signal with the more reliable SPA but using different SPA instances.

By way of example, assume that a zero-mean inference is to be supported by both a sample-mean algorithm and a median detector algorithm. Assume that only a small number of data samples are available. Under this assumption, the median detector algorithm is likely to be more reliable. Suppose that the median detector algorithm supports the zero-mean inference while the sample mean algorithm does not. RESUN creates the composite hypothesis that the mean is zero. To this the hypothesis that the mean is not zero is linked using a **NEGATIVE-EVIDENCE OUTLIER** label. The data samples are then reprocessed by the sample mean algorithm by using SPA instances which delete some of the extreme data values. If the zero-mean inference is supported, the negative evidence SOU is assumed to have been eliminated. If the zero-mean inference is not supported, the signal is reprocessed by the median detector algorithm where different sets of outliers may be chosen.

### **III.3 - Application of IPUS to Radar Signal Understanding**

The IPUS architecture is suitable when a single SPA-instance cannot correctly process all the input signals that can potentially arise in a signal understanding application. In the radar problem, the variety of probability distributions underlying the data along with the different tasks to be carried out in monitoring the environment (clutter mapping and cell indexing) necessitates more than one

SPA-instance. Hence, IPUS is suitable for the radar problem.

In this research we emphasize the WSC. As explained previously, the branch of Fig. III.1.2 corresponding to the WSC is referred to as WSUD/FBES. From the figure, it is clear that tasks of the WSUD/FBES have been subdivided into mapping, indexing and detection. Assuming the mapping and indexing to be done properly, application of the LOD is straight forward.

## Chapter IV

### Description of the Proposed Radar Signal Processing System

#### IV.1 - Data Collection and Preprocessing

Assume that a radar transmits a periodic signal composed of a series of predefined RF pulses. Let  $T$  be the period of the signal and  $\tau_e$  denote the pulse duration.  $T$  is known as the pulse repetition interval (PRI). Assuming rectangular shaped pulses, the envelope of the emitted signal is shown in Fig. IV.1 where  $A$  denotes the pulse amplitude.

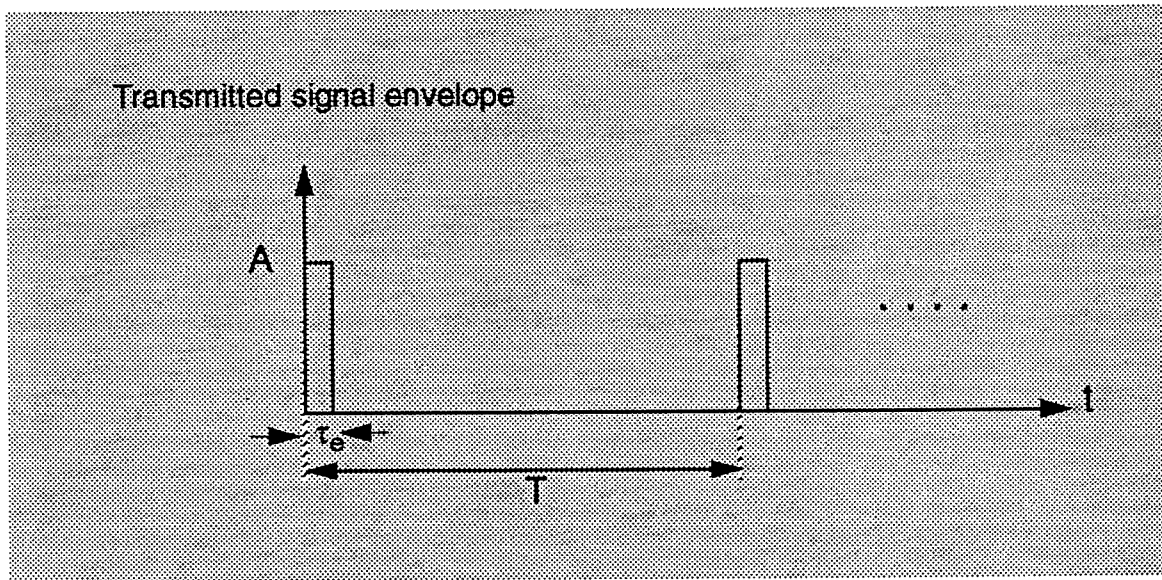


Figure IV.1.1 - Envelope of the Transmitted Signal

For ease of discussion consider a low pulse repetition frequency (PRF) radar for which there is no range ambiguity. During the time interval  $[pT+\tau_e, (p+1)T]$ , of the  $p^{\text{th}}$  PRI,  $p=1,2,3,\dots$ , the radar functions in the receive mode and collects data, due to the  $p^{\text{th}}$  pulse from the azimuth angle,  $\theta_z$ , to which the radar antenna is oriented. The collected data corresponds to returns from different range cells as illustrated in the top view of Fig. IV.1.2 where  $\Delta\theta$  denotes the antenna beam-width

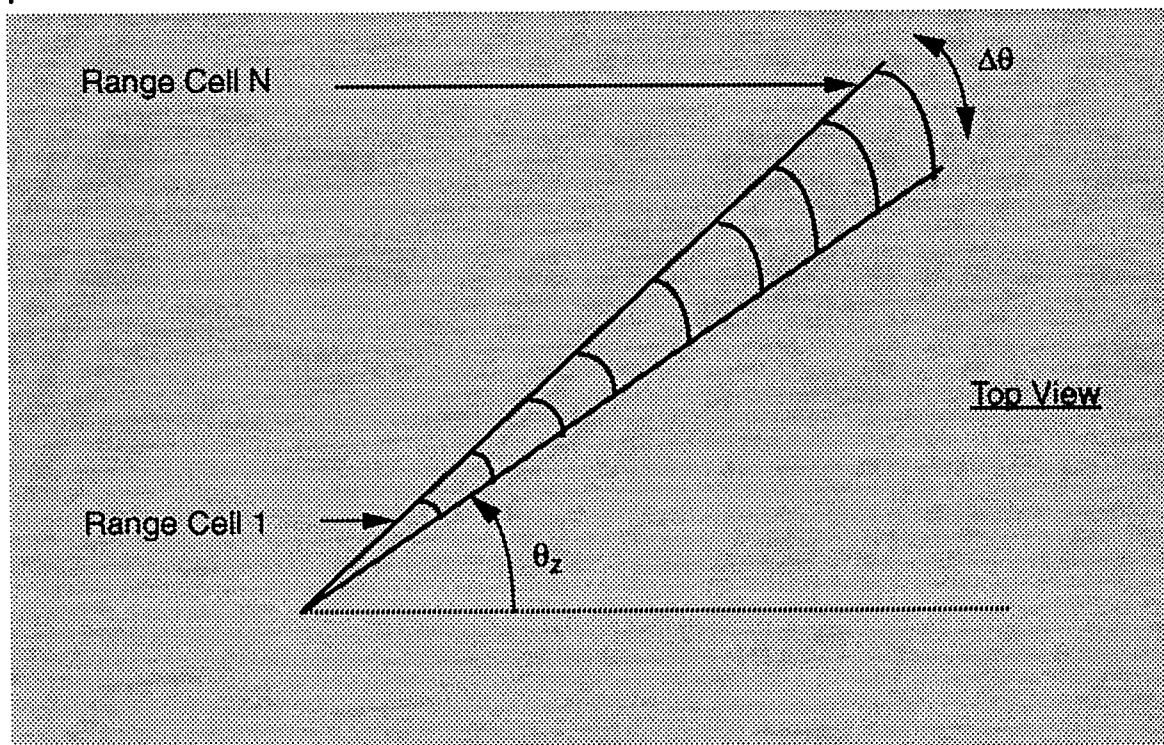


Figure IV.1.2 - Range Cells in a Constant Azimuth Beam

The round trip delay,  $t_d$ , from a given range  $R$  is given by

$$t_d = \frac{2R}{c} \quad (\text{IV-1.1})$$

where  $c$  denotes the velocity of propagation of the electromagnetic wave. For the  $p^{\text{th}}$  period of the transmitted signal, the time interval  $[pT+\tau_e, (p+1)T]$  is subdivided into  $J$  range bins of duration  $\tau_e$ . Each range bin corresponds to a range cell whose range extent is denoted by  $r_e$ . Fig. IV.1.3 shows the different range cells and their corresponding range bins on the time axis for a fixed azimuth angle  $\theta_z$ . Let  $R_k$  and  $R_{k+1}$  denote the ranges to the leading and trailing edges of the  $k^{\text{th}}$  range cell. Also, let  $t_k$  and  $t_{k+1}$  denote the corresponding round trip delay times. Then, using Eq. (IV-1.1) we can write

$$t_k = \frac{2R_k}{c} \quad \text{and} \quad t_{k+1} = \frac{2R_{k+1}}{c} \quad (\text{IV-1.2})$$

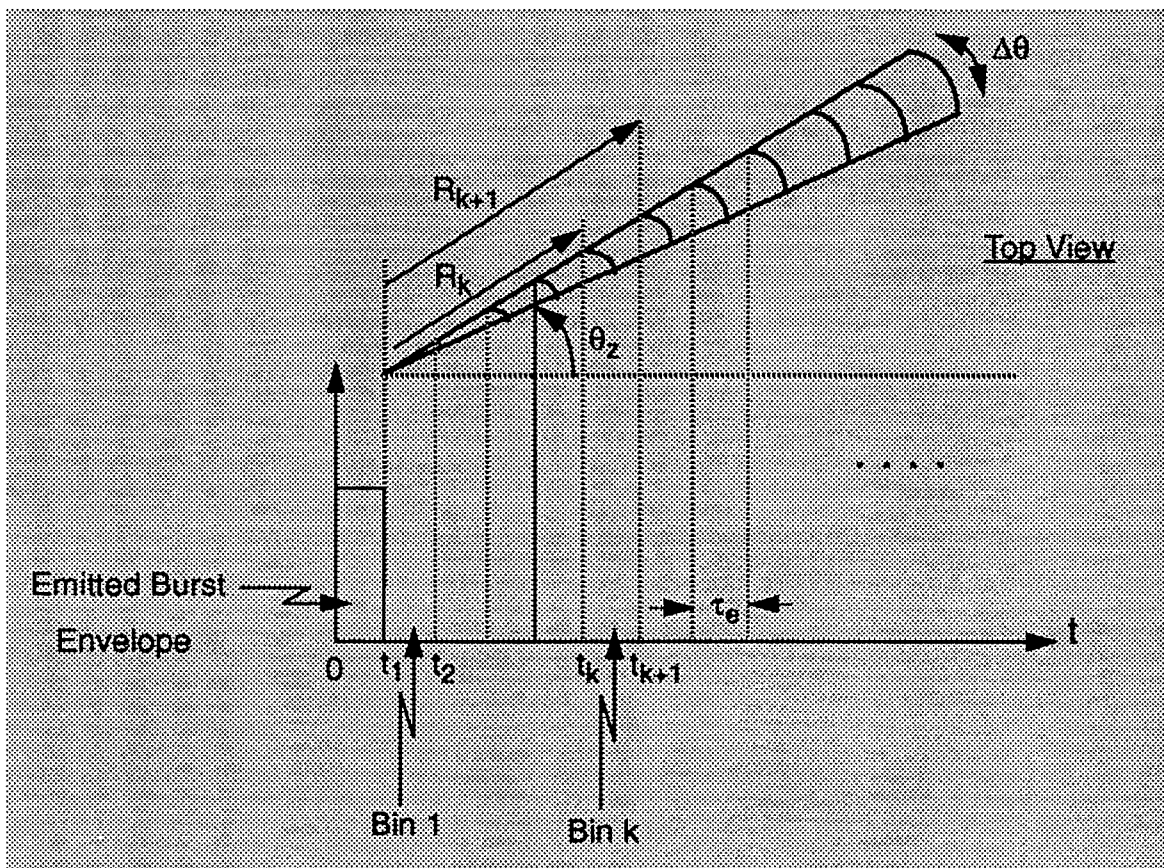


Figure IV.1.3 - Range Cells and Their Corresponding Time Bins

Taking the difference and utilizing the fact that a range bin is defined to be of time extent,  $\tau_e$ , results in

$$t_{k+1} - t_k = \tau_e = \frac{2(R_{k+1} - R_k)}{c} . \quad (\text{IV-1.3})$$

Hence, each range bin of time extent,  $\tau_e$ , corresponds to a range cell of range extent,  $r_e$ , where

$$r_e = R_{k+1} - R_k = c \frac{\tau_e}{2} . \quad (\text{IV-1.4})$$

This process is repeated for different azimuth angles,  $\theta_z$ . The collection of cells corresponding to different ranges and azimuth angles can be represented in a rectangular format, as illustrated in Fig. IV.1.4. The collection of range cells

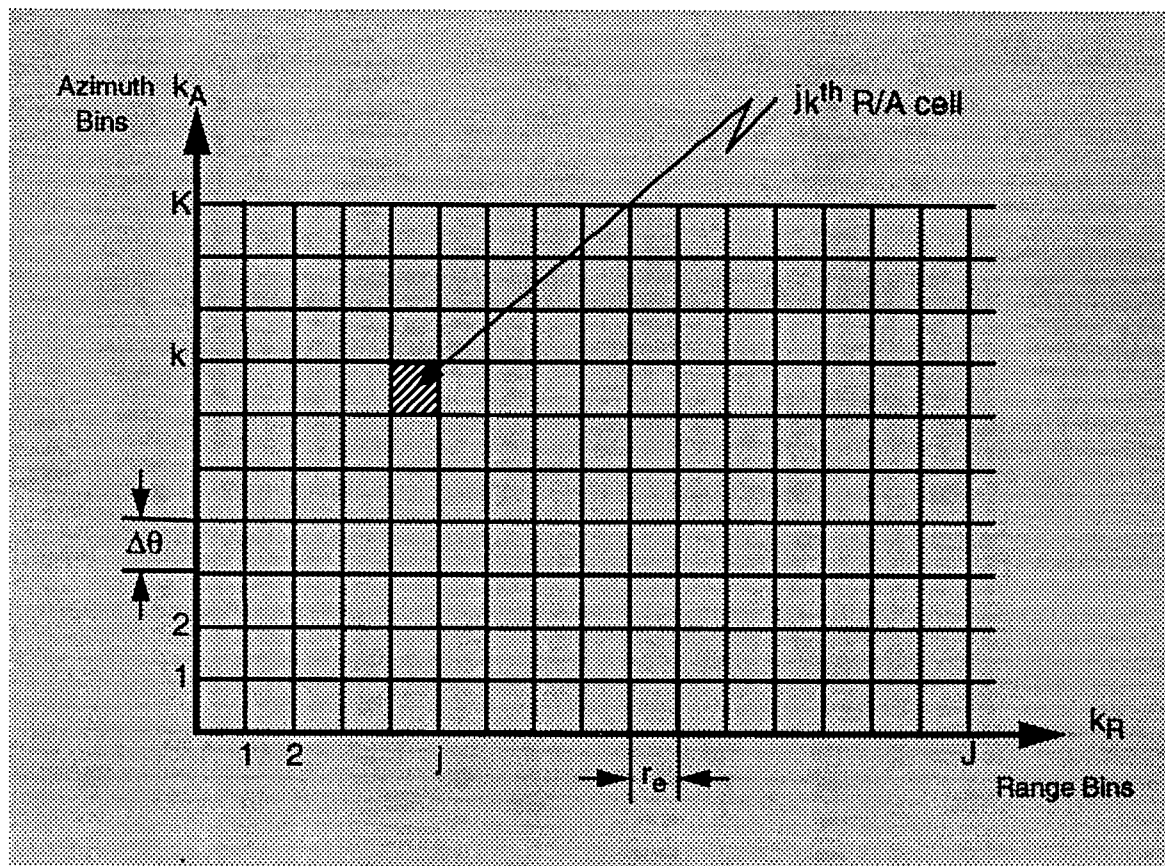


Figure IV.1.4 - Rectangular Format for Representing Cells at Different Ranges and Azimuth Angles

corresponding to a constant azimuth angle is shown in Fig. IV.1.2. For a fixed range, the collection of azimuth cells is as shown in Fig. IV.1.5. Let the range bins be indexed by  $k_R$ ,  $1 \leq k_R \leq J$ , and the azimuth bins be indexed by  $k_A$ ,  $1 \leq k_A \leq K$ . The resolution cell corresponding to  $k_R=j$  and  $k_A=k$  is referred to as the  $jk^{\text{th}}$  range-azimuth (R/A) cell, as illustrated in Fig. IV.1.4.

In practice, the antenna beam dwells on each range-azimuth cell for a time duration, known as the dwell time, that is equal to  $P$  pulse repetition intervals (PRI's). Consequently,  $P$  pulse returns from each range-azimuth cell, spaced  $T$  seconds apart, can be processed. After decomposing the  $P$  received pulses into a sequence of I and Q quadrature components, a Doppler filter bank is implemented by performing a  $M$ -point FFT on each of the  $P$  quadrature component samples

where  $M \geq P$  depending upon whether or not zero padding is used. Let  $y_{Ip}(j,k)$  and  $y_{Qp}(j,k)$ ,  $p=1,2,3,\dots,P$ , denote the I and Q components from the  $p^{\text{th}}$  PRI of the  $jk^{\text{th}}$  range-azimuth cell. Similarly, let  $Y_{Im}(j,k)$  and  $Y_{Qm}(j,k)$ ,  $m=1,2,3,\dots,M$ , denote the  $m^{\text{th}}$  FFT coefficient from the  $jk^{\text{th}}$  range-azimuth cell. In addition to computing the temporal data magnitudes,  $y_p(j,k)$ , from the I and Q quadrature components for each PRI, the magnitude of each Fourier coefficient,  $Y_m(j,k)$ , is computed, as

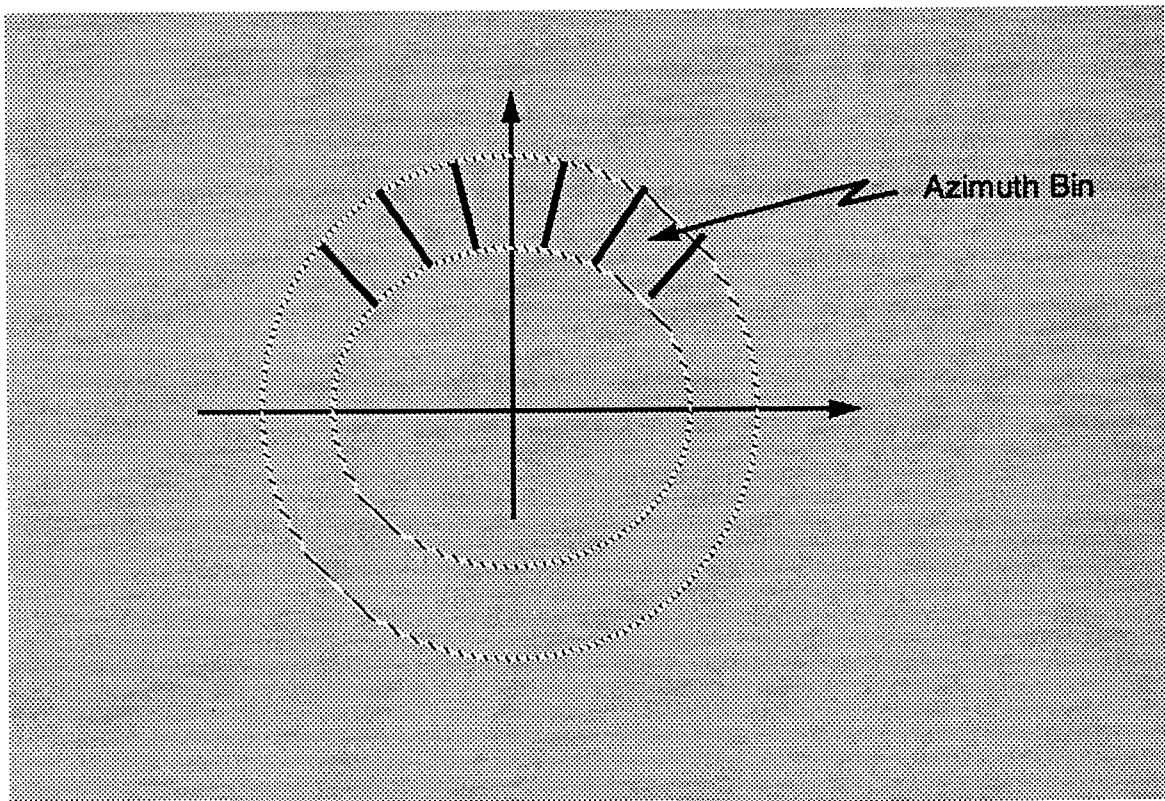
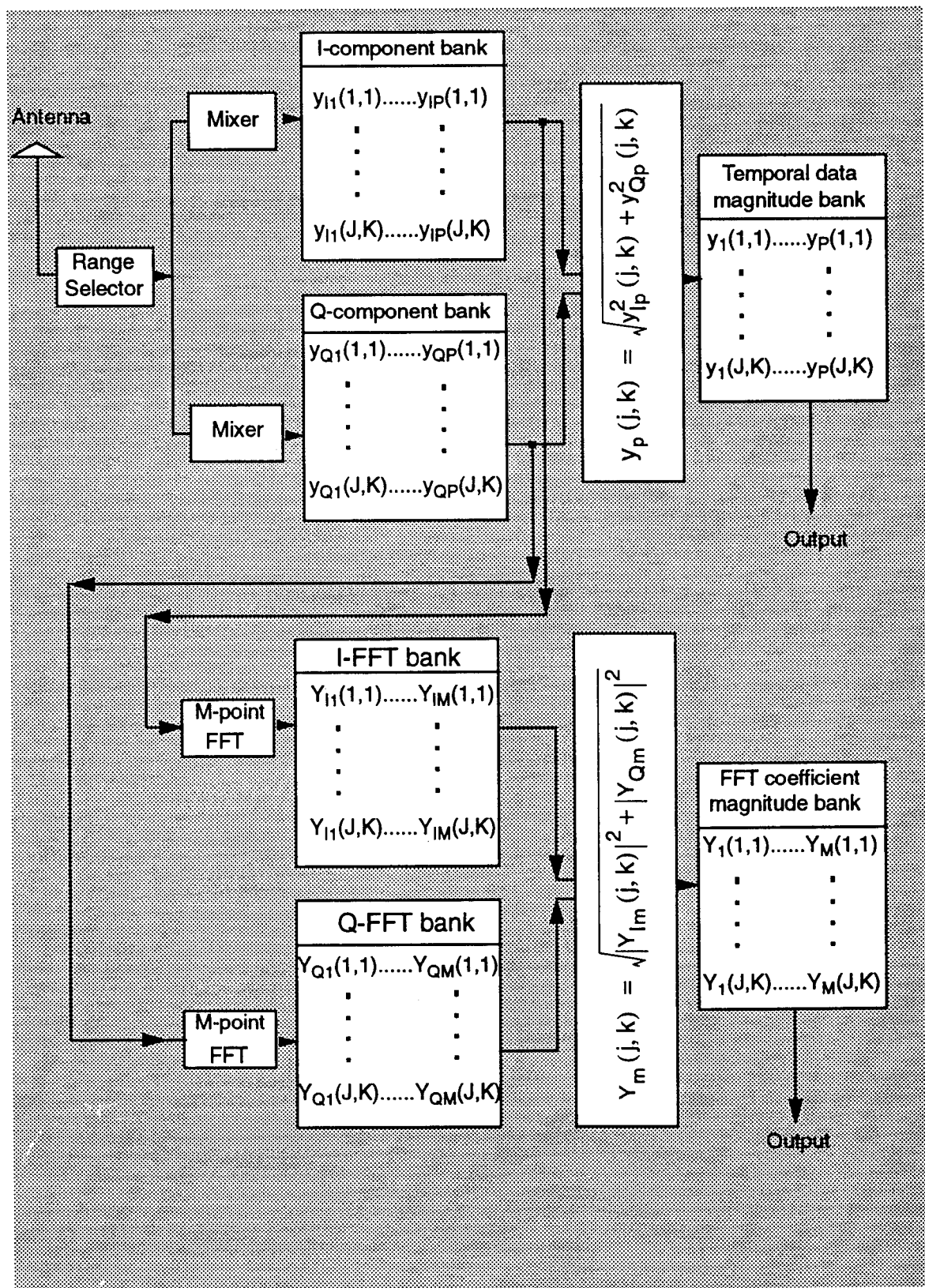


Figure IV.1.5 - Collection of Azimuth Cells for a Fixed Range

shown in Fig. IV.1.6, to form the FFT coefficient magnitudes.

The collection of cells corresponding to different ranges, azimuth angles, and Doppler frequencies can be represented in a 3-dimensional cubic format, as illustrated in Fig. IV.1.7. Let the Doppler bins be indexed by  $k_D$ ,  $1 \leq k_D \leq M$ . The resolution cell corresponding to  $k_R=j$ ,  $k_A=k$ , and  $k_D=m$  is referred to as the  $jk^{\text{th}}$  range-azimuth-Doppler (R/A/D) cell. The total number of range-azimuth-Doppler cells is given by  $J \times K \times M$ .



*Figure IV.1.6 - Block Diagram of Data Preprocessing Stage*

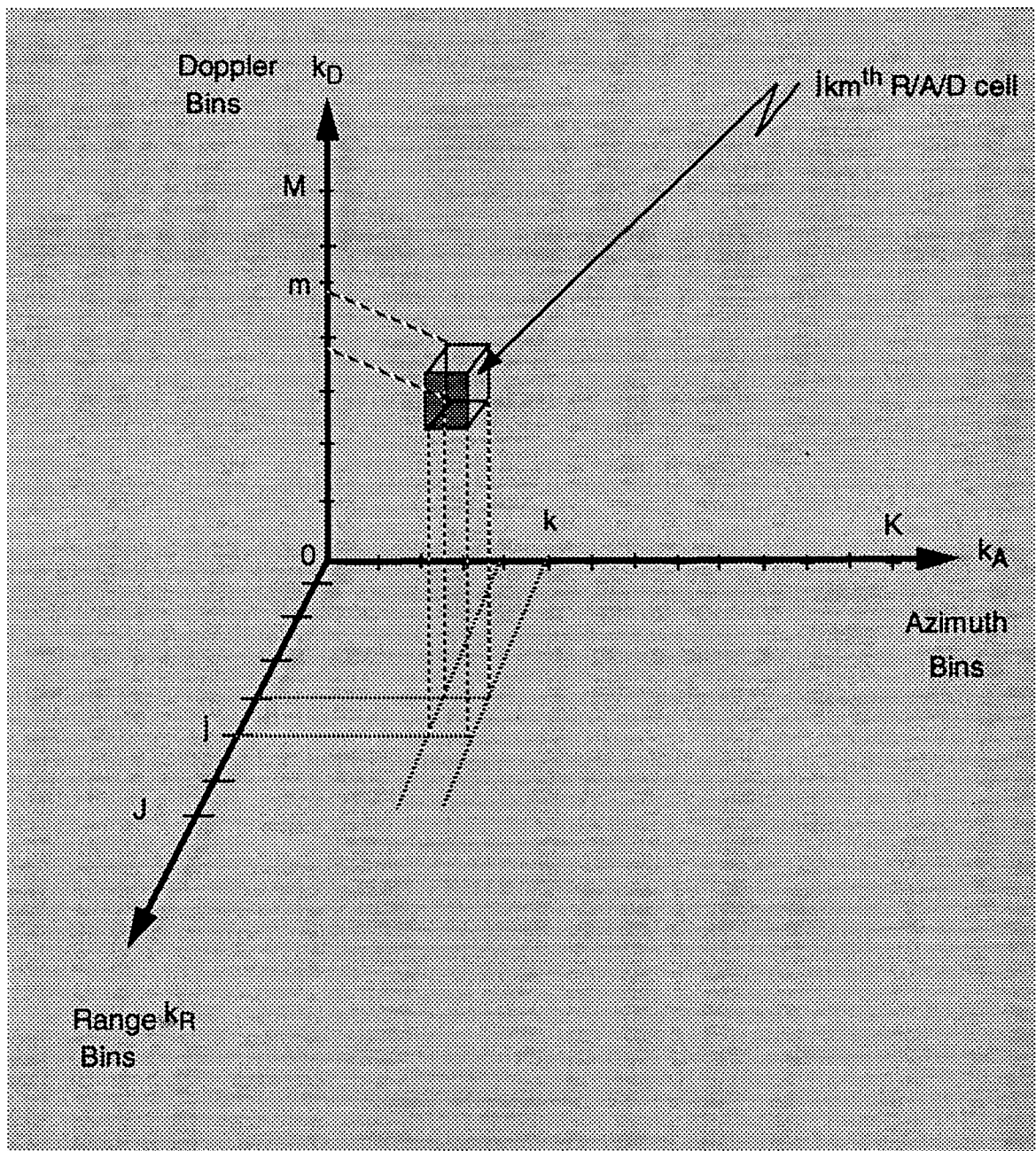


Figure IV.1.7 - Cubic Format for Representing Cells at Different Ranges, Azimuth Angles, and Doppler Frequencies.

The temporal data magnitudes and FFT coefficient magnitudes are used by the mapping processor to enable classification of the R/A/D cells into background noise cells and clutter cells. The mapping approach is described in the next section for the general radar problem.

## IV.2 - Mapping

The purpose of mapping is to declare a R/A/D cell as either a background noise cell or clutter cell. As shown in Fig. IV.1.6, two types of data are formed in the preprocessing stage. These are, temporal data magnitudes,  $y_p(j,k)$ , and FFT coefficient magnitudes,  $Y_m(j,k)$ . The set of  $y_p(j,k)$  magnitudes consists of  $P$  data points for each R/A cell in the  $J \times K$  R/A plane, while, the set of  $Y_m(j,k)$  magnitudes consists of one data point for each R/A/D cell in the  $J \times K \times M$  R/A/D space.

The mapping is done in two stages. First, using  $y_p(j,k)$ , the R/A plane is mapped into background noise (BN) and clutter (CL) R/A cells. Then, using  $Y_m(j,k)$ , the 3-dimensional R/A/D space is mapped into BN and CL R/A/D cells. The necessity for performing mapping in two stages is explained next.

In the first mapping stage, an average  $P(j,k)$  is formed for each R/A cell in the  $J \times K$  R/A plane by averaging the power of the  $P$  temporal data magnitudes,  $y_p(j,k)$  as shown in Equation (IV-2.1),

$$P(j,k) = \frac{1}{P} \sum_{p=1}^P y_p^2(j,k); \quad \begin{matrix} j=1,2,\dots,J \\ k=1,2,\dots,K \end{matrix} \quad (IV-2.1)$$

The average powers  $P(j,k)$  are used to classify BN and CL cells in the R/A plane, as is discussed in the next chapter.

The second stage involves the 3-dimensional R/A/D space. In particular, each cell in the R/A/D space needs to be classified as either BN or CL. The classification performed in the first mapping stage is useful in reducing the effort required in the second stage. If the  $jk^{\text{th}}$  R/A cell is BN, then all of the  $jk m$  Doppler cells,  $m=1,2,\dots,M$ , will also be BN. However, if the  $jk^{\text{th}}$  R/A cell is CL, then the  $jk m$  Doppler cells,  $m=1,2,\dots,M$ , may or may not be CL depending upon the clutter spectrum. Consequently, only the Doppler cells corresponding to R/A cells that have been identified as CL in the first mapping stage need to be examined in the second stage. This reduces considerably the amount of processing needed for

the second mapping stage.

Notice that two-way communications is required between the preprocessing and mapping stages. As shown in Fig. IV.2.1, the preprocessing stage generates the quadrature components, the FFT coefficients, and their magnitudes. The first mapping stage classifies the R/A cells as either BN or CL. For those R/A cells classified as BN, the corresponding Doppler cells are also classified as BN by the second mapping stage. For those R/A cells that are classified as CL, the second mapping stage obtains the FFT coefficient magnitudes. These are then used to classify the remaining R/A/D cells as either BN or CL.

The major focus of this work is to demonstrate how the principles of IPUS can be applied to the radar problem. For that purpose, procedures and rules have been developed that utilize the IPUS capabilities to solve the various stages of the radar problem. Throughout this work the procedures and rules have been tested with non-trivial radar examples. The first procedure, presented in the next chapter, is a mapping technique that classifies cells into BN and CL.

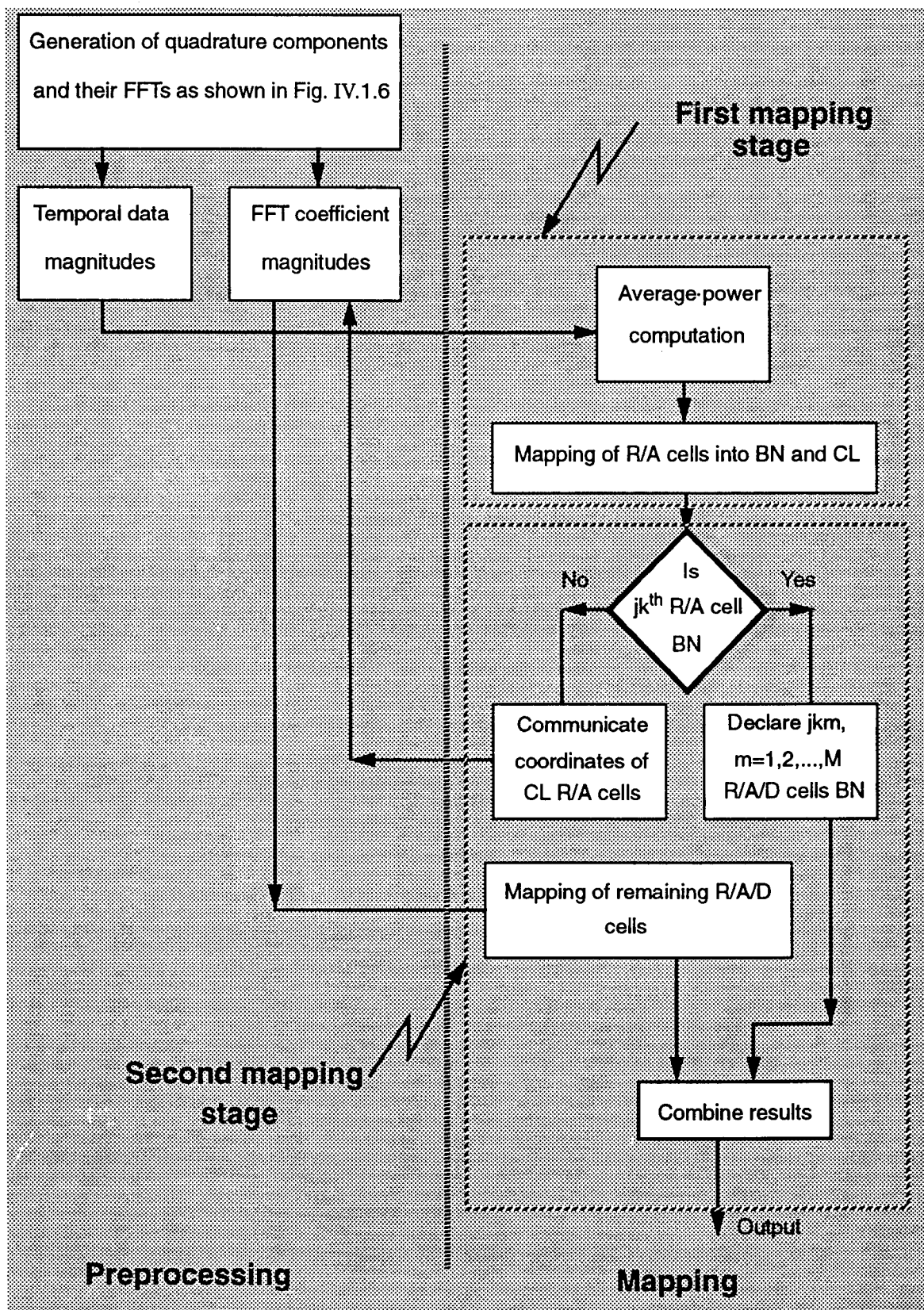


Figure IV.2.1 - Block Diagram of the Preprocessing and Mapping of Data

## Chapter V

### Mapping Procedure

In this chapter a mapping procedure for a surveillance volume subdivided into range-azimuth cells is presented along with examples. Also, extension of the mapping procedure to range-azimuth-Doppler cells is discussed in the last section. General procedures are presented without explanations of how to choose parameters. The explanations are provided in Chapter VII.

#### **V.1 - Introduction**

Assume that  $J \times K$  R/A cells are scanned by a radar antenna. Furthermore, for simplicity, assume that the dwell time is equal to the PRI so that only a single pulse is processed from each cell, i.e.  $P=1$ . In this case, an FFT is not possible and the block diagram of the preprocessing stage reduces to that shown in Fig V.1.1. When an FFT is not possible, the block diagram of the preprocessing and

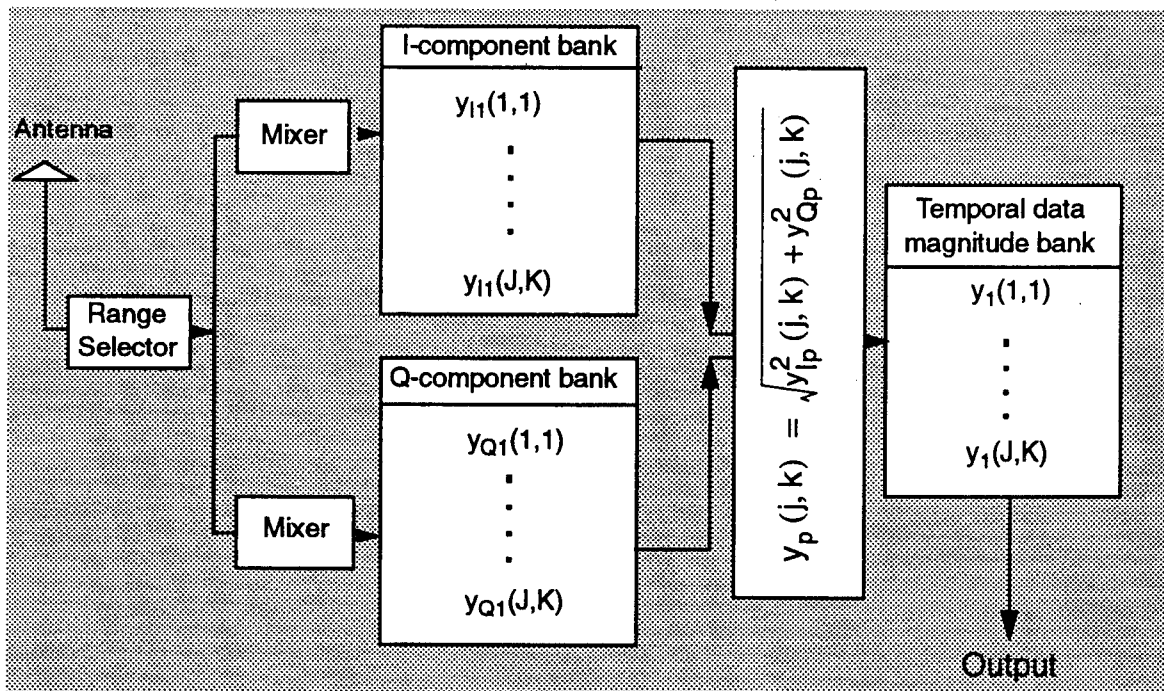


**Figure V.1.1 - Block Diagram of Data Preprocessing Stage for  $P=1$**

mapping stages, shown in Fig. IV.2.1, simplifies to Fig. V.1.2. Only  $J \times K$  temporal data magnitudes  $y(j,k)$  are available to the mapping stage. In this case, only  $J \times K$  R/A cells need to be mapped into BN and CL cells and the mapping process of

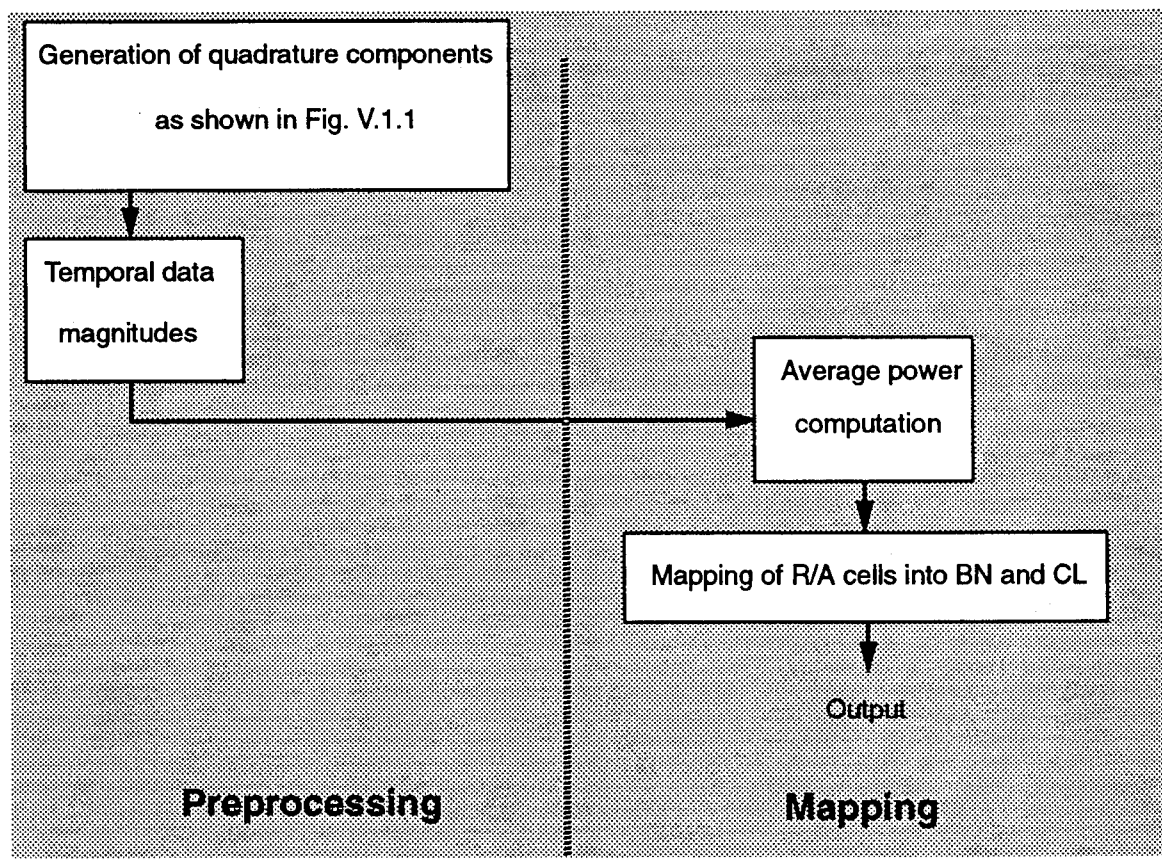


Figure V.1.2 - Block Diagram of Preprocessing and Mapping Stages for  $P=1$

Fig. IV.2.1 reduces to the first mapping stage alone. As explained in Section IV.2, an average power  $P(j,k)$  is formed for every R/A cell in the  $J \times K$  R/A plane. For  $P=1$ , Eq. (IV-2.1) becomes

$$P(j,k) = y_1^2(j,k); \quad \begin{matrix} j=1,2,\dots,J \\ k=1,2,\dots,K. \end{matrix} \quad (V.1-1)$$

At this point, the R/A plane consists of two different types of regions that need to be identified. These are clear regions, where BN alone is present, and clutter patches, where both CL and additive BN are present. Let's, first, examine

the nature of the BN and CL in order to understand the theory behind the procedure developed for mapping.

## **V.2 - Observations on BN and CL Cells**

Assuming additive BN and CL, the following observations are based on many computer generated examples of a BN region containing CL patches where the clutter-to-noise ratio (CNR) is assumed to be greater than 0 dB. The BN envelope is assumed to be Rayleigh while the CL envelope may be either Rayleigh, K-distributed, Weibull or lognormal.

### **V.2.1 - Observations on BN Cells**

The following observations on BN cells were noted:

- On an average, the BN data values are smaller than the CL data values.
- Large data values may exist in a BN cell that may be higher than some data values of a CL cell.
- Large data values in the BN tend to be isolated points.
- The number of BN data significantly larger than the average is relatively small. Fig. V.2.1 shows a typical BN data histogram.

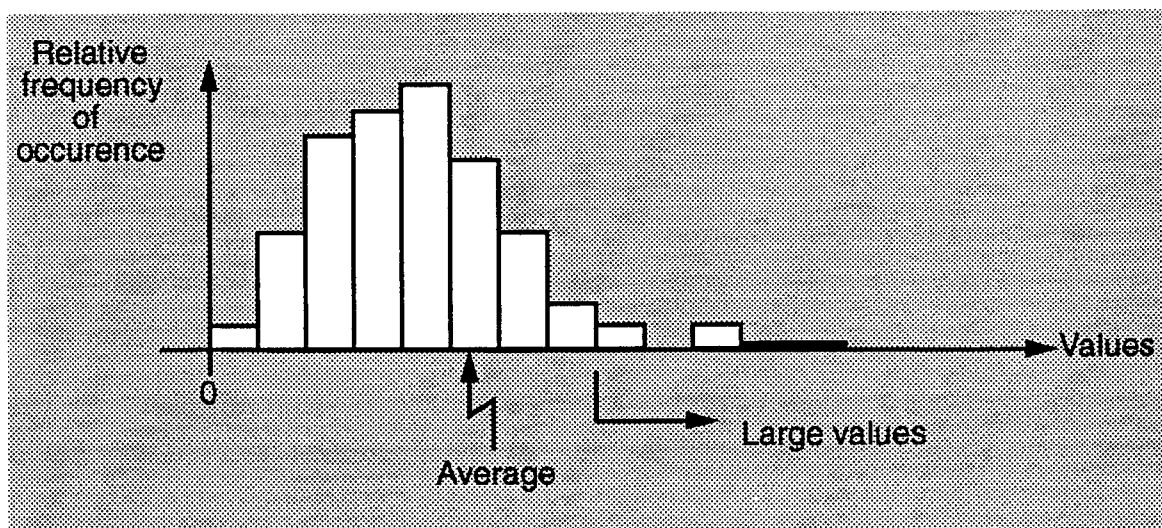


**Figure V.2.1 - Example of a BN Histogram**

- The relatively small number of large BN data are distributed sparsely throughout the surveillance volume.

### **V.2.2 - Observations on CL Cells**

The following observations on CL cells were noted:

- On an average, CL data values are higher than BN data values.
- A CL region contains additive CL and BN.
- Small data values may exist in a CL cell that may be smaller than some data values of a BN cell.
- The large CL data values tend to be larger than most of the large BN data values assuming positive CNR.
- Whereas the BN data values are distributed over the entire surveillance volume, the CL data values are distributed only over the clutter regions.
- Large data values in the CL tend to be clustered.

Fig. V.2.2 shows an example of the distribution of large values of BN data denoted by (x) and large values of CL data denoted by (o). Notice that the large

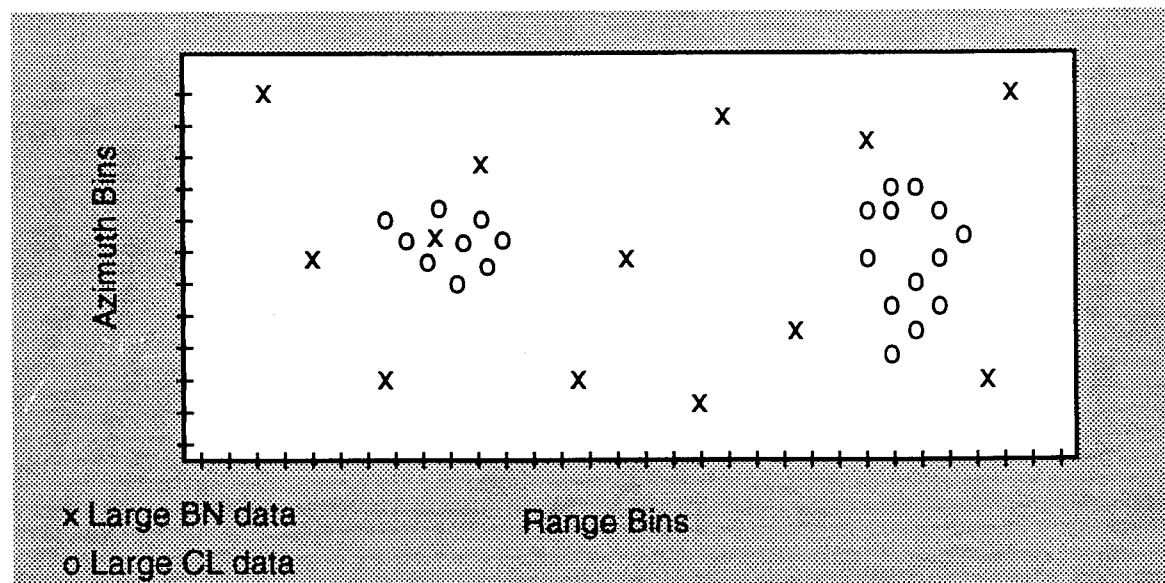


Figure V.2.2 - Concentration of large data in a scanned volume

BN data values are sparsely distributed over a large area while large values of CL are concentrated in small regions, the CL regions.

### **V.3 - Mapping Procedure**

Using the fact that clutter patches, on an average, have stronger radar returns, the mapping processor begins by setting a threshold that results in a specified fraction of BN cells, as explained in Chapter VII. Image processing is then used to establish the background noise and clutter patches. If the final image contains a significantly different fraction of BN than originally established by the initial threshold, the process is repeated with a new threshold. The mapping processor iterates until it is satisfied that the final scene is consistent with the latest specified threshold. Finally, clutter patch edges are detected using an image processing technique.

The mapping procedure consists of two steps. The first step is the identification of CL patches within BN. The second is the detection of clutter patch edges and their enhancement. These two steps are explained next.

#### **V.3.1 - Separation of CL Patches from BN**

Identification of CL patches within BN is performed by the following steps: thresholding, quantization, correction and assessment.

##### **V.3.1.1 - Thresholding and Quantization**

Identification of CL patches within BN starts by setting a threshold  $q$  that results in a specified fraction of BN cells. Then a quantized volume is formed as follows: all R/A cells with average power less than  $q$  are given a value of 0 (zero) and all R/A cells with average power above  $q$  are given a value of 1 (unity). Let  $Q(j,k)$  represent the quantized value of the  $jk^{\text{th}}$  R/A cell. Then,

$$Q(j,k) = \begin{cases} 1 & \text{if } P(j,k) \geq q \\ 0 & \text{if } P(j,k) < q \end{cases} \quad j=1,2,\dots,J \text{ and } k=1,2,\dots,K \quad (\text{V.3-1})$$

where  $P(j,k)$ , the average power of the  $jk^{\text{th}}$  R/A cell, is defined in Eq. (V.1-1).

Fig. V.3.1 shows the computer generated CL patches and BN region that are to be separated by the mapping procedure. A, B, C, and D denote the CL patches. Fig. V.3.2 shows a typical contour plot of the quantized R/A volume.

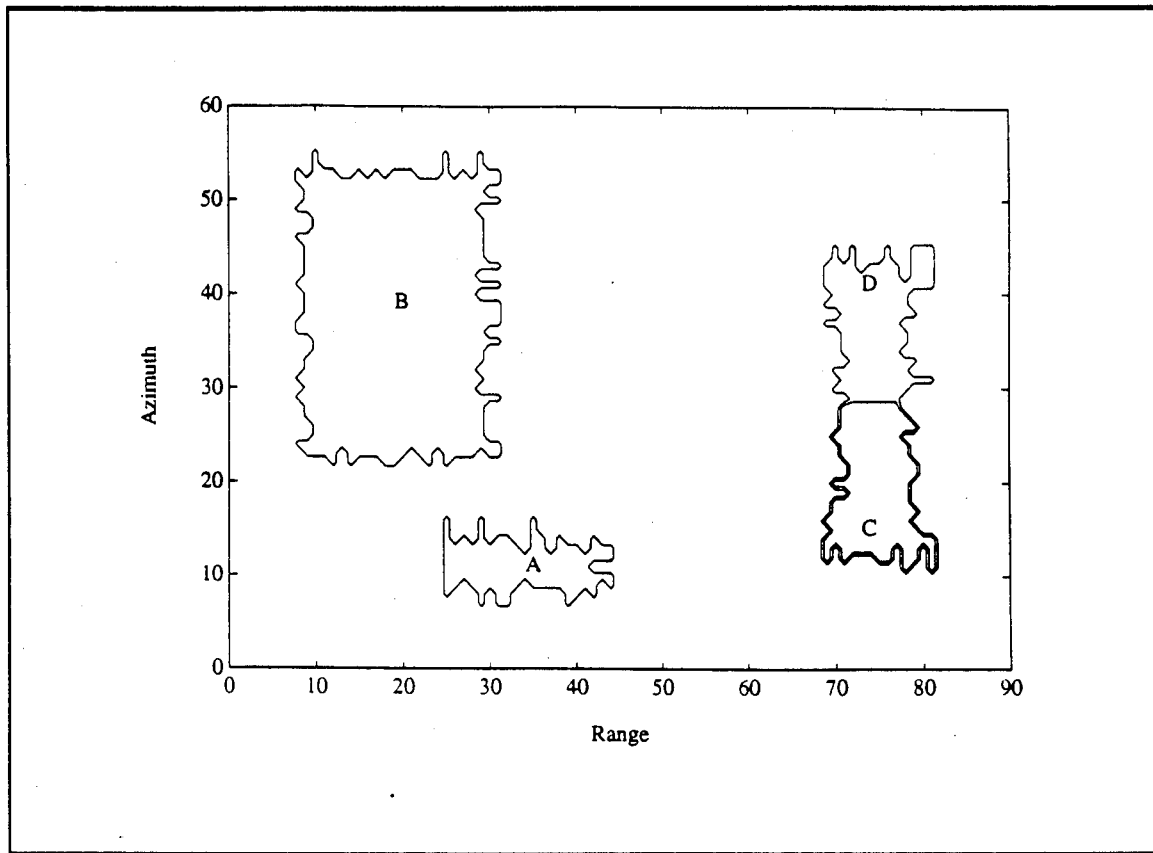
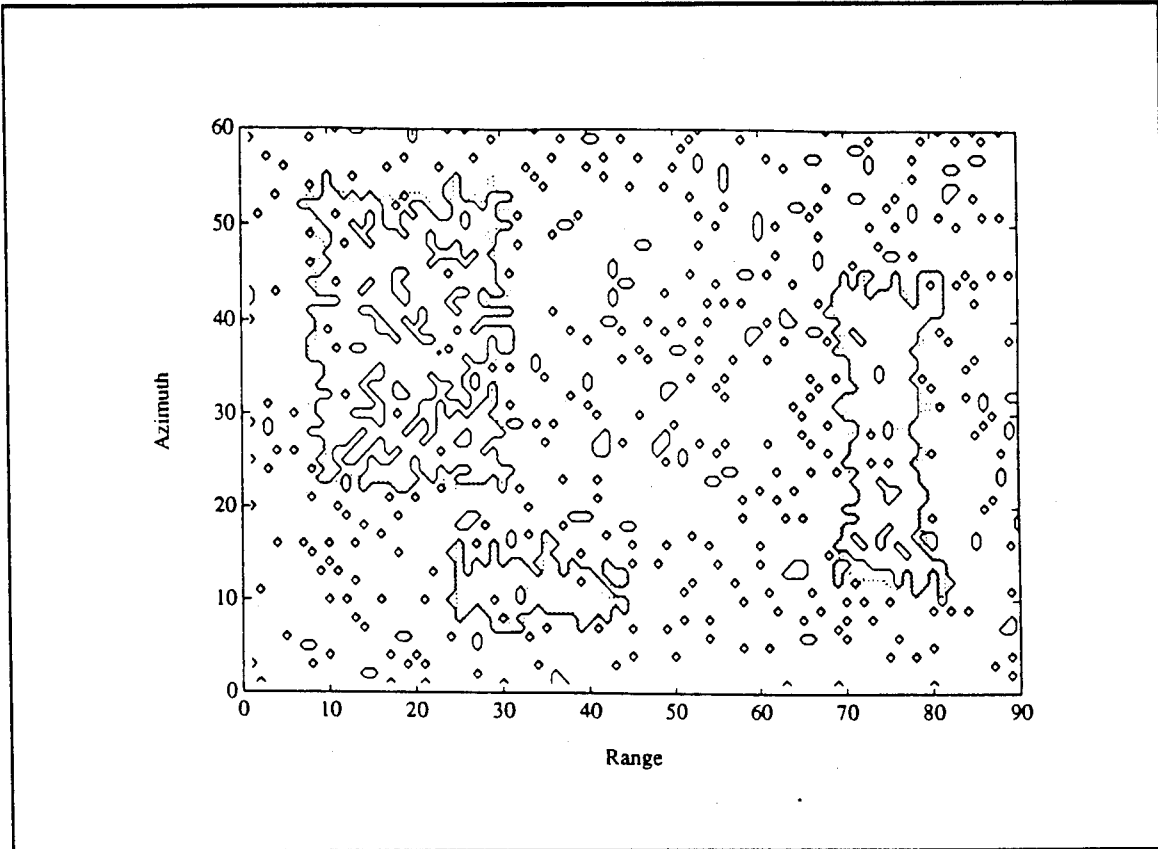


Figure V.3.1 - Example of a Generated R/A Volume that is to be Separated by the Mapping Procedure

Initially, let R/A cells with a quantized value of 1 be declared as CL cells and R/A cells with a quantized value of 0 be declared as BN cells. By comparing Figs. V.3.1 and V.3.2, note that the quantized version differs from the original. This is due to the fact that even though the average powers of BN cells are expected to fall under the threshold while the average powers of CL cells are expected to fall above the threshold, typically,

some BN cells have an average power that falls above the threshold and some CL cells have an average power that falls under the threshold. Also, as explained in Chapter VII, the first setting of the threshold, which is somewhat arbitrary, is likely not to be the best for identifying CL patches within BN.



*Figure V.3.2 - Example of a Quantized R/A Volume*

### **V.3.1.2 - Correction**

After quantization, the next step is to correct misclassified BN and CL cells. Consider a set of  $3 \times 3$  R/A cells. As shown in Fig. V.3.3, let the center cell be referred to as the test cell and the surrounding cells be referred to as the neighboring cells. Assume that a clutter patch cannot be formed by a single cell. In this case, every test cell in the clutter patch has at least one neighboring cell that belongs to the same clutter patch.

A test cell belonging to a clutter patch that has at least one neighboring BN cell is referred to as a CL edge cell. On the other hand, a test cell that belongs to a CL patch for which none of the neighboring cells are in the BN is referred to as an inner CL cell.

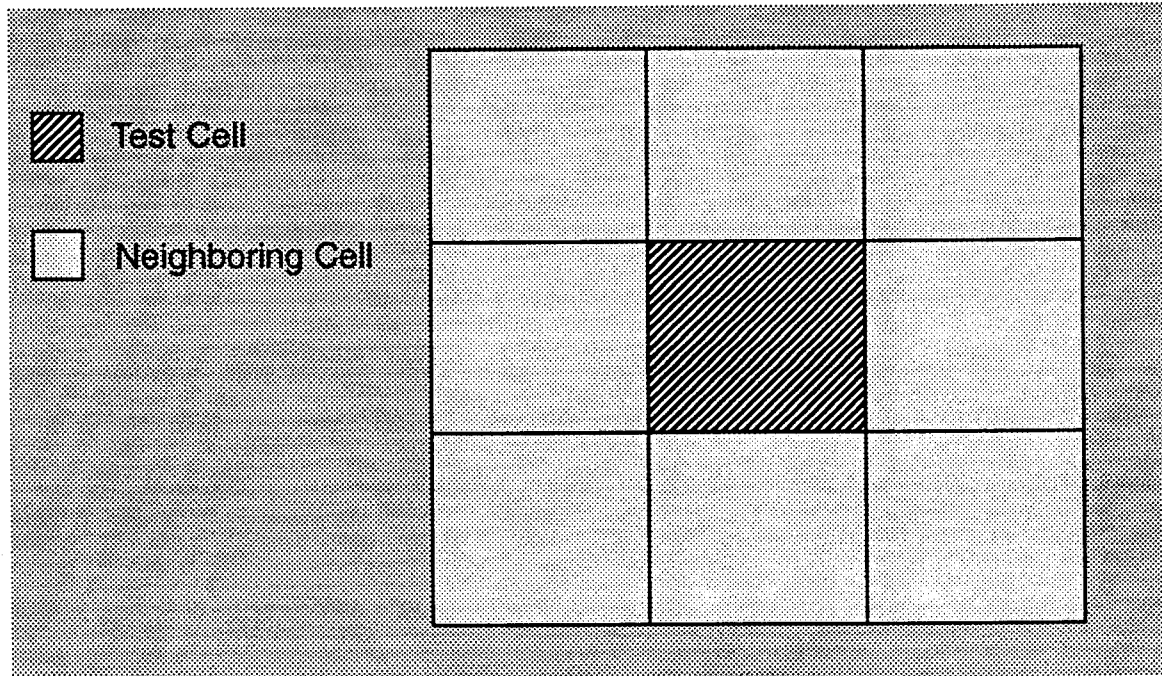


Figure V.3.3 - 3x3 R/A Cells

The proposed correction technique consists of transforming the quantized volume into a "corrected" volume. The transformation consists of the following steps:

- 1. As explained in Chapter VII, choose the necessary number of CL neighboring cells, NCQ, for a test cell in the quantized volume to be declared as a CL cell in the corrected volume. NCQ can take one of the following values: 5,6,7,8.
- 2. For every test cell in the quantized volume count the number of neighboring CL cells. If the number is greater than or equal to NCQ declare the test cell as a CL cell in the corrected volume. Otherwise, declare the test cell as a BN cell in the corrected volume.

When all the cells of the quantized volume have been tested, a "corrected" volume consisting of declared BN or CL R/A cells is obtained. Notice that a cell type is not updated until the entire correction is done. Fig. V.3.4 shows an example of a "corrected" volume. Notice that the latter volume has larger homogeneous regions than the quantized one.

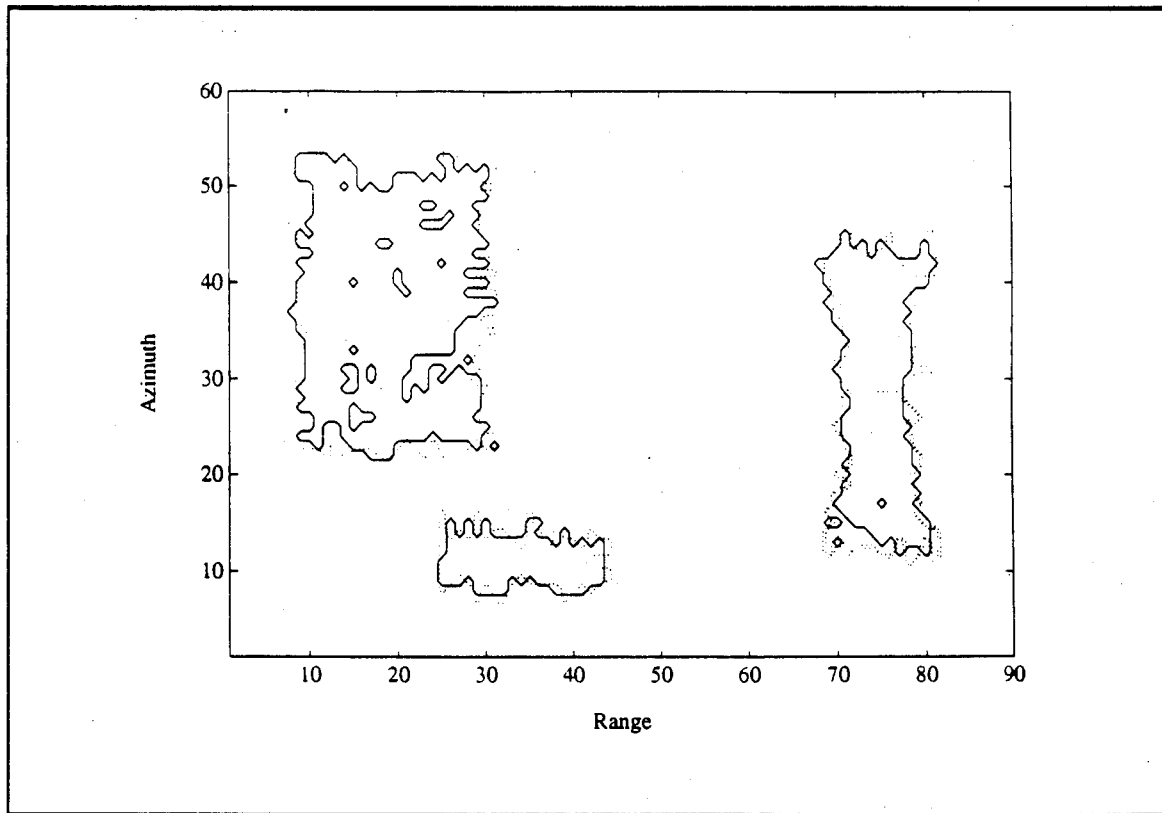


Figure V.3.4 - Example of a "Corrected" R/A Volume

Because NCQ is chosen to be relatively large (i.e. NCQ=5,6,7 or 8), BN cells that were incorrectly identified in the quantized volume as CL cells due to their large power tend to be reclassified as BN cells. Also, inner CL cells in the quantized volume are recognized as CL cells in the "corrected" volume. Meanwhile, most of the CL edge cells in the quantized volume are recognized as BN cells in the "corrected" volume. This results in an over-correction where most of the CL edge cells are identified as BN. As an example, when NCQ=8, only inner CL cells in the quantized volume are recognized as CL cells in the "corrected" vol-

ume and all CL edge cells in the quantized volume are recognized as BN cells in the "corrected" volume. In order to recover the edge cells, a second-correction stage is needed where the first "corrected" volume will be transformed into a second "corrected" volume. Let the first "corrected" volume be referred to as the "corrected-quantized" volume (CQV) and the second "corrected" volume be referred to as the "corrected-corrected" volume (CCV). The following steps are used to transform the CQV into the CCV:

- 1 - As explained in Chapter VII, choose the necessary number of CL neighboring cells, NCC, for a test cell in the CQV to be declared as a CL cell in the CCV. NCC can take one of the following values: 1,2,3 or 4.
- 2 - For every test cell in the CQV count the number of neighboring CL cells. If the number is greater than or equal to NCC declare the test cell as a CL cell in the CCV. Otherwise, declare the test cell as a BN cell in the CCV.

Figure V.3.5 shows the CCV obtained by transforming the CQV of Fig. V.3.4.

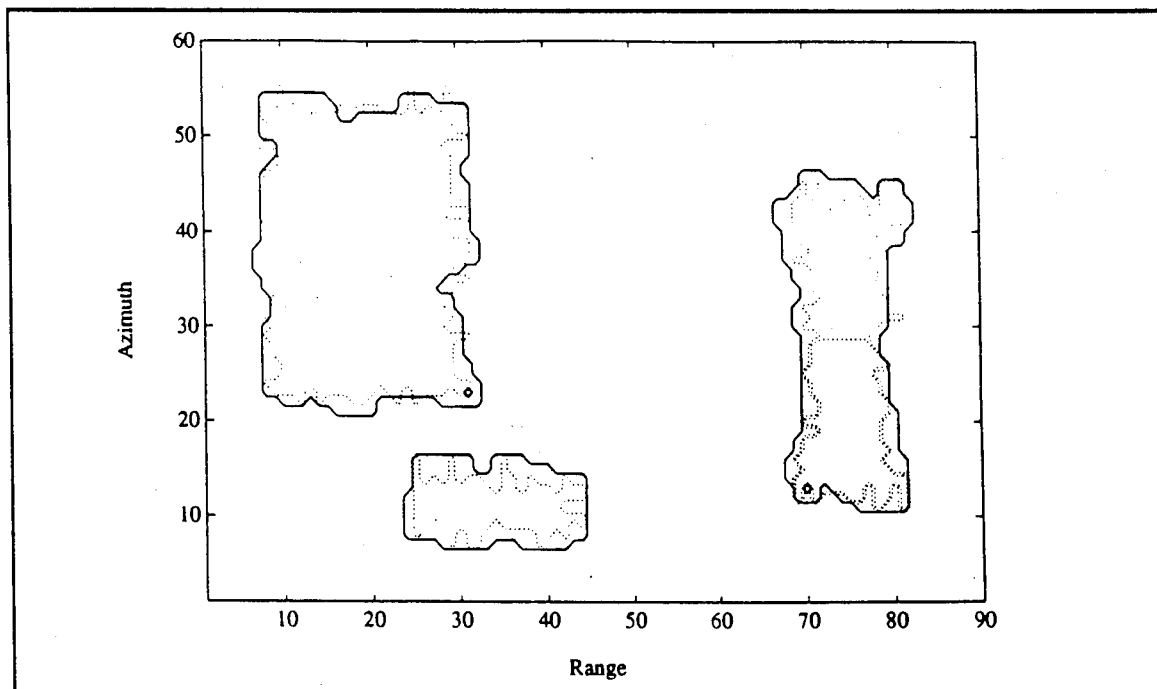


Figure V.3.5 - Example of the CCV Corresponding to the CQV of Fig. V.3.4

### **V.3.1.3 - Assessment**

Let BNQP, BNCQP and BNCCP denote the percentage of BN cells in the “quantized”, “corrected-quantized” and “corrected-corrected” volumes, respectively. BNQP is pre-specified so as to determine the threshold for the quantized volume, whereas BNCQP and BNCCP are computed after the CQV and the CCV are obtained.

The assessment process consists of comparing BNCQP and BNCCP to BNQP in order to determine whether or not the percentages of the BN cells after correction are consistent with the percentage of BN cells in the quantized volume. When there is no consistency, further quantization, correction and assessment are performed until consistency is obtained.

The thresholding/quantization, first-correction, second-correction, and assessment stages are used to find the best threshold to separate between BN and CL patches. Once BNQP has been set, a threshold is computed. Then corrections are made to try and build the BN region and CL patches. The correction stages re-label some of the above-threshold cells as BN cells if they are likely to belong to the BN, and some of the below-threshold cells as CL cells if they are likely to belong to a CL patch, based on the choices for NCQ and NCC. Depending on how good or how bad of a choice is the threshold, many or few cells are relabeled, respectively. At the end of the procedure, BNCCP is computed and compared to BNQP. If the values are within a certain range, few cells would have been relabeled, the threshold is accepted and the assessment passes. Otherwise, many cells would have been relabeled and the threshold is rejected. The iterative process then continues by setting another threshold through the choice of a new value for BNQP.

Rules for choosing NCQ, NCC and BNQP and for determining when consistency of the percentages are obtained are explained in Chapter VII.

### **V.3.1.4 - Smoothing**

Examples have shown in many cases that when the percentages are consistent, clutter declared patches may contain isolated BN declared cells. Because small powers can arise in a CL patch as explained in Section V.2, it is most likely that isolated BN cells in CL patches are CL cells. The smoothing process is used to detect these isolated cells and label them adequately by transforming the CCV into a smoothed volume (SV). The smoothing technique consists of the following steps:

- 1 - Choose the necessary number of CL neighboring cells, NS, for a BN identified test cell in the CCV to be declared as a CL cell in the SV where NS can take one of the following values: 5,6,7, or 8.
- 2 - For every BN identified cell in the CCV count the number of neighboring CL cells. If the number is greater than or equal to NS, declare the test cell as a CL cell in the SV. Otherwise, declare the test cell as a BN cell in the SV.

Fig. V.3.6 shows an example of the smoothed volume corresponding to the CCV of Fig. V.3.5. Note that the CL patches are smooth and do not contain any isolated points.

### **V.3.2 - Detection of Clutter Patch Edges and Edge Enhancement**

#### **V.3.2.1 - Detection of Clutter Patch Edges**

After smoothing, each cell in the SV has been declared as either a CL or BN cell. The next step is to determine which of the CL cells are located on the edges of the CL patches. This is important for subsequent radar signal processing if reference cells for estimating parameters of a test cell are to be chosen properly.

Identification of CL edge (CLE) cells is done by the use of an image processing technique referred to in the image processing literature as unsharp masking [24, 25]. It consists of the following steps:

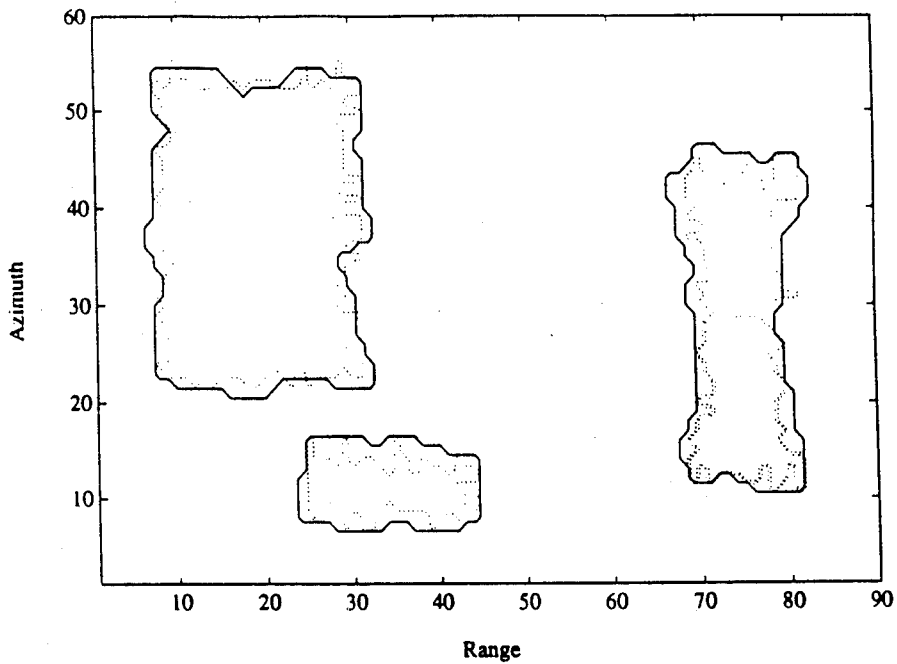


Figure V.3.6 - Example of the SV Corresponding to the CCV of Fig. V.3.5

1 - A weighting filter consisting of a  $3 \times 3$  array of cells is constructed, as shown in Fig. V.3.7, where the center cell has a weight given by  $w(0,0)=8$  and the neighboring cells have weights given by  $w(-1,-1)=w(0,-1)=w(1,-1)=w(-1,0)=w(1,0)=w(-1,1)=w(0,1)=w(1,1)=-1$ . The center cell is positioned on the test cell. Notice that the weights of the filter cells sum to zero. In particular,

$$\sum_{m=-1}^1 \sum_{n=-1}^1 w(m, n) = 0 \quad (V.3-2)$$

2 - Assume the weighting filter is centered at the  $jk^{\text{th}}$  cell in SV. The cells corresponding to the  $3 \times 3$  array of the weighting filter have quantized values as illustrated in Fig. V.3.8. By definition,

$w(-1, -1) = -1$	$w(0, -1) = -1$	$w(1, -1) = -1$
$w(-1, 0) = -1$	$w(0, 0) = 8$	$w(1, 0) = -1$
$w(-1, 1) = -1$	$w(0, 1) = -1$	$w(1, 1) = -1$

*Figure V.3.7 - Weighting Filter*

$SQ(j-1, k-1)$	$SQ(j, k-1)$	$SQ(j+1, k-1)$
$SQ(j-1, k)$	$SQ(j, k)$	$SQ(j+1, k)$
$SQ(j-1, k+1)$	$SQ(j, k+1)$	$SQ(j+1, k+1)$

*Figure V.3.8 - Quantized Values of the 3x3 Array Corresponding to the  $jk^{th}$  Cell*

$$SQ(j,k) = \begin{cases} 1 & \text{if the } jk^{\text{th}} \text{ cell in SV is declared as CL} \\ 0 & \text{if the } jk^{\text{th}} \text{ cell in SV is declared as BN} \end{cases} \quad (V.3-3)$$

where

$j=1,2,\dots,J$  and  $k=1,2,\dots,K$ .

To avoid filter cells falling outside SV, the coordinates of the  $jk^{\text{th}}$  cell at which the filter is centered are constrained to  $j=2,3,\dots,J-1$ , and  $k=2,3,\dots,K-1$ .

3 - Form the sum

$$S = \sum_{m=-1}^1 \sum_{n=-1}^1 w(m, n) SQ(j+m, k+n) . \quad (V.3-4)$$

- If  $S$  is equal to zero, all cells have the same assigned value. This can arise only when the test cell is not an edge cell.
- If  $S$  is positive, the test cell is an edge cell and is labeled as such.
- If  $S$  is negative, the test cell cannot be an edge cell. On the other hand, one or more of the neighboring cells are guaranteed to be an edge cell.

The three situations are illustrated in Figs. V.3.9-a, b, c and d, where the black and white cells represent BN and CL cells, respectively. In Figs. V.3.9-a and V.3.9-b,  $S=0$  because all 9 cells are in BN and CL, respectively. Observe that the test cell is not an edge cell. In Fig. V.3.9-c,  $S=4>0$ . Note that the test cell is an edge cell. Finally, in Fig. V.3.9-d,  $S=-2<0$  and the test cell is not an edge cell.

At the end of the edge detection procedure, each cell in the original volume has been labeled as either CL, BN or CLE cell. At this point, the mapping is done. The final volume is referred to as the mapped volume (MV).

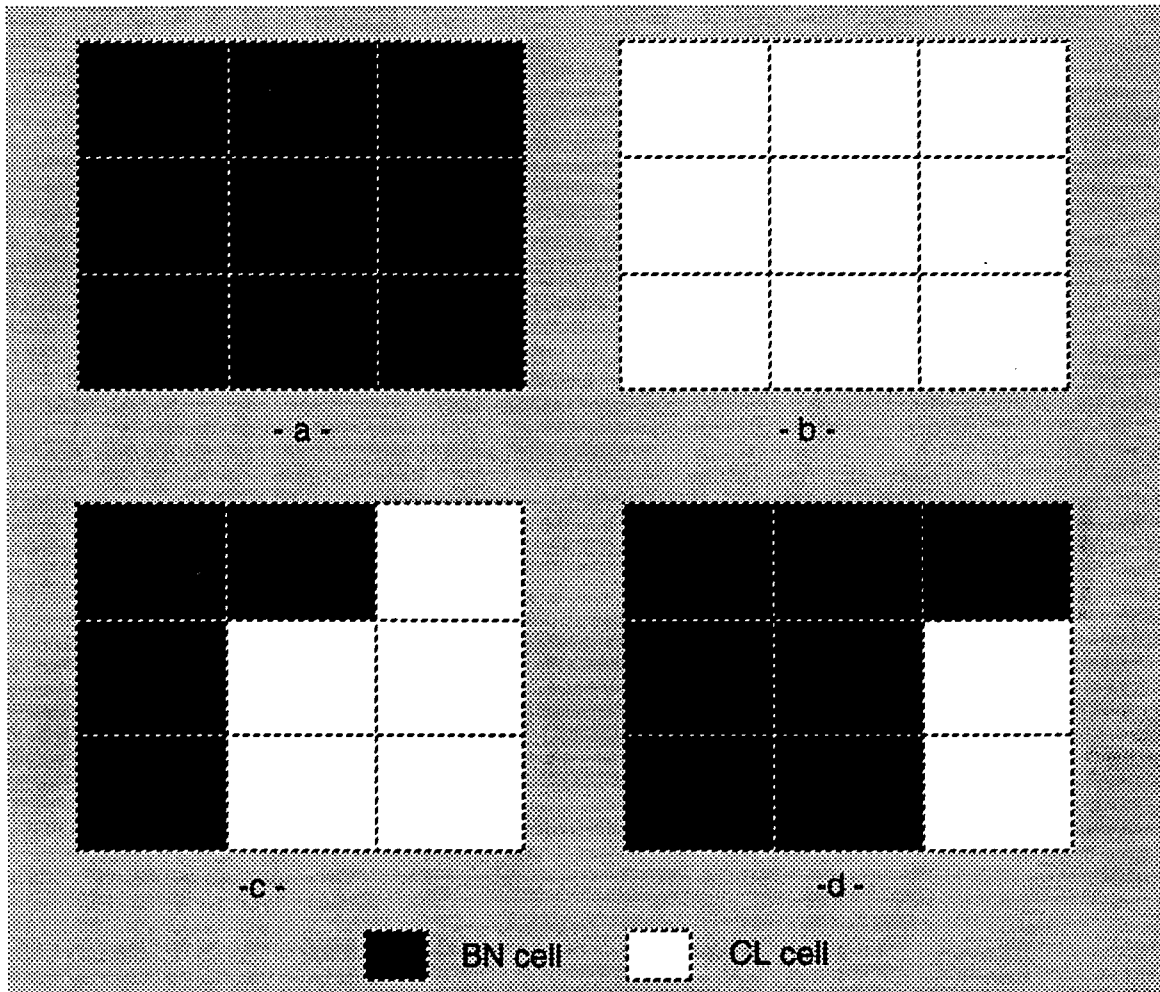


Figure V.3.9 - Example of Unsharp Masking Technique

-a-  $S=0$ , -b-  $S=0$ , -c-  $S>0$ , -d-  $S<0$

### V.3.2.2 - Enhancement of Clutter Patch Edges

The edges detected after smoothing tend not to follow the irregular edges that may actually exist. Consequently, the edges are further enhanced by examining the power levels of cells just outside the edge cells and on the edge cells. If the power levels of these cells exceed the threshold set in the quantization stage, they are declared as edge cells. Otherwise, they are declared as BN cells.

At the end of the edge enhancement procedure, edges are detected and each cell in the original volume is labeled as either CL, BN or CLE cell.

### **V.3.3 - Conclusion**

The mapping procedure consists of the following steps: thresholding/quantization, correction, assessment, smoothing, edge enhancement, and edge detection, as shown in Fig. V.3.10. The feedback loop that connects the assessment procedure to the thresholding/quantization, first-correction, and second-correction blocks is controlled by IPUS, as will be explained later on in Chapter VII.

### **V.4 - Examples of the Mapping Procedure**

Before presenting examples to illustrate how the mapping procedure performs a separation between BN and CL patches, a brief review of the mapping procedure is first given. Then, three different examples of the mapping procedure are presented. The generated scene and the distributions of the clutter patch data are shown for every example. Also, only the results corresponding to the initial and final choices of BNQP are illustrated in each case. The in-between settings of BNQP are listed in tables.

#### **V.4.1 - Introduction**

The mapping procedure begins by selecting a threshold such that the percentage of BN cells relative to the total number of cells is equal to a specified value, denoted by BNQP. Two correction stages then ensue. In the first-correction stage, each cell in the quantized volume, denoted by QV, is tested by a 3x3 mask centered on the test cell. The test cell is labeled as BN only if less than NCQ of the eight neighboring cells are declared as CL in the QV volume where NCQ is a parameter specified by the user. In the following discussion it will be shown that the first-correction stage tries to restore the right tail of the BN PDF which had been severely distorted by the quantization. After the first-correction stage, the corrected volume is denoted by CQV. The second-correction stage attempts to correctly reclassify the edges of the CL patches. This is done by testing each cell in CQV using, once again, a 3x3 mask centered on the test cell. The test cell is labeled as BN if less than NCC of the eight neighboring cells are declared as CL in the CQV

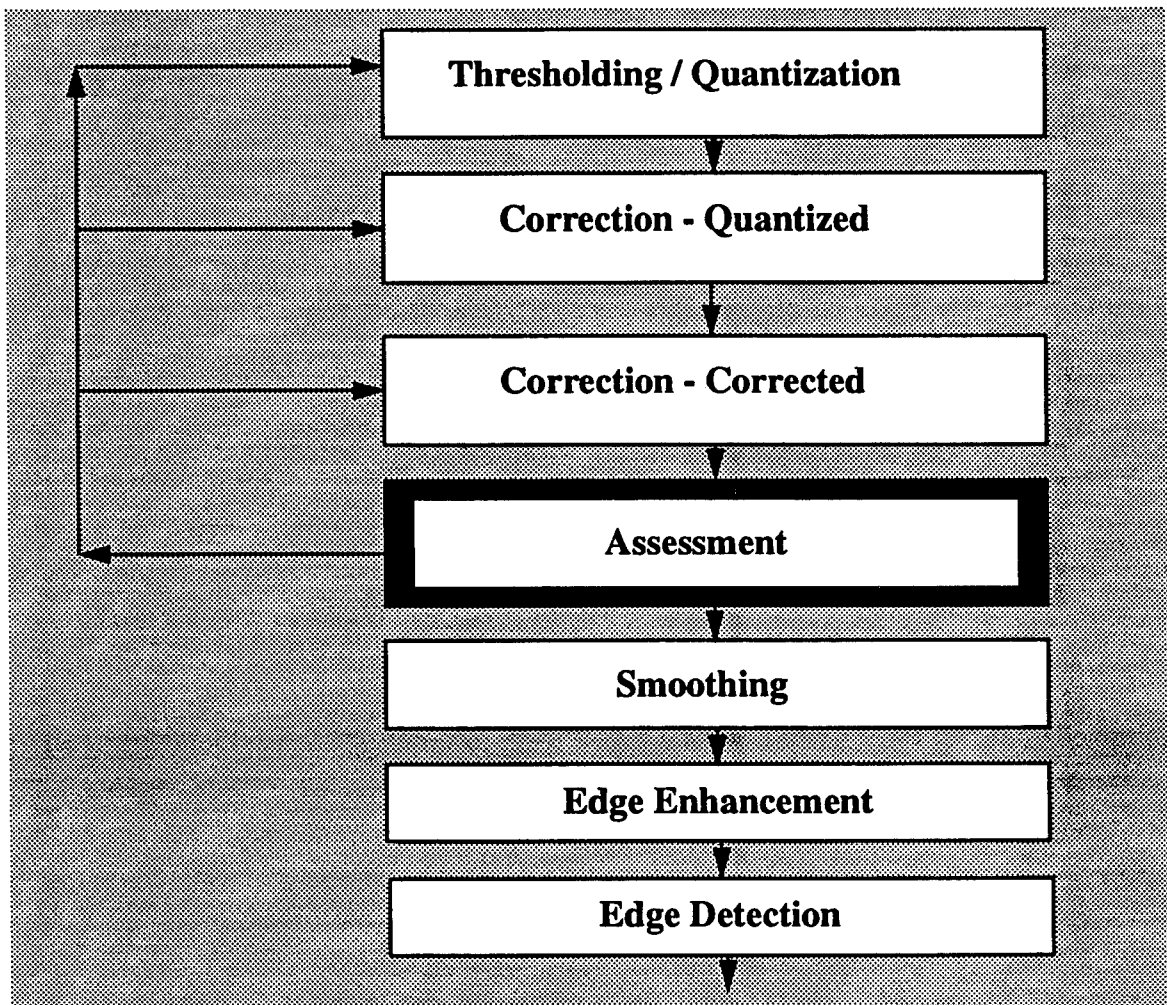


*Figure V.3.10 - Block Diagram of the Mapping Procedure*

volume where NCC is a parameter specified by the user. Typical values for NCQ are 5,6,7,8 while typical values for NCC are 1,2,3,4. In the following discussion it will be shown that the second-correction stage attempts to restore the shapes of both the BN and CL PDFs. After the second-correction stage, the corrected volume is denoted by CCV. The percentage of BN cells relative to the total number of cells in the CCV volume is denoted by BNCCP. BNCCP is compared to BNQP. If the difference  $IBNCCP - BNQPI$  is smaller than a pre-specified value, the iteration process ends and some additional processing is done to enhance and label the edges. As explained in Chapter VII, if the difference is not too large, additional iterations are made with new values for NCQ and NCC. If these do not lead to con-

vergence or if the difference is too large, the whole process is repeated by selecting a new threshold. If the difference is large, the new value for BNQP is chosen to be the previous BNCCP. Otherwise, the new value of BNQP is chosen to be half way in between the previous values of BNQP and BNCCP.

#### **V.4.2 - Examples**

In the following examples, it is assumed that the radar scans over  $120^\circ$  in the azimuthal direction and has a beamwidth of  $2^\circ$ . Hence, the azimuthal axis is subdivided into 60 bins. Also, the length of a range cell is given by  $c\tau/2$  where  $c=3\times 10^8$  meters/second is the speed of the light and  $\tau$  is the radar pulse width. Assuming a pulse width of  $\tau=1\mu\text{s}$  and a maximum range of  $R_{\text{max}}=13.5$  km, the range axis is divided into  $\frac{R_{\text{max}}}{(c\tau)/2} = 90$  bins. Consequently, this subdivision of the entire surveillance volume yields a total of 5400 range-azimuth cells.

In all examples presented in this dissertation clutter plus noise data in a given cell are obtained by simply adding the envelopes of the CL and BN values for that cell. Of course, the envelope of the sum of two random processes does not equal the sum of the envelopes. Nevertheless, it is possible to develop the important concepts of mapping and indexing using any set of random variables. The sum of envelopes approach was chosen in order to simplify the many computer simulations required by this research. Specifically, it was not necessary to first generate random processes whose envelopes are Weibull, Lognormal, and K-distributed.

The following three examples illustrate, respectively, the cases of an easy, difficult but resolvable, and difficult but not resolvable problems. These examples are discussed throughout this work.

##### **V.4.2.1 - Example 1**

Consider a surveillance volume containing four homogeneous clutter patches, denoted by A, B, C, and D. Clutter patches C and D are contiguous and form a single nonhomogeneous clutter patch C/D. Let CNR denote the CL to BN

Clutter	CNR (dB)	Data Distribution	Shape Parameter	Number of cells
A	10	Rayleigh	None	117
B	20	K-distributed	10.0	1423
C	30	Lognormal	0.01	146
D	40	Weibull	5.00	146

Table V.4.1 - CL Patch Parameters

average power ratio. Table V.4.1 lists the parameters of each CL patch. In addition, the BN, which is spread throughout the surveillance volume, is Rayleigh distributed

In this example, 66.07% of the total scanned volume is occupied by BN alone. Also, CL patch C contains the same number of cells as CL patch D. Figures V.4.1 and V.4.2 show the CL patch boundaries and the three-dimensional envelope plot for the surveillance volume, respectively. The probability density functions and histograms of the background noise and clutter patches are shown in Fig. V.4.3. Comparing Figures V.4.3.a and b, notice that some of the BN data are larger than some of the clutter data of clutter patches A and B.

The iteration process begins with the threshold set such that 10% of the sorted data are below the threshold, i.e BNQP=10%. Although the value of 10% is arbitrary, the initial setting of BNQP should be low. With the setting at 10%, the contour plot of the quantized volume is shown in Figure V.4.4. In this figure, the closed solid line contours surround the BN declared regions and the rest is CL. Notice that a lot of BN cells have data exceeding the threshold because the threshold was set very low. This results in a lot of small BN regions. For the purpose of comparison, the boundaries of the original CL patches are shown in dotted lines. With, NCQ set to 8 and NCC set to 1, the contour plots resulting from the first and second-corrections, respectively, are shown in Figures V.4.5 and V.4.6.

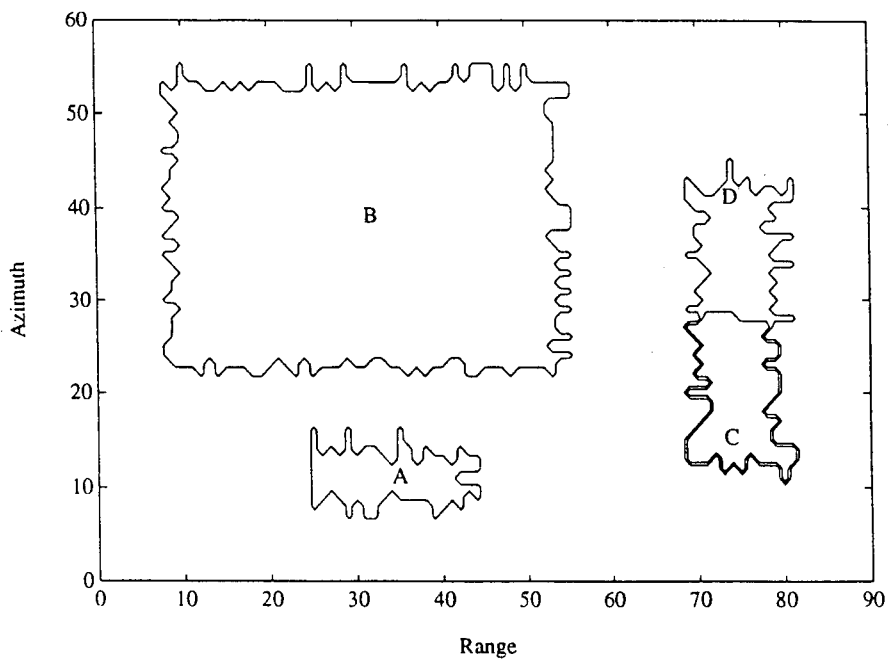


Figure V.4.1 - Boundaries of the CL Regions

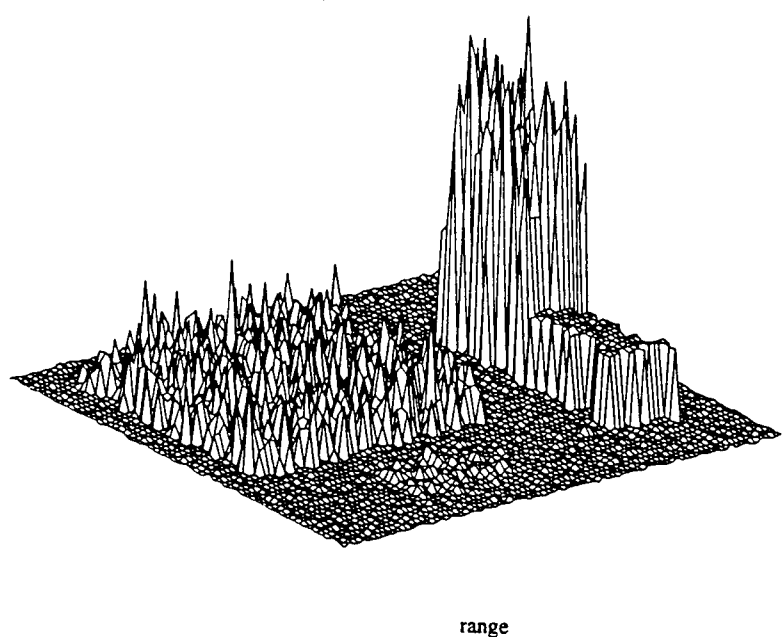
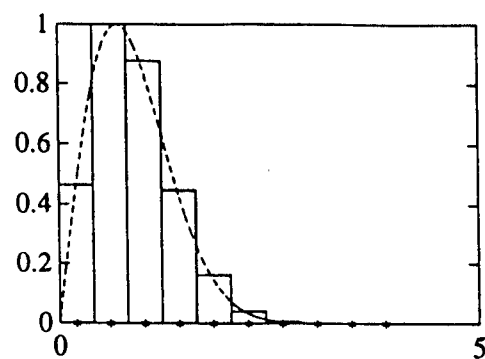
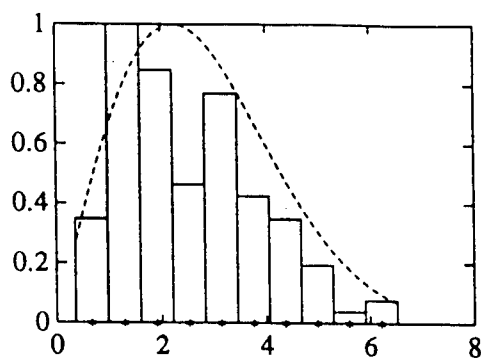


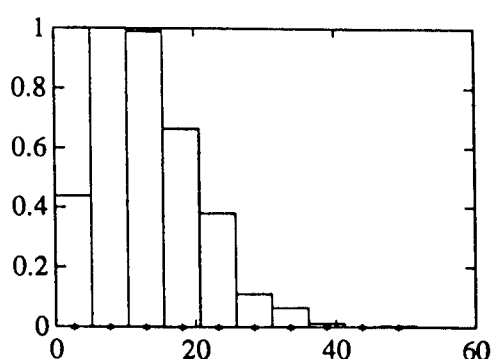
Figure V.4.2 - 3-D Envelope Plot of the Surveillance Volume



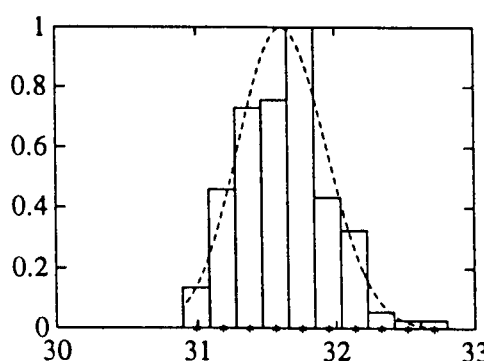
- a -



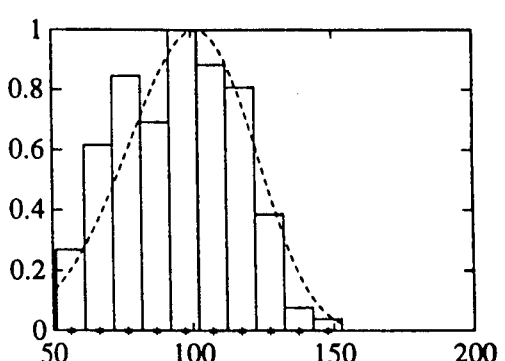
- b -



- c -



- d -



- e -

Figure V.4.3 - Probability Density Functions and Histograms of the Background Noise and Clutter Patches (a) Rayleigh distributed background noise, (b) Rayleigh distributed CL A, (c) K-distributed CL B, (d) Lognormal distributed CL C, (e) Weibull distributed CL D

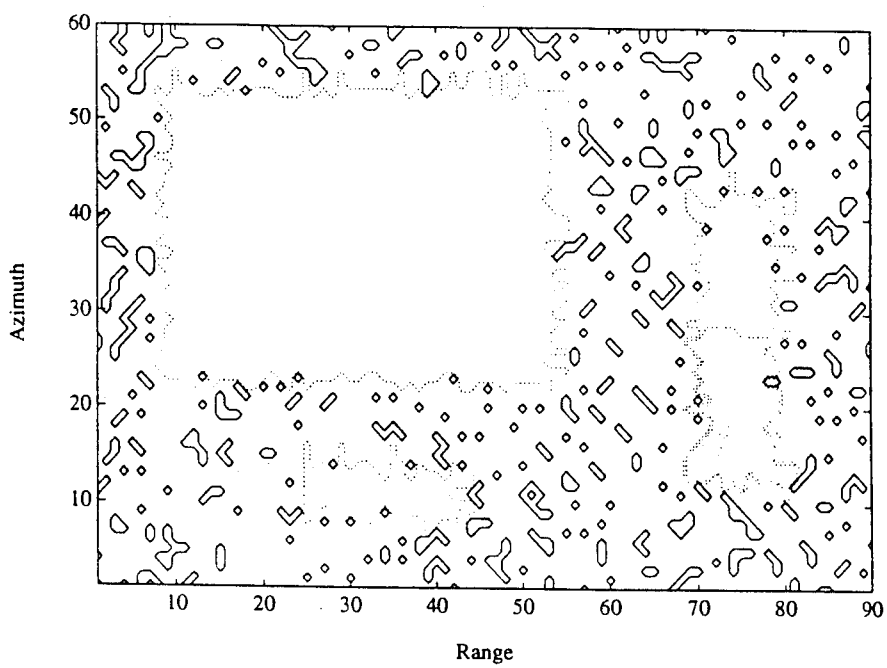


Figure V.4.4 - Contour plot of the Quantized Volume with BNQP=10%

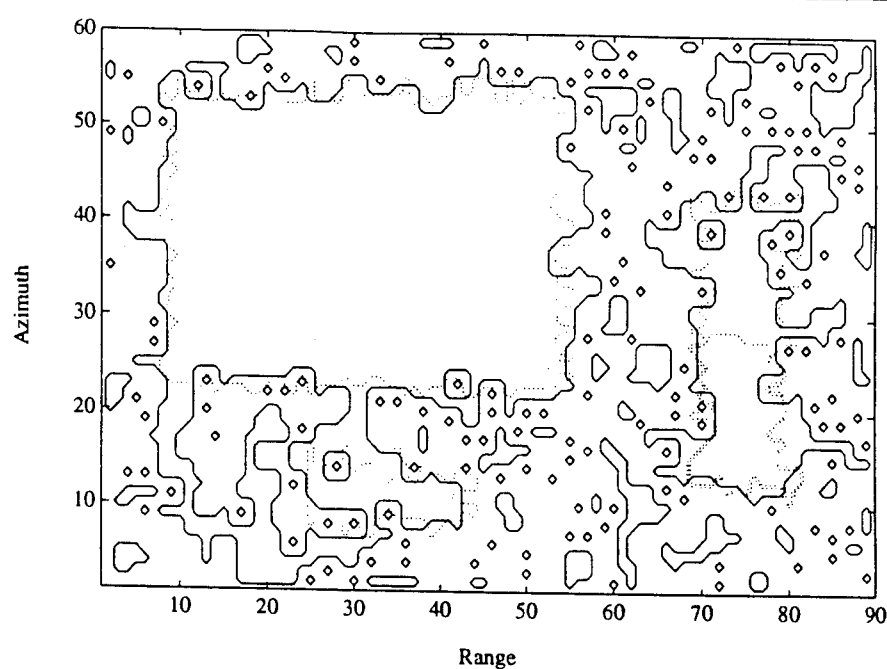


Figure V.4.5 - Contour Plot of the First-Correction Volume with NCQ=8

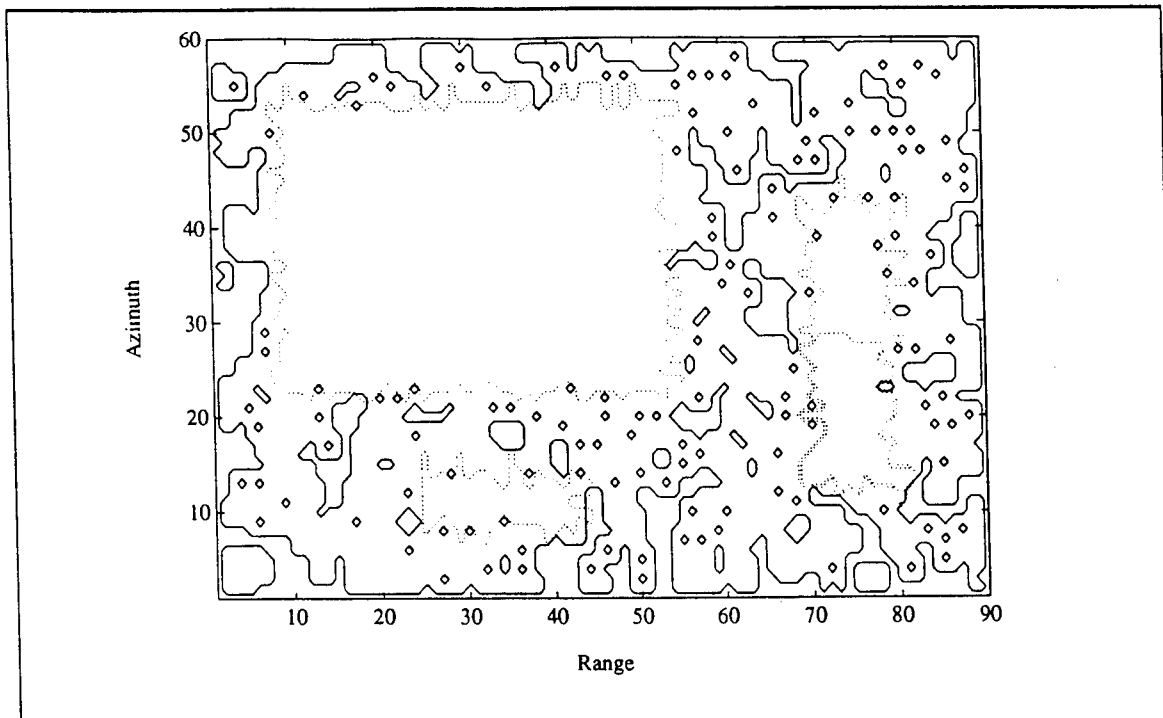


Figure V.4.6 - Contour Plot of the Second-Correction Volume with NCC=1

As shown in Table V.4.2, when BNQP=10% and (NCQ,NCC)=(8,1), BNC-CP=22% which results in  $|IBNQP-BNCCPI|=12\%$  being large. A new threshold is then chosen so that BNQP=22% which is the previous value obtained for BNCCP. The iterative process continues until it is found for BNQP=63.37%, NCQ=5, and NCC=3, that  $|IBNQP-BNCCPI|=|63.37-64.17|<1\%$ . In particular, for these parameter values,  $|IBNQP-BNCCPI|=|63.37-64.17|<1\%$ . At this stage the assessment passes and the iterative process stops.

Figures V.4.7-9 show the contour plots obtained after quantization, first-correction and second-correction, respectively, when BNQP=63.37%, NCQ=5 and NCC=3. Note first from Figure V.4.7 that even with this setting of BNQP, where the threshold is very close to its true value, some of the BN data exceed the threshold and form very small CL patches, and some of the CL data in every patch falls below the threshold causing holes in the CL patch. Figure V.4.8 shows how most of the erroneously declared BN and CL cells have been correctly re-classified as CL and BN cells, respectively. Next, the edges are augmented as

shown in Figure V.4.9. However, comparing the resulting edge contour to the ideal contour shows that not all the edges have been recovered even though the CL patches have been identified.

BNQP (%)	Parameter Values	
10.00 (guess)	NCQ=8 NCC=1	BNCQP=51.56 BNCCP=22.00
22.00 latest BNCCP	NCQ=8 NCC=1	BNCQP=68.28 BNCCP=50.39
50.39 latest BNCCP	NCQ=7 NCC=1	BNCQP=70.93 BNCCP=63.37
63.37 latest BNCCP	NCQ=5 NCC=1	BNCQP=67.35 BNCCP=59.72
63.37 same as latest BNQP	NCQ=5 NCC=3	BNCQP=67.35 BNCCP=64.17

Table V.4.2 - Settings of BNQP

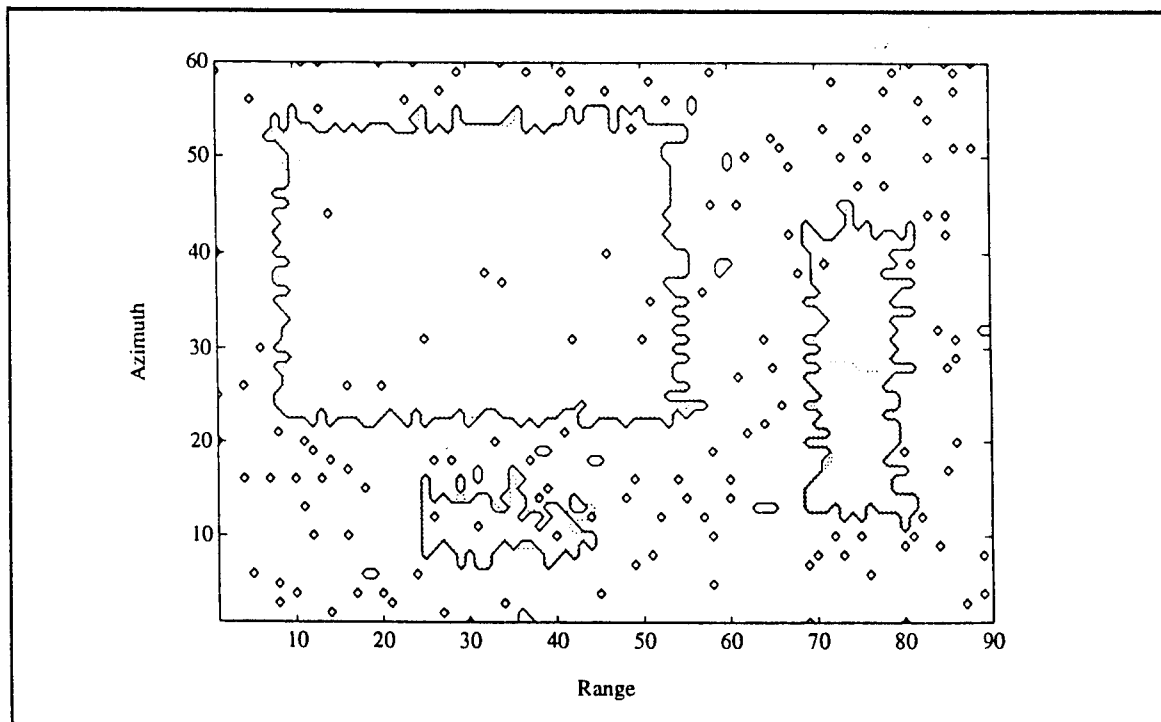


Figure V.4.7 - Contour Plot of the Quantized Volume with BNQP=63.37%

Next, smoothing, edge enhancement and edge detection are performed.

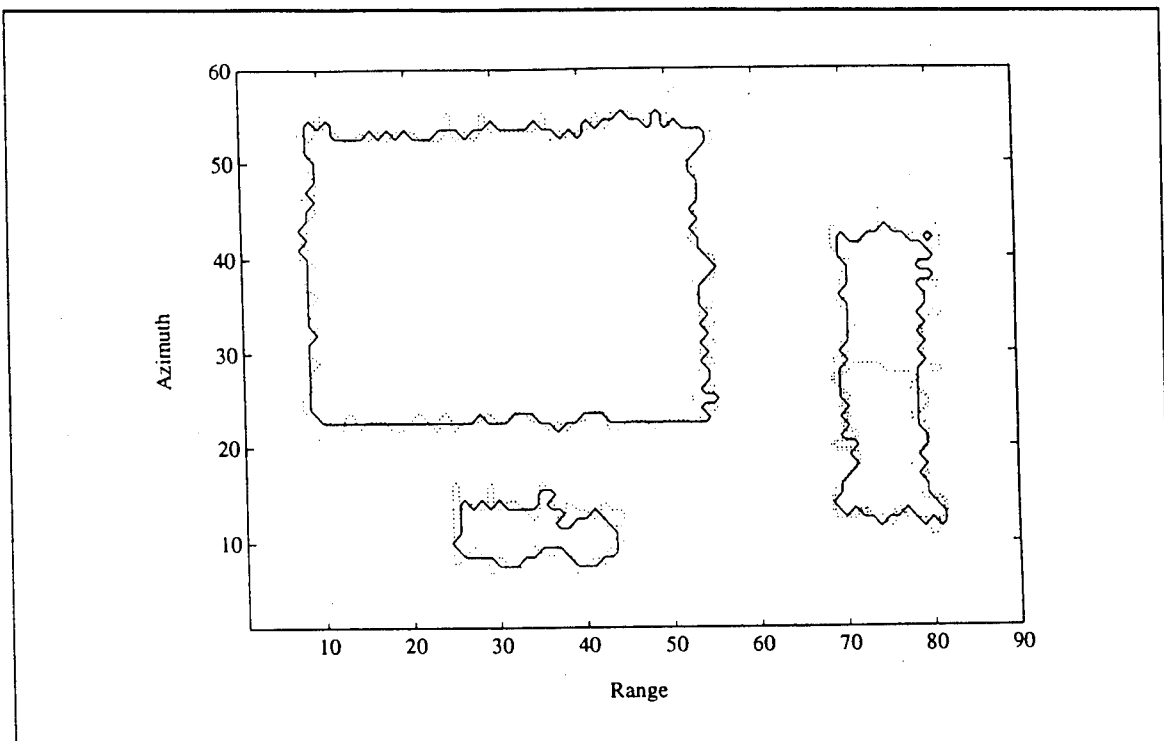


Figure V.4.8 - Contour Plot of the First-Correction Volume with NCQ=5

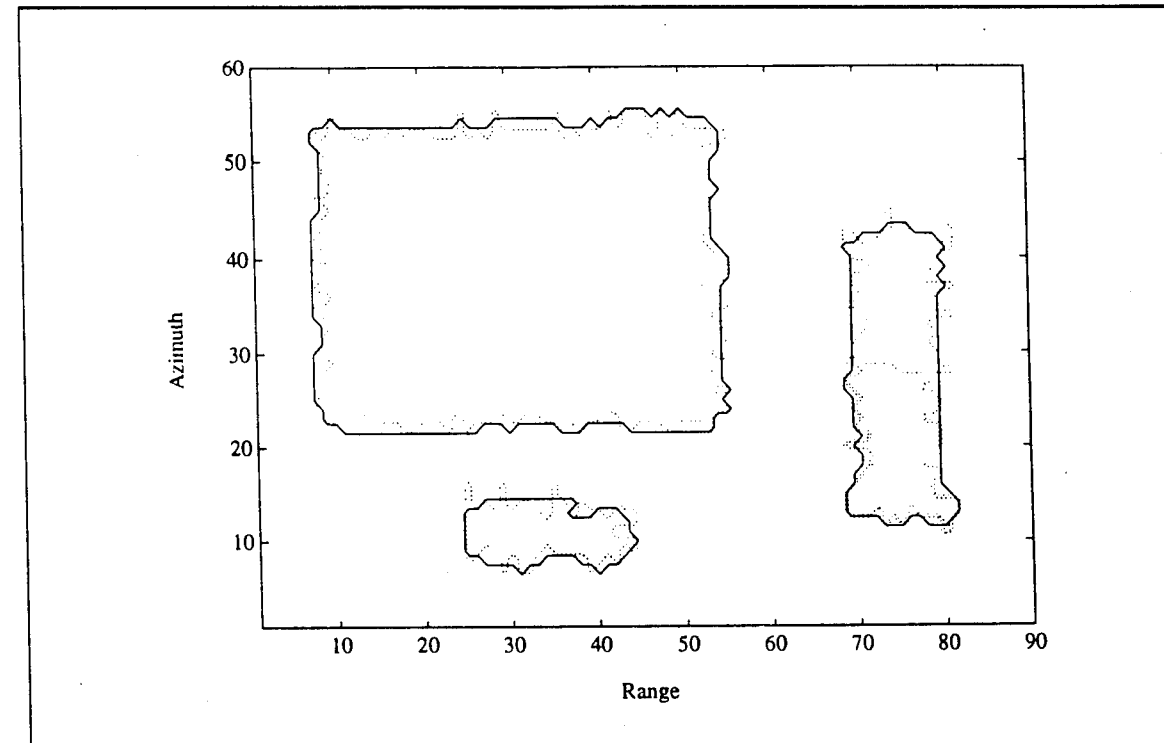


Figure V.4.9 - Contour Plot of the Second-Correction Volume with NCC=3

The results are shown in Figures V.4.10-12, respectively. First, comparing Figures V.4.9 and V.4.10, note that smoothing did not result in any change from the mapped volume. This is because the regions of Figure V.4.9 do not contain any holes whereas the purpose of smoothing is to remove holes. Comparing the edge enhanced regions in Figure V.4.11 (in solid lines) to the ideal one (in dotted lines), one can see how close the two sets of regions have become. In fact, at the end of edge enhancement, 65.54% of the total number of cells are declared BN whereas ideally the BN percentage of the generated scene was 66.07%. Note that, only 10 CL cells were misidentified and associated with the BN. Out of these 6 had data values under the threshold (BNQP=63.37%). Also, 39 BN cells were misidentified and associated with the CL. Of these, 21 had data values above the threshold.

These result in the ratios

$$\frac{\text{misidentified CL cells above the threshold}}{\text{total number of CL cells}} = 0.22 \% \quad (\text{V-4.1})$$

and

$$\frac{\text{misidentified BN cells below threshold}}{\text{total number of BN cells}} = 0.50 \% \quad (\text{V-4.2})$$

Figure V.4.12 shows the edges in the edge detected volume.

An assessment of the mapping procedure results in 3 CL patches with the number of cells for each patch as listed in Table V.4.3. By comparing Tables V.4.1 and V.4.3, notice how close are the number of cells.

Clutter	Number of cells
A	113
C+D	304
B	1444

Table V.4.3 - CL Patch Parameters after Assessment

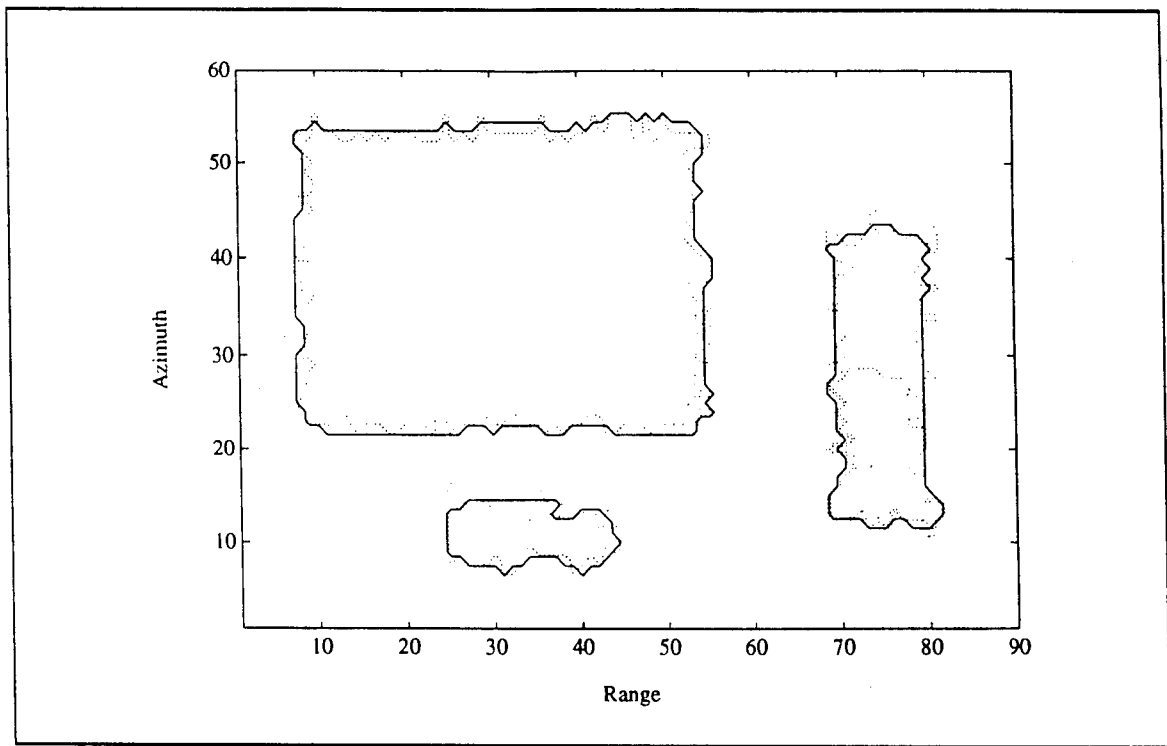


Figure V.4.10 - Contour Plot of the Smoothed Volume with NS=7

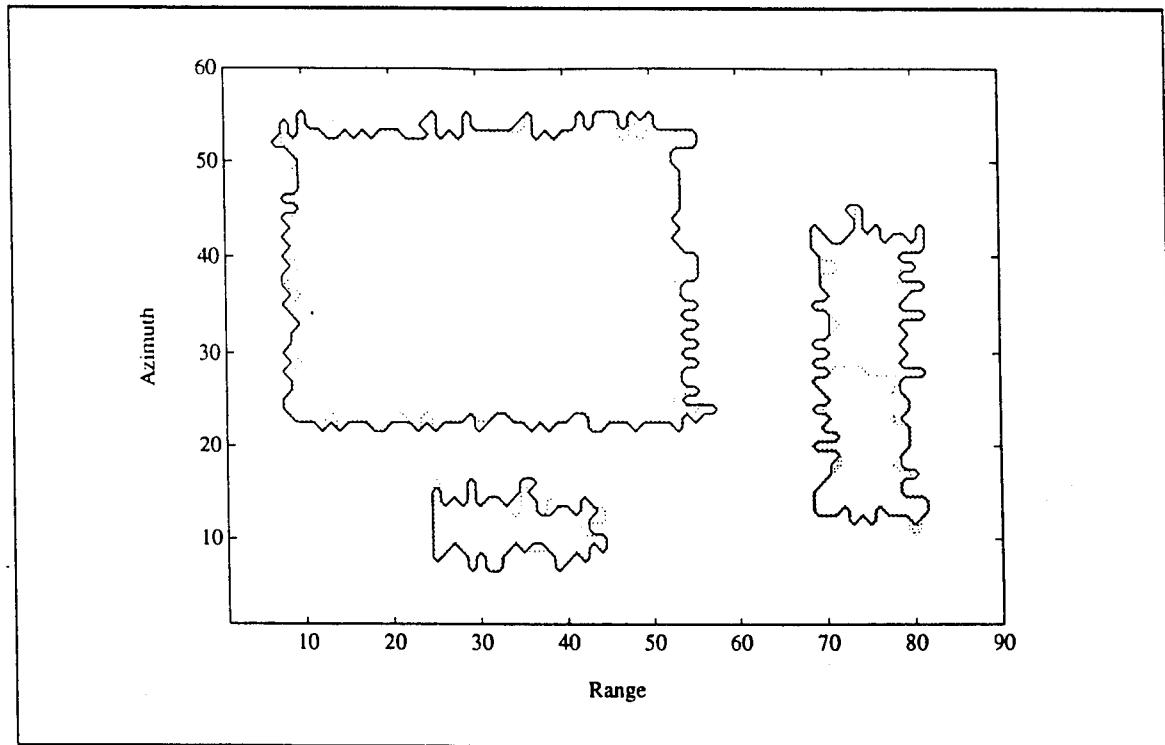


Figure V.4.11 - Contour Plot of the Edge Enhanced Volume

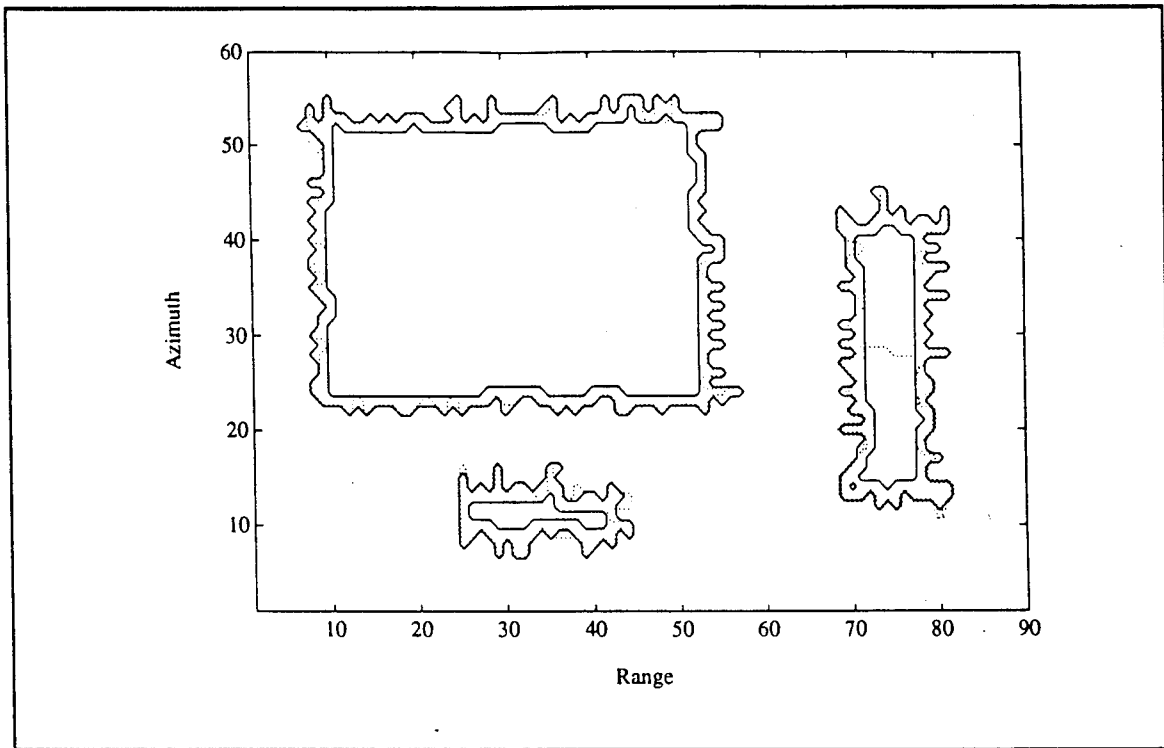


Figure V.4.12 - Contour Plot of the Edge Detected Volume

#### V.4.2.2 - Example 2

Consider, a surveillance volume containing four homogeneous clutter patches, denoted by A, B, C, and D, as shown in Figure V.4.13. Clutter patches C and D are contiguous and form a single nonhomogeneous clutter patch C/D. Table V.4.4 lists the parameters of each CL patch. In addition, the BN which is spread throughout the surveillance volume is Rayleigh distributed.

Clutter	CNR (dB)	Data Distribution	Shape Parameter	Number of cells
A	10	K-distributed	1.5	117
B	10	Weibull	1.0	672
C	10	Lognormal	1.0	151
D	10	Rayleigh	None	151

Table V.4.4 - CL Patch Parameters

In this example, 79.80% of the total scanned volume is occupied by BN alone. Also, CL patch C contains approximately the same number of cells as CL patch D. Figures V.4.13 and V.4.14 show the CL patch boundaries and the three-dimensional envelope plot for the surveillance volume, respectively. The probability density functions and histograms of the background noise and clutter patches are shown in Fig. V.4.15. In this example, not only is the CNR for every patch low but the shape parameters of the PDFs from which the CL data have been generated are such that the CL in patches A, B, and C is very spiky, as shown by the long tails in Figure V.4.15.b, c, and d. The shape of the histograms for CL patches A, B, and C is such that a lot of CL data overlap the BN data in value making it difficult to separate between the BN and CL patches just by setting a threshold.

The iteration process begins with the threshold, once again, arbitrarily set such that 10% of the sorted data are below the threshold, i.e BNQP=10%. With this setting, the contour plot of the quantized volume is shown in Figure V.4.16. In this figure, the closed solid line contours surround the BN declared regions and the rest is CL. Notice that a lot of BN cells have data exceeding the threshold because the threshold was set very low. This results in a lot of small BN regions. For the purpose of comparison, the boundaries of the original CL patches are shown in dotted lines. With, NCQ set to 8 and NCC set to 1, the contour plots resulting from the first and second-corrections, respectively, are shown in Figures V.4.17 and V.4.18.

As shown in Table V.4.5, when BNQP=10% and (NCQ,NCC)=(8,1), BNCCP=20.59% which results in  $|BNQP-BNCCP|=10.59\%$  being large. A new threshold is then chosen so that BNQP=20.59% which is the previous value obtained for BNCCP. The iterative process continues until it is found for BNQP=75.78%, NCQ=5, and NCC=1, that  $|BNQP-BNCCP|<1\%$ . In particular, for these parameter values  $|BNQP-BNCCP|=|75.78-75.31|<1\%$ . At this stage the assessment passes and the iterative process stops.

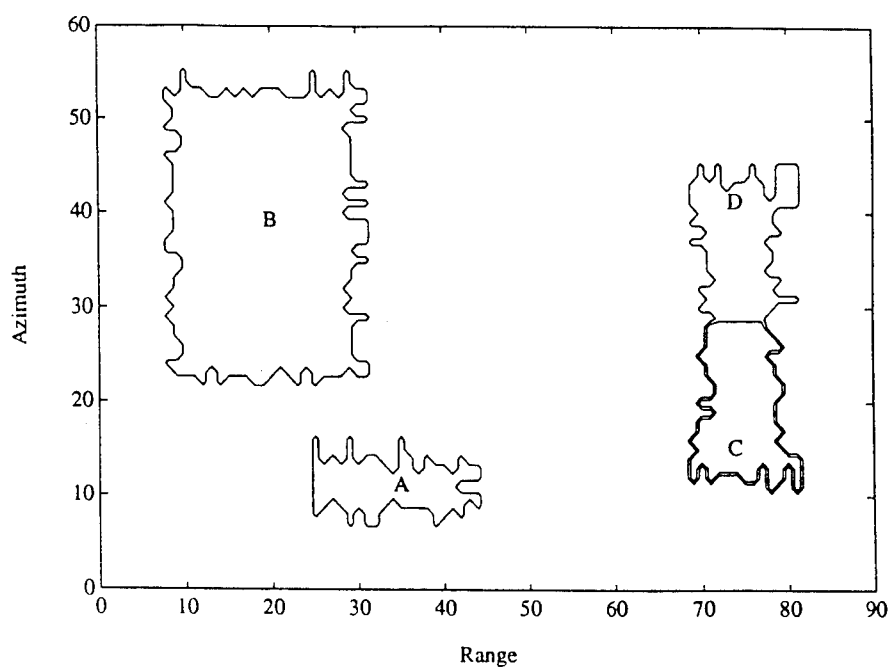


Figure V.4.13 - Boundaries of the CL Regions

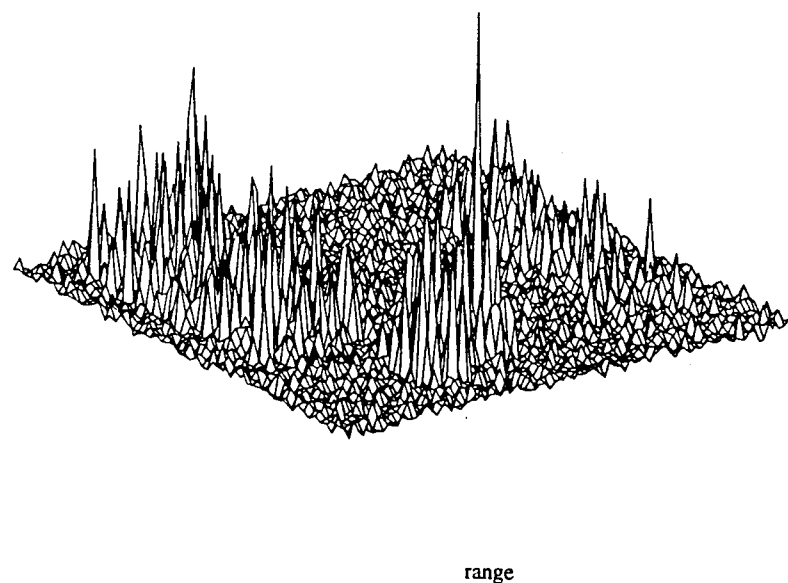
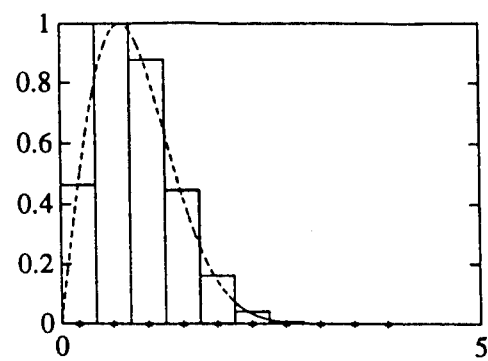
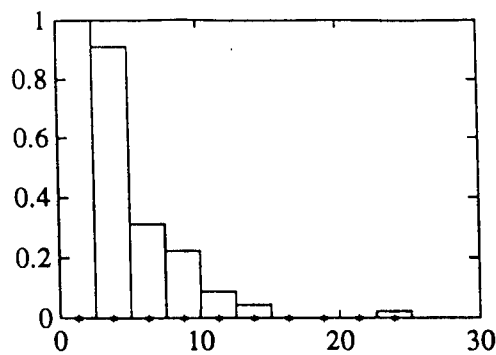


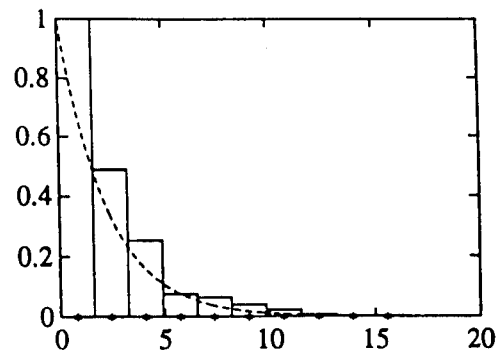
Figure V.4.14 - 3-D Plot of the Surveillance Volume



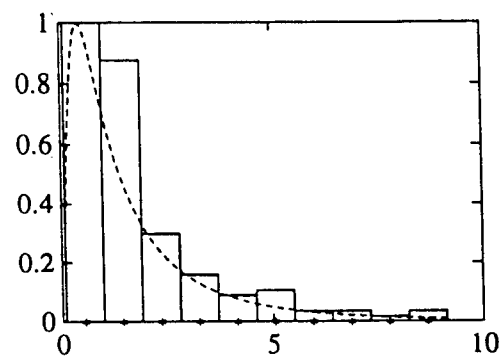
- a -



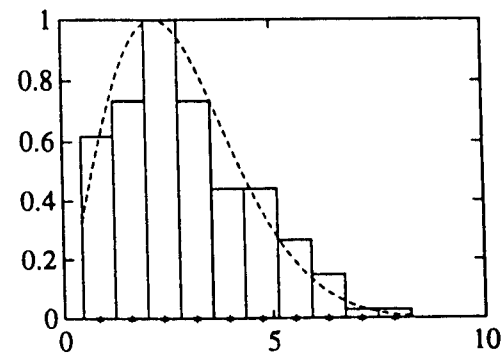
- b -



- c -



- d -



- e -

Figure V.4.15 - Probability Density Functions and Histograms of the Background Noise and Clutter Patches (a) Rayleigh distributed background noise, (b) K-distributed CL A, (c) Weibull CL B, (d) Lognormal distributed CL C, (e) Rayleigh distributed CL D

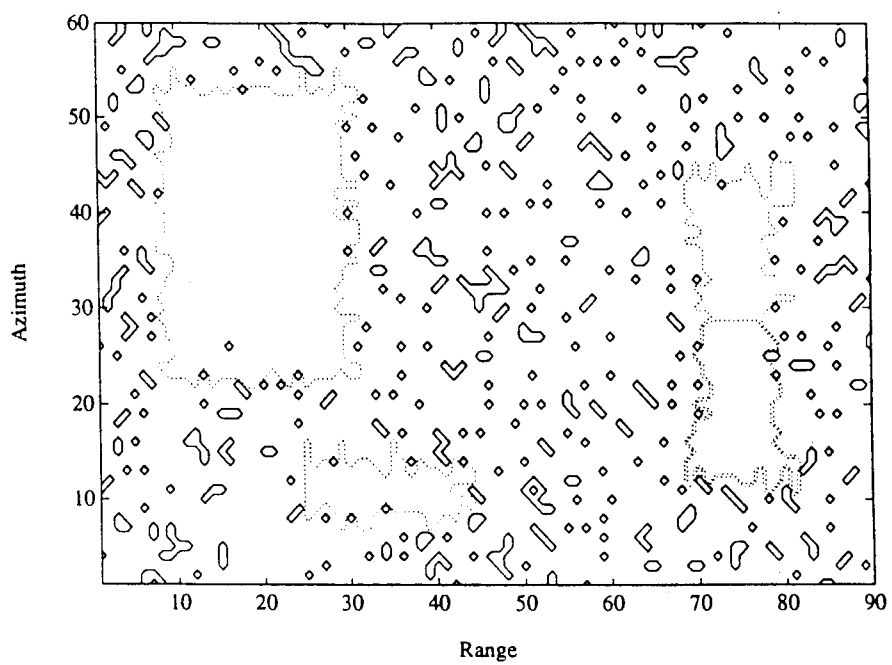


Figure V.4.16 - Contour Plot of the Quantized Volume with BNQP=10%

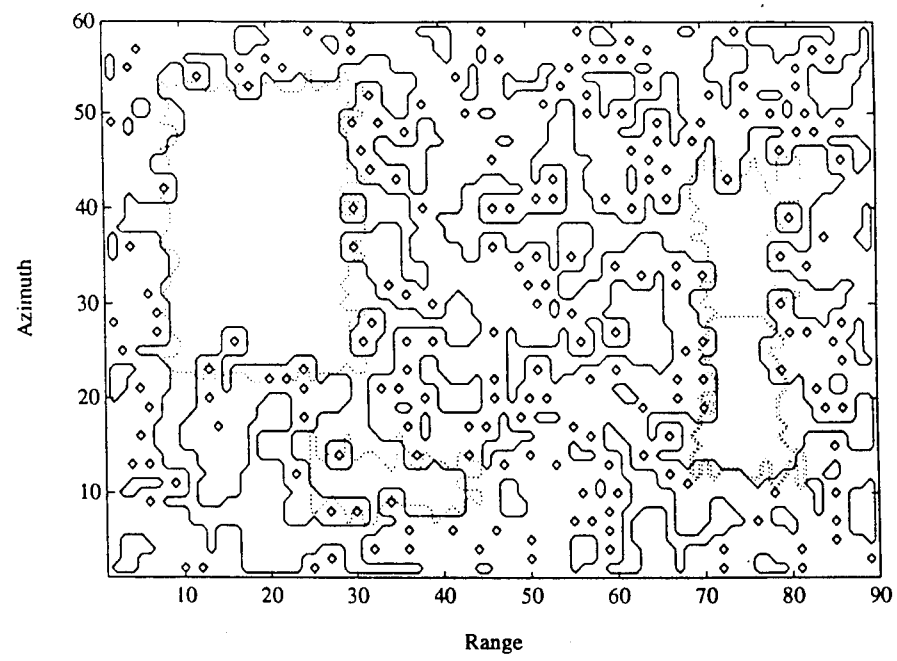


Figure V.4.17 - Contour Plot of the First-Correction Volume with NCQ=8

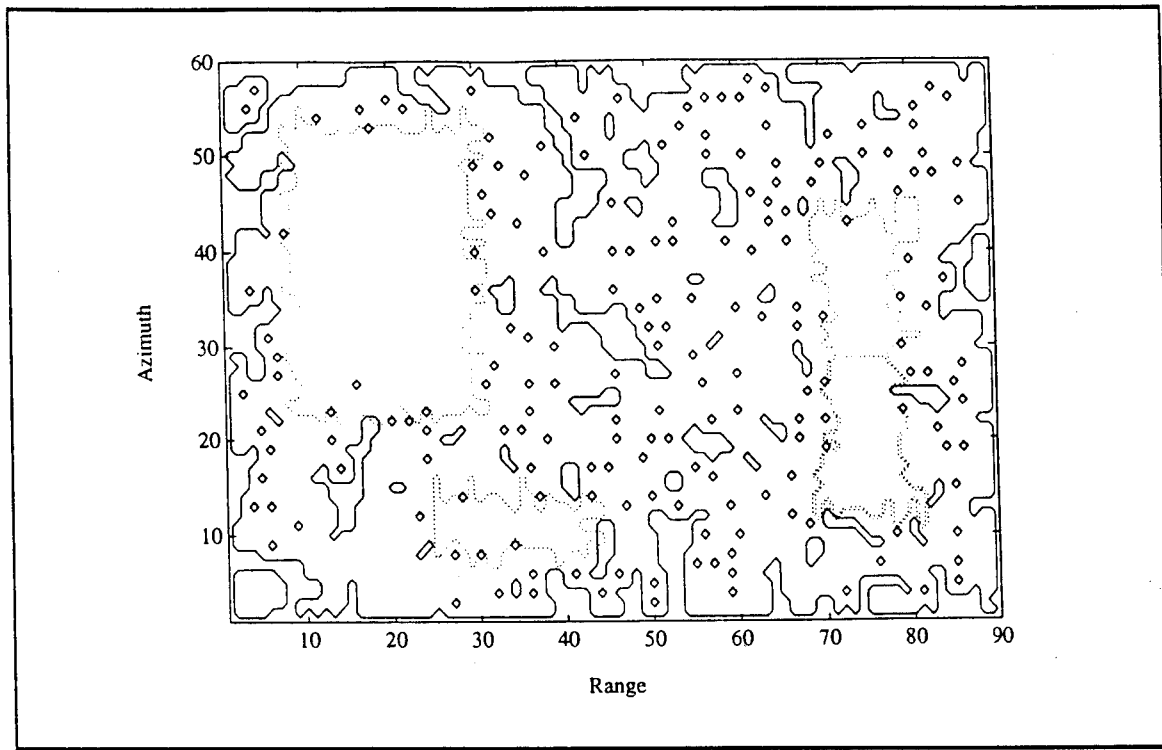


Figure V.4.18 - Contour Plot of the Second-Correction Volume with NCC=1

BNQP (%)	Parameter Values	
10.00 (guess)	NCQ=8 NCC=1	BNCQP=56.35 BNCCP=20.59
20.59 latest BNCCP	NCQ=8 NCC=1	BNCQP=77.43 BNCCP=48.04
48.04 latest BNCCP	NCQ=7 NCC=1	BNCQP=84.11 BNCCP=72.30
72.30 latest BNCCP	NCQ=5 NCC=1	BNCQP=82.17 BNCCP=73.94
72.30 same as latest BNQP	NCQ=5 NCC=3	BNCQP=82.17 BNCCP=79.26
75.78 half way rule	NCQ=5 NCC=1	BNCQP=83.50 BNCCP=75.31

Table V.4.5 - Settings of BNQP

Figures V.4.19-21 show the contour plots obtained after quantization, first-

correction and second-correction, respectively, when BNQP=75.78%, NCQ=5 and NCC=1. First, note from Figure V.4.19 that even with this setting of BNQP where the threshold is very close to its true value, a lot of BN data exceed the threshold and form very small CL patches, and also, a lot of the CL data in every patch falls below the threshold causing holes in the CL patch. Figure V.4.20 shows how most of the erroneously declared BN and CL cells have been correctly reclassified as CL and BN cells, respectively. Next, the edges are augmented as shown in Figure V.4.21. However, comparing the resulting edge contour to the ideal one shows that not all the edges have been completely recovered even though the CL patches have been identified. Also, notice in this case that the CL patches are not homogeneous and contain holes in them.

Next, smoothing, edge enhancement and edge detection are performed. The results are shown in Figures V.4.22-24, respectively. First, comparing Figures V.4.21 and V.4.22, note that the smoothing reclassified the BN declared cells causing holes inside the CL as CL cells. Comparing the edge enhanced regions in Figure V.4.23 (in solid lines) to the ideal one (in dotted lines), one can see how close the two sets of regions have become. In fact, at the end of edge enhancement, 80.31% of the total number of cells are declared BN where as ideally the BN percentage of the generated scene was 79.80%. Note that, 86 CL cells were misidentified and associated with the BN. Out of these 72 had data values under the threshold (BNQP=79.59%). Also, 58 BN cells were misidentified and associated with the CL. Of these, 32 had data values above the threshold. These result in

$$\frac{\text{misidentified CL cells above the threshold}}{\text{total number of CL cells}} = 1.28 \% \quad (\text{V-4.3})$$

$$\frac{\text{misidentified BN cells below the threshold}}{\text{total number of BN cells}} = 0.60 \% \quad (\text{V-4.4})$$

Figure V.4.24 shows the edges of the edge detected volume.

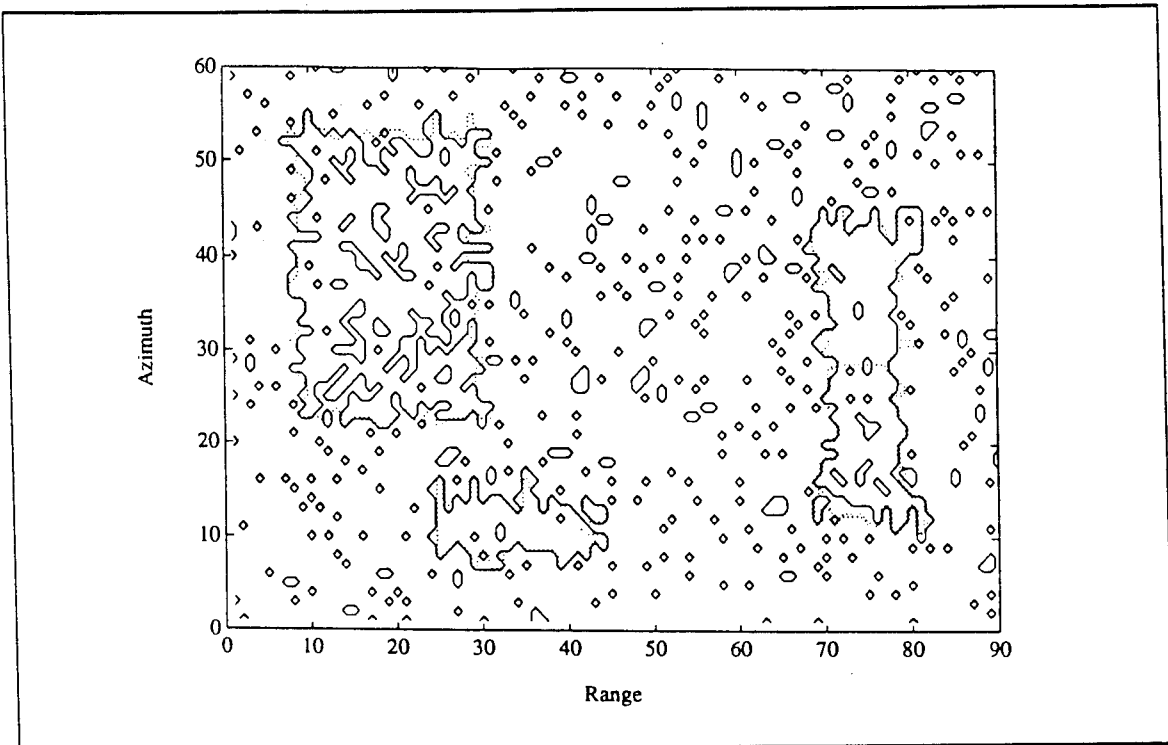


Figure V.4.19 - Contour Plot of the Quantized Volume with BNQP=75.78%

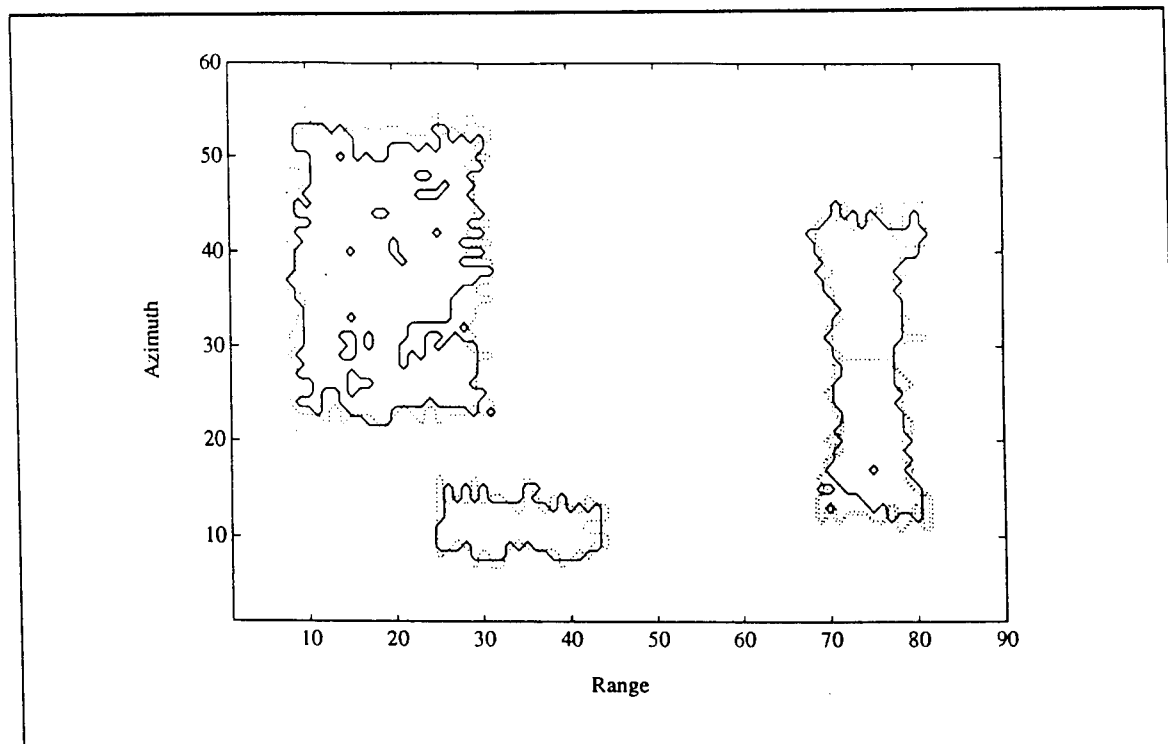


Figure V.4.20 - Contour Plot of the First-Correction Volume with NCQ=5

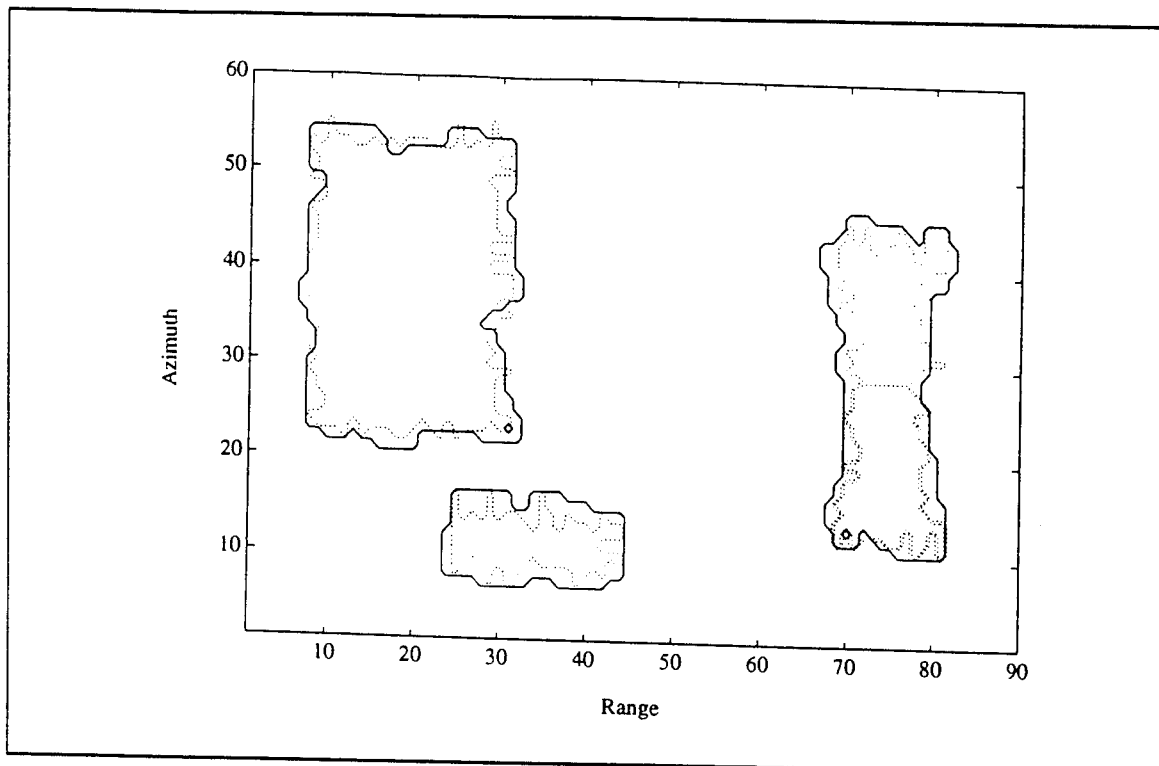


Figure V.4.21 - Contour Plot of the Second-Correction Volume with NCC=1

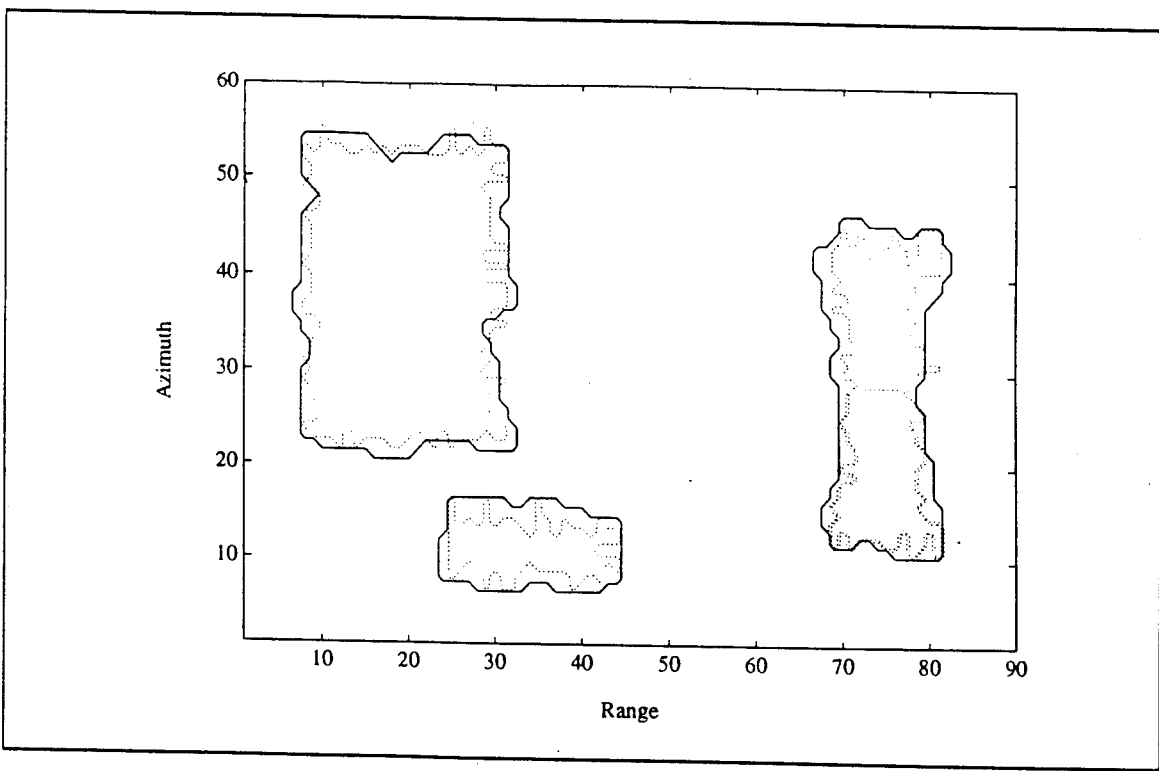


Figure V.4.22 - Contour Plot of the Smoothed Volume with NS=7

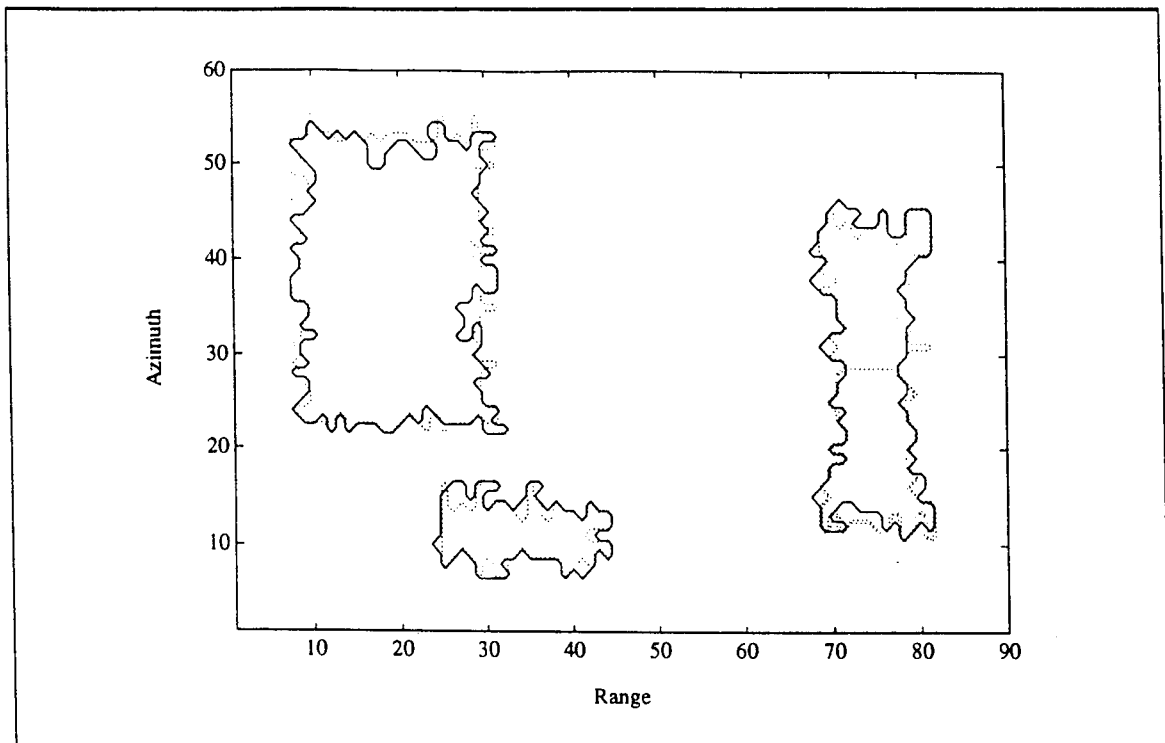


Figure V.4.23- Contour Plot of the Edge Enhanced Volume

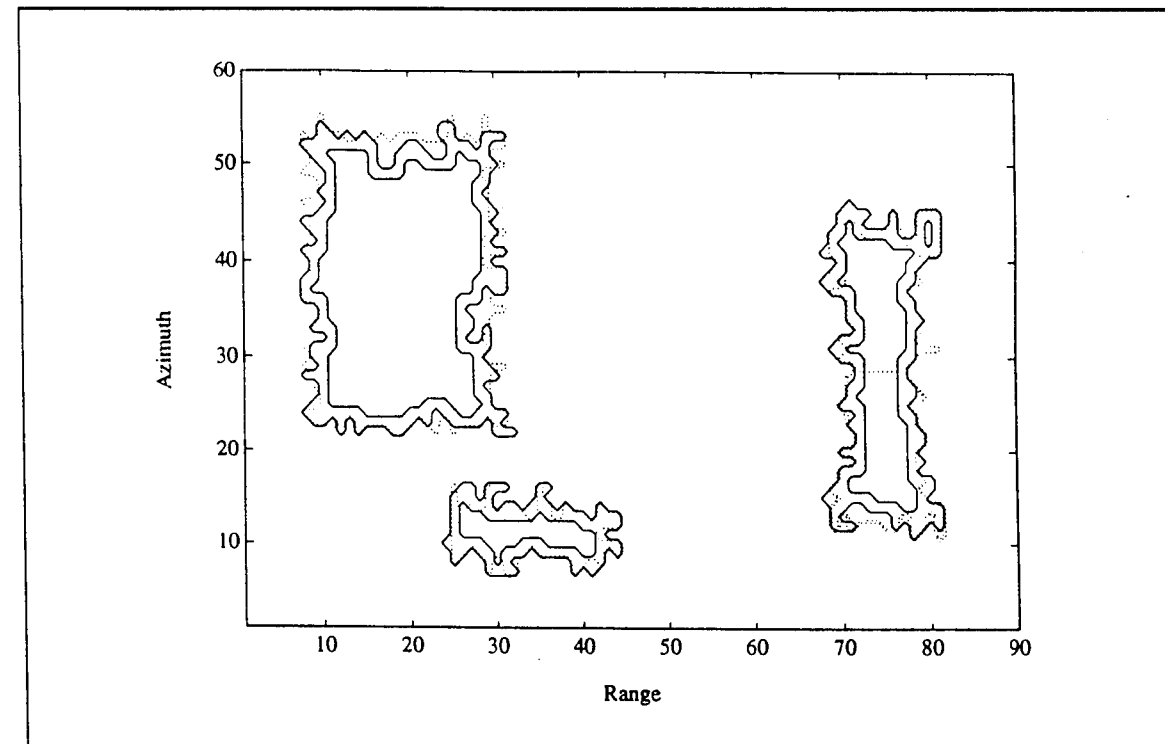


Figure V.4.24 - Contour Plot of the Edge Detected Volume

An assessment of the mapping procedure results in 3 CL patches with the number of cells for each patch as listed in Table V.4.6. By comparing Tables V.4.4 and V.4.6, notice how close are the number of cells.

Clutter	Number of cells
A	133
C+D	308
B	622

Table V.4.6 - CL Patch Parameters after Assessment

#### V.4.2.3 - Example 3

Consider a surveillance volume containing four homogeneous clutter patches, denoted by A, B, C, and D, as shown in Figure V.4.25. Clutter patches C and D are contiguous and form a single nonhomogeneous clutter patch C/D. Table V.4.7 lists the parameters of each CL patch. In addition, the BN is Rayleigh distributed.

Clutter	CNR (dB)	Data Distribution	Shape Parameter	Number of cells
A	10	Rayleigh	None	117
B	10	K-distributed	10.0	298
C	10	Lognormal	0.01	161
D	10	Weibull	10.0	162

Table V.4.7 - CL Patch Parameters

In this example, 86.33% of the total scanned volume is occupied by BN alone. Also, CL patch C contains approximately the same number of cells as CL patch D. Figures V.4.25 and V.4.26 show the CL patch boundaries and the three-dimensional plot of the surveillance volume, respectively. Notice in Figure V.4.26 how small are some of the CL data compared to the BN data, and how large are

some of the BN data compared to the CL data. This is due to the fact that the CNR for each patch is low. (Assuming a SNR of 10dB in order to obtain reasonable detections in the absence of CL, CNR=10dB implies equal signal and CL powers. For values of CNR less than 10dB, the signal would be larger than CL and no WSC would be available). In this example the mapping procedure is tested on a situation where the CNR for every CL patch is low. The probability density functions and histograms of the background noise and clutter patches are shown in Fig. V.4.27. Comparing the histograms in Figures V.4.27.a, b, c, and e, notice that some of the BN data are higher than some of the CL data in patches A, B, and D. Also, observe that overlapping between the histograms of the BN with CL patches A and B is noticeable.

The iteration process begins with the threshold, once again, set such that 10% of the sorted data are below the threshold, i.e BNQP=10%. With this setting, the contour plot of the quantized volume is shown in Figure V.4.28. In this figure, the closed solid line contours surround the BN declared regions and the rest is CL. Notice that a lot of BN cells have data that exceed the threshold because the threshold was set very low. This results in a lot of small BN regions. For purpose of comparison, the boundaries of the original CL patches are shown in dotted lines. With NCQ set to 8 and NCC set to 1, the contour plots resulting from the first and second-corrections are shown in Figures V.4.29 and V.4.30, respectively.

As shown in Table V.4.8, when BNQP=10% and (NCQ,NCC)=(8,1), BNCCP=20.04% which results in  $|BNQP-BNCCP|=10.04\%$  being large. A new threshold is then chosen so that BNQP=20.04% which is the previous value obtained for BNCCP. The iterative process continues until it is found for BNQP=84.70%, NCQ=5, and NCC=3, that  $|BNQP-BNCCP|<1\%$ . For these parameter values,  $|BNQP-BNCCP|=|84.70-85.46|<1\%$ . At this stage the assessment passes and the iterative process stops.

Figures V.4.31-33 show the contour plots obtained after quantization, first-correction and second-correction, respectively, when BNQP=84.70%, NCQ=5 and NCC=3. First, note from Figure V.4.31 that even with this setting of BNQP, where the threshold is very close to its true value some of the BN data exceed the threshold and form very small CL patches, and some of the CL data in every patch falls below the threshold causing holes in the CL patch. Figure V.4.32 shows how most of the erroneously declared BN and CL cells have been correctly reclassified as BN and CL cells, respectively. Next, the edges are augmented as shown in Figure V.4.33. However, comparing the resulting contour to the ideal one shows that even though the CL patches have been identified, the edges are not completely recovered.

BNQP (%)	Parameter Values	
10.00 (guess)	NCQ=8 NCC=1	BNCQP=56.17 BNCCP=20.04
20.04 latest BNCCP	NCQ=8 NCC=1	BNCQP=77.98 BNCCP=43.78
43.78 latest BNCCP	NCQ=8 NCC=1	BNCQP=90.78 BNCCP=82.65
82.65 latest BNCCP	NCQ=7 NCC=1	BNCQP=91.17 BNCCP=84.70
84.70 latest BNCCP	NCQ=5 NCC=1	BNCQP=87.61 BNCCP=82.00
84.70 same as latest BNQP	NCQ=5 NCC=3	BNCQP=87.61 BNCCP=85.46

*Table V.4.8 - Settings of BNQP*

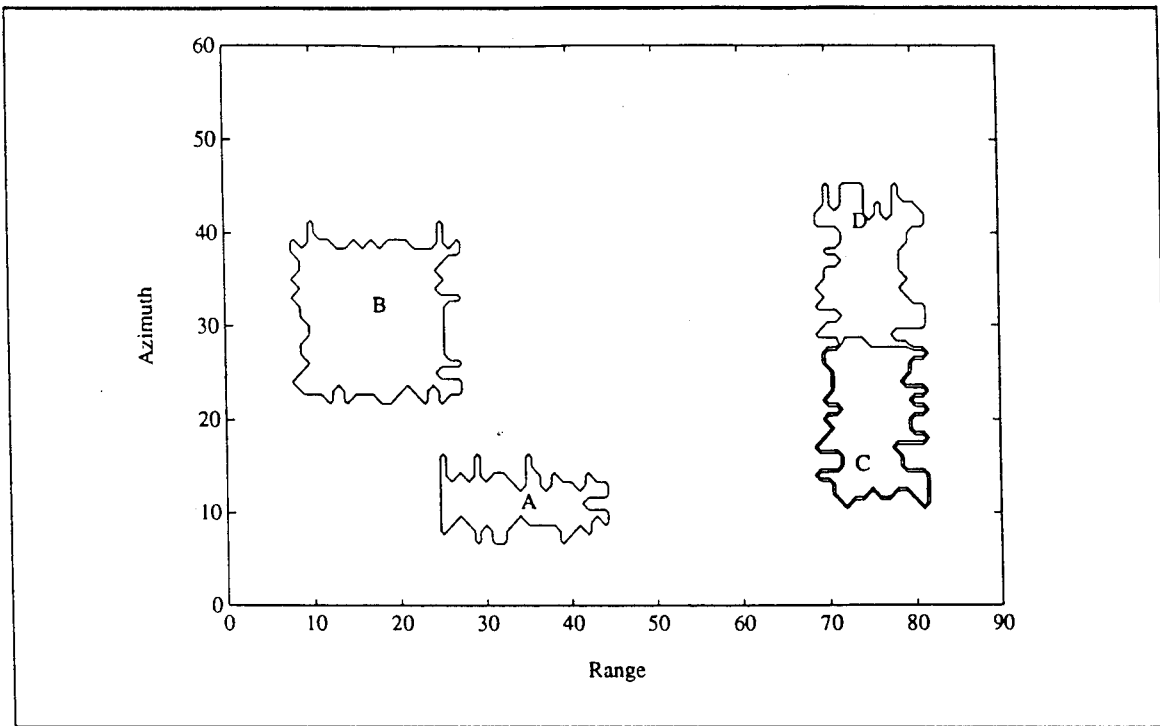


Figure V.4.25 - Boundaries of the CL Regions

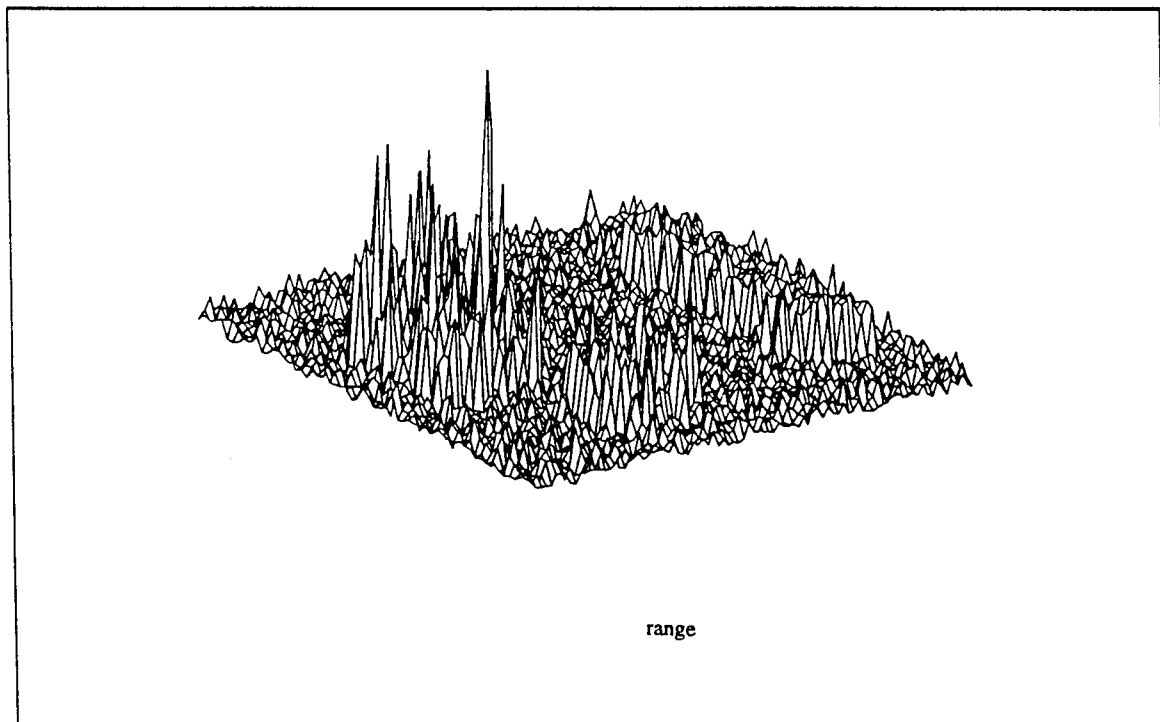
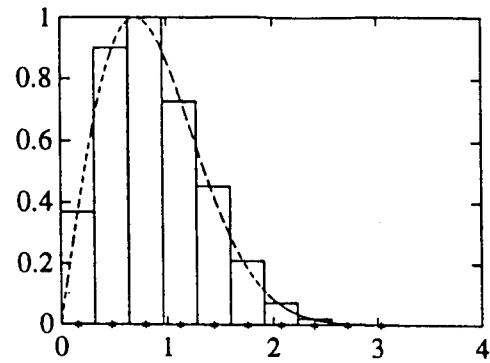
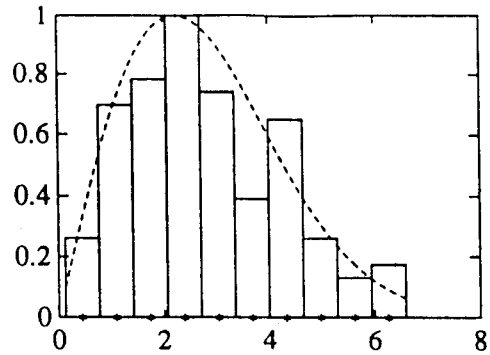


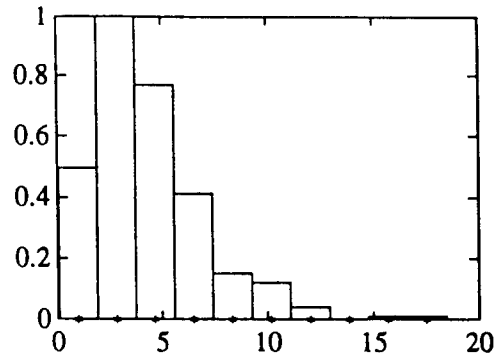
Figure V.4.26 - 3-D Plot of the Surveillance Volume



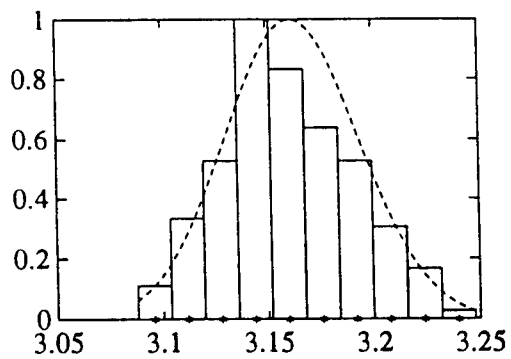
- a -



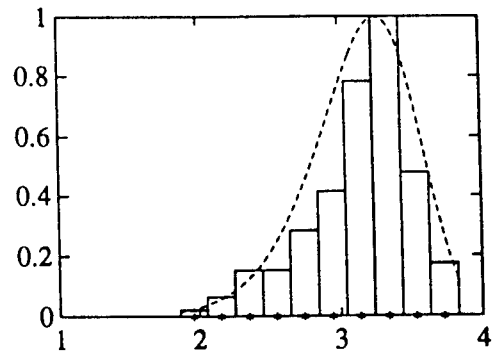
- b -



- c -



- d -



- e -

Figure V.4.27 - Probability Density Functions and Histograms of the Background Noise and Clutter Patches (a) Rayleigh distributed background noise, (b) Rayleigh distributed CL A, (c) K-distributed CL B, (d) Lognormal distributed CL C, (e) Weibull distributed CL D

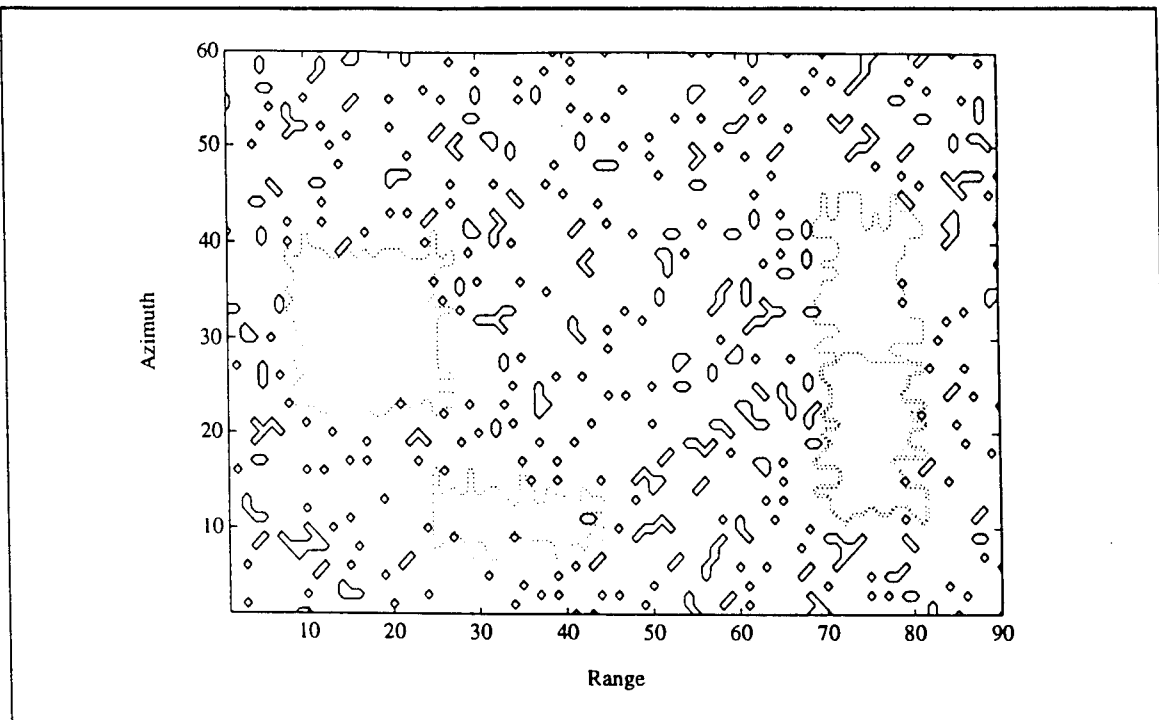


Figure V.4.28 - Contour Plot of the Quantized Volume with BNQP=10%

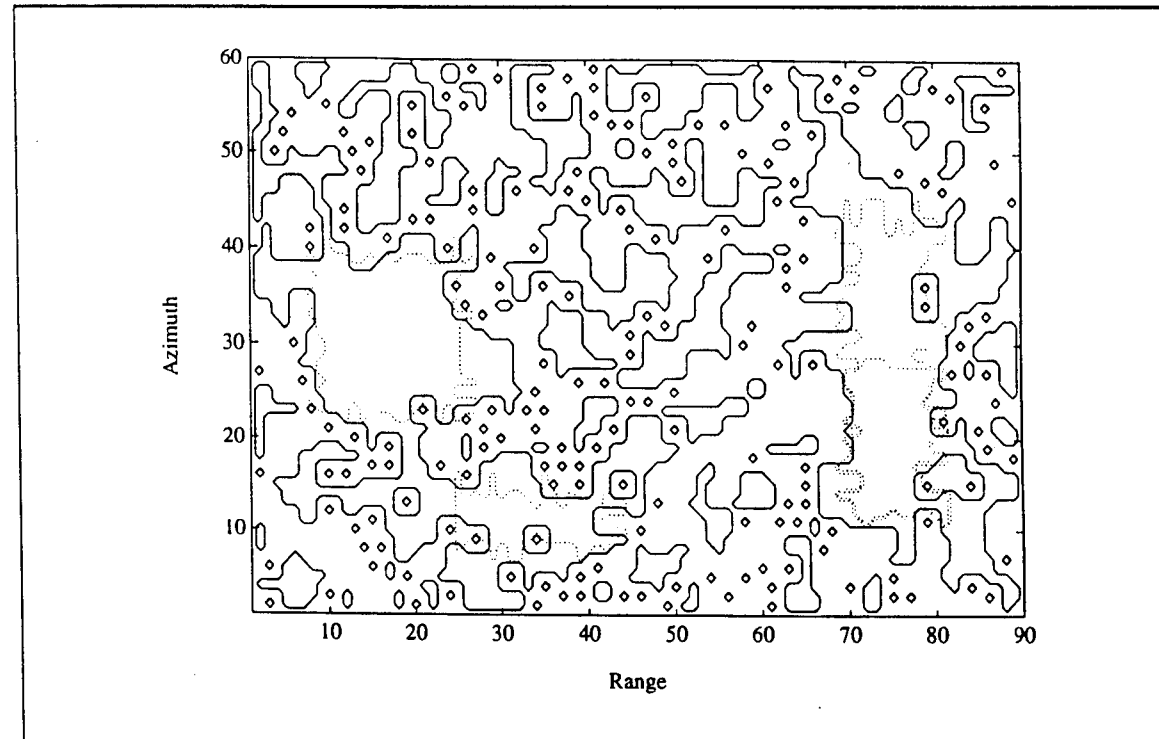


Figure V.4.29 - Contour Plot of the First-Correction Volume with NCQ=8

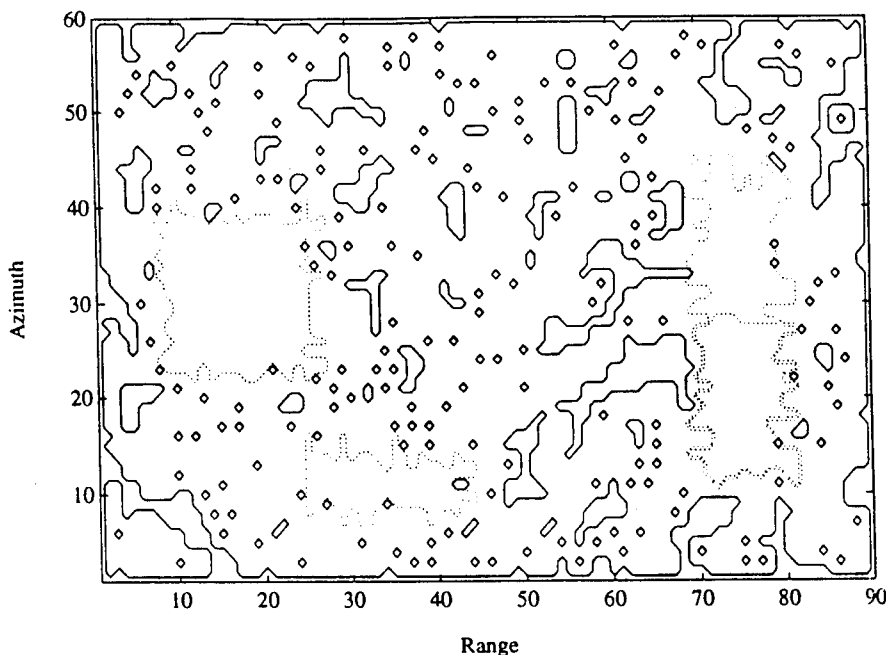


Figure V.4.30 - Contour Plot of the Second-Correction Volume with NCC=1

Next, smoothing, edge enhancement and edge detection are performed. The results are shown in Figures V.4.34-36, respectively. First, comparing Figures V.4.33 and V.4.34, note that smoothing did not result in any change from the mapped volume. This is because the regions of Figure V.4.33 do not contain any holes whereas the purpose of smoothing is to remove holes. Comparing the edge enhanced regions in Figure V.4.35(in solid lines) to the ideal one (in dotted lines), one can see how close the two sets of regions have become. In fact, at the end of edge enhancement, 85.72% of the total number of cells are declared BN where as ideally the BN percentage of the generated scene was 86.33%. Note that only 6 CL cells were misidentified and associated with the BN. Out of these 5 had data values under the threshold (BNQP=84.70%). Also, 39 BN cells were misidentified and associated with the CL. Of these, 10 had data values above the threshold. These result in

$$\frac{\text{misidentified CL cells above the threshold}}{\text{total number of CL cells}} = 0.13 \% \quad (\text{V-4.5})$$

and

$$\frac{\text{misidentified BN cells below the threshold}}{\text{total number of BN cells}} = 0.62 \% \quad (\text{V-4.6})$$

Figure V.4.36 shows the edges of the edge detected volume.

An assessment of the mapping procedure results in 3 CL patches with the number of cells for each patch as listed in Table V.4.9. By comparing Tables V.4.7 and V.4.9, notice how close are the number of cells.

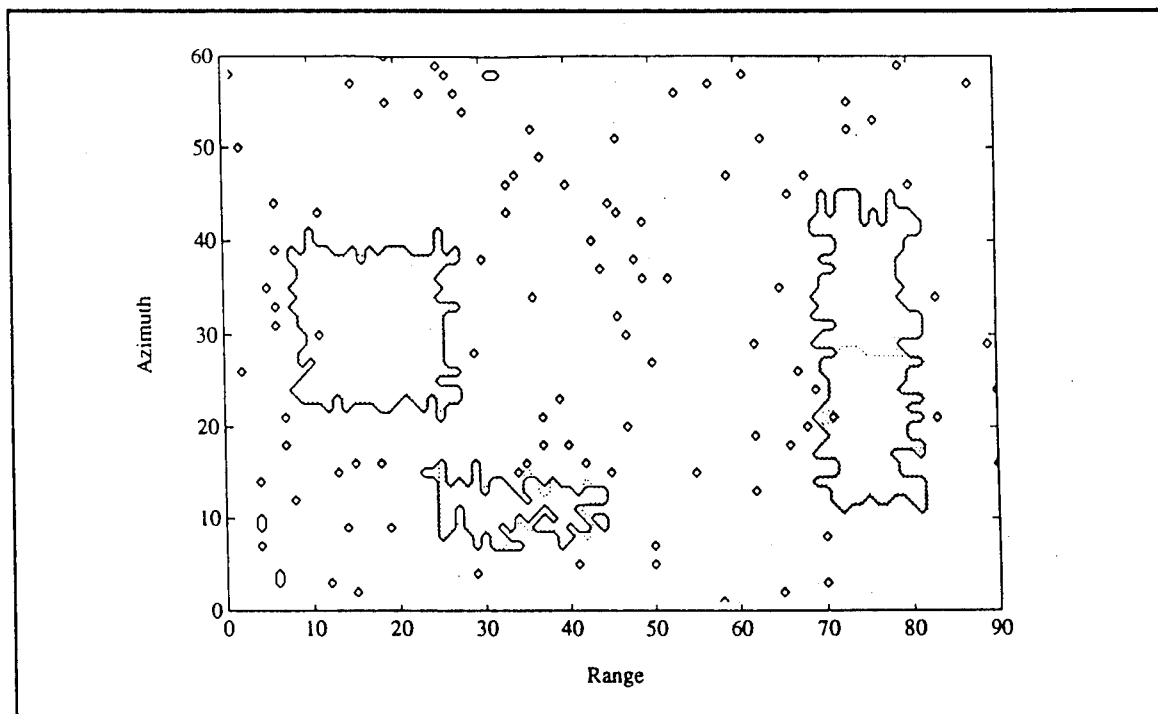


Figure V.4.31 - Contour Plot of the Quantized Volume with BNQP=84.70%

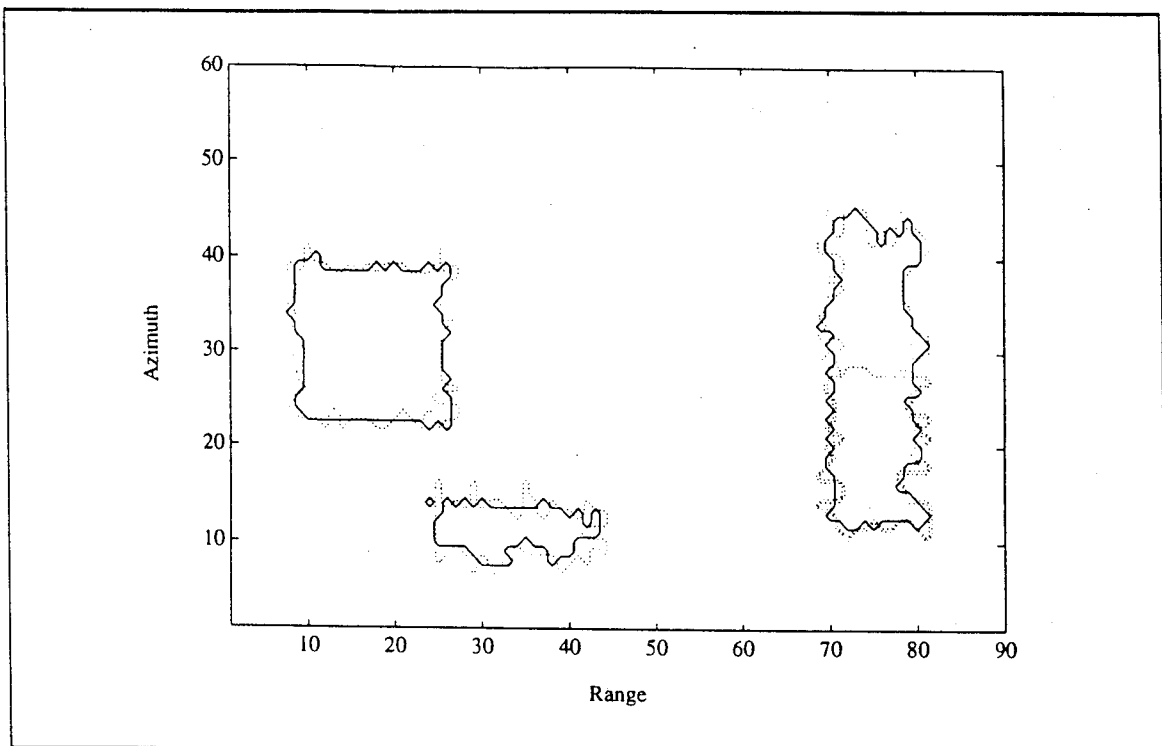


Figure V.4.32 - Contour Plot of the First-Correction Volume with NCQ=5

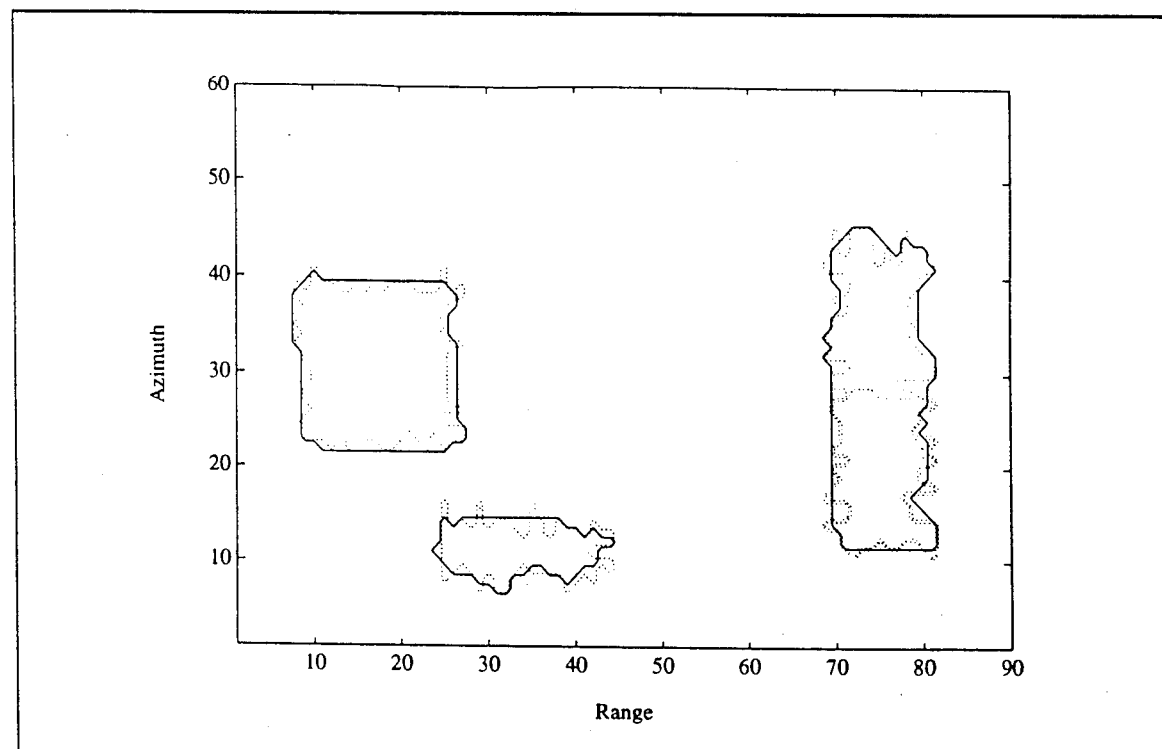


Figure V.4.33 - Contour Plot of the Second-Correction Volume with NCC=3

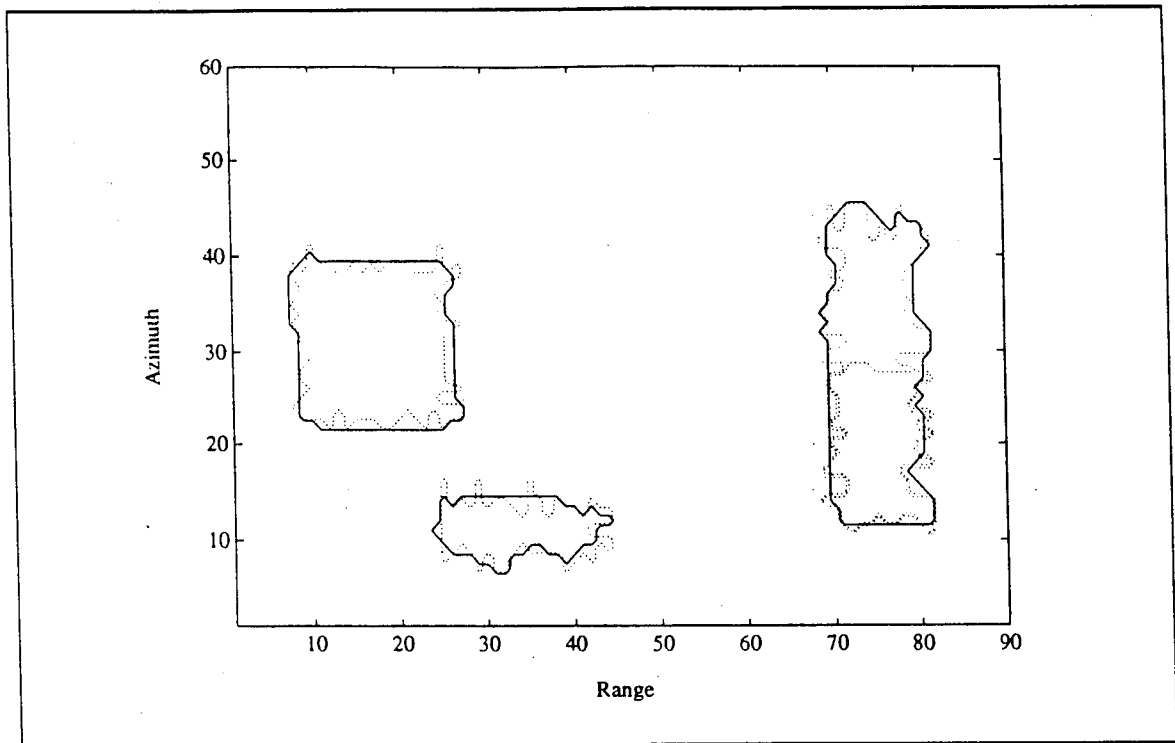


Figure V.4.34 - Contour Plot of the Smoothed Volume with NS=7

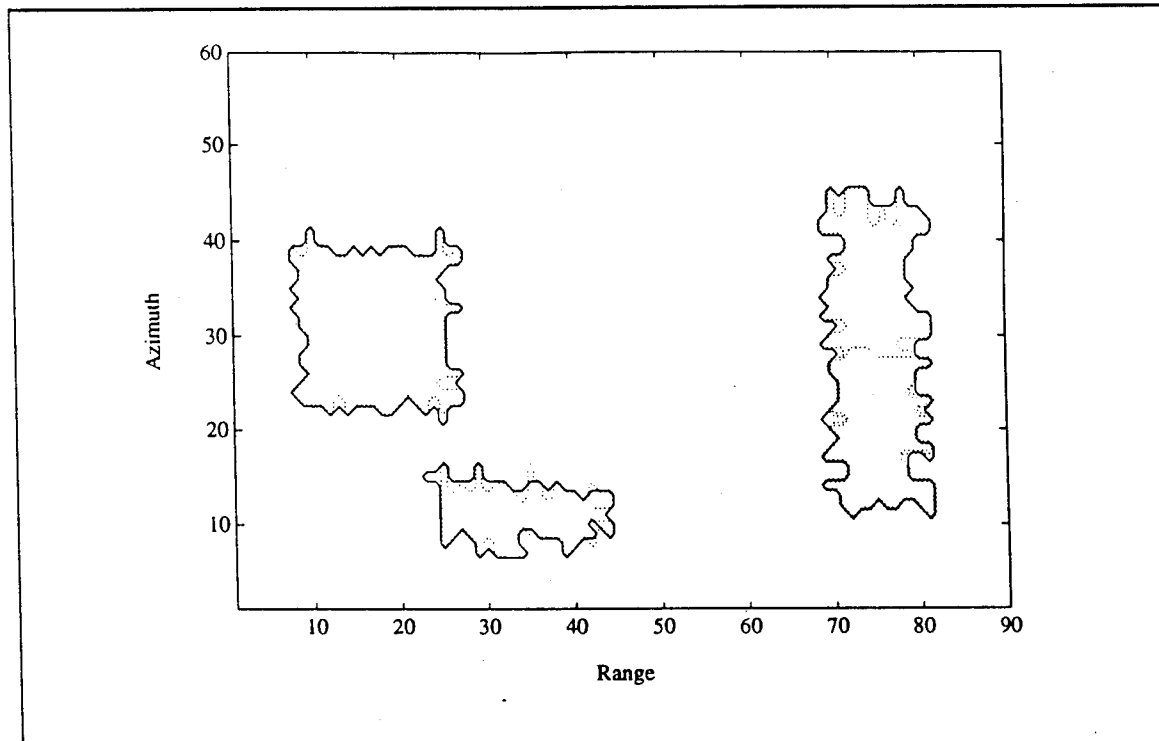


Figure V.4.35 - Contour Plot of the Edge Enhanced Volume

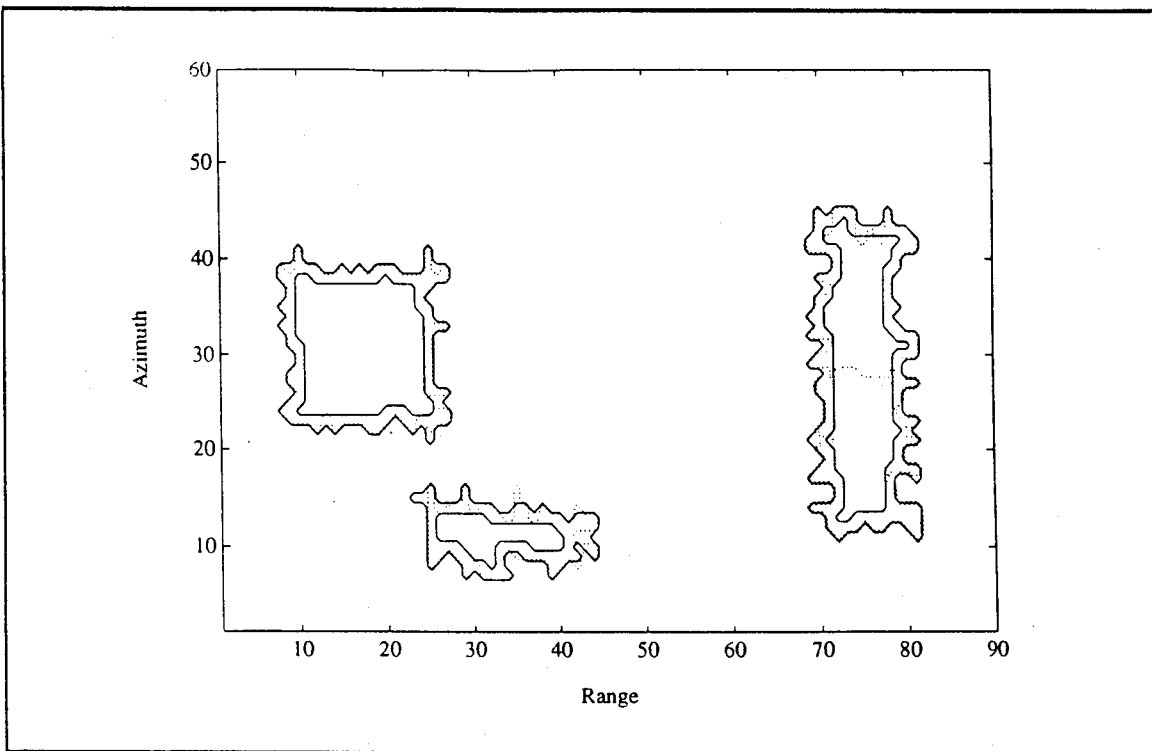


Figure V.4.36 - Contour Plot of the Edge Detected Volume

Clutter	Number of cells
A	124
C+D	341
B	306

Table V.4.9 - CL patch parameters after assessment

## V.5 - Convergence of the Mapping Procedure

### V.5.1 - Introduction

Consider an image containing two regions where the PDFs for each region have nicely separated peaks as shown in Fig. V.5.1 (a) and the overall PDF for both regions is as shown in Fig. V.5.1 (b). In practice, a histogram is generated that approximates the overall PDF. Note that the individual PDF of each region is

unknown. However, because the individual PDFs are adequately separated, the overall histogram will be bimodal and separation between the two regions is readily obtained by placing the threshold  $T_1$  between the two peaks as shown in Fig. V.5.1 (b). Cells with data values lower than  $T_1$  are declared as belonging to region 1, while cells with data values higher than  $T_1$  are declared as belonging to region 2.

Now consider the slightly overlapping PDFs as shown in Figs. V.5.2 (a) and (b). Although the overall PDF of the data regions is again bimodal, there is now noticeable overlap between the tails. Once again, a threshold  $T_1$  is used to separate between the two regions. However, now a significant number of cells will be misclassified and corrections should be made to the extent possible.

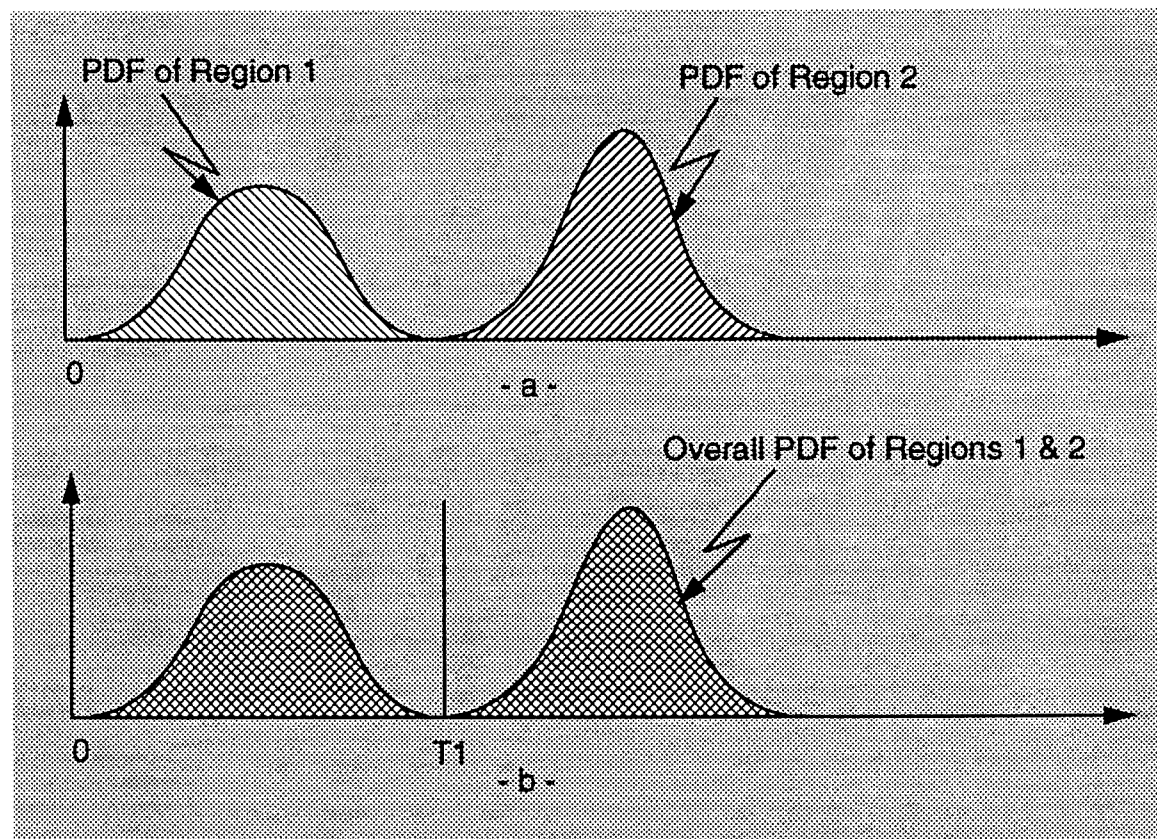


Figure V.5.1 - Non-overlapping PDFs of Two Distinct Regions  
 (a) Individual PDFs for Each Region, (b) Overall PDF for Both Regions

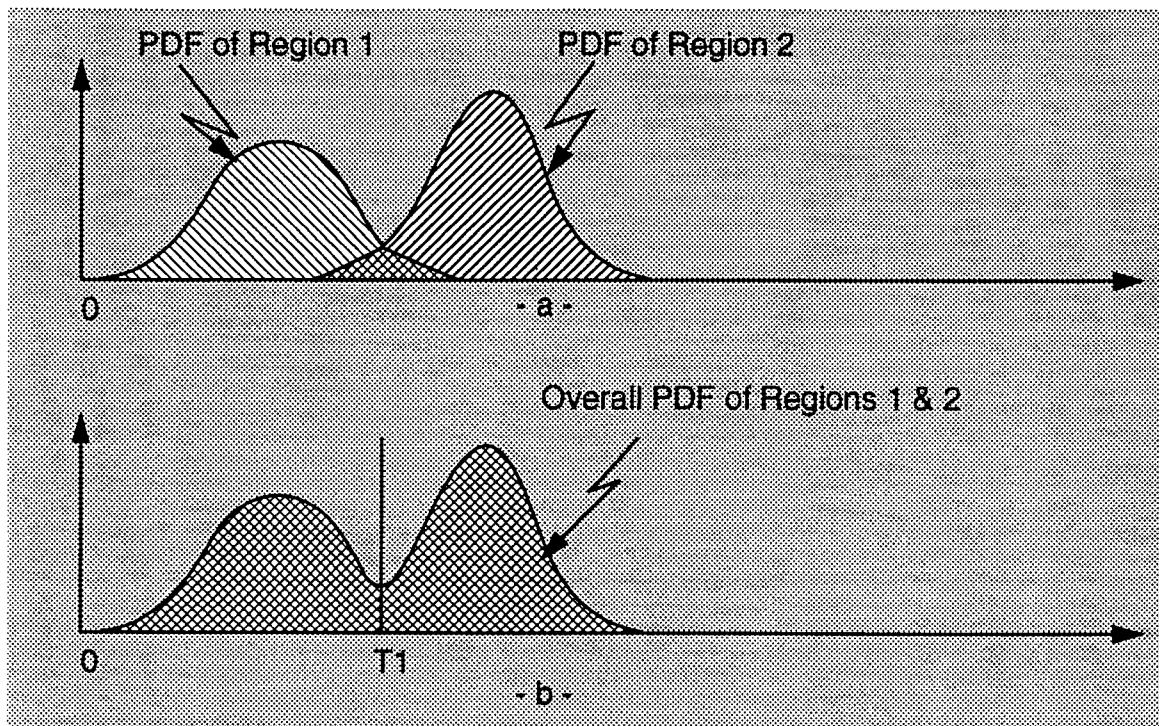


Figure V.5.2 - Overlapping PDFs of Two Distinct Regions with a Small Overlapping Area

(a) Individual PDFs for Each Region. (b) Overall PDF for Both Regions

Fig. V.5.3 shows a more complicated case where the two regions now have major overlap between the tails. The overall PDF of the data from both regions is now unimodal and it is not possible to choose a threshold that separates the two regions without significant misclassifications.

In this section, it is shown that the mapping procedure described previously can adaptively choose a threshold and correct misclassifications so as to obtain good approximations to the PDFs of each region. The mapping procedure enables the region having the smallest envelopes, on average, to be separated from the remaining regions. By successive application of the mapping procedure, it is possible to first separate out the region with the smallest envelopes, followed by the region with the next smallest envelopes, and so forth. In the first application of the mapping procedure to a radar surveillance volume, region 1 consists of the BN while region 2 consists of the entire set of CL patches.

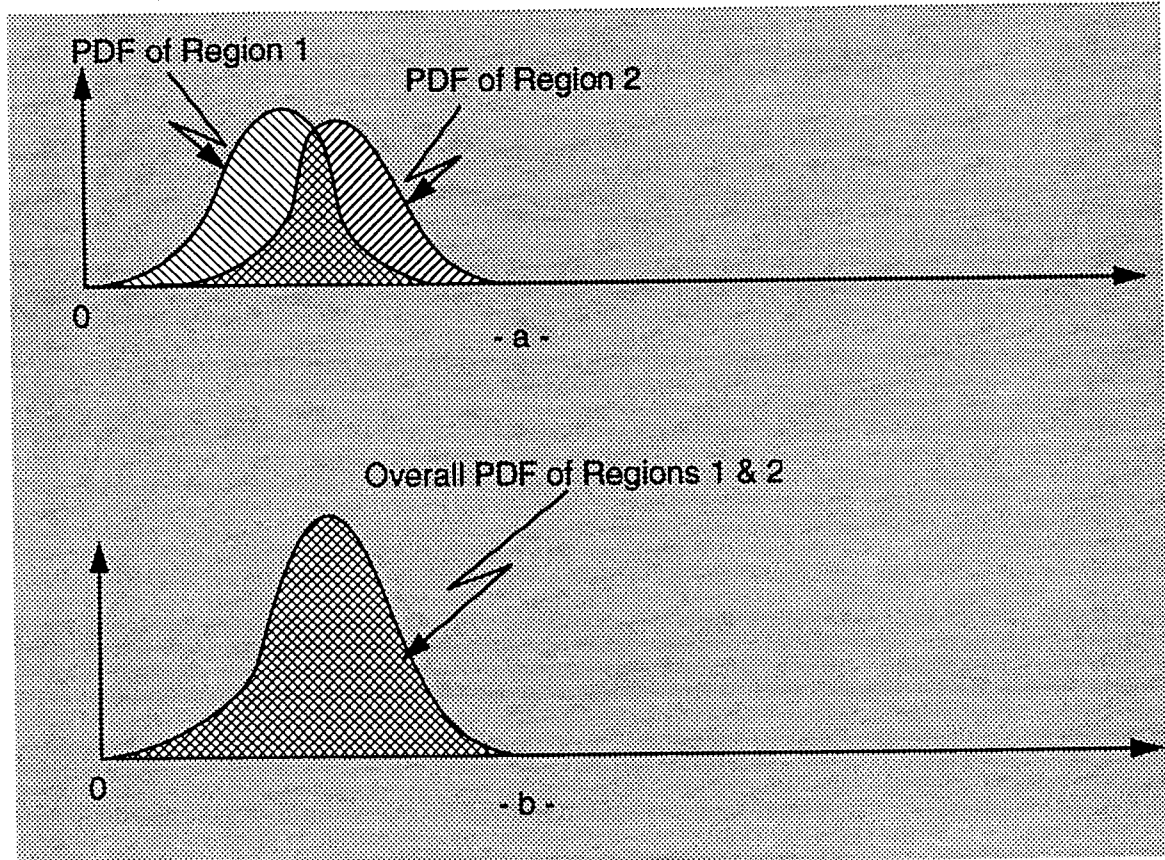


Figure V.5.3 - Overlapping PDFs of Two Distinct Regions with a Big Overlapping Area

(a) Individual PDFs for Each Region, (b) Overall PDF for Both Regions

### V.5.2 - Separation Between BN and CL Patches

An important observation relative to selection of the threshold, via specification of BNQP, is made when considering a surveillance volume that consists only of BN. The objective is to determine the range of threshold settings for which the mapping procedure declares the entire surveillance volume as BN. For this purpose, we consider the situation where the entire scene consists of BN and the data are generated from a Rayleigh PDF.

For the scenario under consideration, the whole scene is homogeneous BN and the mapping, if done correctly, should identify the entire volume as a single BN region. Table V.5.1 shows the values of BNCCP obtained for different set-

BNQP (%)	Threshold Value	BNCCP (%)
10	0.32	19.48
20	0.47	42.80
30	0.59	71.61
40	0.72	89.06
50	0.84	96.26
60	0.95	99.85
70	1.10	100.00
80	1.29	100.00
90	1.53	100.00

Table V.5.1 - BN Percentages and Threshold Values Corresponding to the Rayleigh Distributed BN

tings of BNQP. Notice from the table that a single region results only when the threshold exceeds 70% of the data. As shown in Fig.V.5.4, the mapping procedure correctly reclassifies all cells corresponding to values above the threshold as

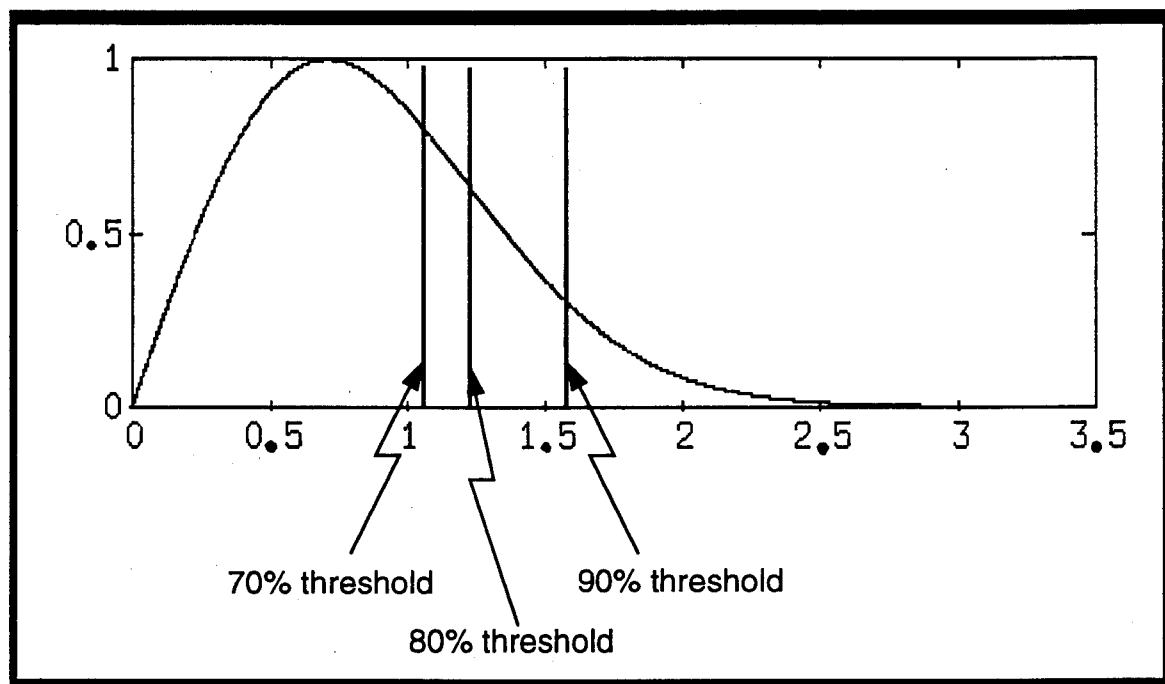


Figure V.5.4 - PDF of the Rayleigh Distributed Patch

long as the threshold is sufficiently towards the tail of the PDF. In general, it is observed that the mapping procedure works best provided the threshold is adequately positioned towards the tail of the PDF.

Another parameter that arises in the mapping procedure is BNCQP which denotes the percentage of background noise cells after the first-correction relative to the total number of cells in the surveillance volume. To gain insight into the relationship between BNQP, BNCQP and BNCCP, we return to example number 2, previously discussed in Section V.4.2.2, where a lot of CL patch data overlap with the BN data in a manner similar to Figure V.5.6. In Table V.5.2, different values of these parameters are tabulated as the mapping procedure converges to the end result. If the test cell is to be declared as CL, recall that at least NCQ and NCC neighboring cells are required to be declared as CL in the QV and CQV during the first and second-corrections, respectively.

Table V.5.3 tracks the mapping procedure during the first-correction stage (denoted by  $QV \rightarrow CQV$ ), during the second-correction stage (denoted by  $CQV \rightarrow CCV$ ) and at the end of the two correction stages (denoted by  $QV \rightarrow CCV$ ). All percentages given are with respect to the total number of cells in the surveillance volume. Initially, the threshold is set such that BNQP percent of the total number of cells are below the threshold. The first-correction stage requires that at least NCQ of the neighboring cells be above the threshold if the test cell is to be classified as a CL cell. Under the column headed by  $QV \rightarrow CQV$ ,  $(CL \rightarrow BN)_1$  denotes the percentage of the total number of cells in the surveillance volume that were above the threshold but are reclassified as BN cells during the first-correction stage. Similarly,  $(BN \rightarrow CL)_1$  denotes the percentage of the total number of cells in the surveillance volume that were below the threshold but are reclassified as CL cells after the first-correction stage. Note that the difference,  $(CL \rightarrow BN)_1 - (BN \rightarrow CL)_1$ , is the net percentage of the total number of cells in the surveillance volume that have been reclassified from CL to BN cells after the first-correction stage. Similar statements apply for (1) the second-correction stage to  $(CL \rightarrow BN)_2$ ,

$(BN \rightarrow CL)_2$ , and  $(CL \rightarrow BN)_2$ -  $(BN \rightarrow CL)_2$  under the column headed by  $CQV \rightarrow CCV$  and (2) for the combined results of the two correction stages to  $(CL \rightarrow BN)$ ,  $(BN \rightarrow CL)$ , and  $(CL \rightarrow BN)$ -  $(BN \rightarrow CL)$  under the column headed by  $QV \rightarrow CCV$ . Note that

$$(CL \rightarrow BN) - (BN \rightarrow CL) = [(CL \rightarrow BN)_1 - (BN \rightarrow CL)_1] + [(CL \rightarrow BN)_2 - (BN \rightarrow CL)_2]. \quad (V.5-1)$$

BNQP (%) (NCQ,NCC)	BNCQP (%)	BNCCP (%)	BNCQP-BNCCP	BNCCP-BNQP
10.00 (8,1)	56.35	20.59	35.76	10.59
20.59 (8,1)	77.43	48.04	29.39	27.45
48.04 (7,1)	84.11	72.30	11.81	24.26
72.30 (5,1)	82.17	73.94	8.23	1.64
72.30 (5,3)	82.17	79.26	2.91	6.96
75.78 (5,1)	83.50	75.31	8.19	0.27

*Table V.5.2 - BN Percentages of Example 2 of Section V.4.2.2*

BNQP (%) (NCQ,NCC)	QV $\rightarrow$ CQV		CQV $\rightarrow$ CCV		QV $\rightarrow$ CCV	
	$(CL \rightarrow BN)_1$ (%)	$(BN \rightarrow CL)_1$ (%)	$(CL \rightarrow BN)_2$ (%)	$(BN \rightarrow CL)_2$ (%)	$(CL \rightarrow BN)$ (%)	$(BN \rightarrow CL)$ (%)
10.00 (8,1)	49.83	3.46	3.70	39.46	10.61	0.00
20.59 (8,1)	59.35	2.48	2.96	32.35	27.48	0.00
48.04 (7,1)	38.07	1.98	0.61	12.43	27.48	3.20
72.30 (5,1)	13.93	4.04	0.09	8.31	9.63	7.96
72.30 (5,3)	13.93	4.04	0.65	3.56	11.31	4.33
75.78 (5,1)	11.85	4.11	0.04	8.22	7.59	8.04

*Table V.5.3 - CL-to-BN and BN-to-CL Transitions in Example 2 of Section V.4.2.2*

Also,

$$\begin{aligned} \text{BNCQP-BNQP} &= (\text{CL} \rightarrow \text{BN})_1 - (\text{BN} \rightarrow \text{CL})_1 \\ \text{BNCCP-BNCQP} &= (\text{CL} \rightarrow \text{BN})_2 - (\text{BN} \rightarrow \text{CL})_2 \\ \text{BNCCP-BNQP} &= (\text{CL} \rightarrow \text{BN}) - (\text{BN} \rightarrow \text{CL}) \\ &= [\text{BNCQP-BNQP}] + [\text{BNCCP-BNCQP}]. \end{aligned} \quad (\text{V.5.2})$$

The mapping procedure involves iterations which continue until the difference  $\text{BNCCP-BNQP}$  is sufficiently small. From Eq.(V.5-2), it is seen that convergence results when

$$(\text{CL} \rightarrow \text{BN}) \approx (\text{BN} \rightarrow \text{CL}). \quad (\text{V.5-3})$$

Consequently, near convergence, the combined effect of the two correction stages should result in the percentage of CL cells reclassified as BN cells being approximately equal to the percentage of BN cells reclassified as CL cells. Alternatively, from Eq.(V.5.2), convergence results when

$$[\text{BNCQP-BNQP}] \approx - [\text{BNCCP-BNCQP}] \quad (\text{V.5-4})$$

or equivalently, when

$$[(\text{CL} \rightarrow \text{BN})_1 - (\text{BN} \rightarrow \text{CL})_1] \approx - [(\text{CL} \rightarrow \text{BN})_2 - (\text{BN} \rightarrow \text{CL})_2]. \quad (\text{V.5-5})$$

Thus, near convergence, the net percentage of cells that have been reclassified from CL to BN cells during the first-correction stage should approximately equal the negative of the net percentage of cells that have been reclassified from CL to BN cells during the second-correction stage. These observations are helpful in coming up with rules for determining the next setting of the parameters in the iteration process.

By way of example, when  $\text{BNQP}=10\%$ , the threshold is such that 10% of the total number of cells in the surveillance volume fall below the threshold while 90% fall above. The situation is pictured in Fig. V.5.5 (b). With reference to Table V.5.3, when  $\text{NCQ}=8$ , 49.83% of the total cells in the surveillance volume which

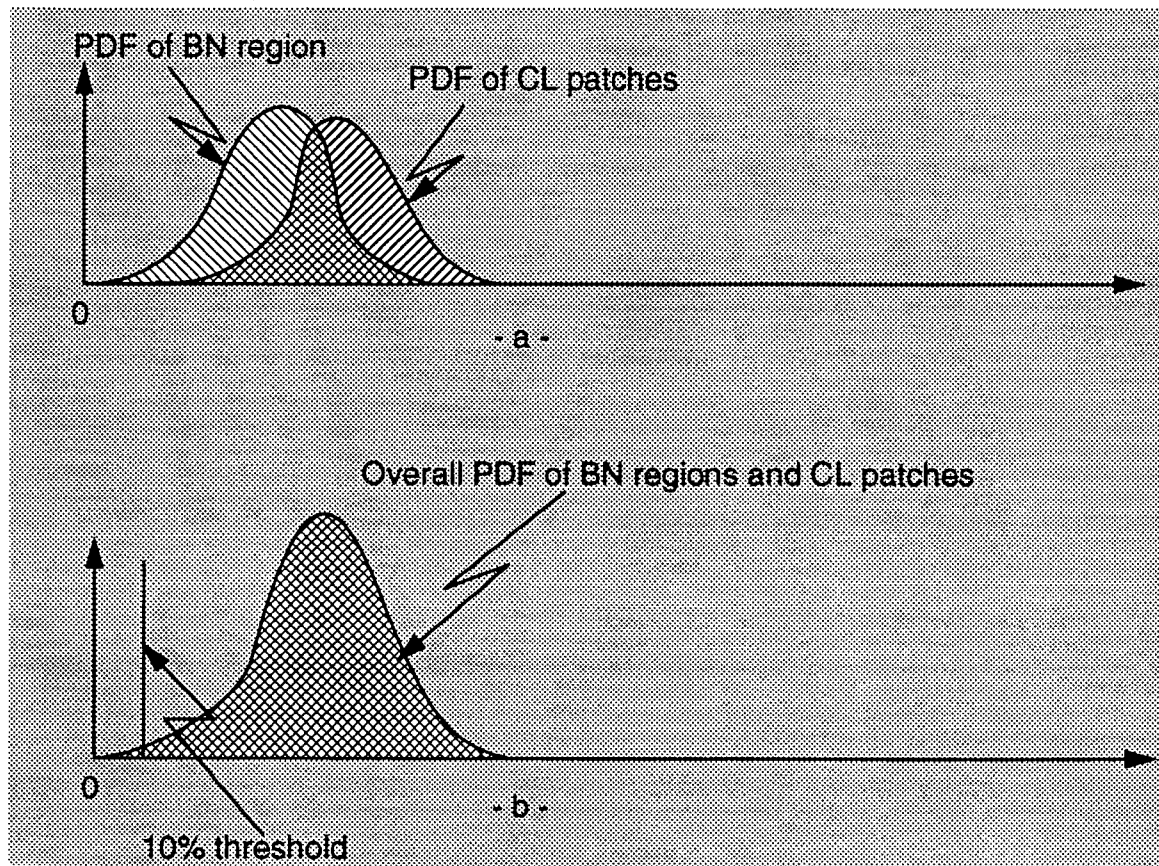


Figure V.5.5 - Overlapping PDFs of BN Region and CL Patches  
(a) Individual PDFs for each Region, (b) Overall PDF for both Regions

were classified as CL cells because they were above the threshold, are reclassified as BN cells after the first-correction stage whereas 3.46%, which were classified as BN cells because they were below the threshold, are reclassified as CL cells. The net percentage of cells reclassified as BN is  $49.83\%-3.46\%=46.37\%$ . For the second-correction stage, with  $NCC=1$ , 3.70% of the total cells in the CQV surveillance volume, which were classified as CL cells after the first-correction stage, are reclassified as BN cells because they don't have at least one neighboring CL cell. Similarly, 39.46% of the total cells in the CQV surveillance volume, which were classified as BN cells, are reclassified as CL cells because they have one or more neighboring CL cells. The last row of Table V.5.3 corresponds to a situation close to convergence. When the threshold is set such that 75.78% of the

total number of cells in the surveillance volume are below the threshold, the combined effect of the two correction stages results in

$$(CL \rightarrow BN) = 7.59\% \approx (BN \rightarrow CL) = 8.04\%. \quad (V.5-6)$$

Similarly,

$$[(CL \rightarrow BN)_1 - (BN \rightarrow CL)_1] = 8.74\% \approx - [(CL \rightarrow BN)_2 - (BN \rightarrow CL)_2] = 8.18\%. \quad (V.5-7)$$

Equivalently, from Table V.5.2,

$$[BNCQP - BNQP] = 7.72\% \approx - [BNCCP - BNCQP] = 8.19\%. \quad (V.5.8)$$

Insight into the manner by which the PDF's of BN and CL are modified during the correction stages is obtained by examining pertinent amplitude histograms for the various surveillance volumes QV, CQV, and CCV. The overall amplitude histogram for the generated data of the QV volume is shown in Fig. V.5.6 (a). Note that the histogram is unimodal and it is not possible to distinguish between the BN and the CL cells. In fact, by just looking at the histogram one would not suspect that more than one region exists. When the threshold is set at 0.37 such that BNQP=10%, many of the BN cells are classified as CL due to the low threshold. The amplitude histograms for the BN and CL cells in the QV volume are shown in Figs. V.5.6 (b) and (c), respectively. Note that the BN histogram is truncated to a cell amplitude of 0.35.

The amplitude histograms for the CQV volume resulting from the first-correction stage are shown in Fig. V.5.6 (d) and (e). Comparing Fig. V.5.6 (d) with Fig. V.5.6 (b), it is seen that many cells with amplitudes above the threshold value of 0.35 have been reclassified as BN. The amplitude histograms for the CCV volume resulting from the second-correction stage are shown in Figs. V.5.6 (f) and (g). Note the further enhancement of the right tail of the BN amplitude histogram. This enhancement is due to the image processing and is in spite of the low threshold value.

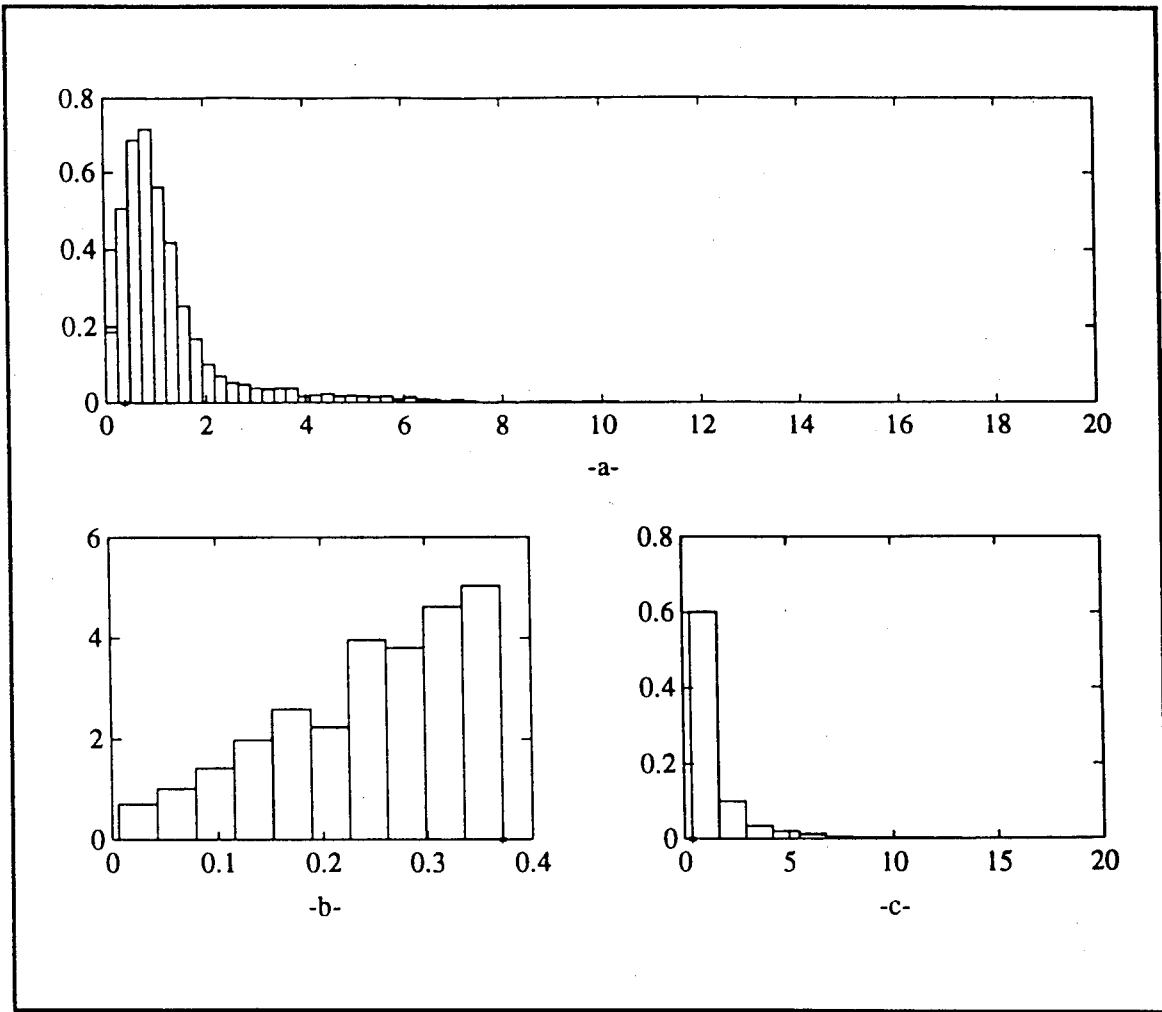


Figure V.5.6 - Region Histograms Corresponding to BNQP=10%, NCQ=8 and NCC=1 (a) Overall histogram of the generated data, (b) BN histogram at the quantization stage, (c) CL histogram at the quantization stage

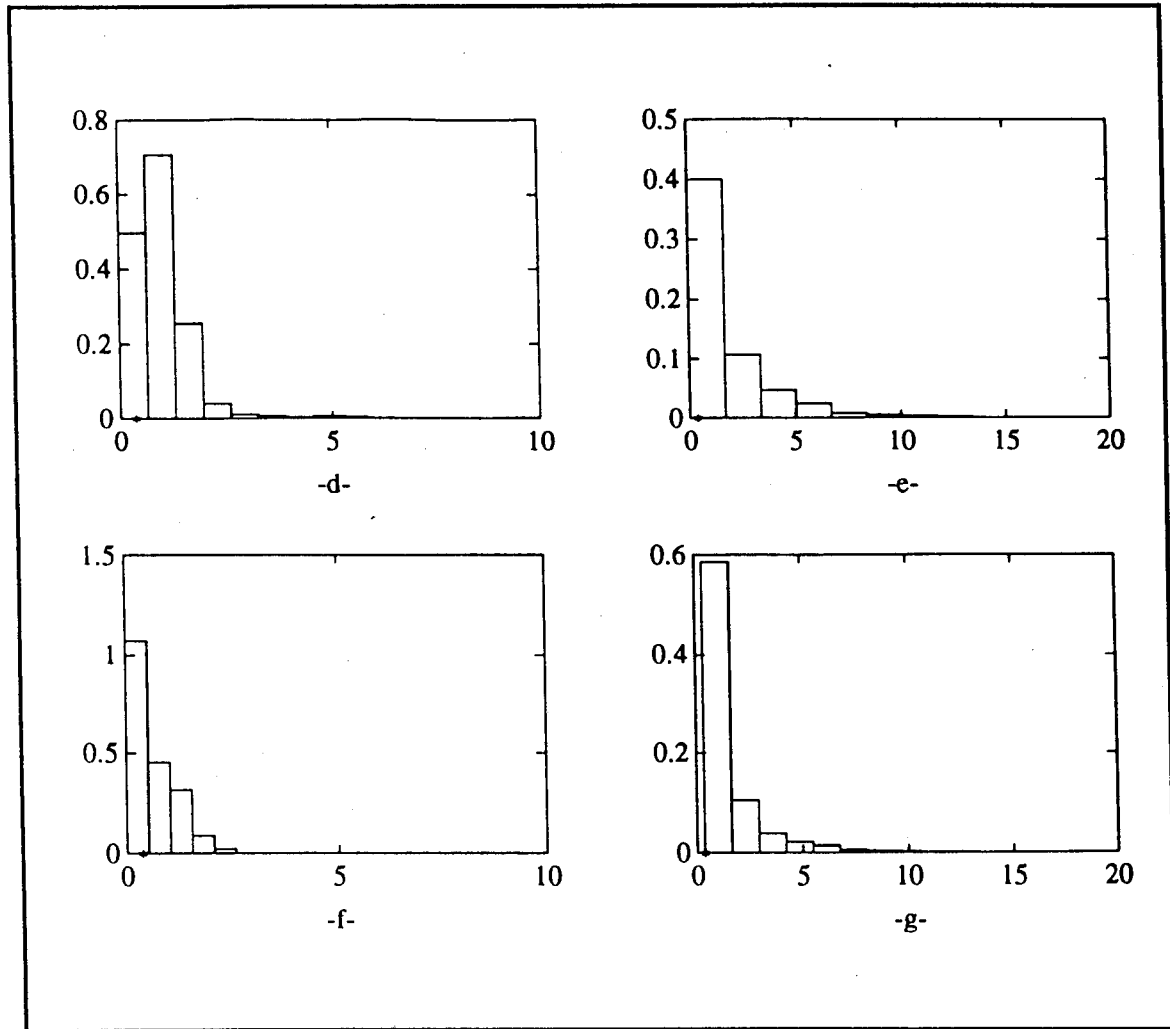


Figure V.5.6 - Region Histograms Corresponding to BNQP=10%, NCQ=8 and NCC=1 (d) BN histogram at the first-correction stage, (e) CL histogram at the first-correction stage, (f) BN histogram at the second-correction stage, (g) CL histogram at the second-correction stage

During the iteration process the threshold is gradually increased and converges to a value in the vicinity of 1.51 for which  $BNQP=75.78\%$ . In Fig. V.5.7 (a), this threshold is shown in the overall histogram for the QV volume. The amplitude histograms for the BN and CL cells in the QV volume are shown in Fig. V.5.7 (b) and (c), respectively. Note that the amplitudes of the BN cells fall below 1.51 whereas those of the CL cells fall above 1.51. The results of the first and second-correction stages and the edge enhancement stage are shown in Figs. V.5.7 (d) and (e), Figs. V.5.7 (f) and (g), and Figs. V.5.8 (h) and (i), respectively. To provide

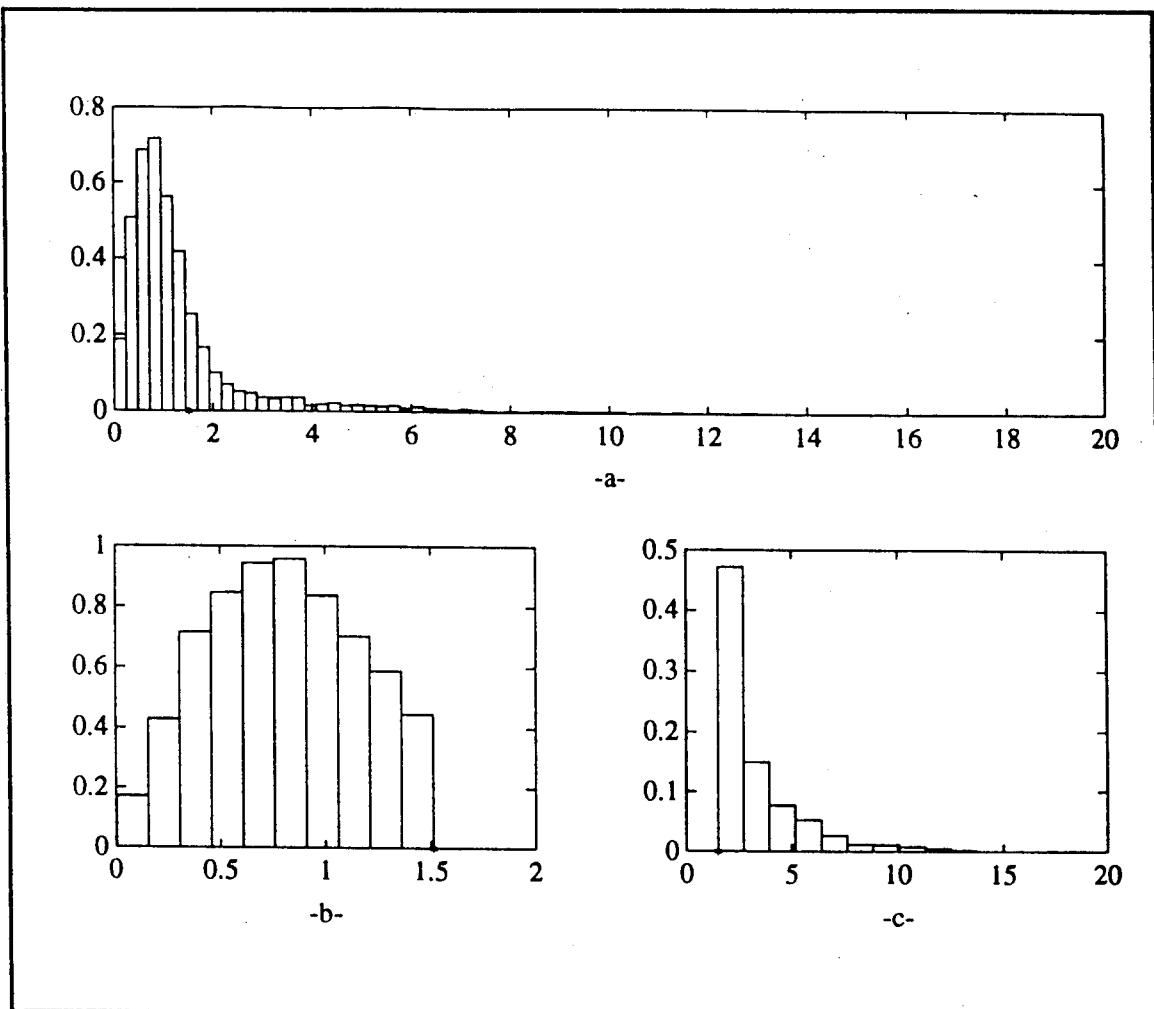


Figure V.5.7 - Region Histograms Corresponding to  $BNQP=75.78\%$ ,  $NCQ=5$ ,  $NCC=1$  (a) Overall histogram of the generated data, (b) BN histogram at the quantization stage, (c) CL histogram at the quantization stage

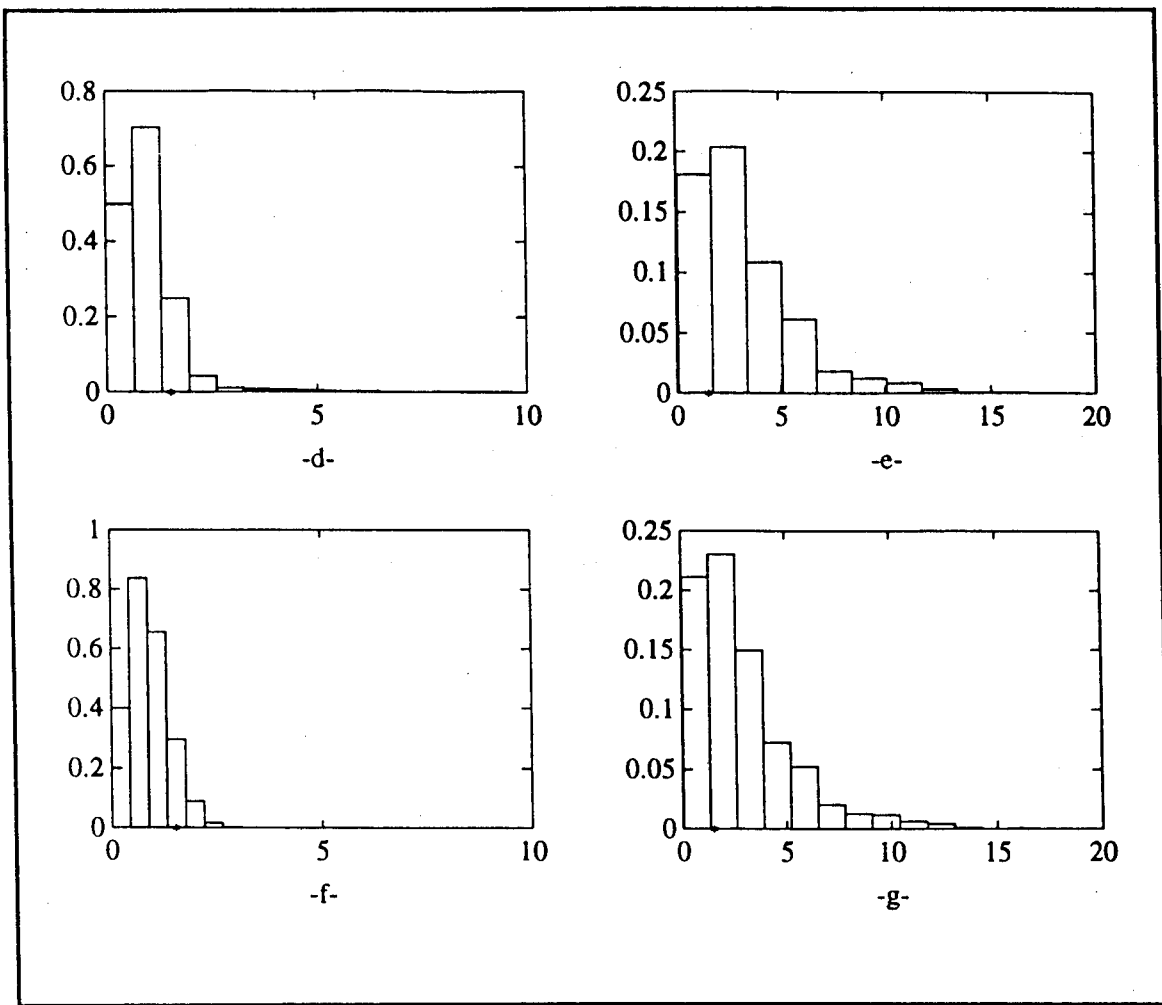


Figure V.5.7 - Region Histograms Corresponding to BNQP=75.78%, NCQ=5, NCC=1 (d) BN histogram at the first-correction stage, (e) CL histogram at the first-correction stage, (f) BN histogram at the second-correction stage, (g) CL histogram at the second-correction stage

as a basis for comparison, the actual BN and CL amplitude histograms are shown in Figs V.5.7 (j) and (k). The strong similarity between the amplitude histograms of Figs. V.5.7 (h) and (i) and those of Figs. V.5.7 (j) and (k) indicates that the mapping procedure has converged satisfactorily. Note how nicely the final histograms of Figs. V.5.7 (h) and (i) have evolved from the original histograms of Figs. V.5.6 (b) and (c).

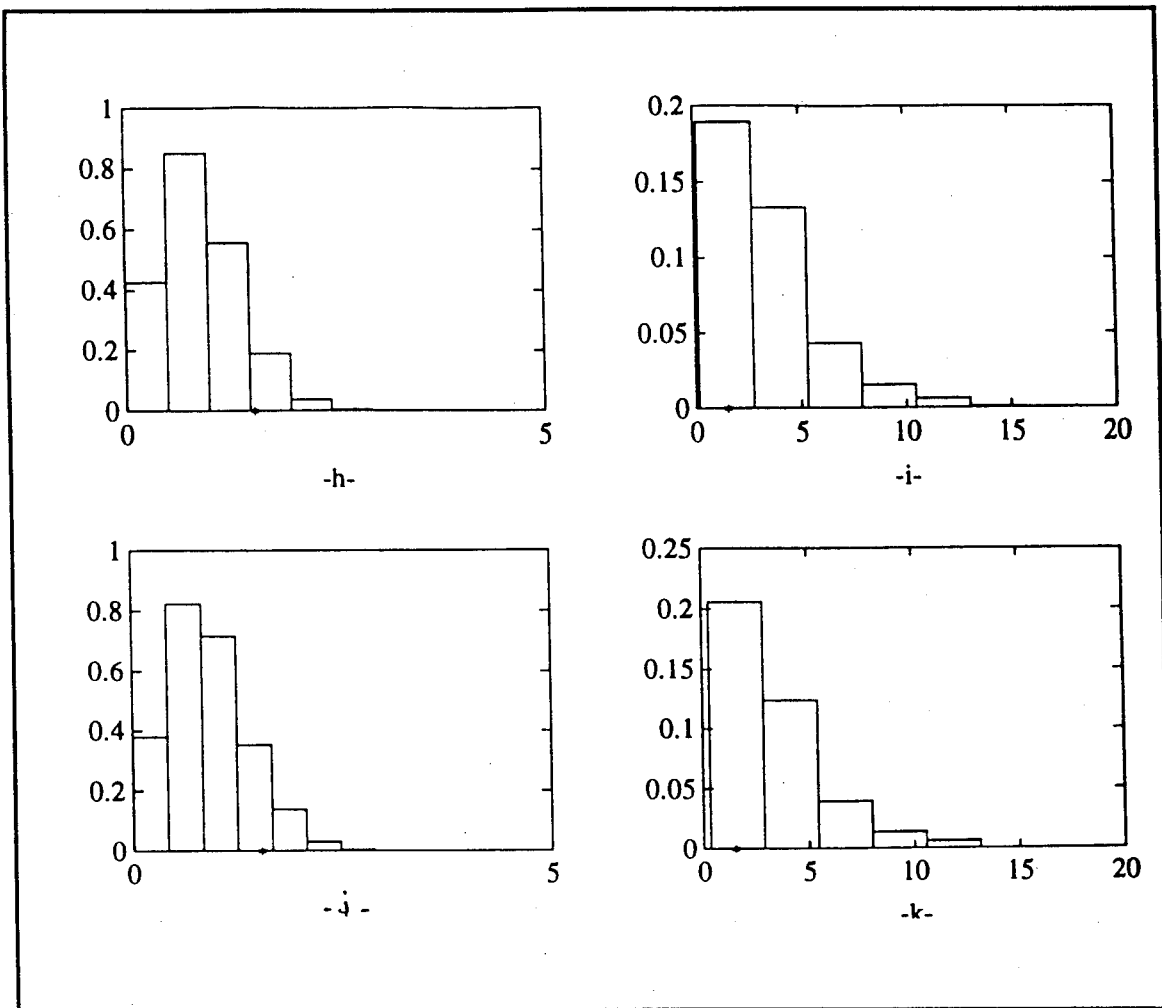


Figure V.5.7 - Region Histograms Corresponding to BNQP=75.78%, NCQ=5, NCC=1 (h) BN histogram at the mapped volume, (i) CL histogram at the mapped volume, (j) Actual BN histogram of the generated data, (k) Actual CL histogram at the generated data

In general, the first-correction stage begins to establish the right tail of the BN amplitude histogram and reshape the CL amplitude histogram by reclassifying mislabelled BN cells. The second-correction stage reshapes both the bodies and the tails of the BN and CL histograms by recovering the CL edges.

## **V.6 - Extension of the Mapping Procedure to R/A/D Cells**

Assume that the dwell time is  $P=M>1$ . In this case, an FFT is possible and the block diagram of the preprocessing and mapping of data is as shown in Fig. IV.2.1. As explained in Section IV.2, the mapping consists of two stages. The first mapping stage operates on R/A cells while the second one operates on R/A/D cells.

Once the R/A surveillance volume has been mapped into BN and CL cells, as explained in Section V.3, the second mapping stage starts by declaring as BN cells all R/A/D cells corresponding to R/A cells previously declared as BN in the first mapping stage. Meanwhile, the FFT magnitudes of R/A cells previously declared as CL in the first mapping stage are obtained from the preprocessing blocks to enable classification of the remaining R/A/D cells as either BN or CL cells.

Note that a row of range cells, having a fixed azimuth, in the R/A volume corresponds to a R/D plane in the R/A/D volume. Also, a row of azimuth cells, having a fixed range in the R/A volume corresponds to an A/D plane in the R/A/D volume. These are illustrated in Figs. V.6.1 (a) and (b), respectively. Hence, range and azimuth rows of BN declared cells in the R/A volume correspond to a R/D and A/D planes, respectively, of BN declared cells in the R/A/D volume and no additional processing is needed for such a plane.

Mapping of the R/A/D volume is done on a plane-by-plane basis. Either a R/D plane (with parameterized azimuth) or an A/D plane (with parameterized range) can be considered. The best choice consists of that which would involve the least processing. For example, if there are more R/D BN declared planes than A/D BN declared planes in the R/A/D volume, the best choice in this case would then be to process R/D planes, and vice-versa.

Assume that R/D plane-by-plane processing has been chosen. The mapping procedure becomes a two-dimensional problem, and, thresholding/quantiza-

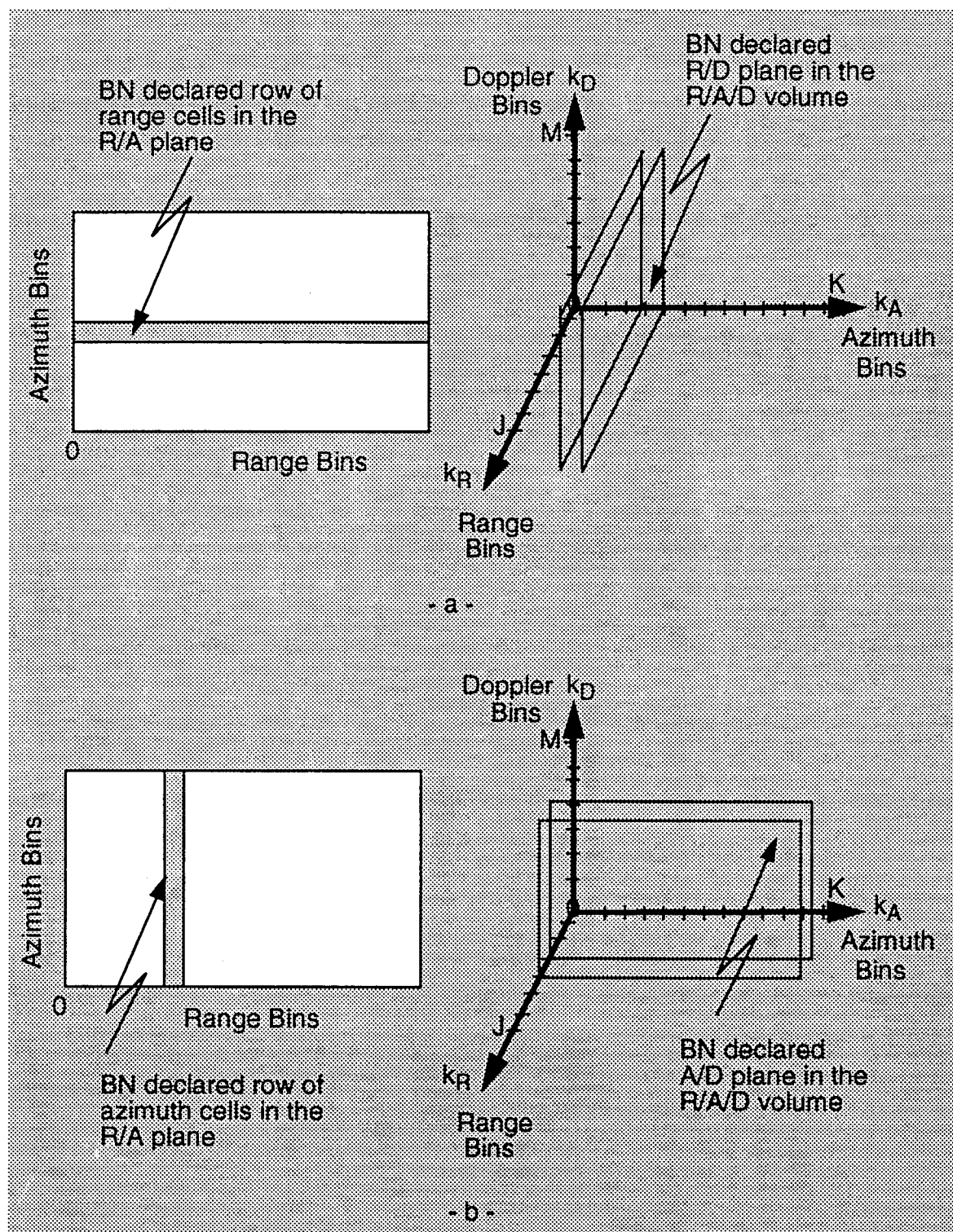


Figure V.6.1 - BN Declared Rows and their Corresponding BN Declared Planes (a) BN row of range cells and BN R/D plane, (b) BN row of azimuth cells and BN A/D plane

tion, first-correction, second-correction, smoothing, edge-enhancement and edge detection are performed as explained in Section V.3.

When the second mapping stage is done, the R/A/D volume will consist of a R/A/D BN region and R/A/D CL patches in the form of three-dimensional objects.

### **V.7 - Conclusion**

In summary, a mapping procedure was presented in chapter V that allows for distinguishing between BN and CL patches. The procedure was illustrated with examples that show how the mapping procedure works, even under very hard conditions as in the example of Section V.4.2.2, where the histograms of the CL patches and BN region overlap to the extent that the total histogram is unimodal such that one wouldn't suspect the presence of more than one distribution.

It is to be noticed that there was no discussion in this chapter of the rules that govern the choice of the parameters BNQP, NCQ, and NCC. These rules will be introduced later in Chapter VII along with the role of IPUS in the mapping procedure.

## Chapter VI

### Indexing Procedure

#### **VI.1 - Introduction**

As explained in Table II.3.1, and shown in the examples of Section V.4.2, the mapping procedure subdivides the surveillance volume into BN regions and CL patches and labels the cells in the surveillance volume as either BN or CL cells.

In this research it is assumed that the BN is white and sufficiently weaker than a desired target return such that the SSC is applicable and detections can be obtained using the conventional Gaussian receiver with little degradation in performance. Consequently, no additional indexing is needed for the BN cells.

On the other hand, more processing is needed on CL cells before the detection process can begin. This is because (1) CL patches may be nonhomogeneous containing two or more CL subpatches, (2) in each CL patch, or CL subpatch if it exists, either the SSC, WSC, or ISC will apply, (3) for each WSC CL patch or subpatch, its probability density function (PDF) must be approximated. Also, for each ISC CL patch or subpatch, its covariance matrix must be approximated. All these steps need to be implemented during the indexing stage and are explained in this chapter.

The indexing procedure starts with an assessment stage by which (1) CL patches and the BN region are identified by assigning a unique identification number to all cells within a CL patch or BN region, and (2) CNR and number of cells in each CL patch are determined. The next stage, called the subpatch investigation stage, consists of determining the existence of CL subpatches. If CL subpatches are found, the assessment stage is then carried out, once again, for the entire surveillance volume. The final stage of the indexing procedure is the PDF approxima-

tion stage where the PDF for each WSC CL patch is approximated. The assessment, CL subpatch investigation and PDF approximation stages are explained next.

## **VI.2 - Assessment Stage**

As explained above, assessment is carried out (1) to assign a unique number to the BN region and each CL patch, (2) to estimate the CNR for each CL patch, and (3) to classify CL patches as either SSC, WSC or ISC regions.

### **VI.2.1 - Identification of the BN Region and CL Patches**

When the mapping is completed, recall that the mapped volume has a value of 0 assigned to BN cells and a value of 1 assigned to the CL cells. Therefore, nothing more needs to be done for the BN region as all of its cells are already indexed by the number 0. On the other hand, all cells in each of the CL patches are assigned a value of 1. Thus, a numbering procedure has to be implemented to enable the computer to distinguish between the various CL patches. The approach taken in this work is to assign every cell in the first patch investigated the number 1, every cell in the second patch investigated the number 2, and so on until all patches have been indexed with consecutive integers. In this way, all cells in each CL patch are assigned a unique number.

If a cell belongs to a new CL patch, the key to the numbering is the ability to recognize this fact. This is done by considering a mask of 5 cells as shown in Figure VI.2.1 where the white cells represent neighboring cells and the shaded one is the test cell to be numbered. Since the surveillance volume has previously been augmented by adding rows of BN to its left, top, right, and bottom edges, there is no problem positioning this mask for each test cell in the original unaugmented surveillance volume.

Let  $M(i,j)$  be the value assigned to the  $ij$ th cell in the mapped volume where,

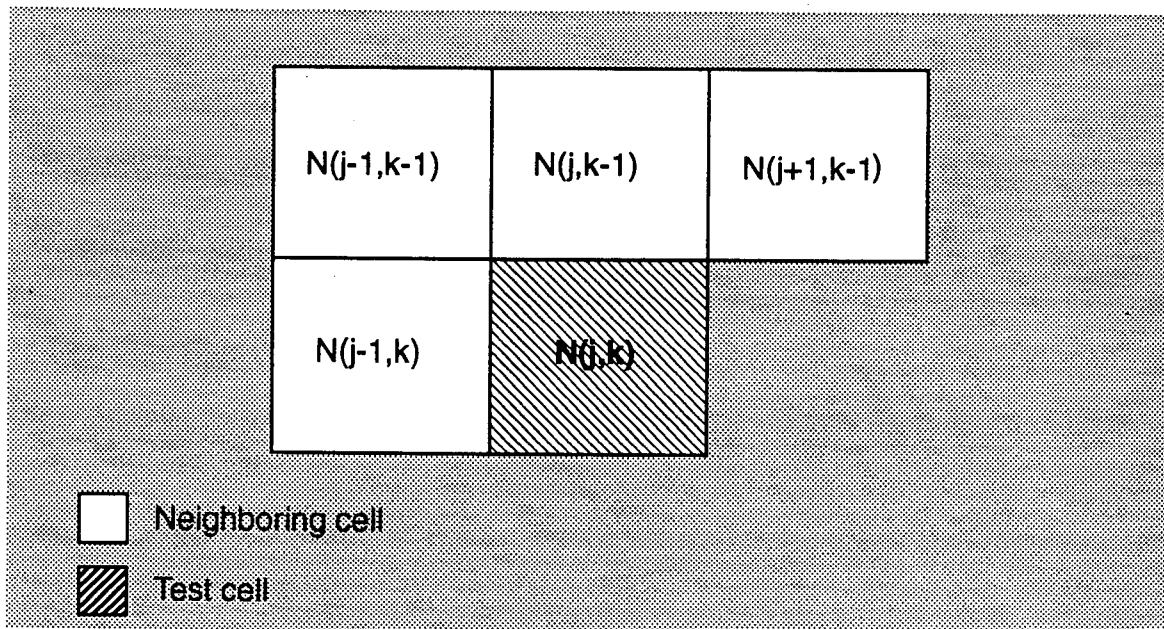


*Figure VI.2.1 - Mask Used in Numbering*

$$M(i,j) = \begin{cases} 0 & \text{if } ij\text{th cell is declared as BN} \\ 1 & \text{if } ij\text{th cell is declared as CL.} \end{cases} \quad (\text{VI.2-1})$$

Assuming that the test cell to be numbered is the  $jk^{\text{th}}$  cell in the original unaugmented surveillance volume, let the assigned number be denoted by  $N(j,k)$ . Also, let  $G$  denote the unique number assigned to the CL patch previously investigated and  $H$  the minimum positive number assigned to the neighboring cells. Then, by definition, we have that

$$N(j,k) = \begin{cases} 0 & \text{if } M(j,k)=0 \\ (G+1) & \text{if all neighboring cells are numbered 0} \\ H & \text{if at least one of the neighboring cells is numbered nonzero.} \end{cases} \quad (\text{VI.2-2})$$

The number G is incremented by unity whenever a new CL patch is detected.

Because a CL patch boundary may be sharply shaped, as shown in the example of Figure VI.2.2, the numbering procedure may end up by assigning two different numbers for different cells of the same CL patch. This anomaly is avoided by further testing the neighboring cells of the cell to be numbered as follows:

1 - For the given cell to be numbered, look up the numbers assigned to the set of neighboring cells  $(j-1,k-1)$ ,  $(j,k-1)$ ,  $(j+1,k-1)$ , and  $(j-1,k)$ ,

2 - Take the minimum nonzero number of those in step 1,

3 - Reassign all nonzero numbered neighboring cells the minimum nonzero number from step 2,

4 - Revisit all the cells in the surveillance volume that have previously been numbered. If any cell is assigned a nonzero number identical to one of those in step 1, reassign that cell the minimum nonzero number of step 2.

For example, with respect to Figure VI.2.2, the above steps have the effect of assigning a value of 1 to all cells of the CL patch shown.

Once numbering is completed, the BN cells are assigned a value of 0, and every CL patch is assigned a unique positive number.

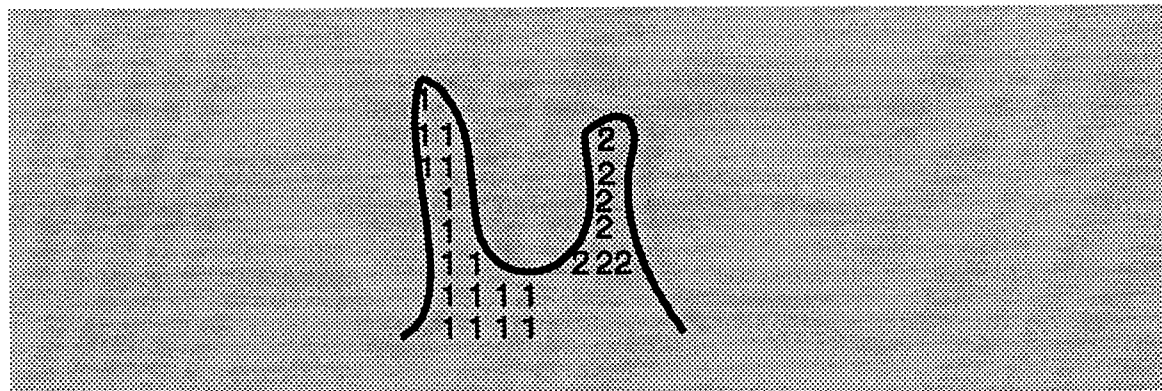


Figure VI.2.2 - Example of a Sharply Shaped Boundary

### **VI.2.2 - Computation of CNRs**

The CNR for CL patch  $k$  is given by  $[(\bar{d}_k - \bar{n}) / \bar{n}]^2$ , expressed in dB, where  $\bar{d}_k$  is the sample average of the CL plus BN values distributed over CL patch  $k$  and  $\bar{n}$  is the sample average of the BN values distributed over the BN region.

### **VI.2.3 - Classification of CL Patches**

Throughout this work the minimum target signal-to-noise ratio (SNR) is assumed to be 10 dB so that targets are readily detected when they appear in the BN region. The classification of a CL patch as a SSC, WSC, or ISC then depends on its CNR. Ranges of the CNR for the strong, weak, and intermediate signal cases are given in Table VI.2.1. The bounds for this work were chosen based on experience gained through computer simulations. For example, when CNR=8 dB, the average signal power is 2 dB larger than the average CL power. Nevertheless, non-Gaussian CL tends to be spiky. Consequently, even when CNR=8 dB, there are regions where the CL is much larger than the signal. Consequently, 8 dB is chosen as the lower bound on CNR for WSC. Also, when CNR=5 dB, the average signal power is 5 dB larger than the average CL power. At this level, the CL typically dominates the signal at only a few isolated points. Thus, 5 dB is chosen as the upper bound on CNR for SSC. ISC is defined to fall between the two bounds.

Classification	CNR
SSC	CNR < 5 dB
ISC	5 dB ≤ CNR ≤ 8 dB
WSC	CNR > 8 dB

*Table VI.2.1 - Classification of a CL Patch*

When a CL patch is classified as SSC, the returns from this patch are processed by the same detector as that used for the BN region. Only the threshold needs to be adjusted properly. When a CL patch is classified as ISC, the general-

ized likelihood ratio test [19] is used to process the associated returns. Finally, when a CL patch is classified as WSC, it is necessary to determine the associated PDF so that the appropriate processor can be selected from the library of weak signal detectors.

### **VI.3 - CL Subpatch Investigation Stage**

Recall that mapping consists of appropriately selecting a threshold to distinguish between BN and CL patches using only the assumption that the BN power, on average, is smaller than the CL power. This same approach may be used, once again to extract that CL subpatch with the lowest average power from a set of contiguous CL subpatches of higher average powers in a given CL patch. In this case, the CL patch containing CL subpatches will be viewed as a volume containing a CL subpatch region with low average power and a set of subpatches with higher average powers occupying the rest of the CL patch area as shown in Figure VI.3.1.

The mapping procedure, therefore, is used to extract the CL subpatch with the lowest average power from among the remaining CL subpatches in a given CL patch. Because numbering has already labelled each patch with a unique number it is straight-forward for the computer program to select a patch and check for the presence of subpatches in it.

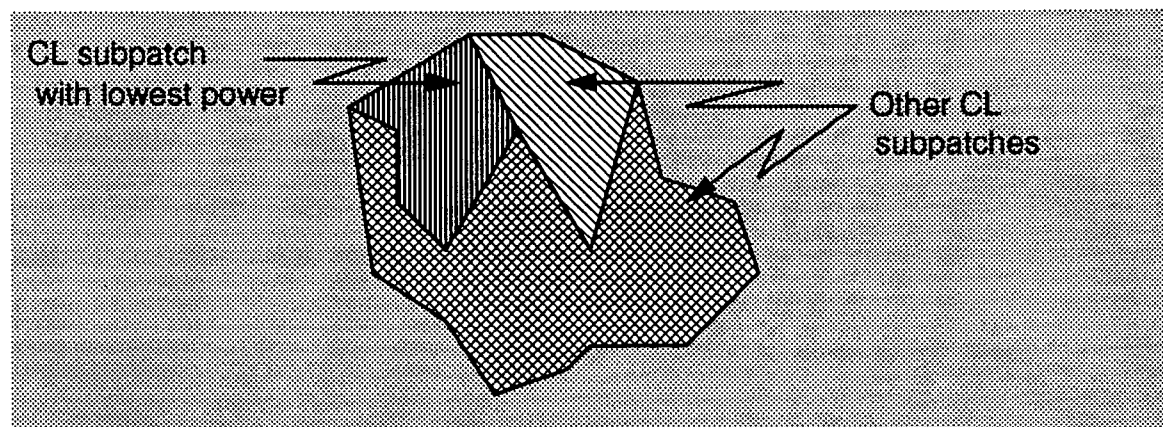


*Figure VI.3.1 - Example a CL Patch Containing CL Subpatches*

For each CL patch, the mapping procedure is performed iteratively until it is hypothesized that every subpatch in a given CL patch is homogeneous and cannot be partitioned further. After all CL subpatches have been extracted, the surveillance volume consists of a BN region and clutter patches that may or may not be contiguous. Notice that every CL subpatch is now referred to as a CL patch.

If CL subpatches are found to exist, assessment is performed once again to (1) allocate, or reallocate, a number for every CL patch in the surveillance volume, (2) compute the CNR for every patch, and (3) classify the CL patches as SSC, WSC, or ISC regions. Assessment and subpatch investigation are described by the flow charts of Figures VI.3.2 and VI.3.3. Figure VI.3.4 shows the order in which assessment and CL subpatch investigation are performed.

Once WSC regions have been identified and numbered, their respective PDFs are approximated as explained in the next section.

#### **VI.4 - PDF Approximation of WSC CL Patches**

The PDF approximation of WSC CL patches follows two steps. During the first step, referred to as test cell selection, a WSC CL patch is selected from among the WSC declared CL patches, a set of test cells is chosen in that CL patch, and reference cells are identified for each test cell that belong to the selected CL patch and that are the closest to the test cell. In the second step, referred to as PDF approximation, the data of the reference cells are processed by the Ozturk algorithm so that the PDF of the test cell can be approximated. The process iterates for the next WSC CL patch until each WSC CL patch in the surveillance volume has its PDF approximated. Test cell selection and PDF approximation, as well as an outlier definition and a PDF approximation strategy, are introduced next.

##### **VI.4.1 - Test Cell Selection**

As explained above, test cell selection involves three steps:

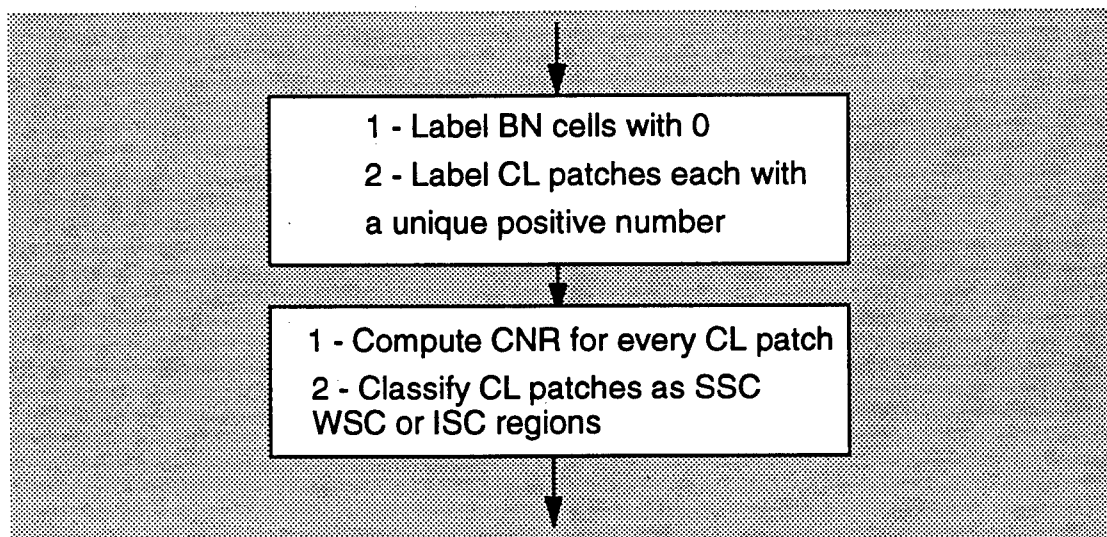


Figure VI.3.2 - Assessment Stage

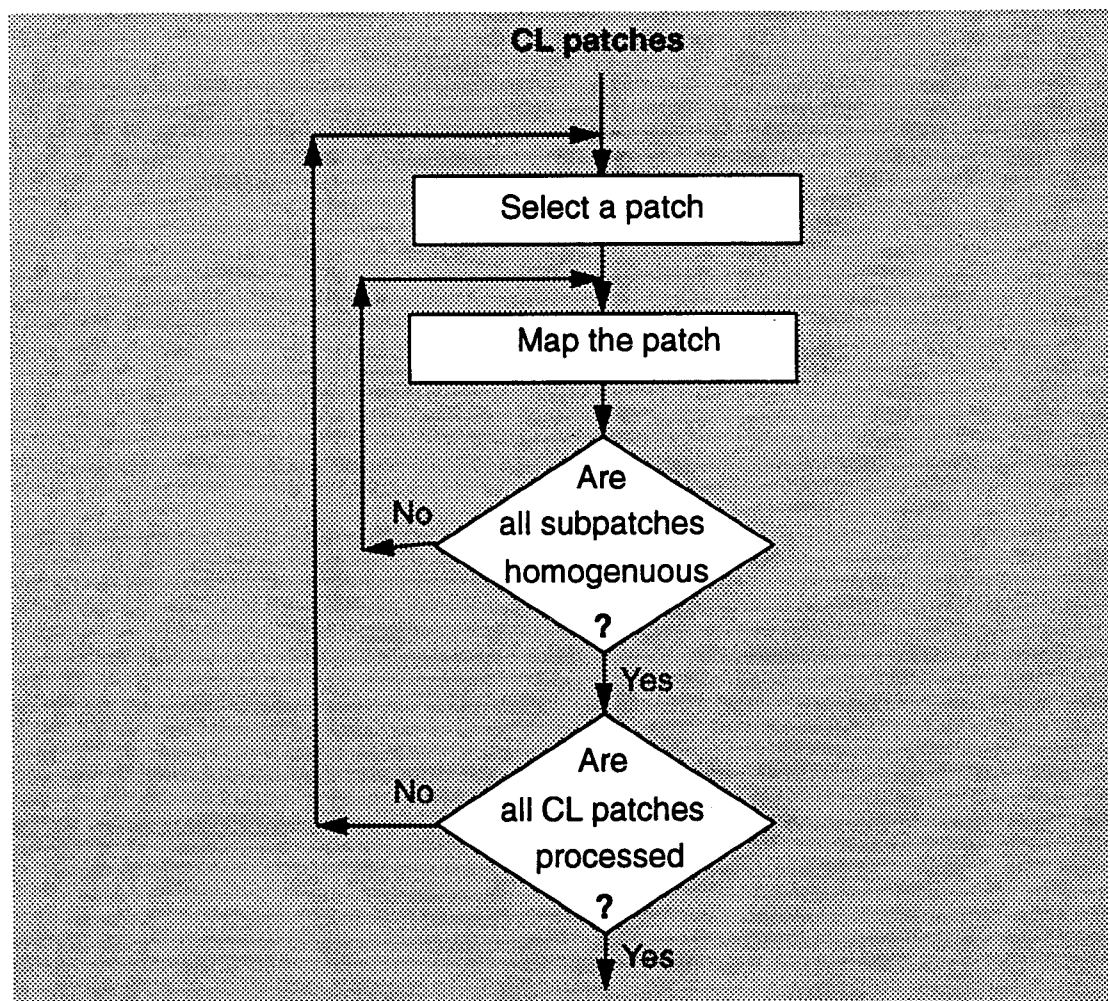


Figure VI.3.3 - CL Subpatch Investigation Stage

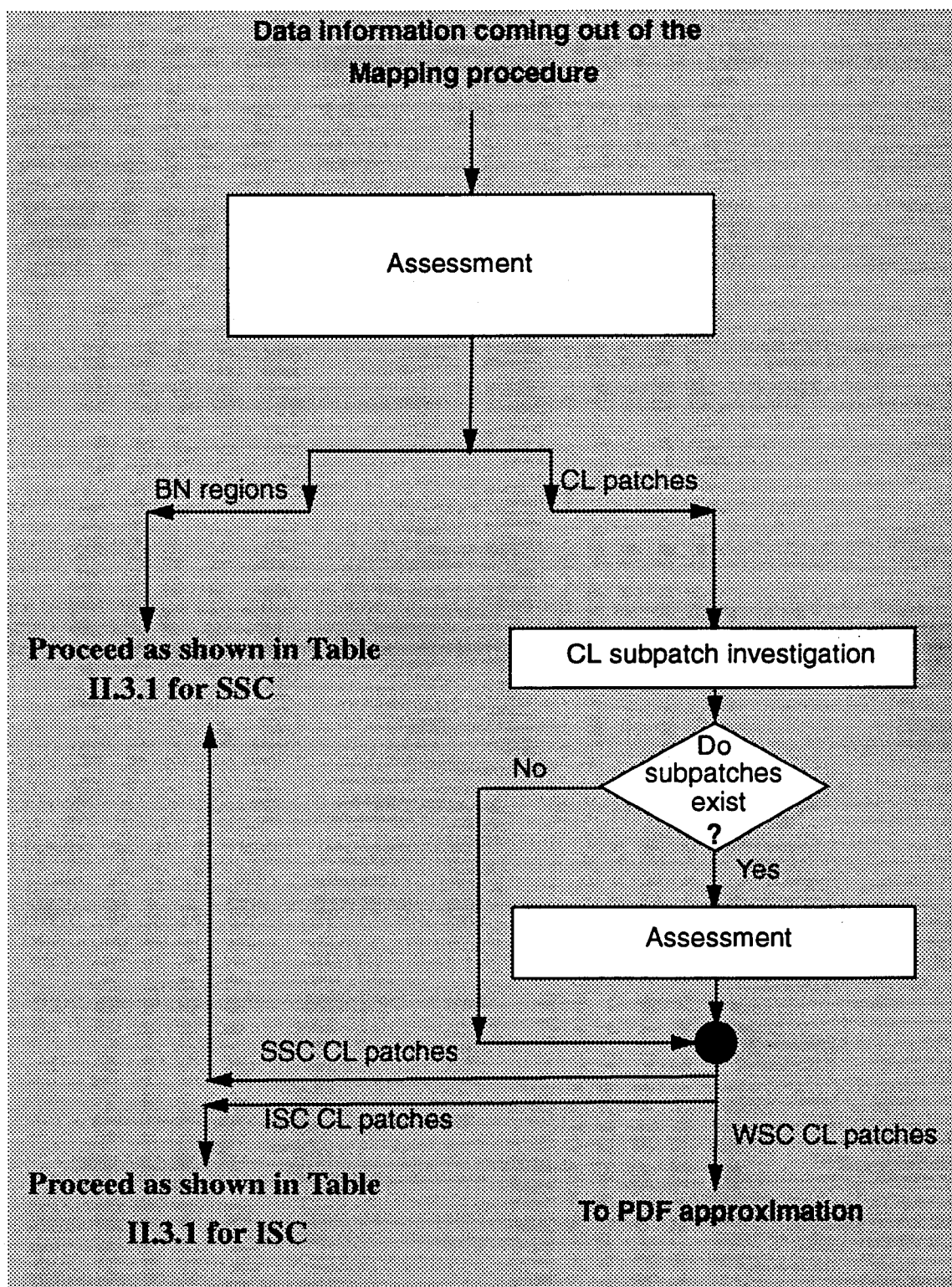


Figure VI.3.4 - Assessment and CL Subpatch Investigation

(i) - A WSC CL patch is chosen from among the WSC declared CL patches. This can be done automatically by the computer program since at this stage every CL patch has been labelled with a unique number.

(ii) - A set of  $N_T$  test cells is then chosen in the WSC CL patch being processed where the value of  $N_T$  depends upon the extent to which the patch needs to be characterized. Note that any cell in the CL patch can be a test cell. A possible choice for the test cells is equally spaced test cells that cover the entire area of the CL patch.

(iii) - Finally, for each test cell, a set of reference cells is selected. The reference cells must be in the same CL patch as the test cell and should be the closest in distance to it because of the assumption that the reference cells are representative of the test cell.

In order to select the reference cells for a given test cell, the program starts by centering a 3x3 mask around the test cell and choosing as reference cells those neighboring cells within the mask that are declared to be in the same CL patch as the test cell. If the desired number of reference cells are not obtained, the program increases the size of the mask by adding one row and one column to each boundary of the 3x3 mask. This results in a 5x5 mask where only the cells in the augmented rows and columns need to be examined. The process of adding one row and one column to each boundary of the previous mask continues until the desired number of reference cells have been obtained.

#### **VI.4.2 - PDF Approximation**

Approximation of the PDF underlying a test cell consists of processing the data in the reference cells. The PDF approximation is performed by the Ozturk algorithm which consists of two modes, referred to as the goodness of fit test mode and the approximation chart mode. These two modes are discussed in the following sections.

#### **VI.4.2.1 - Introduction to Ozturk Algorithm [26]**

The Ozturk algorithm is a recent algorithm based on sample order statistics that has been developed in [27] through [29] and has been reported in [30] for univariate distribution approximation. This algorithm has two modes of operation. In the first mode, the algorithm performs a goodness of fit test. The test determines, to a desired confidence level, whether the random data is statistically consistent with a specified probability distribution. In the second mode of operation, the algorithm approximates the PDF underlying the random data. In particular, by analyzing the random data and without any a priori knowledge, the algorithm identifies from a stored library of PDFs that density function which best approximates the data. Estimates of the location, scale, and shape parameters of the PDF are provided by the algorithm. The algorithm has been found to work reasonably well for observation sizes as small as 75 to 100. Throughout this work, a number of 100 reference cells are selected for each test cell.

#### **VI.4.2.2 - Goodness of Fit Test**

The goodness of fit test determines whether or not the set of data samples provided to the algorithm is statistically consistent with a specified distribution, referred to as the null hypothesis. Let  $N_R$  denote the number of reference cells. For the null hypothesis, the program utilizes a Monte Carlo simulation of 2,000 trials to generate an averaged set of  $N_R$  linked vectors in the UV plane, as shown in Figure VI.4.1. Using the standardized sample order statistics of the data, the program then creates a second system of  $N_R$  linked vectors in the UV plane, as shown in Figure VI.4.1.a. The terminal points of the linked vectors, as well as the shapes of their trajectories, are used in determining whether or not to accept the null hypothesis. The null hypothesis is the distribution against which the sample data is to be tested.

The algorithm provides quantitative information as to how consistent the sample data set is with the null hypothesis distribution by use of confidence con-

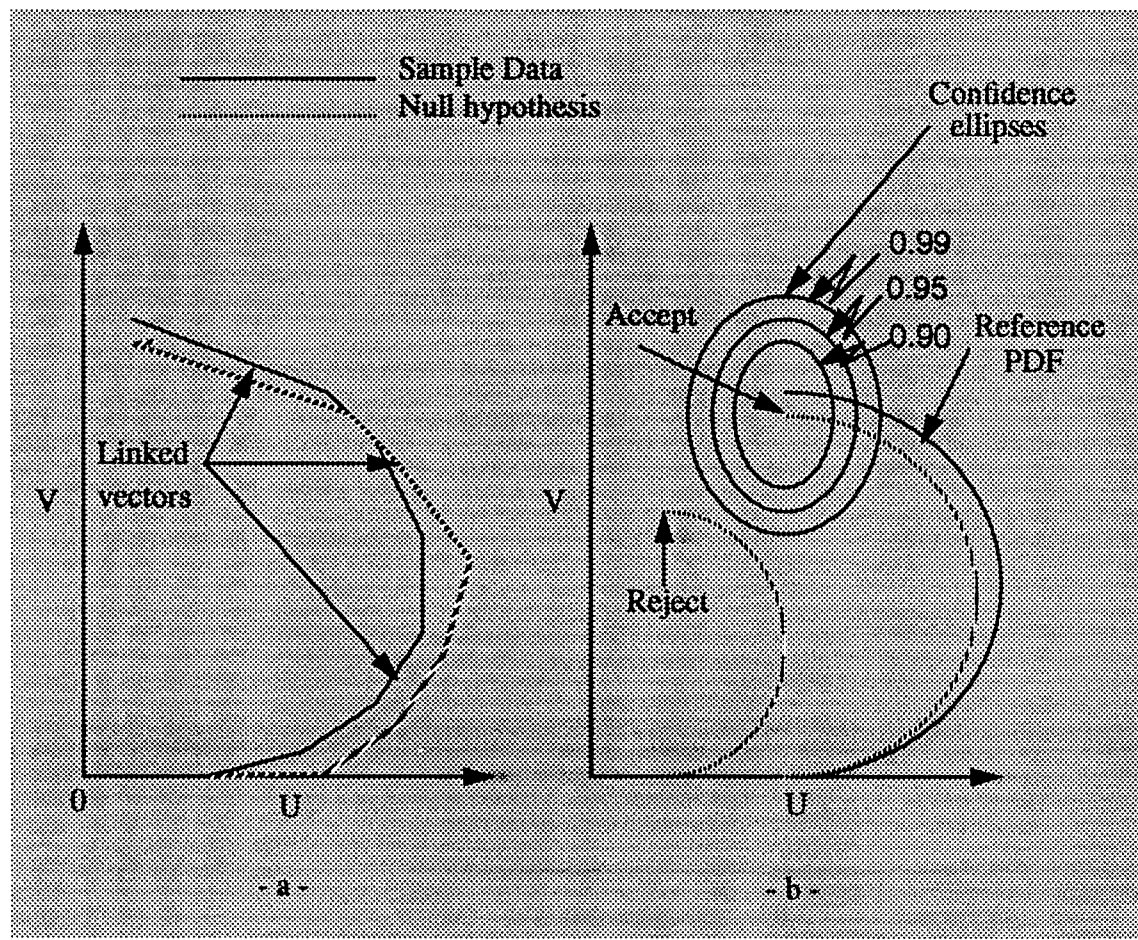


*Figure VI.4.1 - Goodness of Fit Test  
(a) linked vectors and (b) confidence ellipses*

tours where each contour is derived from a specified probability that the end point falls within the contour given that the data comes from the null distribution. An example of these contours is shown in Figure VI.4.1.b for probabilities of 0.9, 0.95, and 0.99. If the end point of the sample data linked vector locus falls within a contour, then the sample data set is said to be statistically consistent with the null hypothesis at a confidence level based on the probability specified for that contour. If the sample data set is truly consistent with the null hypothesis, the system of sample linked vectors is likely to closely follow that for the system of null linked vectors.

#### **VI.4.2.3 - Approximation Chart Mode**

The approximation chart mode is simply an extension of the goodness of fit test mode. Following a similar approach to that outlined in the section for the goodness of fit mode, random samples are generated from a library of different univariate probability distributions. In the goodness of fit test mode, the locus end point was obtained for the null hypothesis and sample size,  $N_R$ . For the approximation chart mode we go one step further by obtaining the locus end point for each distribution from the library of distributions for the given sample size,  $N_R$ , and for various choices of the shape parameter(s). Thus, depending on whether it has a shape parameter or not, each distribution is represented by a trajectory or point in the two dimensional UV plane. The distributions which are plotted on the distribution approximation chart are: (1) Gaussian, (2) Uniform, (3) Exponential, (4) Laplace, (5) Logistic, (6) Cauchy, (7) Extreme Value, (8) Gumbel type-2, (9) Gamma, (10) Pareto, (11) Weibull, (12) Lognormal, (13) Student-T, (14) K-distributed, (15) Beta, and (16) Su-Johnson. Figure VI.4.2 shows an example of the approximation chart. Note that every point in the approximation chart corresponds to a specific distribution. That point closest to the sample data locus end point is chosen as the best approximation to the PDF underlying the random data. This closest point is determined by projecting the sample locus end point to all points on the approximation chart and selecting that point whose perpendicular distance from the sample point is the smallest. Once the PDF underlying the sample data is selected, the shape, location and scale parameters are then approximated.

#### **VI.4.3 - PDF Approximation Metric**

In the goodness of fit test, it is hypothesized that whenever the end point of the sample data locus falls within the 0.99 probability confidence contour of the null distribution, the PDF underlying the data can be approximated by the null distribution. Because the confidence contours are neither circular nor exactly elliptical, analytically determining whether the locus end point falls within the contour is

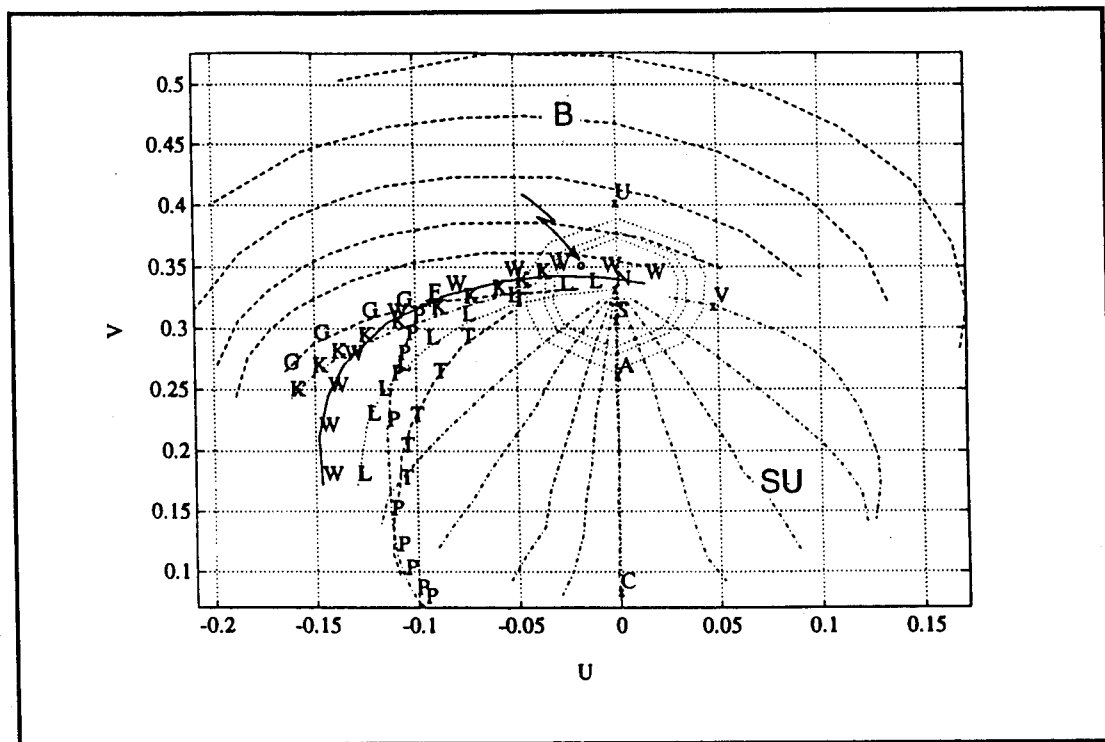


Figure VI.4.2 - Approximation Chart: N=Normal, U=Uniform, E=Negative Exponential, A=Laplace, S=Logistic, C=Cauchy, V=Extreme Value, T=Gumbel type-2, G=Gamma, P=Pareto, W=Weibull, L=Lognormal, K=K-distributed, B=Beta, and SU=Su-Johnson

a difficult computational problem. Thus, by definition, the sample data is declared to be from the null distribution provided the locus end point of the sample linked vectors is within the locus end point of the null distribution by a distance that is less than half the length of the minor axis of the 0.99 confidence contour.

Although the approximation chart can accommodate a wide variety of PDFs, most experimentally measured data for radar clutter envelopes are approximated as arising from either Rayleigh, Weibull, Lognormal, or K-distributed PDFs, as noted in Section I.2. Hence, for ease of implementation, it is assumed throughout this work that the random data in a homogeneous region is generated from and approximated by one of the cited PDFs. In addition, note that because the Weibull PDF becomes the Rayleigh PDF when its shape parameter equals 2, only Weibull, Lognormal, or K distributions are used. The half-length of the minor axis of the 0.99 confidence contour is listed in Table VI.4.1 for the Rayleigh, Weibull,

Lognormal, and K-distributed PDFs for various values of the shape parameters when  $N_R=100$ . For a shape parameter that is not listed in the table, the half-length of the minor axis of the 0.99 confidence contour is approximated by that of the closest shape parameter for the particular PDF. Because the smallest PDF approximation metric that appears in Table VI.4.1 is  $d_{min}=0.13 \times 10^{-1}$ , the null distribution is declared as the approximating distribution without the need to refer to the table whenever the distance between the end points of the sample and null distribution linked vectors is less than  $d_{min}$ .

#### **VI.4.4 - Outliers**

Even though the mapping procedure does a good job in separating the BN and CL regions one or more outliers may exist in a set of reference cells. For example, outliers may arise due to (1) misidentified BN cells in a CL patch or misidentified CL cells in the BN, (2) cells having data values of low probability of occurrence, and (3) cells containing signals from strong targets.

Outliers can cause a problem in correctly approximating the PDF underlying a set of data by significantly altering the set of linked vectors generated by the Ozturk algorithm. To illustrate this, a set of  $N_R= 100$  reference data, referred to as set A, are generated from the Lognormal distribution with shape parameter 0.01. The histogram of this set is plotted in Figure VI.4.3. Also, another set, referred to as set B, is formed which contains 97 data points from set A and three data points with very small values to constitute the outliers in the set. Figure VI.4.4 shows the histogram of this second set. Note from the histogram that the three data points have resulted in an isolated bar. The two sets are processed by the Ozturk algorithm and have their locus end points plotted in the approximation charts of Figures VI.4.5 and VI.4.6. Note how the end point in Figure VI.4.6 for the set containing outliers (set B) is far removed from the Lognormal PDF from which 97 out of the 100 data points of set B were generated. To understand the cause, Figures VI.4.7 and VI.4.8 show the plots of the goodness of fit test for set A and set B, respectively, where the null hypothesis is the Lognormal PDF with shape pa

PDF	Shape Parameter	Half -length of the minor axis
Rayleigh	-	$0.47 \times 10^{-1}$
Weibull	0.1	$0.25 \times 10^{-1}$
	0.5	$0.41 \times 10^{-1}$
	1.0	$0.41 \times 10^{-1}$
	2.0	$0.47 \times 10^{-1}$
	3.0	$0.47 \times 10^{-1}$
	4.0	$0.45 \times 10^{-1}$
	5.0	$0.44 \times 10^{-1}$
	10.0	$0.44 \times 10^{-1}$
Lognormal	0.01	$0.48 \times 10^{-1}$
	0.05	$0.45 \times 10^{-1}$
	0.1	$0.43 \times 10^{-1}$
	0.2	$0.42 \times 10^{-1}$
	0.3	$0.42 \times 10^{-1}$
	0.4	$0.46 \times 10^{-1}$
	1.0	$0.41 \times 10^{-1}$
	5.0	$0.28 \times 10^{-1}$
	10.0	$0.13 \times 10^{-1}$
K-distribution	0.01	$0.13 \times 10^{-1}$
	0.1	$0.37 \times 10^{-1}$
	1.0	$0.29 \times 10^{-1}$
	5.0	$0.47 \times 10^{-1}$
	10.0	$0.47 \times 10^{-1}$
	20.0	$0.49 \times 10^{-1}$
	40.0	$0.49 \times 10^{-1}$
	50.0	$0.49 \times 10^{-1}$

Table VI.4.1 - PDF Approximation Metric for Different PDFs.  $N_R=100$

parameter 0.01. Comparing the two Figures, it is noted that the linked vectors in set B are smaller than those of set A causing the locus end point for set B to fall way below the end point for set A and, therefore, outside the confidence ellipses. This

is due to the fact that the amplitudes of the linked vectors are proportional to the magnitude of the standardized data which depend on the mean and standard deviation of the set. The three outliers do not significantly affect the mean of the set but do increase the variance tremendously causing the standardized data and, therefore, the amplitudes of the linked vectors to become smaller. In this example, the mean and standard deviation for set A are equal to 32.54 and 4.69, respectively, while the mean and standard deviation for set B are equal to 31.63 and 18.08, respectively. This example illustrates what can happen when three BN cells with small data values are misidentified and associated with a set of CL cells.

One way to identify outliers within a region is to compute the mean  $m$  and standard deviation  $\sigma$  within that region and call as an outlier any cell whose data value falls outside the interval  $[m-2\sigma, m+2\sigma]$ . This method is used to identify outliers within a set of selected reference cells. When this method is applied to set B, whose histogram is shown in Figure VI.4.4, the three outliers are identified and removed from the set.

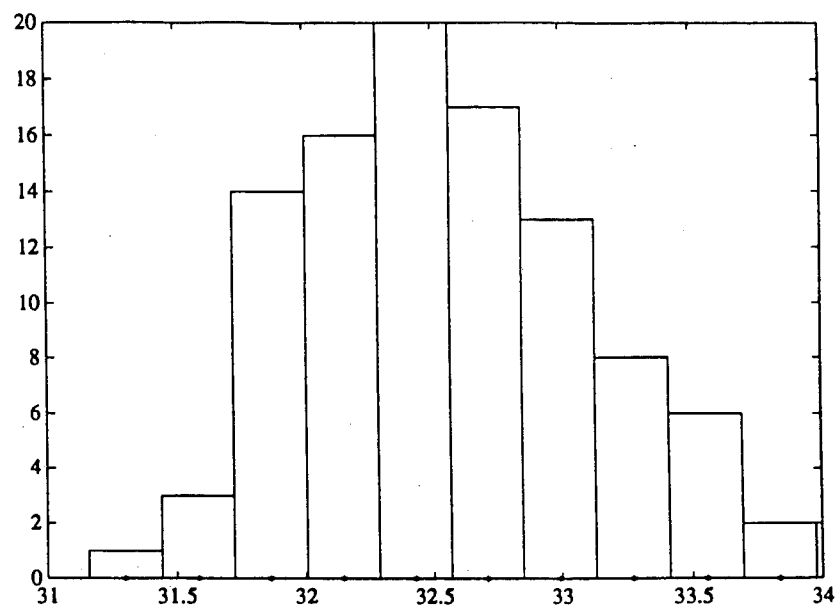


Figure VI.4.3 - Histogram of Set A

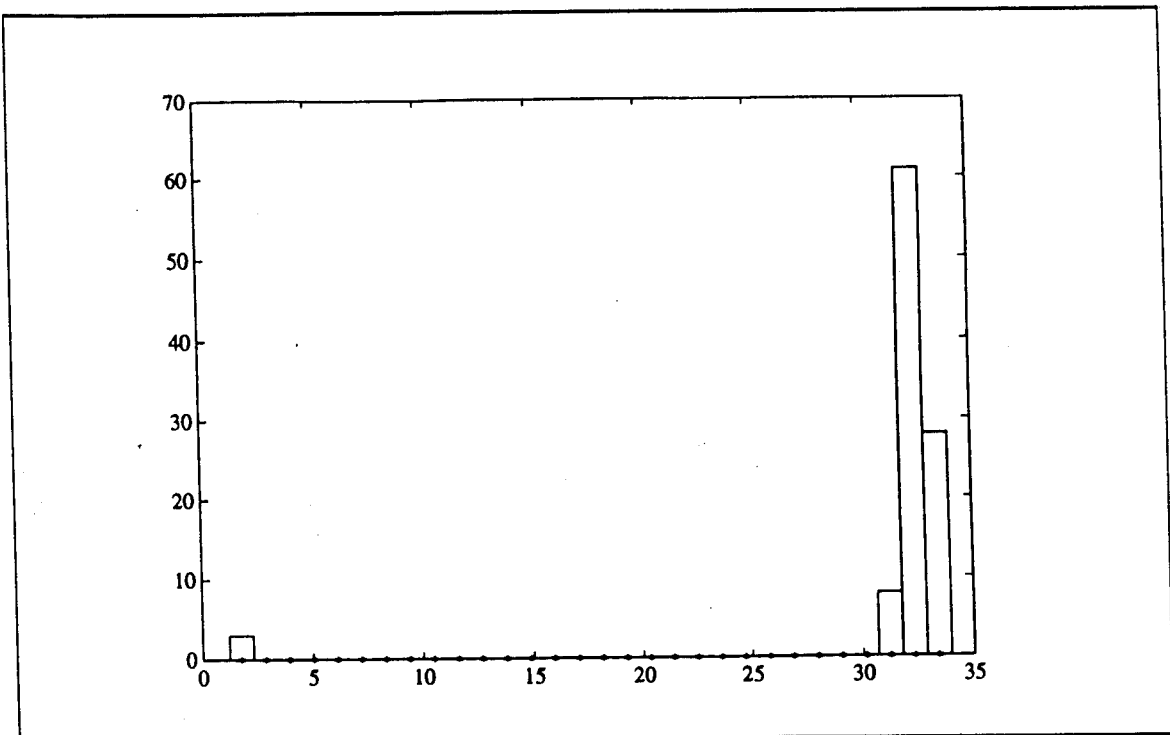


Figure VI.4.4 - Histogram of Set B

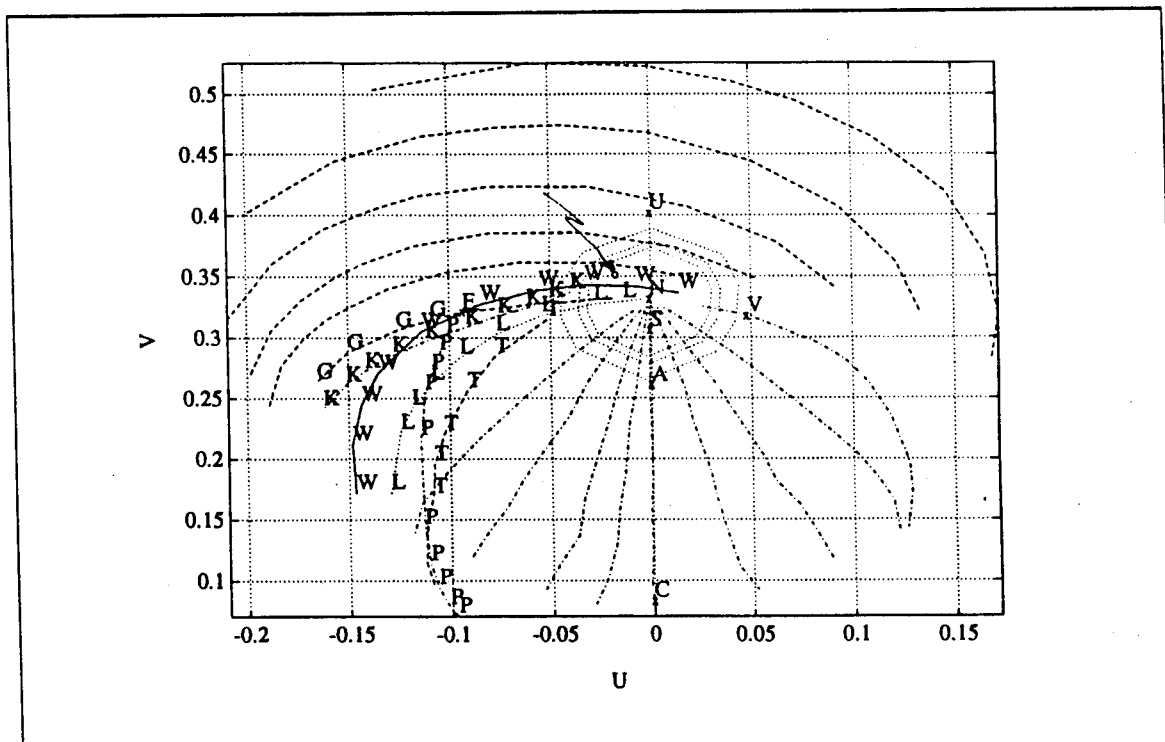
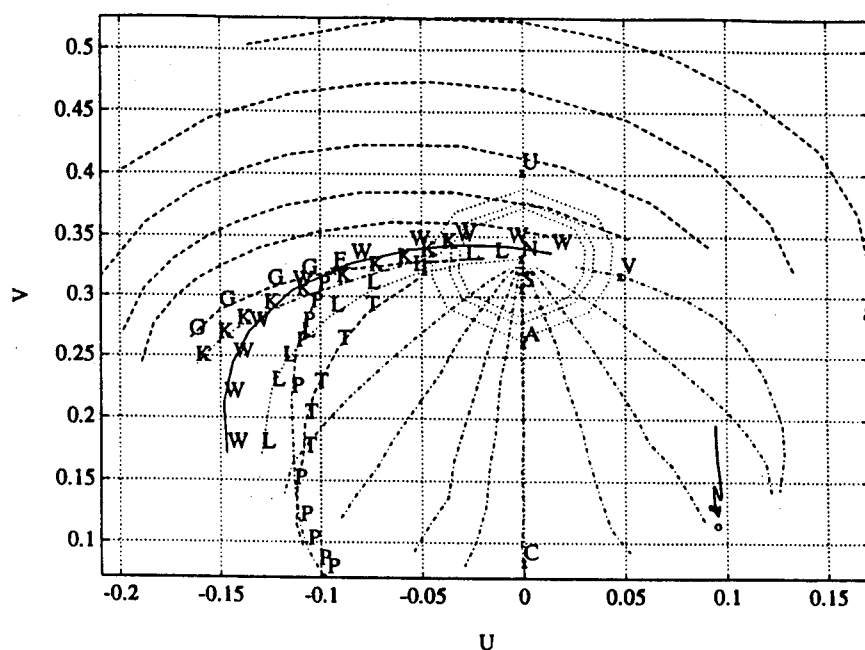
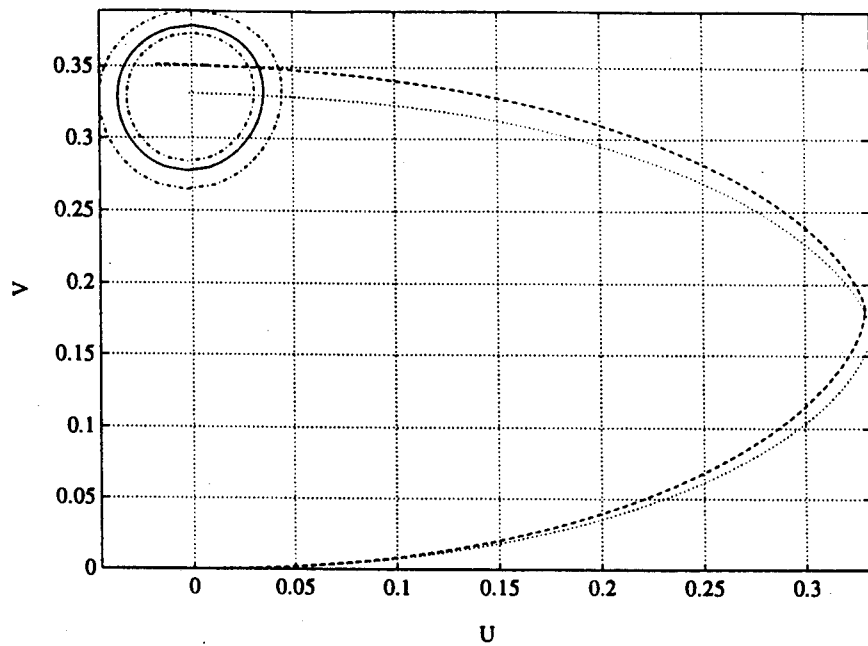


Figure VI.4.5 - Approximation Chart for the End Point of Set A



*Figure VI.4.6 - Approximation Chart for the End Point of Set B*



*Figure VI.4.7 - Goodness of Fit Test for Set A*

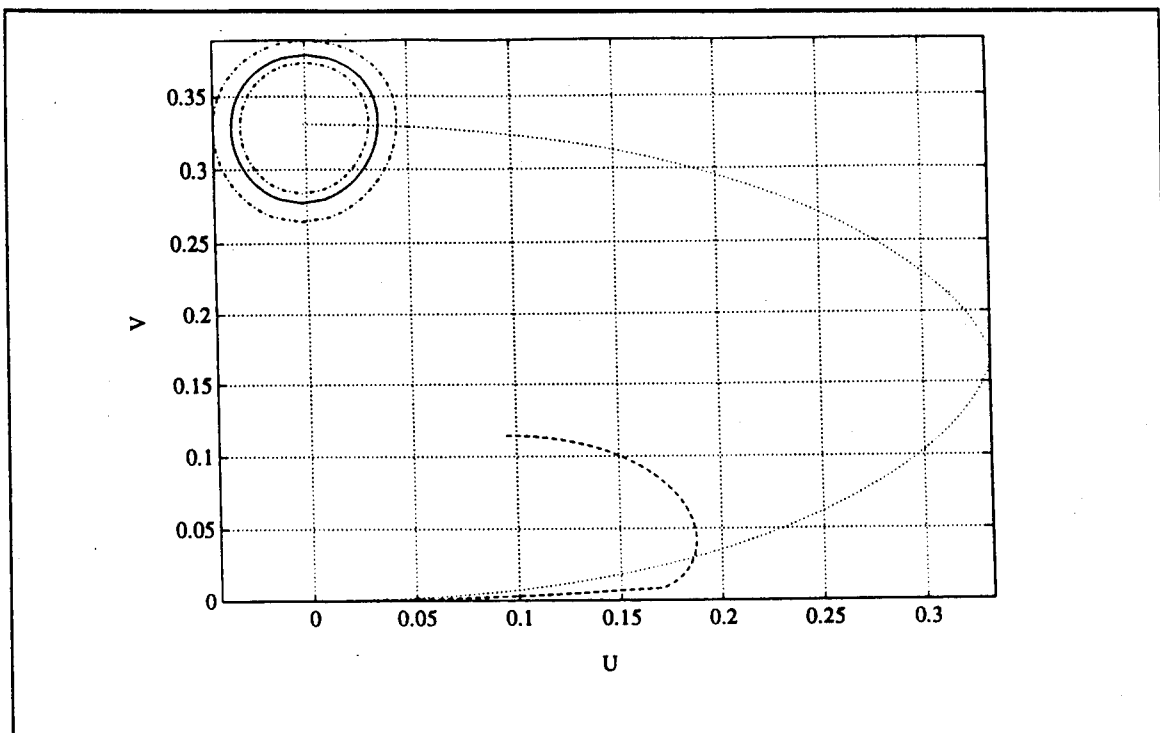


Figure VI.4.8 - Goodness of Fit Test for Set B

#### **VI.4.5 - PDF Approximation Strategy**

As mentioned in Section VI.4.3, CL data are generated in this work from either the Weibull, Lognormal, or K-distributed distributions. Consequently, the strategy for approximating the PDF underlying a CL patch consists of the following steps:

- 1 - Select a total of  $N_T$  test cells that are evenly spread throughout the CL patch.
- 2 - For each test cell, choose its closest  $N_R=100$  reference cells as described in Section VI.4.1.
- 3 - Using the Ozturk algorithm, determine the distance between the locus end point of the data linked vectors and its projection onto the Weibull, Lognormal, and K-distributed trajectories.
- 4 - Discard those PDFs for which the distances in step 3 exceed the correspond-

ing distances obtained from Table VI.4.1.

5 - If all possible PDFs are discarded in step 4, excise any outliers that may exist from the data and proceed to step 3.

6 - Use IPUS, as discussed in the next chapter, to determine the best PDF(s) to approximate the data.

Steps 1 through 5 are now illustrated through examples.

## **VI.5 - Examples**

In this section, indexing is performed on the same examples considered in Section V.4 where the mapping procedure was carried out. Discussion of each example ends with a table indicating the approximations to be used for the PDFs underlying selected test cells in the CL patches. The quality of the approximations is discussed in Chapter VII for each of the examples.

### **VI.5.1 - Example 1**

Consider the example of Section V.4.2.1 where the parameters of the generated scene, previously given in Table V.4.1, are repeated in Table VI.5.1.

Clutter Patch	CNR (dB)	Data Distribution	Shape Parameter	Number of cells
A	10	Rayleigh	None	117
B	20	K-distributed	10.0	1423
C	30	Lognormal	0.01	146
D	40	Weibull	5.00	146

**Table VI.5.1 - CL Patch Parameters**

### **(i) - Assessment**

The indexing procedure starts by first assessing the mapped volume. This consists of labeling the CL patches, estimating CNR for each patch, and counting the number of cells in each patch. The results are presented in Table VI.5.2.

Clutter Patch	Clutter Patch Label	CNR (dB)	Number of cells
A	1	9.04	113
C+D	2	36.66	304
B	3	23.31	1444

Table VI.5.2 - Assessment Parameters

CL patches labeled 1, 2 and 3, are shown in Figure VI.5.1. By comparing Table VI.5.1 with Table VI.5.2, it is seen that reasonable results are obtained for the CNRs and numbers of cells. Since the CL patch labeled as 2 consists of C+D, its CNR and number of cells, respectively, are approximated by the average of the CNRs and the sum of the number of cells for C and D.

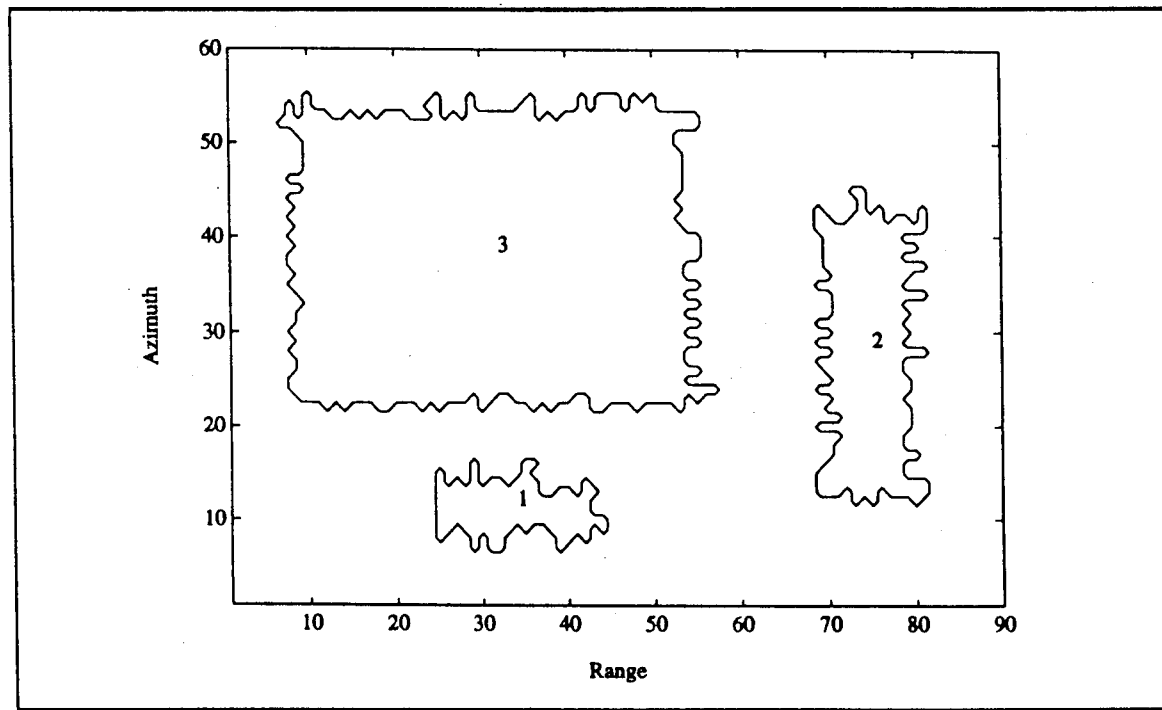


Figure VI.5.1 - Contour Plot of the Mapped Volume after Numbering

## (ii) - CL Subpatch Investigation

The next step in the indexing procedure consists of identifying subclutter

patches within a CL patch. This is done by selecting a CL patch and applying the mapping procedure to it. If one or more subpatches exist, the procedure attempts to first identify the subpatch having the lowest average power. If a subpatch does not exist, the procedure attempts to recognize this situation.

Let PLQP, PLCQP, and PLCCP represent the percentage number of cells of the subpatch with the lowest power among the possible subpatches of a CL patch in the quantized, first-corrected and second-corrected stages, respectively. Tables VI.5.3, 4, and 5 show the results of the mapping procedure applied, respectively, to CL patches 1, 2, and 3. For both CL patches 1 and 3, the mapping procedure results with PLCCP being equal to 100%, reflecting the conclusion that the subpatches with the lowest average power in CL patches 1 and 3 occupy 100% of the area in each patch. Therefore, it is concluded that both CL patches 1 and 3 are homogeneous and do not contain any subpatches. On the other hand, mapping of CL patch 2 results with PLCCP=48.75%. This indicates that CL patch 2 contains at least two subpatches and the subpatch with the lowest power occupies 48.75% of the total area of patch 2. This is consistent with the generated surveillance volume, where CL patch C has a smaller power than CL patch D and C occupies 50% of the total area of CL patch 2.

Clutter Patch 1		
PLQP (%)		
10.00 (guess)	NCQ=8 NCC=1	PLCQP=70.59 PLCCP=20.59
20.59 previous PLCCP	NCQ=8 NCC=1	PLCQP=94.12 PLCCP=82.35
82.35 previous PLCCP	NCQ=8 NCC=1	PLCQP=100.0 PLCCP=100.0

Table VI.5.3 - Mapping Procedure Applied to CL Patch 1

Clutter Patch 2		
PLQP (%)		
10.00 (guess)	NCQ=8 NCC=1	PLCQP=39.38 PLCCP=7.50
20.00 previous PLCCP	NCQ=8 NCC=1	PLCQP=59.38 PLCCP=43.12
43.12 previous PLCCP	NCQ=7 NCC=1	PLCQP=55.00 PLCCP=49.38
49.38 previous PLCCP	NCQ=5 NCC=1	PLCQP=50.62 PLCCP=46.25
49.38 previous PLCCP	NCQ=5 NCC=3	PLCQP=50.62 PLCCP=48.75

Table VI.5.4 - Mapping Procedure Applied to CL Patch 2

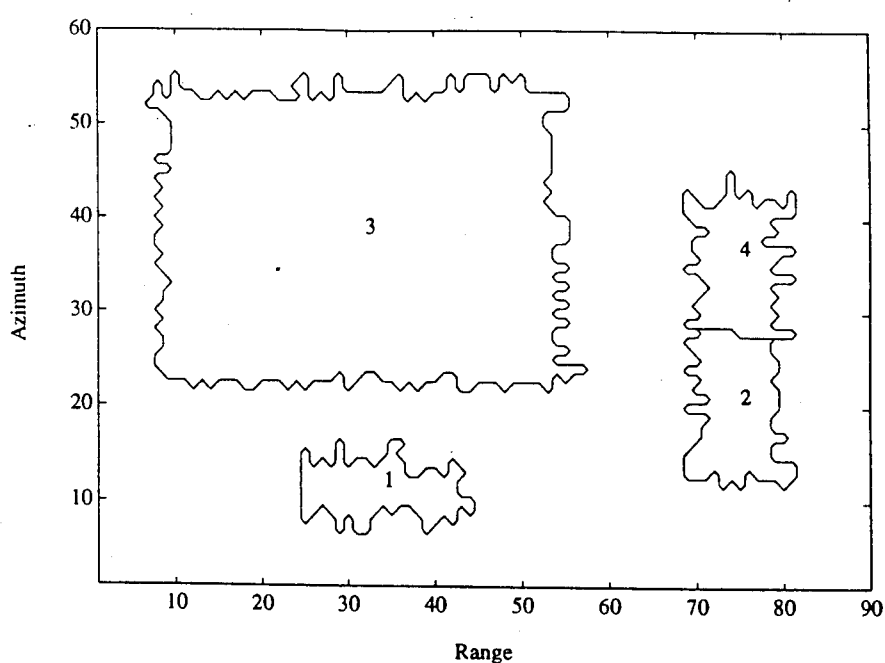
Clutter Patch 3		
PLQP (%)		
10.00 (guess)	NCQ=8 NCC=1	PLCQP=50.25 PLCCP=12.19
12.19 previous PLCCP	NCQ=8 NCC=1	PLCQP=58.51 PLCCP=16.61
16.61 previous PLCCP	NCQ=8 NCC=1	PLCQP=73.62 PLCCP=28.80
28.80 (guess)	NCQ=8 NCC=1	PLCQP=92.57 PLCCP=66.19
66.19 previous PLCCP	NCQ=8 NCC=1	PLCQP=100.0 PLCCP=100.0

Table VI.5.5 - Mapping Procedure Applied to CL Patch 3

### **(iii) - Assessment**

Finally, mapping was applied to CL patches 2 and 4 with the result that both patches were judged to be homogeneous.

Treating each identified subpatch as a patch, assessment is done once more to relabel all subpatches in the surveillance volume. Results of the assessment are tabulated in Table VI.5.6. Now the surveillance volume is identified to include four CL patches where CL patches 1, 2, 3, and 4 coincide with CL patches A, C, B, and D, respectively, of the original scene. Note how close are the number of cells and CNR for every patch when comparing Tables VI.5.6 and VI.5.1. Note also that using the values of Table VI.2.1, every CL patch in the surveillance volume has been identified as a WSC region. Also, using the ranges of the CNR for the strong, weak, and intermediate signal cases, as given in Table VI.2.1, classification of the CL patches is shown in column 5 of Table VI.5.6. Figure VI.5.2 shows the result of the numbering of the new mapped volume.



**Figure VI.5.2 - Contour Plot of the Mapped Volume after Numbering**

Clutter Patch	Clutter Patch Label	CNR (dB)	Number of cells	Classification
A	1	9.04	113	WSC
C	2	30.63	151	WSC
B	3	23.31	1444	WSC
D	4	40.54	146	WSC

*Table VI.5.6 - Assessment Parameters*

**(iv) - Steps 1-5 of the PDF Approximation Strategy**

As detailed in Section VI.4.5, the first step in the PDF approximation strategy is to select a total of  $N_T$  test cells that are evenly spread throughout the CL patch. For each of the four CL patches listed in Table VI.5.6, let  $N_T=5$ . Assume each CL patch is scanned from left to right and from top to bottom. In each CL patch let the first cell scanned be numbered 1. The last cell scanned in each patch is assigned a number equal to the total number of cells in that patch. The test cells selected for CL patches 1, 2, 3, and 4 are listed in the first column of Tables VI.5.7, 8, 9, and 10, respectively. Note that the test cells are evenly spread throughout each CL patch.

The second step in the PDF approximation strategy is to choose for each test cell the closest  $NR=100$  reference cells as detailed in Section VI.4.1.

Using the Ozturk algorithm, the third step is to determine the distance between the locus end point of the data linked vectors and its projection onto the Weibull, Lognormal, and K-distributed trajectories. The distance, shape, scale, and location parameters for the approximating PDF's are tabulated in columns 4, 5, 6, and 7, respectively, of Tables VI.5.7, 8, 9, and 10. The (U,V) coordinates of the data locus end point are listed in column 8 of the tables. Finally, column 3 provides a ranking based on the smallest distance between the approximating PDF

and the data locus end point.

Step 4 is to discard those PDFs for which the distances in step 3 exceed the corresponding distances obtained from Table VI.4.1. In Tables VI.5.7, 8, 9, and 10, the results are indicated by either  $\times$  or  $\checkmark$ , respectively, depending upon whether the PDFs are discarded or not.

In the shaded background rows of Table VI.5.8, related to CL patch 2, note that all possible PDFs are discarded. Consequently, step 5 is implemented where outliers that exist are excised from each set of reference cells. Steps 3 and 4 are then repeated and the results presented with a white background in Table VI.5.8. With the outliers removed, note that the distance measure for one or more of the approximating PDFs has become significantly smaller.

Test Cell No.	PDF	Rank	Distance	Shape	Scale	Location	(U,V)
1	W	1	$0.72 \times 10^{-2} \checkmark$	2.12	3.20	0.58	(-0.0298, 0.3503)
	L	5	$0.22 \times 10^{-1} \checkmark$	0.18	7.48	-4.18	
	K	3	$0.17 \times 10^{-1} \checkmark$	50.0	0.43	0.77	
28	W	2	$0.90 \times 10^{-2} \checkmark$	2.14	3.26	0.54	(-0.0293, 0.3320)
	L	5	$0.24 \times 10^{-1} \checkmark$	0.18	7.76	-4.47	
	K	3	$0.18 \times 10^{-1}$	50.0	0.43	0.75	
57	W	1	$0.74 \times 10^{-2} \checkmark$	1.94	3.01	0.74	(-0.0376, 0.3500)
	L	5	$0.24 \times 10^{-1} \checkmark$	0.21	6.74	-3.50	
	K	3	$0.13 \times 10^{-1} \checkmark$	50.0	0.43	0.69	
85	W	2	$0.13 \times 10^{-1} \checkmark$	2.06	3.16	0.63	(-0.0313, 0.3561)
	L	6	$0.28 \times 10^{-1} \checkmark$	0.19	7.38	-4.10	
	K	3	$0.21 \times 10^{-1} \checkmark$	50.0	0.43	0.73	
113	W	1	$0.23 \times 10^{-2} \checkmark$	2.01	3.09	0.69	(-0.0330, 0.3455)
	L	5	$0.18 \times 10^{-1} \checkmark$	0.20	7.02	-3.75	
	K	2	$0.11 \times 10^{-1} \checkmark$	50.0	0.43	0.73	

Table VI.5.7 - PDF Approximation for CL Patch 1

Test Cell No.	PDF	Rank	Distance	Shape	Scale	Location	(U,V)
1	W	17	$0.24 \times 10^{-0}$ <del>X</del>	5.00	9.00	24.12	(-0.0952, 0.1143)
	L	19	$0.25 \times 10^{-0}$ <del>X</del>	0.76	1.97	30.20	
	K	20	$0.26 \times 10^{-0}$ <del>X</del>	32.0	0.72	28.99	
1 w/o 3 Outliers	W	2	$0.87 \times 10^{-2}$ ✓	2.60	1.39	31.30	(-0.0177, 0.3512)
	L	4	$0.21 \times 10^{-1}$ ✓	0.10	5.02	27.50	
	K	6	$0.27 \times 10^{-1}$ ✓	50.0	0.16	31.58	
38	W	23	$0.29 \times 10^{-0}$ <del>X</del>	0.73	1.81	30.84	(0.1281, 0.1361)
	L	21	$0.27 \times 10^{-0}$ <del>X</del>	0.81	2.27	29.80	
	K	20	$0.26 \times 10^{-0}$ <del>X</del>	50.0	0.72	28.09	
38 w/o 4 Outliers	W	1	$0.63 \times 10^{-2}$ ✓	2.82	1.46	31.30	(-0.0122, 0.3486)
	L	4	$0.18 \times 10^{-1}$ ✓	0.06	7.81	24.77	
	K	14	$0.31 \times 10^{-1}$ ✓	50.0	0.15	31.67	
76	W	24	$0.30 \times 10^{-0}$ <del>X</del>	0.74	1.81	30.79	(0.1310, 0.1360)
	L	21	$0.27 \times 10^{-0}$ <del>X</del>	1.10	1.29	30.67	
	K	20	$0.26 \times 10^{-0}$ <del>X</del>	50.0	0.71	28.09	
76 w/o 4 Outliers	W	1	$0.20 \times 10^{-2}$ ✓	2.52	1.25	31.43	(-0.0202, 0.3406)
	L	3	$0.11 \times 10^{-1}$ ✓	0.13	3.62	28.89	
	K	5	$0.21 \times 10^{-1}$ ✓	50.0	0.14	31.66	
114	W	26	$0.31 \times 10^{-0}$ <del>X</del>	0.52	1.19	31.02	(0.1581, 0.1563)
	L	23	$0.29 \times 10^{-0}$ <del>X</del>	1.84	0.37	31.41	
	K	21	$0.27 \times 10^{-0}$ <del>X</del>	50.0	0.84	27.16	
114 w/o 5 Outliers	W	12	$0.28 \times 10^{-1}$ ✓	2.45	1.19	31.41	(-0.0235, 0.3143)
	L	3	$0.14 \times 10^{-1}$ ✓	0.18	2.57	29.86	
	K	11	$0.28 \times 10^{-1}$ ✓	50.0	0.14	31.60	
151	W	26	$0.31 \times 10^{-0}$ <del>X</del>	0.52	1.19	31.02	(0.1581, 0.1563)
	L	23	$0.29 \times 10^{-0}$ <del>X</del>	1.85	0.38	31.41	
	K	21	$0.27 \times 10^{-0}$ <del>X</del>	50.0	0.84	27.16	
151 w/o 5 Outlier	W	10	$0.28 \times 10^{-1}$ ✓	2.44	1.19	31.48	(-0.0235, 0.3147)
	L	3	$0.14 \times 10^{-1}$ ✓	0.18	2.58	29.85	
	K	11	$0.28 \times 10^{-1}$ ✓	50.0	0.14	31.60	

Table VI.5.8 - PDF Approximation for CL Patch 2

Test Cell No.	PDF	Rank	Distance	Shape	Scale	Location	(U,V)
1	W	5	$0.17 \times 10^{-1}$ ✓	1.62	13.1	0.82	(-0.0476, 0.3235)
	L	1	$0.25 \times 10^{-2}$ ✓	0.34	20.4	-9.04	
	K	3	$0.75 \times 10^{-2}$ ✓	15.6	3.90	-1.19	
361	W	6	$0.24 \times 10^{-1}$ ✓	1.67	13.7	1.65	(-0.0438, 0.3171)
	L	1	$0.49 \times 10^{-2}$ ✓	0.33	21.4	-8.75	
	K	4	$0.15 \times 10^{-1}$ ✓	15.8	3.94	-0.01	
722	W	3	$0.19 \times 10^{-1}$ ✓	2.67	22.1	-4.93	(-0.0154, 0.3620)
	L	5	$0.32 \times 10^{-1}$ ✓	0.07	1.15	-101.14	
	K	7	$0.35 \times 10^{-1}$ ✓	50.0	2.43	-0.14	
1083	W	1	$0.33 \times 10^{-2}$ ✓	1.63	11.8	3.41	(-0.0508, 0.3433)
	L	5	$0.22 \times 10^{-1}$ ✓	0.31	19.8	-6.95	
	K	2	$0.11 \times 10^{-1}$ ✓	35.0	2.34	1.51	
1444	W	1	$0.36 \times 10^{-2}$ ✓	2.20	16.9	-1.17	(-0.0285, 0.3393)
	L	3	$0.11 \times 10^{-1}$ ✓	0.19	37.7	-24.57	
	K	4	$0.12 \times 10^{-1}$ ✓	50.0	2.18	0.26	

Table VI.5.9 - PDF Approximation for CL Patch 3

Test Cell No.	PDF	Rank	Distance	Shape	Scale	Location	(U,V)
1	W	5	$0.44 \times 10^{-1}$ ✓	4.30	86.9	16.66	(0.0165, 0.3811)
	L	6	$0.52 \times 10^{-1}$ ✗	0.01	2625	-2529.01	
	K	20	$0.72 \times 10^{-1}$ ✗	50.0	6.34	57.92	
37	W	5	$0.36 \times 10^{-1}$ ✓	3.88	79.5	23.66	(0.0102, 0.3751)
	L	6	$0.44 \times 10^{-1}$ ✓	0.01	2628	-2532.56	
	K	18	$0.63 \times 10^{-1}$ ✗	50.0	6.35	57.54	
73	W	2	$0.78 \times 10^{-2}$ ✓	5.00	96.2	17.69	(0.0119, 0.3630)
	L	5	$0.23 \times 10^{-1}$ ✓	0.01	2547	-2508.77	
	K	19	$0.60 \times 10^{-1}$ ✗	50.0	6.16	58.36	
110	W	1	$0.52 \times 10^{-2}$ ✓	5.00	99.3	5.24	(0.0153, 0.3317)
	L	5	$0.16 \times 10^{-1}$ ✓	0.01	2616	-2520.22	
	K	18	$0.56 \times 10^{-1}$ ✗	50.0	6.32	58.84	
146	W	1	$0.47 \times 10^{-2}$ ✓	4.37	92.2	11.62	(0.0080, 0.3430)
	L	3	$0.14 \times 10^{-1}$ ✓	0.01	2736	-2640.34	
	K	18	$0.48 \times 10^{-1}$ ✓	50.0	6.61	56.10	

Table VI.5.10 - PDF Approximation for CL Patch 4

## VI.5.2 - Example 2

Consider now the example of Section V.4.2.2 where the parameters of the generated scene, previously given in Table V.4.4, are repeated in Table VI.5.11.

Clutter Patch	CNR (dB)	Data Distribution	Shape Parameter	Number of cells
A	10	K-distributed	1.5	117
B	10	Weibull	1.0	672
C	10	Lognormal	1.0	151
D	10	Rayleigh	None	151

Table VI.5.11 - CL Patch Parameters

### (i) - Assessment

Following the same strategy discussed in Section VI.5.1, results of the assessment stage are presented in Table VI.5.12.

Clutter Patch	Clutter Patch Label	CNR (dB)	Number of cells
A	1	12.03	133
C+D	2	8.22	308
B	3	8.65	622

Table VI.5.12 - Assessment Parameters

CL patches 1, 2 and 3, are shown in Figure VI.5.3. Comparison of Tables VI.5.11 and VI.5.12 shows that reasonable results are obtained for the CNRs and number of cells.

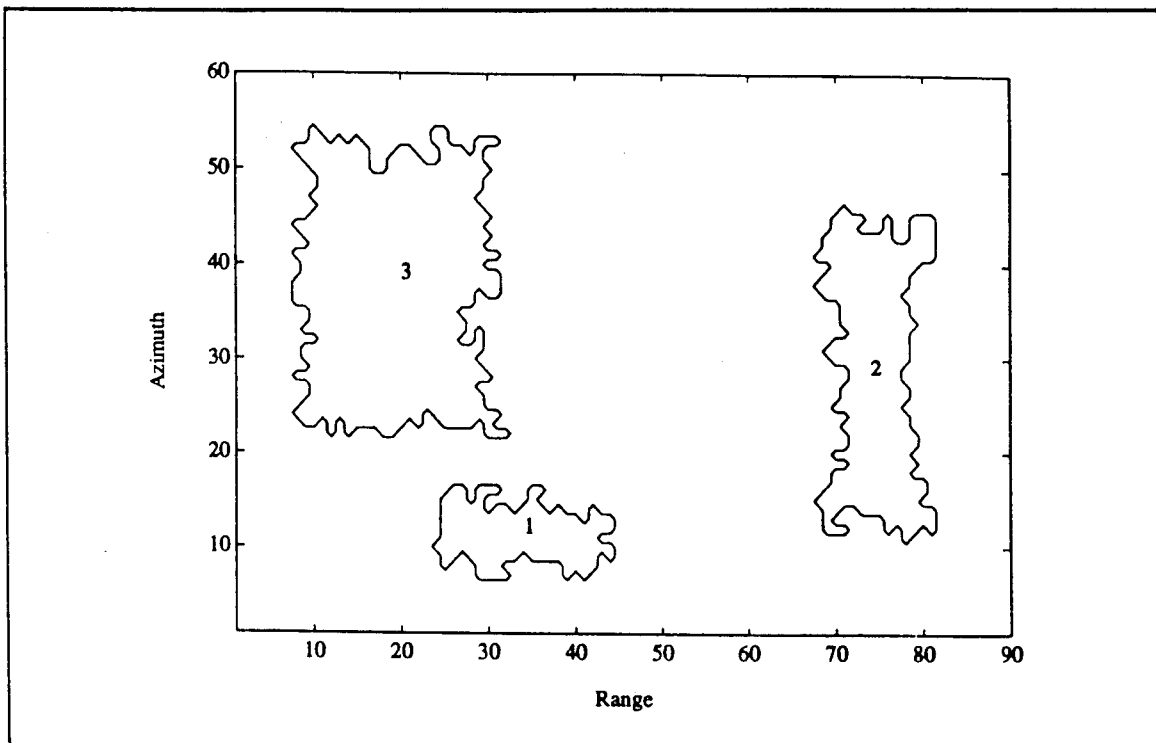


Figure VI.5.3 - Contour Plot of the Mapped Volume after Numbering

**(ii) - CL Subpatches Investigation**

Tables VI.5.13, 14, and 15 show the results of the mapping procedure ap-

Clutter Patch 1		
PLQP (%)		
10.00 (guess)	NCQ=8 NCC=1	PLCQP=36.73 PLCCP=8.16
20.00 modified PLQP	NCQ=8 NCC=1	PLCQP=71.43 PLCCP=28.57
28.57 previous PLCCP	NCQ=8 NCC=1	PLCQP=87.76 PLCCP=55.10
55.10 previous PLCCP	NCQ=8 NCC=1	PLCQP=100.0 PLCCP=100.0

Table VI.5.13 - Mapping Procedure Applied to CL Patch 1

Clutter Patch 2		
PLQP (%)		
10.00 (guess)	NCQ=8 NCC=1	PLCQP=60.38 PLCCP=19.50
19.50 previous PLCCP	NCQ=8 NCC=1	PLCQP=81.76 PLCCP=49.06
49.06 previous PLCCP	NCQ=8 NCC=1	PLCQP=94.97 PLCCP=81.76
81.76 previous PLCCP	NCQ=8 NCC=1	PLCQP=100.0 PLCCP=100.0

Table VI.5.14 - Mapping Procedure Applied to CL Patch 2

Clutter Patch 3		
PLQP (%)		
10.00 (guess)	NCQ=8 NCC=1	PLCQP=63.36 PLCCP=22.12
22.12 previous PLCCP	NCQ=8 NCC=1	PLCQP=89.63 PLCCP=62.90
62.90 previous PLCCP	NCQ=8 NCC=1	PLCQP=100.0 PLCCP=100.0

Table VI.5.15 - Mapping Procedure Applied to CL Patch 3

plied, respectively to CL patches 1, 2, and 3. For CL patches 1, 2, and 3, the mapping procedure results with PLCCP being equal to 100% reflecting the conclusion that the subpatches with the lowest power in CL patches 1, 2, and 3 occupy 100% of the area in each patch. Therefore, it is concluded that all of these CL patches are homogeneous and do not contain any subpatches.

In fact, CL patch 2 consists of subpatches C and D. By using expert system rules, it is shown in Chapter VII that CL patch 2 can be further separated.

### **(iii) - Assessment**

Because CL subpatch identification does not result in finding any subpatch within CL patches 1,2 and 3, the mapped volume is not changed and assessment is not necessary.

### **(iv) - Steps 1-5 of the PDF Approximation Strategy**

Tables VI.5.16, VI.5.17, and VI.5.18 list the results of steps 1-5 of the PDF approximation strategy applied to CL patches 1, 2, and 3, respectively.

Test Cell No.	PDF	Rank	Distance	Shape	Scale	Location	(U,V)
1	W L K	5 1 2	0.16x10 <sup>-1</sup> ✓ 0.31x10 <sup>-2</sup> ✓ 0.57x10 <sup>-2</sup> ✓	1.40 0.40 9.93	4.54 6.67 1.90	0.20 -2.93 -1.00	(-0.0566, 0.3207)
33	W L K	5 3 1	0.13x10 <sup>-1</sup> ✓ 0.73x10 <sup>-2</sup> ✓ 0.17x10 <sup>-2</sup> ✓	1.37 0.41 8.61	4.57 6.63 2.09	0.23 -2.80 -1.10	(-0.0604, 0.3232)
66	W L K	6 2 5	0.44x10 <sup>-1</sup> ✗ 0.16x10 <sup>-1</sup> ✗ 0.35x10 <sup>-1</sup> ✗	0.86 0.77 1.71	2.93 3.14 4.36	1.48 0.37 -0.36	(-0.0802, 0.2751)
66 w/o 3 outliers	W L K	4 3 1	0.13x10 <sup>-1</sup> ✓ 0.82x10 <sup>-2</sup> ✓ 0.16x10 <sup>-2</sup> ✓	1.30 0.45 6.96	3.82 5.26 2.03	0.68 -1.64 -0.58	(-0.0651, 0.32116)
99	W L K	5 1 3	0.23x10 <sup>-1</sup> ✓ 0.65x10 <sup>-3</sup> ✓ 0.11x10 <sup>-1</sup> ✓	1.27 0.48 6.23	4.11 5.35 2.35	0.62 -1.59 -0.79	(-0.0636, 0.3113)
133	W L K	7 3 6	0.56x10 <sup>-1</sup> ✗ 0.29x10 <sup>-1</sup> ✗ 0.48x10 <sup>-1</sup> ✗	0.73 0.83 1.73	2.39 2.82 4.93	2.05 0.85 -0.23	(-0.0732, 0.2641)
133 w/o 4 outliers	W L K	5 1 2	0.18x10 <sup>-1</sup> ✓ 0.21x10 <sup>-2</sup> ✓ 0.71x10 <sup>-2</sup> ✓	1.36 0.42 8.80	4.08 5.77 1.93	0.55 -2.06 -0.62	(-0.0586, 0.3181)

*Table VI.5.16 - PDF Approximation for CL Patch 1*

Test Cell No.	PDF	Rank	Distance	Shape	Scale	Location	(U,V)
1	W	8	$0.57 \times 10^{-1} \times$	0.73	1.08	1.47	(-0.0725, 0.2622)
	L	3	$0.30 \times 10^{-1} \checkmark$	0.84	1.27	0.93	
	K	6	$0.50 \times 10^{-1} \times$	1.71	2.02	0.41	
77	W	7	$0.85 \times 10^{-1} \times$	0.72	1.09	1.53	(-0.0813, 0.2659)
	L	2	$0.21 \times 10^{-1} \checkmark$	0.85	1.27	0.99	
	K	5	$0.41 \times 10^{-1} \times$	1.47	2.19	0.51	
154	W	2	$0.18 \times 10^{-1} \checkmark$	1.34	2.56	0.91	(-0.0740, 0.3510)
	L	7	$0.37 \times 10^{-1} \checkmark$	0.40	3.98	-1.07	
	K	4	$0.29 \times 10^{-1} \checkmark$	1.92	1.16	0.08	
231	W	3	$0.93 \times 10^{-2} \checkmark$	2.08	4.06	0.24	(-0.0316, 0.3338)
	L	2	$0.67 \times 10^{-2} \checkmark$	0.21	8.63	-4.97	
	K	4	$0.93 \times 10^{-2} \checkmark$	50.0	0.55	0.42	
308	W	1	$0.01 \times 10^{-3} \checkmark$	1.99	3.99	0.25	(-0.0335, 0.3435)
	L	4	$0.16 \times 10^{-1} \checkmark$	0.20	9.10	-5.52	
	K	2	$0.94 \times 10^{-2} \checkmark$	50.0	0.56	0.29	

Table VI.5.17- PDF Approximation for CL Patch 2

Test Cell No.	PDF	Rate	Distance	Shape	Scale	Location	(U,V)
1	W	3	$0.69 \times 10^{-2} \checkmark$	0.90	2.06	0.87	(-0.0997, 0.3072)
	L	6	$0.19 \times 10^{-1} \checkmark$	0.69	2.45	-0.12	
	K	1	$0.26 \times 10^{-2} \checkmark$	1.69	2.94	-0.30	
156	W	1	$0.13 \times 10^{-2} \checkmark$	1.13	2.66	0.52	(-0.0830, 0.2397)
	L	5	$0.25 \times 10^{-1} \checkmark$	0.52	3.51	-1.02	
	K	4	$0.13 \times 10^{-1} \checkmark$	4.00	2.08	-0.65	
311	W	4	$0.13 \times 10^{-1} \checkmark$	1.17	2.50	0.88	(-0.0743, 0.3181)
	L	3	$0.11 \times 10^{-1} \checkmark$	0.52	3.21	-0.45	
	K	1	$0.48 \times 10^{-3} \checkmark$	4.47	1.78	-0.12	
466	W	4	$0.13 \times 10^{-1} \checkmark$	1.17	3.12	0.81	(-0.0743, 0.3174)
	L	3	$0.11 \times 10^{-1} \checkmark$	0.52	3.99	-0.84	
	K	1	$0.11 \times 10^{-2} \checkmark$	4.41	2.25	-0.45	
622	W	5	$0.24 \times 10^{-1} \checkmark$	0.76	2.13	1.43	(-0.0965, 0.2867)
	L	1	$0.33 \times 10^{-2} \checkmark$	0.79	2.57	0.31	
	K	3	$0.16 \times 10^{-1} \checkmark$	1.36	4.03	-0.19	

Table VI.5.18 - PDF Approximation for CL Patch 3

### VI.5.3 - Example 3

Finally, consider the example of Section V.4.2.3 where the parameters of the generated scene, previously given in Table V.4.7, are repeated in Table VI.5.19.

Clutter Patch	CNR (dB)	Data Distribution	Shape Parameter	Number of cells
A	10	Rayleigh	None	117
B	10	K-distributed	10.0	298
C	10	Lognormal	0.01	161
D	10	Weibull	10.0	162

Table VI.5.19 - CL Patch Parameters

### (i) - Assessment

Following the same strategy discussed in Section VI.5.1, results of the assessment stage are presented in Table VI.5.20.

Clutter Patch	Clutter Patch Label	CNR (dB)	Number of cells
A	1	9.34	124
C+D	2	10.63	341
B	3	13.47	306

Table VI.5.20 - Assessment Parameters

CL patches 1, 2 and 3, are shown in Figure VI.5.4. Comparison of Tables VI.5.19 and VI.5.20 shows that reasonable results are obtained for the CNRs and number of cells.

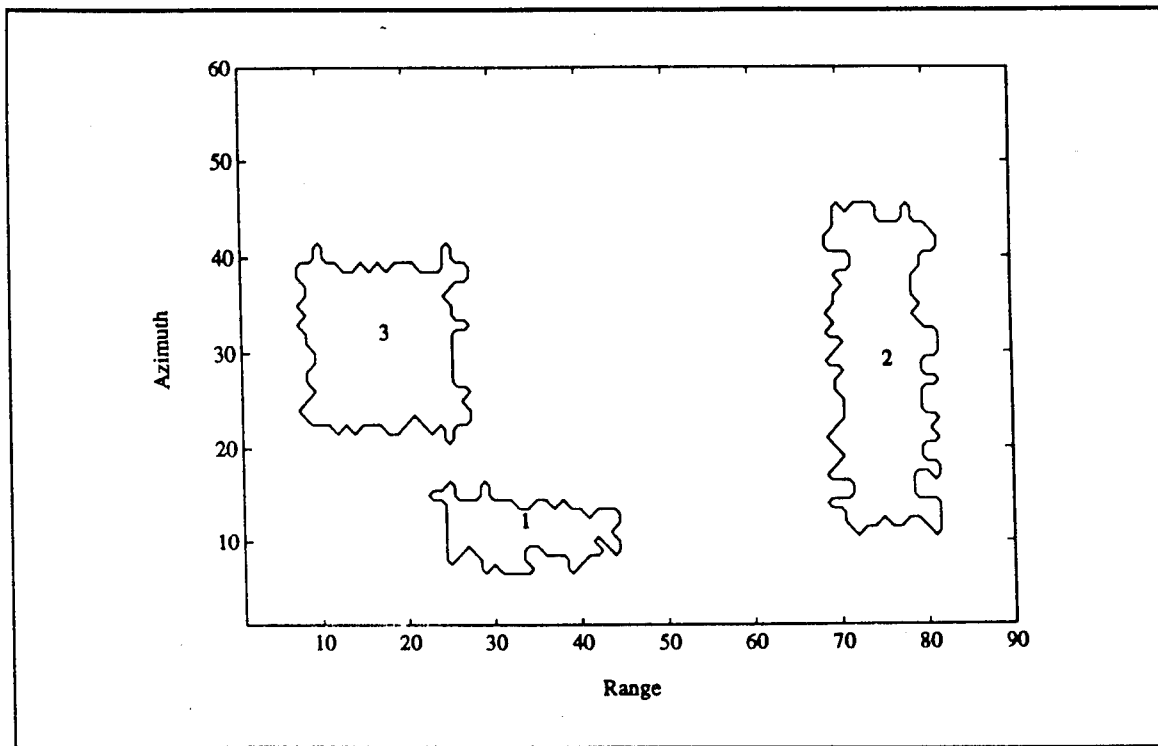


Figure VI.5.4 - Contour Plot of the Mapped Volume after Numbering

**(ii) - CL Subpatch Investigation**

Tables VI.5.21, 22, and 23 show the results of the mapping procedure ap-

Clutter Patch 1		
PLQP (%)		
10.00 (guess)	NCQ=8 NCC=1	PLCQP=48.94 PLCCP=8.51
20.00 modified PLQP	NCQ=8 NCC=1	PLCQP=82.98 PLCCP=51.06
51.06 previous PLCCP	NCQ=8 NCC=1	PLCQP=100.0 PLCCP=100.0

Table VI.5.21 - Mapping Procedure Applied to CL Patch 1

Clutter Patch 2		
PLQP (%)		
10.00 (guess)	NCQ=8 NCC=1	PLCQP=42.93 PLCCP=11.62
11.62 previous PLCCP	NCQ=8 NCC=1	PLCQP=53.54 PLCCP=13.64
13.64 previous PLCCP	NCQ=8 NCC=1	PLCQP=64.14 PLCCP=18.69
18.69 previous PLCCP	NCQ=8 NCC=1	PLCQP=77.27 PLCCP=32.32
32.32 previous PLCCP	NCQ=8 NCC=1	PLCQP=94.44 PLCCP=69.70
69.70 previous PLCCP	NCQ=8 NCC=1	PLCQP=100.0 PLCCP=100.0

Table VI.5.22 - Mapping Procedure Applied to CL Patch 2

Clutter Patch 3		
PLQP (%)		
10.00 (guess)	NCQ=8 NCC=1	PLCQP=46.53 PLCCP=14.36
14.36 previous PLCCP	NCQ=8 NCC=1	PLCQP=70.30 PLCCP=26.24
26.24 previous PLCCP	NCQ=8 NCC=1	PLCQP=92.08 PLCCP=66.83
66.83 previous PLCCP	NCQ=8 NCC=1	PLCQP=100.0 PLCCP=100.0

Table VI.5.23 - Mapping Procedure Applied to CL Patch 3

plied, respectively, to CL patches 1, 2, and 3. For CL patches 1, 2, and 3, the mapping procedure results with PLCCP being equal to 100% reflecting the conclusion that the subpatches with the lowest power in CL patches 1, 2, and 3 occupy 100% of the area in each patch. Therefore, it is concluded that all CL patches

are homogeneous and do not contain any subpatches.

As in example 2, CL patch 2 consists of subpatches C and D. In Chapter VII it is shown that expert system rules are unable, in this case, to further subdivide the CL patch. However, it is also shown that the PDFs of subpatches C and D are very similar with identical power levels. Consequently, the inability to subdivide CL patch 2 is not a serious problem.

### **(iii) - Assessment**

Because the CL subpatch identification does not result in finding any subpatches within CL patches 1, 2, and 3, the mapped volume is not changed and assessment is not necessary.

### **(iv) - Steps 1-5 of the PDF Approximation Strategy**

Tables VI.5.24, VI.5.25, and VI.5.26 list the results of steps 1-5 of the PDF approximation strategy applied to CL patches 1, 2, and 3, respectively.

Test Cell No.	PDF	Rate	Distance	Shape	Scale	Location	(U,V)
1	W	3	$0.30 \times 10^{-1}$ ✓	2.20	3.90	-0.01	(-0.0250, 0.3733)
	L	7	$0.44 \times 10^{-1}$ ✗	0.13	12.4	-9.01	
	K	5	$0.39 \times 10^{-1}$ ✓	50.0	0.49	0.40	
31	W	3	$0.27 \times 10^{-1}$ ✓	2.32	3.98	-0.07	(-0.0233, 0.3702)
	L	7	$0.41 \times 10^{-1}$ ✓	0.12	12.9	-9.60	
	K	4	$0.36 \times 10^{-1}$ ✓	50.0	0.49	0.42	
62	W	2	$0.97 \times 10^{-2}$ ✓	2.00	3.69	-0.32	(-0.0342, 0.3529)
	L	5	$0.25 \times 10^{-1}$ ✓	0.20	8.41	-5.00	
	K	3	$0.17 \times 10^{-1}$ ✓	50.0	0.51	0.54	
93	W	3	$0.28 \times 10^{-1}$ ✓	2.32	3.98	-0.07	(-0.0238, 0.3709)
	L	7	$0.41 \times 10^{-1}$ ✓	0.12	13.0	-9.60	
	K	4	$0.37 \times 10^{-1}$ ✓	50.0	0.49	0.41	
124	W	3	$0.28 \times 10^{-1}$ ✓	2.10	3.77	0.12	(-0.0276, 0.3727)
	L	7	$0.41 \times 10^{-1}$ ✓	0.15	10.8	-7.53	
	K	4	$0.36 \times 10^{-1}$ ✓	50.0	0.49	0.39	

*Table VI.5.24 - PDF Approximation for CL Patch 1*

Test Cell No.	PDF	Rank	Distance	Shape	Scale	Location	(U,V)
1	W	15	$0.94 \times 10^{-1} \times$	5.00	3.06	1.24	(0.0308, 0.2437)
	L	14	$0.94 \times 10^{-1} \times$	0.01	81.0	-76.96	
	K	20	$0.11 \times 10^{-0} \times$	50.0	0.19	2.89	
1 w/o 5 Outliers	W	2	$0.13 \times 10^{-1} \checkmark$	2.39	1.20	3.07	(-0.0227, 0.3554)
	L	6	$0.26 \times 10^{-1} \checkmark$	0.13	3.58	0.52	
	K	4	$0.25 \times 10^{-1} \checkmark$	50.0	0.14	3.24	
85	W	15	$0.11 \times 10^{-0} \times$	5.00	3.04	1.19	(0.0282, 0.2214)
	L	14	$0.11 \times 10^{-0} \times$	0.01	80.5	-76.56	
	K	18	$0.13 \times 10^{-0} \times$	36.5	0.22	2.84	
85 w/o 6 Outliers	W	1	$0.79 \times 10^{-2} \checkmark$	2.19	1.03	3.14	(-0.0281, 0.3509)
	L	5	$0.23 \times 10^{-1} \checkmark$	0.17	2.51	1.51	
	K	3	$0.18 \times 10^{-1} \checkmark$	50.0	0.13	3.23	
171	W	22	$0.18 \times 10^{-0} \times$	0.49	0.24	3.68	(0.0365, 0.2186)
	L	14	$0.12 \times 10^{-0} \times$	0.01	80.0	-76.24	
	K	18	$0.14 \times 10^{-0} \times$	50.0	0.19	2.78	
171 w/o 5 Outliers	W	12	$0.32 \times 10^{-1} \checkmark$	2.35	1.16	2.97	(-0.0258, 0.3105)
	L	3	$0.17 \times 10^{-1} \checkmark$	0.22	2.05	1.91	
	K	11	$0.30 \times 10^{-1} \checkmark$	43.8	0.15	3.13	
256	W	15	$0.47 \times 10^{-1} \times$	4.70	2.45	1.71	(-0.0005, 0.2915)
	L	12	$0.40 \times 10^{-1} \times$	0.05	9.86	-5.89	
	K	18	$0.55 \times 10^{-1} \times$	50.0	0.16	2.98	
256 w/o 3 Outliers	W	1	$0.39 \times 10^{-2} \checkmark$	2.29	1.14	2.98	(-0.0256, 0.3468)
	L	5	$0.18 \times 10^{-1} \checkmark$	0.16	2.88	1.07	
	K	4	$0.17 \times 10^{-1} \checkmark$	50.0	0.14	3.11	
341	W	23	$0.19 \times 10^{-0} \times$	0.39	0.16	3.72	(0.0469, 0.2188)
	L	14	$0.12 \times 10^{-0} \times$	0.01	94.1	-90.21	
	K	19	$0.14 \times 10^{-0} \times$	50.0	0.22	2.57	
341 w/o 7 Outlier	W	8	$0.24 \times 10^{-1} \checkmark$	2.36	1.21	2.95	(-0.0253, 0.3186)
	L	1	$0.94 \times 10^{-2} \checkmark$	0.18	2.56	1.42	
	K	7	$0.24 \times 10^{-1} \checkmark$	50.0	0.14	3.12	

Table VI.5.25 - PDF Approximation for CL Patch 2

Test Cell No.	PDF	Rank	Distance	Shape	Scale	Location	(U,V)
1	W L K	14 6 10	$0.73 \times 10^{-1} \times$ $0.47 \times 10^{-1} \times$ $0.62 \times 10^{-1} \times$	0.96 0.72 3.03	2.90 3.07 3.06	2.39 1.41 0.29	(-0.0530, 0.2596)
1 w/o 3 Outliers	W L K	12 3 10	$0.33 \times 10^{-1} \checkmark$ $0.16 \times 10^{-1} \checkmark$ $0.29 \times 10^{-1} \checkmark$	2.23 0.24 35.3	5.36 8.91 0.81	0.03 -4.35 0.54	(-0.0291, 0.3098)
76	W L K	14 6 10	$0.71 \times 10^{-1} \times$ $0.45 \times 10^{-1} \times$ $0.59 \times 10^{-1} \times$	0.98 0.69 3.33	3.00 3.26 2.97	2.39 1.30 0.58	(-0.0519, 0.2632)
76 w/o 3 Outliers	W L K	10 2 7	$0.29 \times 10^{-1} \checkmark$ $0.13 \times 10^{-1} \checkmark$ $0.25 \times 10^{-1} \checkmark$	2.18 0.24 38.6	5.39 9.20 0.79	0.05 -4.61 0.48	(-0.0300, 0.3135)
153	W L K	5 1 2	$0.17 \times 10^{-1} \checkmark$ $0.39 \times 10^{-2} \checkmark$ $0.58 \times 10^{-2} \checkmark$	1.31 0.45 7.51	3.49 4.78 1.81	1.61 -0.48 0.49	(-0.0626, 0.3176)
229	W L K	3 7 4	$0.36 \times 10^{-1} \checkmark$ $0.57 \times 10^{-1} \times$ $0.45 \times 10^{-1} \checkmark$	1.50 0.35 42.9	4.20 6.70 0.82	1.29 -2.14 0.24	(-0.0673, 0.3742)
306	W L K	3 6 4	$0.25 \times 10^{-1} \checkmark$ $0.44 \times 10^{-1} \checkmark$ $0.33 \times 10^{-1} \checkmark$	1.50 0.36 31.5	4.22 6.59 0.95	1.23 -2.02 0.18	(-0.0645, 0.3623)

Table VI.5.26 - PDF Approximation for CL Patch 3

## **VI.6 - Extension of the Indexing Procedure to R/A/D Cells**

It is possible to extend the indexing procedure to the three dimensional R/A/D plane. The same steps used in indexing the R/A plane are followed. Namely, (1) an assessment stage is utilized to assign a unique number to the BN region and each 3-dimensional CL patch, compute the CNR for each CL patch, and classify CL patches as to whether they are SSC, WSC, or ISC regions, (2) a CL subpatch investigation stage is utilized to subdivide nonhomogeneous CL patches into contiguous CL subpatches, and (3) a random data analysis stage is utilized to obtain a PDF approximation of WSC CL patches stage.

Even though the indexing procedure for the R/A/D volume follows the same steps as those shown in Figures VI.3.2, VI.3.3, and VI.3.4 for the R/A plane, some changes are needed to apply the indexing algorithms of the R/A plane to the R/A/D volume. These changes are:

(i) - The mask used in the numbering procedure and shown in Figure VI.2.1 becomes a 3 dimensional mask which consists of the 13 previously numbered neighboring cells to the test cell. This is illustrated in Figure VI.6.1 for the  $ijk^{\text{th}}$  test cell.

(ii) - For the choice of the reference cells, a  $3 \times 3 \times 3$  mask of neighboring cells is initially centered around the test cell instead of the  $3 \times 3$  one used for the R/A plane. Then, the mask is augmented by one plane at each of its boundaries resulting in a  $5 \times 5 \times 5$  mask. As was done for the R/A case, the process of adding one row and one column to each boundary of the previous mask continues until the desired number of reference cells have been obtained. Note that the process of choosing a specified number of reference cells in the R/A/D volume results in the cells being closer to the test cell than for the R/A plane. For example, in order to choose 100 reference cells in a homogeneous region, a mask of dimension  $11 \times 11$  is needed in the R/A plane whereas a mask of dimension  $5 \times 5 \times 5$  suffices in the R/A/D volume. Thus, the reference cells are a distance of up to 5 cells away from

the test cell in the R/A plane, whereas the distance is only up to 2 cells away from the test cell in the R/A/D plane.

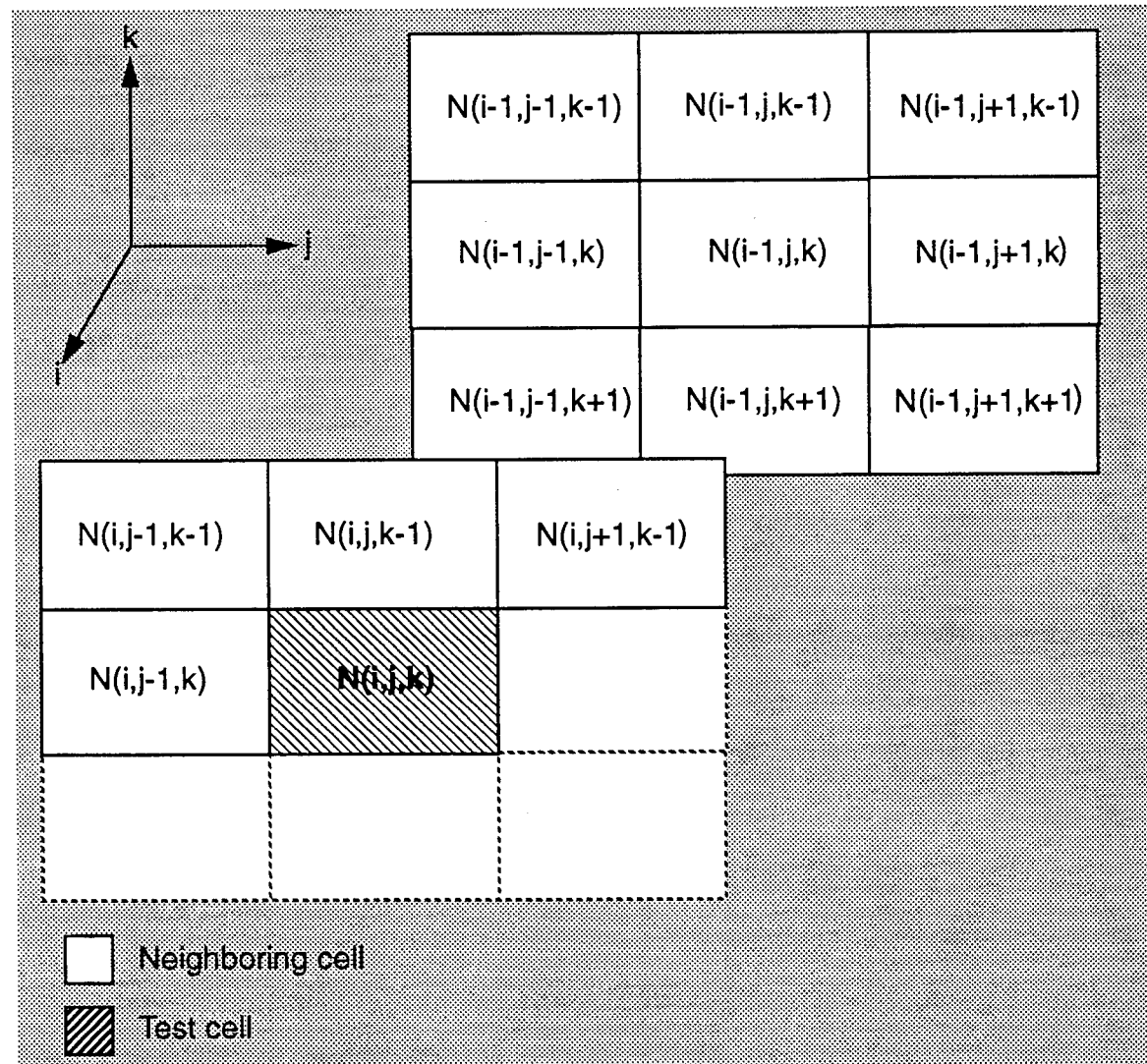


Figure VI.6.1 - Mask Used in Numbering the R/A/D Volume

## VI.7 - Conclusion

In summary, an indexing procedure has been presented that allows for numbering each of the BN region and CL patches with a unique number, extracting CL subpatches, and approximating the PDF of the test cells in the CL patches. The procedure was illustrated with examples that show how the indexing procedure works.

With respect to the indexing procedure presented in Table II.3.1, every step of the WSC has been discussed in this chapter. It should be pointed out that the procedures used for choosing test and reference cells in SSC and ISC are the same as those used for WSC.

Note that detection is not handled in this work because it is assumed that the appropriate detection algorithms to be used are known once the mapping and indexing are handled correctly.

Up to this point, only the signal understanding and detection using a feed forward expert system (SUD/FFES) has been presented. Rules are presented in the next chapter to enable signal understanding and detection with a feed back expert system (SUD/FBES).

## Chapter VII

### Application of IPUS to the Radar Detection Problem

Various aspects of the radar detection problem were illustrated in Figure III.1.1. The IPUS architecture decides whether or not a weak signal situation exists by classifying the data to be processed into either SSC, ISC, or WSC. As explained in Table II.3.1, the SSC uses the LRT, the ISC uses the GLRT, and the WSC uses the LOD.

Thus far, the mapping and indexing stages for the feed-forward expert system (FFES), shown in Figure II.3.2, have been detailed. In this chapter, rules are developed which allow IPUS to supervise (1) the convergence process in the mapping procedure, and (2) the interpretation of the indexing procedure.

Section VII.1 summarizes IPUS concepts. In Sections VII.2 and VII.4, rules are developed for the mapping and indexing procedures, respectively, along with examples which illustrate application of the rules.

#### **VII.1 - Summary of IPUS Concepts**

The following items summarize the concepts upon which IPUS is based:

- Signal processing algorithm (SPA): one or more signal processing algorithms and the corresponding control parameters need to be defined. The set of values assigned to the control parameters at a given instance is referred to as an SPA instance.
- Discrepancy detection: When the signal being monitored by the SPA does not satisfy the requirements of the SPA instance, the output of the SPA is distort-

ed. Recognition that the SPA instance is not properly chosen for the input data stream is referred to as discrepancy detection.

- Diagnosis procedure: Once a discrepancy has been detected, a diagnosis procedure is used to identify the source of the distortion that may have led to the discrepancy.

- Reprocessing procedure: Knowing the source of the distortion, then either parameters of the same SPA can be readjusted or a different SPA can be chosen to reprocess the data.

In the following sections, (1) SPAs are identified along with their sets of control parameters, (2) rules are developed which enable the detection of discrepancies and identification of sources of the distortion, and (3) examples are presented to illustrate the result of reprocessing.

## **VII.2 - Role of IPUS in the Mapping Procedure**

In this section, control by IPUS of the convergence process in the mapping procedure is described.

### **VII.2.1 - IPUS Stages Included in the Mapping Procedure**

#### **VII.2.1.1 - SPA and SPA Instance**

It has been shown in the block diagram of Figure V.3.10 that part of the mapping procedure consists of a set of four blocks linked by feed-forward and feed-back loops. These blocks are: thresholding/quantization, correction-quantized, correction-corrected, and assessment. Recall that these blocks are used to find the best threshold to separate between BN and CL patches.

The parameters associated with the first three blocks are BNQP, NCQ, and NCC, respectively. The assessment block defines whether or not reprocessing through the feed-back loops is needed and, if so, which control parameters should be changed and what values should be assigned. The assessment stage com-

putes BNCQP and BNCCP and compares them to BNQP.

In this application IPUS treats all four blocks as a single SPA. The control parameters for the SPA are BNQP, NCQ, NCC. Any one set of the control parameter values is referred to as an SPA instance.

#### **VII.2.1.2 - Observations on Setting of the Control Parameters**

In this section, different effects of the control parameters are discussed. Note first that the intervals for the allowable values of the control parameters are given in Chapter V and are equal to

$$0\% \leq BNQP \leq 100\%$$

$$5 \leq NCQ \leq 8 \quad (VII.2-1)$$

$$1 \leq NCC \leq 4.$$

Recall that BNQP represents the fraction of BN cells in the quantized volume. It is used to determine the threshold  $q$  for which all cells with data amplitudes below  $q$  are identified as BN and all cells with data amplitudes above  $q$  are identified as CL in the quantized volume.

Also, NCQ is the minimum number of neighboring cells in the quantized volume required to be identified as CL cells for a test cell to be declared as a CL cell in the first-corrected volume. Finally, NCC is the minimum number of neighboring cells in the first-corrected volume required to be identified as CL cells for a test cell to be declared as a CL cell in the second-corrected volume.

BNCQP and BNCCP are computed parameters which represent the BN percentages in the first and second-corrected volumes, respectively.

Define  $BNQP_t$  to be the true value for the fraction of BN cells in the generated scene.

As explained in Section V.3, the mapping processor begins by setting a threshold that results in a specified fraction of BN cells equal to BNQP. The mapping processor iterates until it is satisfied that the latest scene is consistent with the last specified value of BNQP. When the iteration process ends, it is assumed that

$$BNQP \approx BNQP_t. \quad (VII.2-2)$$

#### **(i) - Observations on the Setting of BNQP**

- 1 - Setting BNQP much smaller than BNQP<sub>t</sub>: Many cells have data amplitudes larger than the threshold resulting in a large number of BN cells being declared as CL cells in the quantized volume.
- 2 - Setting BNQP much larger than BNQP<sub>t</sub>: CL patch cells may be misclassified due to the fact that some CL patches have data amplitude values below the threshold. This results in many CL cells being identified as BN cells in the quantized volume.

Conclusion: Because (1) the objective of the mapping procedure is to separate between BN and CL patches, (2) the average power of the BN is the lowest among all regions, and (3) the threshold is set adaptively by the assessment stage, the threshold is always set very low at the beginning so that BN information is gained as the process iterates. The threshold, controlled by the assessment stage, is raised adaptively until  $BNQP \approx BNQP_t$ .

#### **(ii) - Observations on the Setting of NCQ**

Recall that NCQ controls which test cells in the first-corrected volume are to be declared as CL. NCQ is said to be large when its value approaches 8 and small when its value approaches 5. The following observations relative to NCQ take into consideration that the initial setting of BNQP is low and then is increased until BNQP approximates the true value  $BNQP_t$ . Depending on the setting of BNQP with respect to  $BNQP_t$ , four cases exist:

- 1 - BNQP much smaller than BNQP<sub>t</sub>:

- a - Setting NCQ small: In this case, because many CL declared cells exist in the quantized volume due to the low threshold, small NCQ results in the building of a multitude of CL patches which are likely to be so close that they form a single big CL patch in the first-corrected volume.

- b - Setting NCQ high: Here, even though many CL declared cells exist in the quantized volume due to the low threshold, high NCQ results in the building of fewer CL patches than when NCQ is small. This is due to the fact that there must be at least NCQ CL cells neighboring the test cell in the quantized volume, where NCQ is large, in order for the test cell to be declared as a CL cell in the first-corrected volume. In this case, corrections are made and some of the cells previously declared as CL cells in the quantized volume are now declared as BN cells in the first-corrected volume.

- 2 - BNQP close to BNQP<sub>t</sub>: When BNQP is close to its true value, the threshold is high enough to separate between the BN region and CL patches. With either small or large values for NCQ, the CL regions are well approximated. In this case, the choice of NCQ affects the classification of the inner cells of the CL regions. This results because, even though the data amplitudes of CL cells are higher than those of the BN cells, in general, some CL cells with data amplitudes lower than those of the highest BN data values exist and may be lower than the threshold.

- a - Setting NCQ small: All test cells in the quantized volume that have at least NCQ neighboring cells are declared as CL cells in the first-corrected volume. Small NCQ helps to correctly classify the inner CL cells. However, note that small NCQ also results in misclassifying BN cells that are surrounded by at least NCQ declared CL cells.

- b - Setting NCQ high: Every test cell must have a large number of neighboring CL declared cells in the quantized volume for it to be declared as a

CL cell in the first-corrected volume. This causes the procedure to misclassify some of the inner CL cells when too many of the neighboring cells have their data amplitudes falling below the threshold. In this case, the identified CL regions are not homogeneous and contain BN declared "holes".

Conclusion: The value of NCQ should be chosen as large as possible at the beginning of the iterative process when the threshold is set very low to correctly reclassify the maximum number of BN cells misidentified at the thresholding/quantization stage. When the threshold reaches a level where it is close to its convergence value, NCQ should then be chosen small to avoid non-homogeneous CL regions.

### **(iii) - Observations on the Setting of NCC**

Because NCQ truncates the boundaries of the CL regions, NCC is used to augment the edges of the CL declared regions. NCC is said to be large when its value approaches 4 and small when its value approaches 1. In the following discussion it is assumed that the conclusions previously reached on the settings of BNQP and NCQ are taken into consideration so that BNQP is initially set low to be increased until it approaches its true value  $BNQP_t$ , while NCQ is initially set to a large value, to be decreased as BNQP approaches its true value. Four cases are then identified:

#### **- 1 - BNQP much smaller than $BNQP_t$ and NCQ large:**

Because NCQ is set large, many CL edge cells are misclassified and associated with the BN region.

**- a - Setting NCC small:** When NCC is set small, many of the edge cells are correctly reclassified from BN cells to CL cells in the second-corrected volume.

**- b - Setting NCC large:** In this case, only a few misclassified CL

edge cells are correctly reclassified in the second-corrected volume.

- 2 - BNQP close to BNQP<sub>t</sub> and NCQ small:

Because NCQ is small, only a few CL edge cells are associated with the BN.

- a - Setting NCC small: Small NCC causes not only CL edge cells to be recovered but also BN cells to be misclassified in the second-corrected volume.

- b - Setting NCC large: In this case, most of the CL edge cells are correctly classified in the second-corrected volume and only few BN cells are misclassified as CL cells.

Conclusion: NCC results in the recovery of CL edge cells and the misclassification of some BN cells close to the CL edge cells. In order to maximize recovery of the CL edge cells and minimize the misclassification of BN cells, NCC should be set small when NCQ is set large in order to recover a lot of CL edge cells that were lost in the first-correction. On the other hand, NCC should be set large when NCQ is set small because, in this case, only a few CL edge cells need to be recovered.

### **VII.2.1.3 - Discrepancy Detection**

In this section, rules are developed to enable the detection of discrepancies. The assessment stage of the mapping procedure consists of comparing at each step of the iteration the value for BNCCP with the corresponding BNQP. When BNCCP is not sufficiently close to BNQP, the assessment stage is said to fail. This initiates the discrepancy detection stage. Diagnosis identifies the distortion that may have caused the discrepancy and adjusts one or more of the mapping control parameters for reprocessing of the data.

The strategy behind the iterative process of the mapping procedure employs two stages. In the first stage, referred to as the threshold approximation

stage, BNQP is varied iteratively by the mapping processor until, as explained later, it is expected that BNQP is within 10% of its true value  $BNQP_t$ . The second stage, referred to as the threshold fine-tuning stage, consists of iteratively varying BNQP until it converges to within 1% of the last computed value for BNCCP. The two stages are now discussed in detail.

- a - Threshold approximation stage: During this stage, two sets of SPA instances are used on the same data of the surveillance volume. For both sets BNQP and NCC are the same whereas NCQ is equal to 7 for one set and 8 for the other.

Recall that NCQ is used to recognize the CL patches in the surveillance volume. First consider the situation where BNQP approximately equals  $BNQP_t$ . Here the threshold is such that it is possible to do a good job of separating between the BN region and CL patches. Steps are then taken to correct misclassified BN and CL data. Note that misclassifications are due to large BN data exceeding the threshold and small CL data falling below the threshold. At this point, setting NCQ to 7 and 8, respectively, results in very close values for BNCQP and BNCCP due to the facts that (1) the two masks are very similar. (NCQ=8 requires that 8 neighboring cells be declared CL in the quantized volume for a test cell in the first-corrected volume to be declared CL whereas NCQ=7 requires that 7 neighboring cells be declared CL in the quantized volume for a test cell in the first-corrected volume to be declared CL), (2) only a few cells are misclassified in the quantized volume.

Now consider that BNQP is significantly smaller than  $BNQP_t$ . In this case many BN cells are misclassified after quantization. Even though masks with NCQ equal to 7 and 8 are similar, they result in BNCQP and BNCCP being considerably different due to the fact that the large number of misclassified BN cells are so many that they tend to group together. Consequently, changing NCQ from 8 to 7 simply results in additional BN cells grouping together to form additional CL re-

gions and more edges. Because of this

$$BNCP|_{NCQ=7} < BNCP|_{NCQ=8}$$

and

(VII.2-3)

$$BNCCP|_{NCQ=7} < BNCCP|_{NCQ=8}.$$

Because the second-corrected volume represents the scene where CL patches and their edges are assumed to be properly recovered had the threshold BNQP been chosen properly, BNCCP tries to converge to BNQP<sub>t</sub>. Thus, it is logical to begin each iteration by assigning to BNQP the latest computed value of BNCCP|<sub>NCQ=8</sub>. The very first value assigned to BNQP is simply a guess. This value should be such that the threshold is low. In all of our examples, the first value of BNQP is chosen equal to 10%.

Using different scenes with different values for BNQP<sub>t</sub>, it has been determined near convergence that whenever the difference between BNCCP|<sub>NCQ=7</sub> and BNCCP|<sub>NCQ=8</sub> is within 10%, then BNQP is likely to be within 10% of its true value. This is confirmed in Figure VII.2.1 where plots of the quantities BNCCP|<sub>NCQ=8</sub> - BNCCP|<sub>NCQ=7</sub> versus BNQP-BNQP<sub>t</sub> are shown for different values of BNQP<sub>t</sub>. Note that

- i - for different values of BNQP<sub>t</sub>, all plots are such that near convergence the difference BNCCP|<sub>NCQ=8</sub> - BNCCP|<sub>NCQ=7</sub> approaches to 0 when BNQP-BNQP<sub>t</sub> also approaches 0,
- ii - for different values of BNQP<sub>t</sub>, when BNQP-BNQP<sub>t</sub> > -10%, the difference BNCCP|<sub>NCQ=8</sub> - BNCCP|<sub>NCQ=7</sub> < 10%.

As a result of the above, the threshold approximation stage iterates until it is satisfied that

$$BNCCP|_{NCQ=8} - BNCCP|_{NCQ=7} < 10\%. \quad (VII.2-4)$$

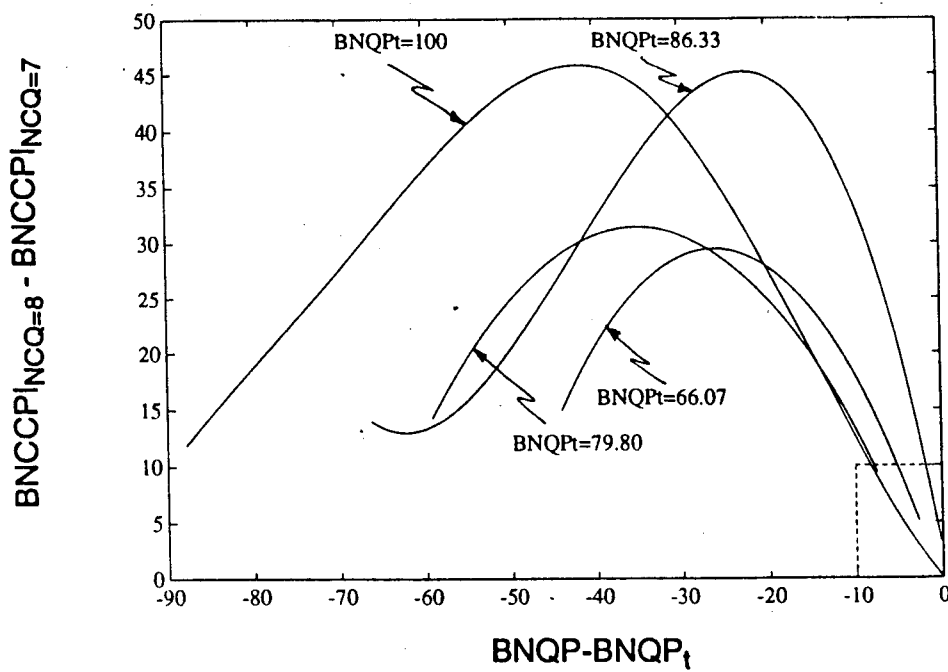


Figure VII.2.1- Plot of  $BNCCPI_{NCQ=8} - BNCCPI_{NCQ=7}$  Versus  $BNQP - BNQP_t$  for Different Values of  $BNQP_t$

In summary, as shown in the flow chart of Figure VII.2.2, a guess for the initial value of BNQP is followed by the execution of the mapping procedure using two different SPA instances. The outputs of the two SPA instances are compared by means of the computed values of BNCCP. If  $BNCCPI_{NCQ=8} - BNCCPI_{NCQ=7}$  is more than 10%, a discrepancy is detected and it is concluded that the value of BNQP differs from its true value by more than 10%. BNQP is then increased to the latest computed value of  $BNCQPI_{NCQ=8}$ . BNQP is varied from one iteration to the next while NCC is kept equal to 1. This choice for NCC agrees with the observations made previously where it was concluded that NCC should be set small when NCQ is set large. In this case NCQ has a large value equal to either 7 or 8.

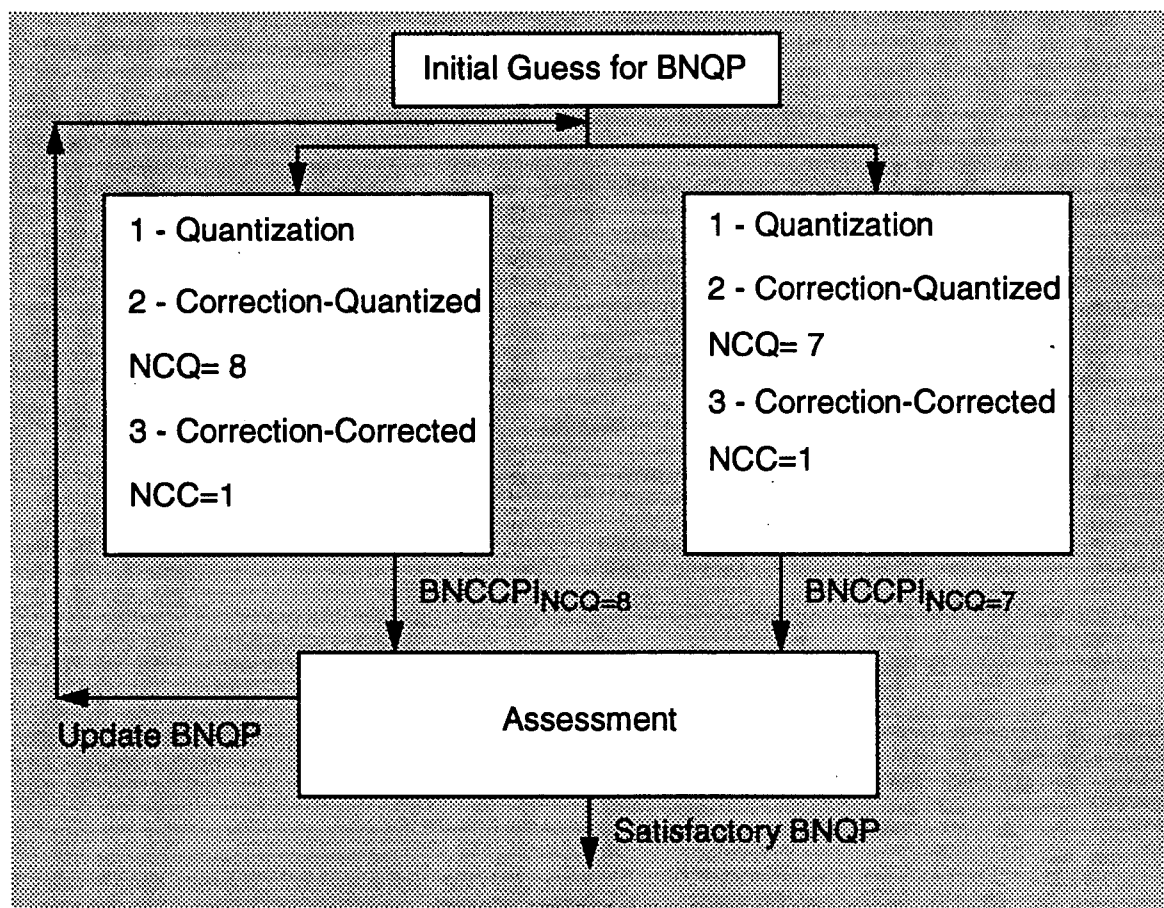


Figure VII.2.2 - Threshold Approximation Stage

The discrepancies that may arise in the threshold approximation stage are due to the fact that two instances of the same SPA result in different interpretations when applied to the same data. As defined in Section III.2.2, such a discrepancy is typified as a fault.

Two fault-type discrepancies are readily identified in the threshold approximation stage. These are as follows:

- 1 -  $BNCCPI_{NCQ=8} - BNCCPI_{NCQ=7} > 10\%$ : As discussed above, the goal of the threshold approximation stage is to obtain a threshold BNQP that is within 10% of its true value. As shown in Figure VII.2.1, this is likely only when  $BNCCPI_{NCQ=8} - BNCCPI_{NCQ=7} < 10\%$ . When the difference between the computed thresholds  $BNCCPI_{NCQ=8} - BNCCPI_{NCQ=7}$  is more than 10%, a fault type of

discrepancy is detected during the assessment stage. The diagnosis process identifies the fact that  $BNQP - BNQP_t < -10\%$  as the source for the distortion causing the discrepancy. The remedy, in this case, is to increase the value of BNQP during the reprocessing stage to the latest computed value for  $BNCCPI_{NCQ=8}$ .

- 2 - initial BNQP set too low: In some cases, when the initial guess for BNQP is too small, the number of BN cells with data exceeding the threshold is so large that when corrections are made, the second-corrected volume results in many CL declared patches or, in the worst case, a single big CL patch. This results in the values of either  $BNCCPI_{NCQ=8}$  or  $BNCCPI_{NCQ=7}$  being even smaller than BNQP. In this case, it is possible to obtain a value for the difference  $BNCCPI_{NCQ=8} - BNCCPI_{NCQ=7}$  that is smaller than 10%. The IPUS control must be suspicious of such a case and declare BNQP-set-too-low as the source for the distortion causing the discrepancy. The remedy, in this case, is to increase the initial value of BNQP during the reprocessing stage. In our examples, we choose to increase BNQP by 10% every time an initial-BNQP-set-too-low fault is obtained.

Table VII.2.1, summarizes the discrepancies that may occur during the threshold approximation stage.

Discrepancy (Fault Type)	Diagnosis (Source of Distortion)	Reprocessing
$BNCCPI_{NCQ=8} - BNCCPI_{NCQ=7}$ is more than 10%	$BNQP - BNQP_t > -10\%$	Assign to BNQP the latest value of $BNCCPI_{NCQ=8}$
$BNCCPI_{NCQ=8} - BNCCPI_{NCQ=7}$ is less than 10% in the early stages of iteration	Initial value of BNQP is too low	Increase BNQP by 10% from its initial value

Table VII.2.1 - Discrepancies in the Threshold Approximation Stage

- b - Threshold fine-tuning stage: At the end of the threshold approximation stage BNQP is likely to be within 10% of its true value  $BNQP_t$ . During the threshold fine-tuning stage, BNQP is varied until BNCCP is within 1% of the corresponding value of BNQP.

During the threshold fine-tuning stage, NCQ is lowered to avoid holes in the CL patches caused by misclassified CL cells whose data values are lower than the threshold. For the same reason BNQP is assigned the latest value of  $BNCCPI_{NCQ=7}$  rather than the latest value of  $BNCCPI_{NCQ=8}$ . In addition, the value of NCC is raised to avoid misclassification of BN cells close to the CL edges. These choices for NCQ and NCC agree with observations mentioned in Section VII.2.1.2.

The following observations on BNQP, NCQ, and NCC are necessary to understand how these parameters should be automatically set in order for BNCCP to converge to within 1% of BNQP.

- 1 - When BNQP is increased while both NCQ and NCC are kept constant, the number of BN cells in the quantized volume is increased and, therefore, both BNCQP and BNCCP are likely to increase.

- 2 - When NCQ is increased while both BNQP and NCC are kept constant, the requirement on a test cell to be declared as a CL cell in the first-corrected volume becomes more stringent and, therefore, the number of CL cells in both corrected volumes are likely to decrease. This tends to increase the number of BN cells causing both BNCQP and BNCCP to increase.

- 3 - When NCC is increased while both BNQP and NCQ are kept constant, the requirement on a test cell to be declared as a CL cell in the second-corrected volume becomes more stringent and, therefore, the number of CL cells in this volume is decreased. Thus, the number of BN cells in the second-corrected volume increases and, consequently, BNCCP increases.

Using the above observations, the following strategy is used by the assessment stage to control the threshold fine-tuning stage,

- 1 - Because BNQP is within 10% of its true value at the beginning of the threshold fine-tuning stage, the threshold is likely to be relatively high. Thus, NCQ should be set to its smallest value of 5 while, as needed, NCC should be incremented iteratively from its minimum value of 1 up to its maximum value of 4.

- 2 - When the inequality in Equation VII.2-4 is not satisfied, BNQP should be increased in small steps. Otherwise, the iterative process diverges when the same rule from the threshold approximation stage is used. The approach taken in this work during the threshold fine-tuning stage consists of assigning a value to BNQP that is half way between its latest value and the latest value of BNCCP, i.e.

$$BNQP = \frac{BNQPI_{latest} + BNCCPI_{latest}}{2} \quad (VII.2-5)$$

- 3 - The condition set forward for ending the threshold fine-tuning stage is given by

$$|BNQP - BNCCP| < 1\%. \quad (VII.2-6)$$

Two cases are possible when the inequality in Equation VII.2-6 is not satisfied: either  $BNQP < BNCCP$  or  $BNQP > BNCCP$ .

- 4 - When the inequality in Equation VII.2-6 is not satisfied and  $BNQP < BNCCP$ , the control parameters should be varied by the diagnosis procedure such that BNCCP is decreased. In this case, NCQ should be made smaller. If none of the allowable values for NCQ result in the inequality in Equation VII.2-6 being satisfied, then BNQP is varied according to Equation VII.2.5.

- 5 - When the inequality in Equation VII.2-6 is not satisfied and  $BNQP > BNCCP$ , the control parameters should be varied by the diagnosis procedure such that BNCCP is increased. In this case, NCC should be made larger. If

none of the allowable values for NCC result in the inequality in Equation VII.2-6 being satisfied, then BNQP is varied according to Equation VII.2.5.

During the threshold approximation stage note that only BNQP was varied. On the other hand, in the threshold fine-tuning stage, any of the parameters BNQP, NCQ, and NCC may be varied.

In summary, as shown in the flow chart of Figure VII.2.3, the threshold fine-tuning stage begins by assigning to BNQP the latest value of  $BNCCPI_{NCQ=7}$ . Once quantization, first-correction, and second-correction stages are completed with pre-selected values for NCQ and NCC, the assessment stage diagnoses the results according to the strategy discussed above, and, depending on the outcome, decides either that reprocessing is necessary with adjusted values for any of the BNQP, NCQ, and NCC parameters, or the threshold fine-tuning stage is completed.

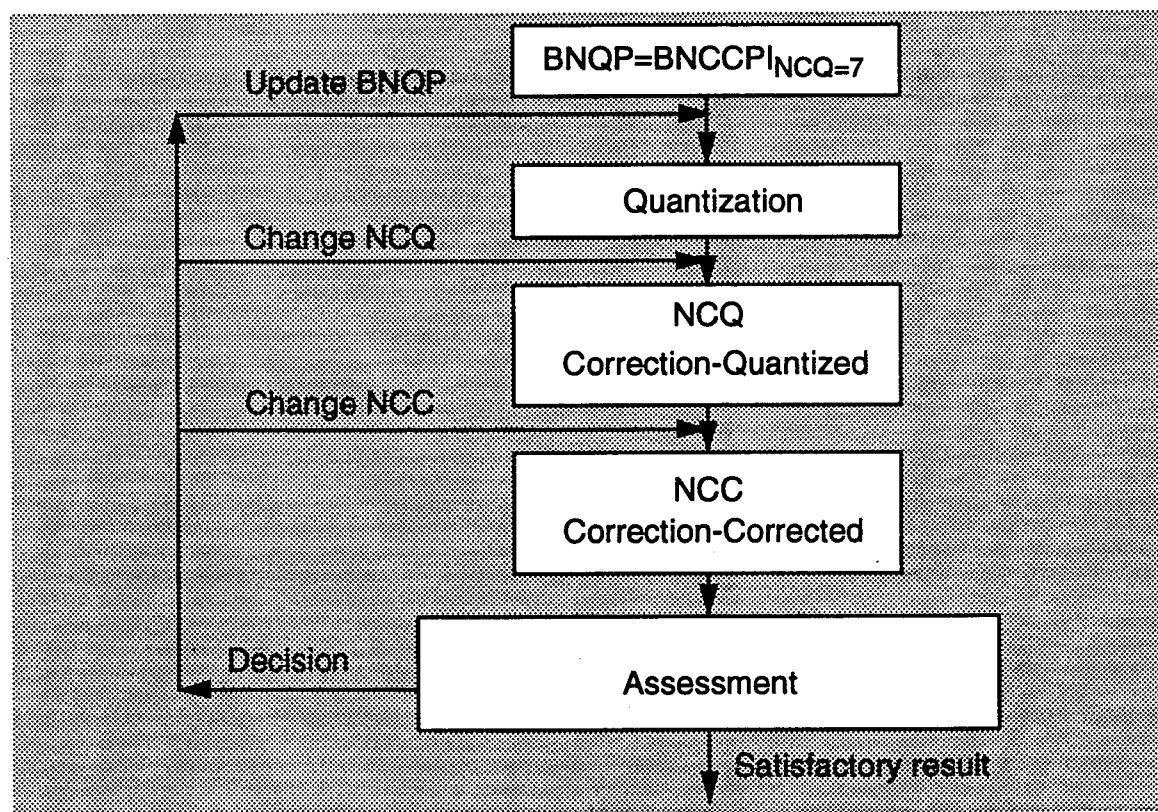


Figure VII.2.3 - Threshold Fine-Tuning Stage

At the end of each iteration of the threshold fine-tuning stage it is expected that the computed value of BNCCP will be within 1% of BNQP. When the inequality in Equation VII.2-6 is not satisfied, a conflict type of discrepancy is detected based on the inconsistency in the expectation that BNCCP will be within 1% of BNQP. Table VII.2.2 summarizes the discrepancies that may occur during the threshold fine-tuning stage.

Discrepancy (Conflict Type)	Diagnosis (Source of Distortion)	Reprocessing
IBNQP - BNCCPI > 1% and BNQP < BNCCP	Either NCQ or BNQP are not well adjusted	Decrease NCQ, otherwise update BNQP
IBNQP - BNCCPI > 1% and BNQP > BNCCP	Either NCC or BNQP are not well adjusted	Increase NCC, otherwise update BNQP

*Table VII.2.2 - Discrepancies in the Threshold Fine-Tuning Stage*

It has been determined through examples that the initial setting of NCQ=5 is adequate for the threshold fine-tuning stage to converge (i.e., in the examples studied it was never necessary to decrease NCQ).

In the following section, examples are presented which illustrate use of the rules developed for both the threshold approximation and threshold fine-tuning stages.

### **VII.3 - Examples**

In this section, tables describing previous results from the mapping procedure of examples 1, 2 and 3 in Chapter V are modified to demonstrate operation of the rules developed in this chapter for both the threshold approximation and threshold fine-tuning stages. In the following examples, define

$$\Delta_1 = \text{BNCCPI}_{\text{NCQ}=8} - \text{BNCCPI}_{\text{NCQ}=7} \quad (\text{VII.3-1})$$

and

$$\Delta_2 = |\text{BNQP} - \text{BNCCPI}|. \quad (\text{VII.3-2})$$

### VII.3.1 - Example 1

First, consider the example presented in Section V.4.2.1. Table VII.3.1 is an expanded version of Table V.4.2 in order to include information about the procedures for the threshold approximation and threshold fine-tuning stages. In the first step of the threshold fine-tuning stage note that  $\Delta_2 > 1\%$  and BNCCP < BNQ-P. Using the decision rules in Table VII.2.2, NCC is increased in the next steps.

BNQP (%)	Parameter Values		$\Delta_i$
Threshold Approximation Stage			
10.00 (guess)	NCQ=8 NCC=1 BNCQP=51.56 BNCCP=22.00	NCQ=7 NCC=1 BNCQP=25.78 BNCCP=7.09	$\Delta_1 > 10\%$
22.00 latest BNCCP	NCQ=8 NCC=1 BNCQP=68.28 BNCCP=50.39	NCQ=7 NCC=1 BNCQP=54.06 BNCCP=25.74	$\Delta_1 > 10\%$
50.39 latest BNCCP	NCQ=8 NCC=1 BNCQP=75.56 BNCCP=68.46	NCQ=7 NCC=1 BNCQP=70.93 BNCCP=63.37	$\Delta_1 < 10\%$
Threshold Fine-Tuning Stage			
63.37 latest BNCCP	NCQ=5 NCC=1 BNCQP=67.35 BNCCP=59.72 < BNQP		$\Delta_2 > 1\%$
63.37 latest BNCCP	NCQ=5 NCC=2 BNCQP=67.35 BNCCP=62.26 < BNQP		$\Delta_2 > 1\%$
63.37 same as lat- est BNQP	NCQ=5 NCC=3 BNCQP=67.35 BNCCP=64.17		$\Delta_2 < 1\%$

Table VII.3.1 - Setting of BNQP in Both of the Threshold Approximation and Threshold Fine-tuning Stages

### VII.3.2 - Example 2

Consider now the example presented in Section V.4.2.2. Table VII.3.2 is an expanded version of Table V.4.5 in order to include information about the procedures for the threshold approximation and threshold fine-tuning stages. In the first step of the threshold fine-tuning stage note that  $\Delta_2 > 1\%$  and BNCCP > BNQP. Using the decision rules in Table VII.2.2, BNQP is increased using the half way rule of equation VII.2-5.

BNQP (%)	Parameter Values			$\Delta_i$
Threshold Approximation Stage				
10.00 (guess)	NCQ=8 NCC=1 BNCQP=56.35 BNCCP=20.59	NCQ=7 NCC=1 BNCQP=23.94 BNCCP=6.33		$\Delta_1 > 10\%$
20.59 latest BNCCP	NCQ=8 NCC=1 BNCQP=77.43 BNCCP=48.04	NCQ=7 NCC=1 BNCQP=53.30 BNCCP=16.94		$\Delta_1 > 10\%$
48.04 latest BNCCP	NCQ=8 NCC=1 BNCQP=91.83 BNCCP=81.70	NCQ=7 NCC=1 BNCQP=84.11 BNCCP=72.30		$\Delta_1 < 10\%$
Threshold Fine-Tuning Stage				
72.30 latest BNCCP	NCQ=5 NCC=1 BNCQP=82.17 BNCCP=79.26 > BNQP			$\Delta_2 > 1\%$
75.78 half way	NCQ=5 NCC=1 BNCQP=83.50 BNCCP=75.31			$\Delta_2 < 1\%$

Table VII.3.2 - Setting of BNQP in Both of the Threshold Approximation and Threshold Fine-tuning Stages

### VII.3.3 - Example 3

Consider now the example presented in Section V.4.2.3. Table VII.3.3 is an expanded version of Table V.4.8 in order to include information about the proce-

BNQP (%)	Parameter Values		$\Delta_i$
Threshold Approximation Stage			
10.00 (guess)	NCQ=8 NCC=1 BNCQP=56.17 BNCCP=20.04	NCQ=7 NCC=1 BNCQP=24.24 BNCCP=6.09	$\Delta_1 > 10\%$
20.04 latest BNCCP	NCQ=8 NCC=1 BNCQP=77.98 BNCCP=43.78	NCQ=7 NCC=1 BNCQP=51.22 BNCCP=14.83	$\Delta_1 > 10\%$
43.78 latest BNCCP	NCQ=8 NCC=1 BNCQP=90.78 BNCCP=82.65	NCQ=7 NCC=1 BNCQP=84.78 BNCCP=66.09	$\Delta_1 > 10\%$
82.65 latest BNCCP	NCQ=8 NCC=1 BNCQP=93.43 BNCCP=89.39	NCQ=7 NCC=1 BNCQP=91.17 BNCCP=84.70	$\Delta_1 < 10\%$
Threshold Fine-Tuning Stage			
84.70 latest BNCCP	NCQ=5 NCC=1 BNCQP=87.61 BNCCP=82.00 < BNQP		$\Delta_2 > 1\%$
84.70 latest BNCCP	NCQ=5 NCC=2 BNCQP=87.61 BNCCP=83.65 < BNQP		$\Delta_2 > 1\%$
84.70 same as lat- est BNQP	NCQ=5 NCC=3 BNCQP=87.61 BNCCP=85.46		$\Delta_2 < 1\%$

Table VII.3.3 - Setting of BNQP in Both of the Threshold Approximation and Threshold Fine-tuning Stages

dures for the threshold approximation and threshold fine-tuning stages. As was the case in example 1, note that  $\Delta_2 > 1\%$  in the first step of the threshold fine-tuning stage and  $BNCCP < BNQP$ . Once again, using the decision rules in Table VII.2.2, NCC is increased.

## **VII.4 - Role of IPUS in the Indexing Procedure**

In this section, control of the indexing procedure by IPUS is described. Recall that the indexing procedure consists of the assessment, CL subpatch investigation and PDF approximation stages. Control by IPUS of these different stages is discussed next.

### **VII.4.1 - IPUS Stages Included in the Assessment Stage**

As explained in Section VI.2, the assessment stage consists of (1) assigning a unique number to the BN region and each CL patch, (2) computing the CNR for each CL patch, and (3) classifying CL patches as either SSC, WSC or ISC regions. Due to the straight forward implementation of these steps, any control by IPUS of the assessment stage is not discussed further.

### **VII.4.2 - IPUS Stages Included in the CL Subpatch Investigation Stage**

The approach used to extract a CL subpatch from a set of contiguous CL subpatches is the same as that used in the mapping procedure to extract the BN from CL patches. Therefore, control by IPUS is needed in the CL subpatch investigation stage.

#### **VII.4.2.1 - SPA and SPA Instance**

Recall that the CL subpatch investigation stage attempts to extract first, if it exists, the CL subpatch having the lowest average power. This part of the CL subpatch investigation stage consists of a set of four blocks linked by feed-forward and feed-back loops. These blocks are: thresholding/quantization, correction-quantized, correction-corrected, and assessment.

The parameters associated with the first three blocks are PLQP, NCQ, and NCC, respectively. The assessment stage computes PLCQP and PLCCP and compares them to PLQP. IPUS treats all four blocks as a single SPA. The control parameters for the SPA are PLQP, NCQ, and NCC. Any single set of the control parameter values is referred to as an SPA instance.

#### **VII.4.2.2 - Observations on the Setting of the Control Parameters**

The observations previously made for the mapping procedure parameters (i.e., BNQP, NCQ, and NCC) also hold for the CL subpatch investigation parameters (i.e., PLQP, NCQ, and NCC).

#### **VII.4.2.3 - Resolution of Discrepancies**

As was the case for the mapping procedure, threshold approximation and threshold fine-tuning stages are used in the CL subpatch investigation stage to enable resolution of discrepancies. Because the procedure for extracting a CL subpatch is the same as that used for separating BN and CL patches, discrepancy detection rules for both procedures are the same. The threshold approximation stage block diagram of Figure VII.2.2 becomes that of Figure VII.4.1 where BNQP and BNCCP have been replaced by PLQP and PLCCP, respectively. Let  $PLQP_t$  represent the true value for PLQP, the threshold approximation stage iterates until it is satisfied that PLQP is within 10% of its true value  $PLQP_t$ . This is satisfied when

$$PLCCPI_{NCQ=8} - PLCCPI_{NCQ=7} < 10\%. \quad (VII.4-1)$$

The threshold fine-tuning stage converges when

$$IPLQP - PLCCPI < 1\%. \quad (VII.4-2)$$

Figure VII.4.2 shows the block diagram of the threshold fine-tuning stage.

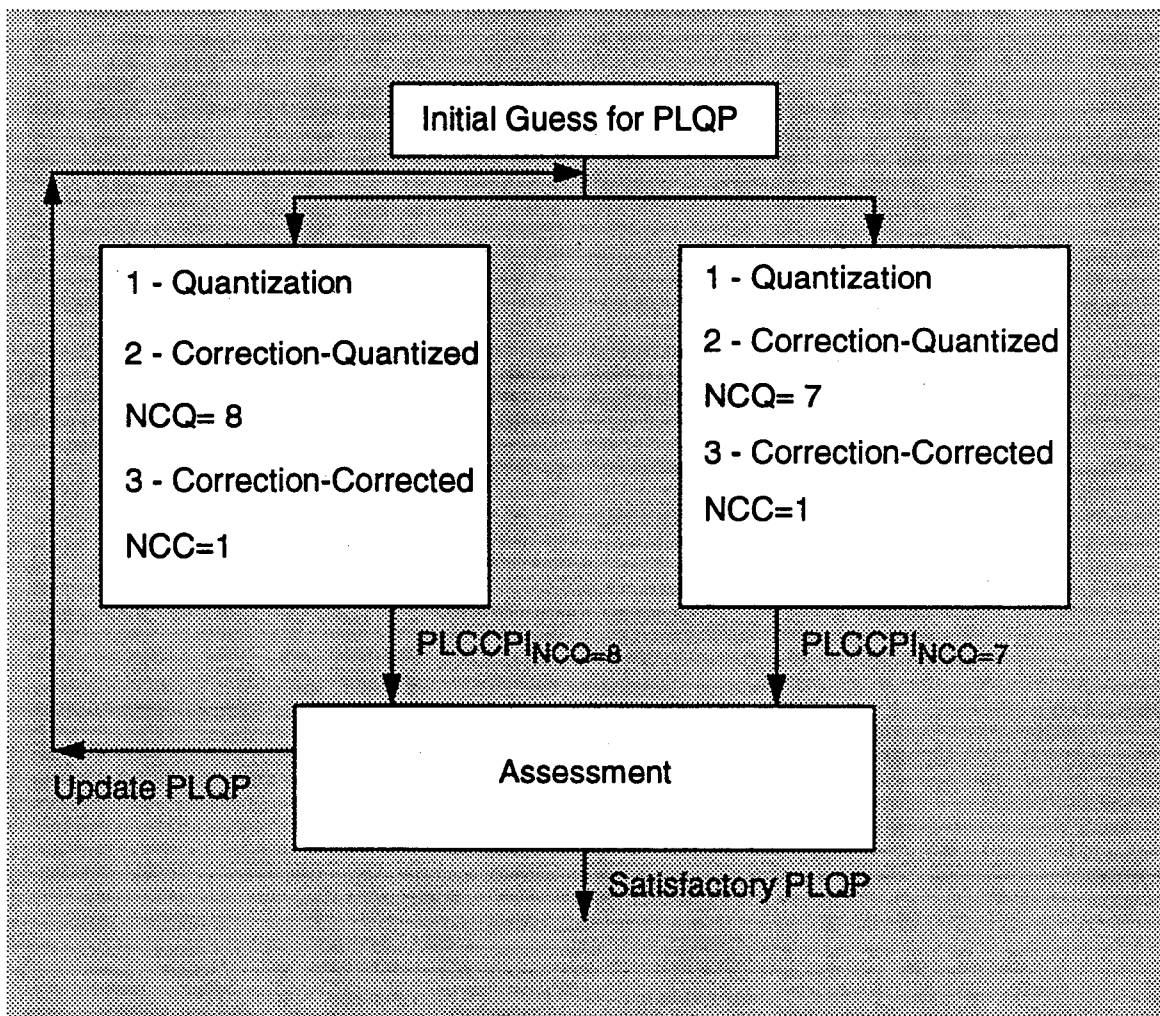


*Figure VII.4.1 - Threshold Approximation Stage*

In addition to the discrepancy rules described in Section VII.2.1.3 for the threshold approximation and fine-tuning stages and summarized in Tables VII.2.1 and VII.2.2, additional rules are introduced next as a result of some more observations on the behavior of PLQP for the case where a CL patch is homogeneous and does not contain subpatches. These are,

- 1 - It is noted that during the threshold approximation stage it is possible that the inequality in Eq. (VII.4-1) will be satisfied with  $PLCCPI_{NCQ=7 \text{ or } 8} = 100\%$ .

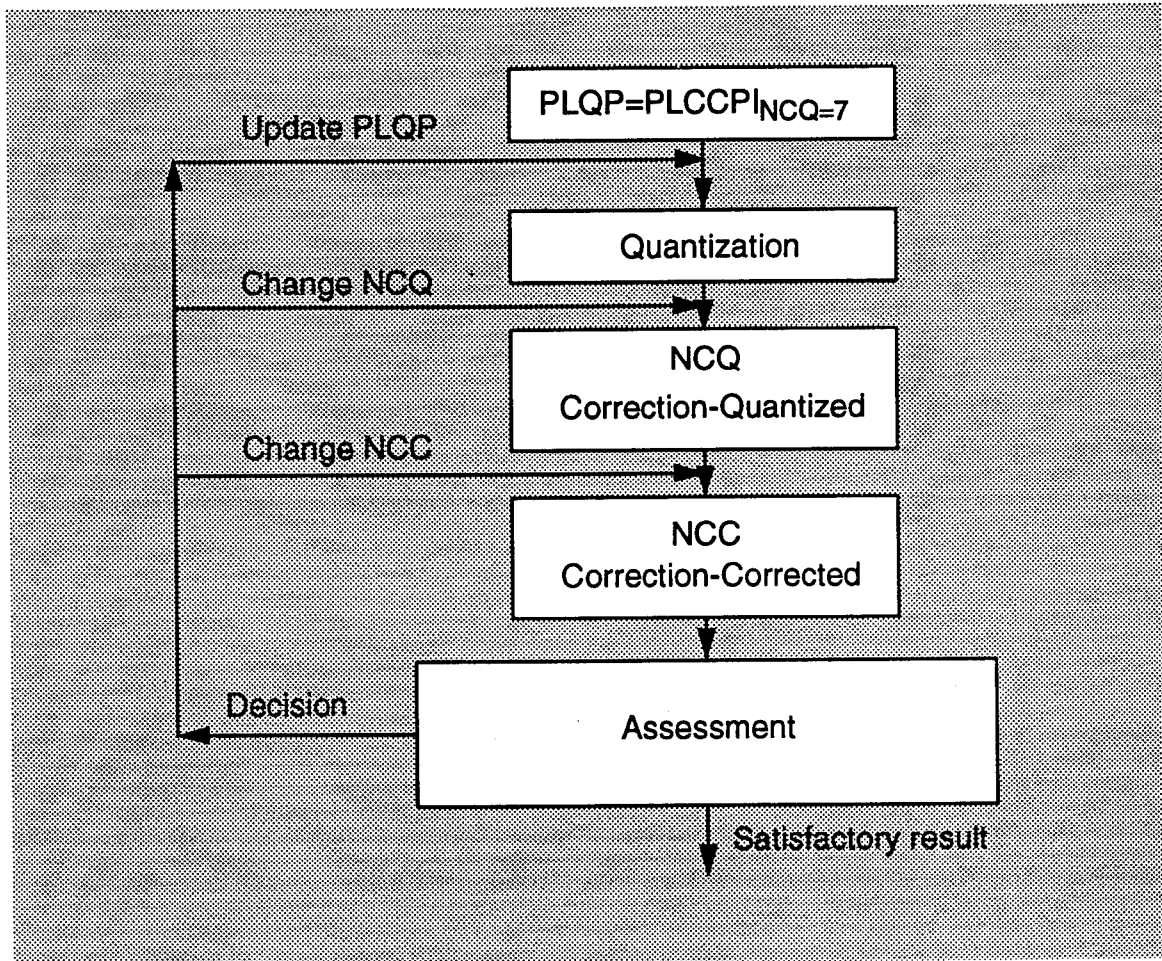


Figure VII.4.2 - Threshold Fine-Tuning Stage

This means that the subpatch with the smallest average power occupies 100% of the CL patch area. Consequently, the CL patch is homogeneous.

- 2 - When the inequality in Eq. (VII.4-1) is met with  $PLCCP|_{NCQ=7}=100\%$ , there is no need for the threshold fine-tuning stage. This is because the initial value of PLQP in the threshold fine-tuning stage would be equal to 100% and any more processing would also result in  $PLCCP=100\%$  regardless of the values chosen for NCQ and NCC.

- 3 - If the threshold fine-tuning stage results in  $PLCCP=100\%$  at any iteration, the threshold fine-tuning stage should end because, as in observation -2-, any more processing will end with  $PLCCP=100\%$  regardless of the values chosen for NCQ and NCC. This, in turn, will make PLQP equal to 100%.

Tables VII.4.1 and VII.4.2 summarize the discrepancies that may occur during the threshold approximation and fine-tuning stages for the CL subpatch investigation.

Discrepancy (Conflict Type)	Diagnosis (Source of Distortion)	Reprocessing
$PLCCP _{NCQ=8} - PLCCP _{NCQ=7}$ is more than 10%	$PLQP - PLQP_t > -10\%$	Assign to PLQP the latest value of $PLCCP _{NCQ=8}$
$PLCCP _{NCQ=8} - PLCCP _{NCQ=7}$ is less than 10% in the early stages of iteration	Initial value of PLQP is too low	Increase PLQP by 10% from its initial value
$PLCCP _{NCQ=8} - PLCCP _{NCQ=7}$ is less than 10% and $PLCCP _{NCQ=7 \text{ or } 8} = 100\%$	CL patch homogeneous	No threshold fine-tuning is needed

*Table VII.4.1 - Discrepancies in the Threshold Approximation Stage*

Discrepancy (Conflict Type)	Diagnosis (Source of Distortion)	Reprocessing
$IPLQP - PLCCP > 1\%$ and $PLQP < PLCCP$	Either NCQ or PLQP are not well adjusted	Decrease NCQ, otherwise update PLQP
$IPLQP - PLCCP > 1\%$ and $PLQP > PLCCP$	Either NCC or PLQP are not well adjusted	Increase NCC, otherwise update PLQP
$IPLQP - PLCCP > 1\%$ and $PLCCP=100\%$	CL patch homogeneous	Stop threshold fine-tuning

*Table VII.4.2 - Discrepancies in the Threshold Fine-Tuning Stage*

Examples are next presented to illustrate the control by IPUS of the CL subpatch investigation.

### **VII.4.3 - Examples**

In this section, tables describing the CL subpatch investigation of examples 1, 2 and 3 in Chapter VI are modified to include the rules developed in this chapter for both the threshold approximation and threshold fine-tuning stages. In the following examples, Define  $\Delta_1 = PLCCPI_{NCQ=8} - PLCCPI_{NCQ=7}$  and  $\Delta_2 = PLQP - PLCCPI$ .

#### **VII.4.3.1 - Example 1**

First consider the example of Section VI.5.1. Tables VII.4.3, VII.4.4 and VII.4.5 are expanded versions of Tables VI.5.3, VI.5.4 and VI.5.5 to include information about the procedures for the threshold approximation and threshold fine-tuning stages. Note in Table VII.4.3 that no threshold fine-tuning is needed for

Clutter Patch 1			
PLQP (%)			$\Delta_i$
Threshold Approximation Stage			
10.00 (guess)	NCQ=8 NCC=1 PLCQP=70.59 PLCCP=20.59	NCQ=7 NCC=1 PLCQP=23.53 PLCCP=2.94	$\Delta_1 > 10\%$
20.59 latest PLCCP	NCQ=8 NCC=1 PLCQP=94.12 PLCCP=82.35	NCQ=7 NCC=1 PLCQP=79.41 PLCCP=38.24	$\Delta_1 > 10\%$
82.35 latest PLCCP	NCQ=8 NCC=1 PLCQP=100.0 PLCCP=100.0	NCQ=7 NCC=1 PLCQP=100.0 PLCCP=100.0	$\Delta_1 < 10\%$

**Table VII.4.3 - Setting of PLQP in Both of the Threshold Approximation and Threshold Fine-tuning Stages**

CL patch 1. This is due to the fact that CL patch 1 is homogeneous and does not contain subpatches. Also in Table VII.4.5 note that the threshold fine-tuning stage needs not be carried out as  $PLCCP=100\%$  in the last row before of the threshold approximation stage. However, when the fine-tuning stage is carried out, PLQP converges to 99.33 %.

Clutter Patch 2			
PLQP (%)			$\Delta_i$
Threshold Approximation Stage			
10.00 (guess)	NCQ=8 NCC=1 PLCQP=39.38 PLCCP=7.50	NCQ=7 NCC=1 PLCQP=9.37 PLCCP=0.00	$\Delta_1 < 10\%$
20.00 (new guess)	NCQ=8 NCC=1 PLCQP=59.38 PLCCP=43.12	NCQ=7 NCC=1 PLCQP=38.12 PLCCP=8.75	$\Delta_1 > 10\%$
43.12 latest PLCCP	NCQ=8 NCC=1 PLCQP=61.88 PLCCP=51.25	NCQ=7 NCC=1 PLCQP=55.00 PLCCP=49.38	$\Delta_1 > 10\%$
Threshold Fine-Tuning Stage			
49.38 latest PLCCP	NCQ=5 NCC=1 PLCQP=50.62 PLCCP=46.25		$\Delta_2 > 1\%$
49.38 same as lat- est PLQP	NCQ=5 NCC=2 PLCQP=50.62 PLCCP=46.88		$\Delta_2 > 1\%$
49.38 same as lat- est PLQP	NCQ=5 NCC=3 PLCQP=50.62 PLCCP=48.75		$\Delta_2 < 1\%$

Table VII.4.4 - Setting of PLQP in Both of the Threshold Approximation and Threshold Fine-tuning Stages

Clutter Patch 3			
PLQP (%)			$\Delta_i$
Threshold Approximation Stage			
10.00 (guess)	NCQ=8 NCC=1 PLCQP=50.25 PLCCP=12.19	NCQ=7 NCC=1 PLCQP=14.61 PLCCP=0.33	$\Delta_1 > 10\%$
12.19 latest PLCCP	NCQ=8 NCC=1 PLCQP=58.51 PLCCP=16.61	NCQ=7 NCC=1 PLCQP=20.28 PLCCP=0.83	$\Delta_1 > 10\%$
16.61 latest PLCCP	NCQ=8 NCC=1 PLCQP=73.62 PLCCP=28.80	NCQ=7 NCC=1 PLCQP=33.97 PLCCP=2.42	$\Delta_1 > 10\%$
28.80 latest PLCCP	NCQ=8 NCC=1 PLCQP=92.57 PLCCP=66.19	NCQ=7 NCC=1 PLCQP=70.03 PLCCP=22.79	$\Delta_1 > 10\%$
66.19 latest PLCCP	NCQ=8 NCC=1 PLCQP=100.0 PLCCP=100.0	NCQ=7 NCC=1 PLCQP=99.83 PLCCP=98.66	$\Delta_1 < 10\%$
Threshold Fine-Tuning Stage			
98.66 latest PLCCP	NCQ=5 NCC=1 PLCQP=100.0 PLCCP=100.0		$\Delta_2 > 1\%$
99.33 half way rule	NCQ=5 NCC=1 PLCQP=100.0 PLCCP=100.0		$\Delta_2 < 1\%$

Table VII.4.5 - Setting of BNQP in Both of the Threshold Approximation and Threshold Fine-tuning Stages

### **VII.4.3.2 - Example 2**

Consider the example of Section VI.5.2. Tables VII.4.6, VII.4.7 and VII.4.8 are expanded versions of Tables VI.5.13, VI.5.14 and VI.5.15 to include information about the procedures for the threshold approximation and threshold fine-tuning stages. In Table VII.4.7 note that the threshold fine-tuning steps, presented in the shaded rows, need not be carried out.

Clutter Patch 1			
PLQP (%)			$\Delta_i$
Threshold Approximation Stage			
10.00 (guess)	NCQ=8 NCC=1 PLCQP=36.73 PLCCP=8.16	NCQ=7 NCC=1 PLCQP=8.16 PLCCP=2.04	$\Delta_1 < 10\%$
20.00 (new guess)	NCQ=8 NCC=1 PLCQP=71.43 PLCCP=28.57	NCQ=7 NCC=1 PLCQP=55.10 PLCCP=10.20	$\Delta_1 > 10\%$
28.57 latest PLCCP	NCQ=8 NCC=1 PLCQP=87.76 PLCCP=55.10	NCQ=7 NCC=1 PLCQP=55.10 PLCCP=10.20	$\Delta_1 > 10\%$
55.10 latest PLCCP	NCQ=8 NCC=1 PLCQP=100.0 PLCCP=100.0	NCQ=7 NCC=1 PLCQP=95.92 PLCCP=79.59	$\Delta_1 > 10\%$
79.59 latest PLCCP	NCQ=8 NCC=1 PLCQP=100.0 PLCCP=100.0	NCQ=7 NCC=1 PLCQP=100.0 PLCCP=100.0	$\Delta_1 < 10\%$

**Table VII.4.6 - Setting of PLQP in Both of the Threshold Approximation and Threshold Fine-tuning Stages**

Clutter Patch 2			
PLQP (%)			$\Delta_i$
Threshold Approximation Stage			
10.00 (guess)	NCQ=8 NCC=1 PLCQP=60.38 PLCCP=19.50	NCQ=7 NCC=1 PLCQP=16.35 PLCCP=0.00	$\Delta_1 > 10\%$
19.50 latest PLCCP	NCQ=8 NCC=1 PLCQP=81.76 PLCCP=49.06	NCQ=7 NCC=1 PLCQP=46.54 PLCCP=8.80	$\Delta_1 > 10\%$
49.06 latest PLCCP	NCQ=8 NCC=1 PLCQP=94.97 PLCCP=81.76	NCQ=7 NCC=1 PLCQP=81.76 PLCCP=57.23	$\Delta_1 > 10\%$
81.76 latest PLCCP	NCQ=8 NCC=1 PLCQP=100.0 PLCCP=100.0	NCQ=7 NCC=1 PLCQP=99.37 PLCCP=94.97	$\Delta_1 < 10\%$
Threshold Fine-Tuning Stage			
94.97 latest PLCCP	NCQ=5 NCC=1 PLCQP=100.0 PLCCP=100.0		$\Delta_2 > 1\%$
97.47 half way rule	NCQ=5 NCC=1 PLCQP=100.0 PLCCP=100.0		$\Delta_2 > 1\%$
98.73 half way rule	NCQ=5 NCC=1 PLCQP=100.0 PLCCP=100.0		$\Delta_2 > 1\%$
99.36 half way rule	NCQ=5 NCC=1 PLCQP=100.0 PLCCP=100.0		$\Delta_2 < 1\%$

Table VII.4.7 - Setting of PLQP in Both of the Threshold Approximation and Threshold Fine-tuning Stages

Clutter Patch 3			
PLQP (%)			$\Delta_i$
Threshold Approximation Stage			
10.00 (guess)	NCQ=8 NCC=1 PLCQP=63.36 PLCCP=22.12	NCQ=7 NCC=1 PLCQP=17.97 PLCCP=0.69	$\Delta_1 > 10\%$
22.12 latest PLCCP	NCQ=8 NCC=1 PLCQP=89.63 PLCCP=62.90	NCQ=7 NCC=1 PLCQP=63.82 PLCCP=19.12	$\Delta_1 > 10\%$
62.90 latest PLCCP	NCQ=8 NCC=1 PLCQP=100.0 PLCCP=100.0	NCQ=7 NCC=1 PLCQP=99.08 PLCCP=94.70	$\Delta_1 < 10\%$

Table VII.4.8 - Setting of BNQP in Both of the Threshold Approximation and Threshold Fine-tuning Stages

### VII.4.3.3 - Example 3

Finally, consider the example of Section VI.5.3. Tables VII.4.9, VII.4.10 and VII.4.11 are expanded versions of Tables VI.5.21, VI.5.22 and VI.5.23 to include information about the procedures for the threshold approximation and threshold fine-tuning stages. Note from Tables VII.4.9 and VII.4.10 and VII.4.11 that no threshold fine-tuning is needed for CL patches 1, 2, and 3. Also, note that the last four shaded rows of Table VII.4.11 need not be carried out.

Clutter Patch 1			
PLQP (%)			$\Delta_i$
Threshold Approximation Stage			
10.00 (guess)	NCQ=8 NCC=1 PLCQP=48.94 PLCCP=8.51	NCQ=7 NCC=1 PLCQP=6.38 PLCCP=0.00	$\Delta_1 < 10\%$
20.00 (new guess)	NCQ=8 NCC=1 PLCQP=82.98 PLCCP=51.06	NCQ=7 NCC=1 PLCQP=46.81 PLCCP=10.64	$\Delta_1 > 10\%$
51.06 latest PLCCP	NCQ=8 NCC=1 PLCQP=100.0 PLCCP=100.0	NCQ=7 NCC=1 PLCQP=95.74 PLCCP=78.72	$\Delta_1 > 10\%$
78.72 latest PLCCP	NCQ=8 NCC=1 PLCQP=100.0 PLCCP=100.0	NCQ=7 NCC=1 PLCQP=100.0 PLCCP=100.0	$\Delta_1 < 10\%$

Table VII.4.9 - Setting of PLQP in Both of the Threshold Approximation and Threshold Fine-tuning Stages

Clutter Patch 2			
PLQP (%)			$\Delta_i$
Threshold Approximation Stage			
10.00 (guess)	NCQ=8 NCC=1 PLCQP=42.93 PLCCP=11.62	NCQ=7 NCC=1 PLCQP=16.67 PLCCP=1.51	$\Delta_1 > 10\%$
11.62 latest PLCCP	NCQ=8 NCC=1 PLCQP=53.54 PLCCP=13.64	NCQ=7 NCC=1 PLCQP=19.19 PLCCP=1.51	$\Delta_1 > 10\%$
13.64 latest PLCCP	NCQ=8 NCC=1 PLCQP=64.14 PLCCP=18.69	NCQ=7 NCC=1 PLCQP=24.24 PLCCP=2.52	$\Delta_1 > 10\%$
18.69 latest PLCCP	NCQ=8 NCC=1 PLCQP=77.27 PLCCP=32.32	NCQ=7 NCC=1 PLCQP=44.95 PLCCP=7.57	$\Delta_1 > 10\%$
32.32 latest PLCCP	NCQ=8 NCC=1 PLCQP=94.44 PLCCP=69.70	NCQ=7 NCC=1 PLCQP=78.79 PLCCP=37.37	$\Delta_1 > 10\%$
69.70 latest PLCCP	NCQ=8 NCC=1 PLCQP=100.0 PLCCP=100.0	NCQ=7 NCC=1 PLCQP=100.0 PLCCP=100.0	$\Delta_1 < 10\%$

Table VII.4.10 - Setting of PLQP in Both of the Threshold Approximation and Threshold Fine-tuning Stages

Clutter Patch 3			
PLQP (%)			$\Delta_i$
Threshold Approximation Stage			
10.00 (guess)	NCQ=8 NCC=1 PLCQP=46.53 PLCCP=14.36	NCQ=7 NCC=1 PLCQP=11.39 PLCCP=1.98	$\Delta_1 > 10\%$
14.36 latest PLCCP	NCQ=8 NCC=1 PLCQP=70.30 PLCCP=26.24	NCQ=7 NCC=1 PLCQP=31.68 PLCCP=5.44	$\Delta_1 > 10\%$
26.24 latest PLCCP	NCQ=8 NCC=1 PLCQP=92.08 PLCCP=66.83	NCQ=7 NCC=1 PLCQP=68.81 PLCCP=24.75	$\Delta_1 > 10\%$
66.83 latest PLCCP	NCQ=8 NCC=1 PLCQP=100.0 PLCCP=100.0	NCQ=7 NCC=1 PLCQP=99.01 PLCCP=93.07	$\Delta_1 < 10\%$
Threshold Fine-Tuning Stage			
93.07 latest PLCCP	NCQ=5 NCC=1 PLCQP=100.0 PLCCP=100.0		$\Delta_2 > 1\%$
96.53 half way rule	NCQ=5 NCC=1 PLCQP=100.0 PLCCP=100.0		$\Delta_2 > 1\%$
98.26 half way rule	NCQ=5 NCC=1 PLCQP=100.0 PLCCP=100.0		$\Delta_2 > 1\%$
99.13 half way rule	NCQ=8 NCC=1 PLCQP=100.0 PLCCP=100.0		$\Delta_2 < 1\%$

Table VII.4.11 - Setting of PLQP in Both of the Threshold Approximation and Threshold Fine-tuning Stages

#### **VII.4.4 - IPUS Stages Included in the PDF Approximation Stage**

Recall that the objective of the PDF approximation stage is to approximate the PDF underlying a particular CL patch region. A six step strategy for PDF approximation was presented in Section VI.4.5. The first 5 steps consisted of (1) selecting a total of  $N_T$  test cells that are evenly spread throughout the CL patch, (2) choosing for each test cell the closest  $N_R=100$  reference cells, as described in Section VI.4.1, (3) Using the Ozturk algorithm to determine the distance between the locus end point of the data linked vectors and its projection onto the Weibull, Lognormal, and K-distributed trajectories, (4) Discarding those PDFs for which the distances in step 3 exceed the corresponding half length of the minor axis obtained from Table VI.4.1, and (5) Excising any outliers that may exist from the data and proceeding to step 3 when all possible PDFs are discarded in step 4. These steps were illustrated through examples in Section VI.5. Step 6 consists of the use of IPUS to determine one or more PDFs to approximate the data in a particular CL patch. Thus, IPUS is needed to complete the PDF approximation stage of the indexing procedure.

In order to be able to identify the SPA, SPA instance, and discrepancies associated with the PDF approximation stage, step 6 of the PDF approximation strategy has to be formulated.

##### **VII.4.4.1 - Step 6 of the PDF Approximation Strategy**

When the five first steps of the PDF approximation strategy are completed, the information available to step 6 consists of (1) identification numbers of the test cells, (2) best PDF(s) to approximate the data of the reference cells in every test cell along with their shape, scale, and location parameters, (3) distance from the locus end point of every test cell to the approximating PDF(s), and (4) (U,V) coordinates of the locus end point for every test cell. This information has been tabulated for the selected examples of Sections VI.5.1, VI.5.2, and VI.5.3.

The following strategy is used in step 6:

- 6.1 - Only those kinds of PDFs among the Weibull, Lognormal and K distributions, denoted by W, L, and K, respectively, that pass step 4 for all of the test cells in the patch are considered as possible approximating kind of PDF(s) for the CL patch.

A violation type of discrepancy occurs when none of the distributions pass step 4 for all of the test cells in the patch. This situation initiates a search for sub-patches within the patch.

- 6.2 - The ranking of each possible approximating type of PDF is summed over all of the test cells in the CL patch. That distribution having the lowest sum is chosen as the best approximation kind, for the underlying CL patch distribution. For example, consider Table VI.5.9 which contains the distribution rankings for each test cell. The sum of the rankings for W, L, and K are 16, 15, and 20, respectively. Consequently, L is chosen as the best approximating kind.

- 6.3 - A check is made to determine whether, indeed, the patch under consideration is homogeneous. If it is, numerical values are determined for the best approximating kind of PDF. If it is not, a fault type of discrepancy occurs and a subpatch search is initiated. The check for homogeneity proceeds by determining whether all of the test cells in the patch fall within the 0.99 confidence contour of the approximating PDF for each test cell. However, in contrast to Section VI.4.3, the length of the minor axis is used as opposed to the half length. The lengths of the minor axes are tabulated in Table VII.4.12 for  $N_R=100$  and various shape parameters. The procedure is carried out as follows:

- 6.3.a - Select the first test cell in the CL patch.
- 6.3.b - Using the best approximating kind of PDF found in - 6.2 -

PDF	Shape Parameter	Length of the minor axis
Rayleigh	-	$0.94 \times 10^{-1}$
Weibull	0.1	$0.50 \times 10^{-1}$
	0.5	$0.82 \times 10^{-1}$
	1.0	$0.82 \times 10^{-1}$
	2.0	$0.94 \times 10^{-1}$
	3.0	$0.94 \times 10^{-1}$
	4.0	$0.90 \times 10^{-1}$
	5.0	$0.88 \times 10^{-1}$
	10.0	$0.88 \times 10^{-1}$
Lognormal	0.01	$0.96 \times 10^{-1}$
	0.05	$0.90 \times 10^{-1}$
	0.1	$0.86 \times 10^{-1}$
	0.2	$0.84 \times 10^{-1}$
	0.3	$0.84 \times 10^{-1}$
	0.4	$0.92 \times 10^{-1}$
	1.0	$0.82 \times 10^{-1}$
	5.0	$0.56 \times 10^{-1}$
	10.0	$0.26 \times 10^{-1}$
K-distribution	0.01	$0.26 \times 10^{-1}$
	0.1	$0.74 \times 10^{-1}$
	1.0	$0.58 \times 10^{-1}$
	5.0	$0.97 \times 10^{-1}$
	10.0	$0.94 \times 10^{-1}$
	20.0	$0.98 \times 10^{-1}$
	40.0	$0.98 \times 10^{-1}$
	50.0	$0.98 \times 10^{-1}$

Table VII.4.12 - Minor Axis Length for Different PDFs,  $N_B=100$

and the shape, parameter associated with the selected test cell, determine the length of the minor axis from Table VII.4.12.

- 6.3.c - Using the (U,V) coordinates for the locus end points, compute the distances between the (U,V) coordinates of the selected test cell and every other test cell.

- 6.3.d - Check the distances computed in - 6.3.c - against the minor axis length obtained in - 6.3.b -. Those test cells within the minor axis length from the selected test cell pass and are indicated by a ✓. The remaining cells are indicated by an X.

- 6.3.e - Select the second test cell in the CL patch and repeat - 6.3.b- through - 6.3.d -.

- 6.3.f - Continue this process until all test cells have been selected.

- 6.3.g - Record the results in a table referred to as the exclusion table. The CL patch is assumed to be homogeneous only if no X's appear in the exclusion table.

- 6.3.h - When only ✓'s appear in the exclusion table, the CL patch is considered to be homogeneous. An approximating PDF is obtained by averaging over all of the test cells the shape, scale, and location parameters of the best approximating kind of PDF obtained in - 6.2 -.

- 6.3.i. - When X's appear in the exclusion table, a fault type of discrepancy occurs. This is discussed in a later section dealing with discrepancies.

Steps - 6.3.a - to - 6.3.h - are now illustrated using the data in Table VI.5.9. As noted in step - 6.2 -, Lognormal is the best PDF approximating kind for the CL patch under consideration. Therefore, using Table VII.4.12, the lengths of the minor axes corresponding to the shape parameter values of the Lognormal PDF found in Table VI.5.9 are listed in Table VII.4.13 for the different test cells. The second column and first row of Table VII.4.13. indicate the assigned numbers of

the test cells. Finally, the remaining entries in the Table represent the distance between the locus end points of the tabulated pairs of test cells.

Length from Table VII.4.12	Cell No.	1	361	722	1083	1444
0.084	1	0	0.007	0.050	0.020	0.025
0.084	361	0.007	0	0.053	0.027	0.027
0.084	722	0.050	0.053	0	0.040	0.026
0.084	1083	0.020	0.027	0.040	0	0.023
0.090	1444	0.025	0.027	0.026	0.023	0

Table VII.4.13 - Distance Between All Pairs of Test Cells for the Data of Table VI.5.9

The exclusion table corresponding to Table VII.4.13 is shown in Table VII.4.14 and consists of ✓'s and ✗'s depending on whether or not the distances in every row of Table VII.4.13 are smaller or larger than the length shown in the first column of the same row. For this example, note that the entries are all ✓'s indicating that all test cells are within the length of the minor axes for the appropriate log-normal distributions. It is concluded that the patch under investigation is homogeneous. This example is completed in Section VII.5.1.

Cell No.	1	361	722	1083	722
1	✓	✓	✓	✓	✓
361	✓	✓	✓	✓	✓
722	✓	✓	✓	✓	✓
1083	✓	✓	✓	✓	✓
1444	✓	✓	✓	✓	✓

Table VII.4.14 - Exclusion Table for the Example of Table VI.5.9

#### **VII.4.4.2 - SPA and SPA Instance**

Steps 1 through 6 of the PDF approximation stage involve the choice of  $N_T$  test cells, the selection of  $N_R$  reference cells for each test cell, use of the Ozturk algorithm to find the best approximating PDF(s) for each test cell, and determination of an approximating PDF when the CL patch is homogeneous or implementation of a subpatch search procedure when the CL patch is nonhomogeneous. These steps, which are diagrammed in Figure VII.4.3, constitute the SPA. A particular setting of the parameters  $N_T$ , and  $N_R$  constitutes an SPA instance.

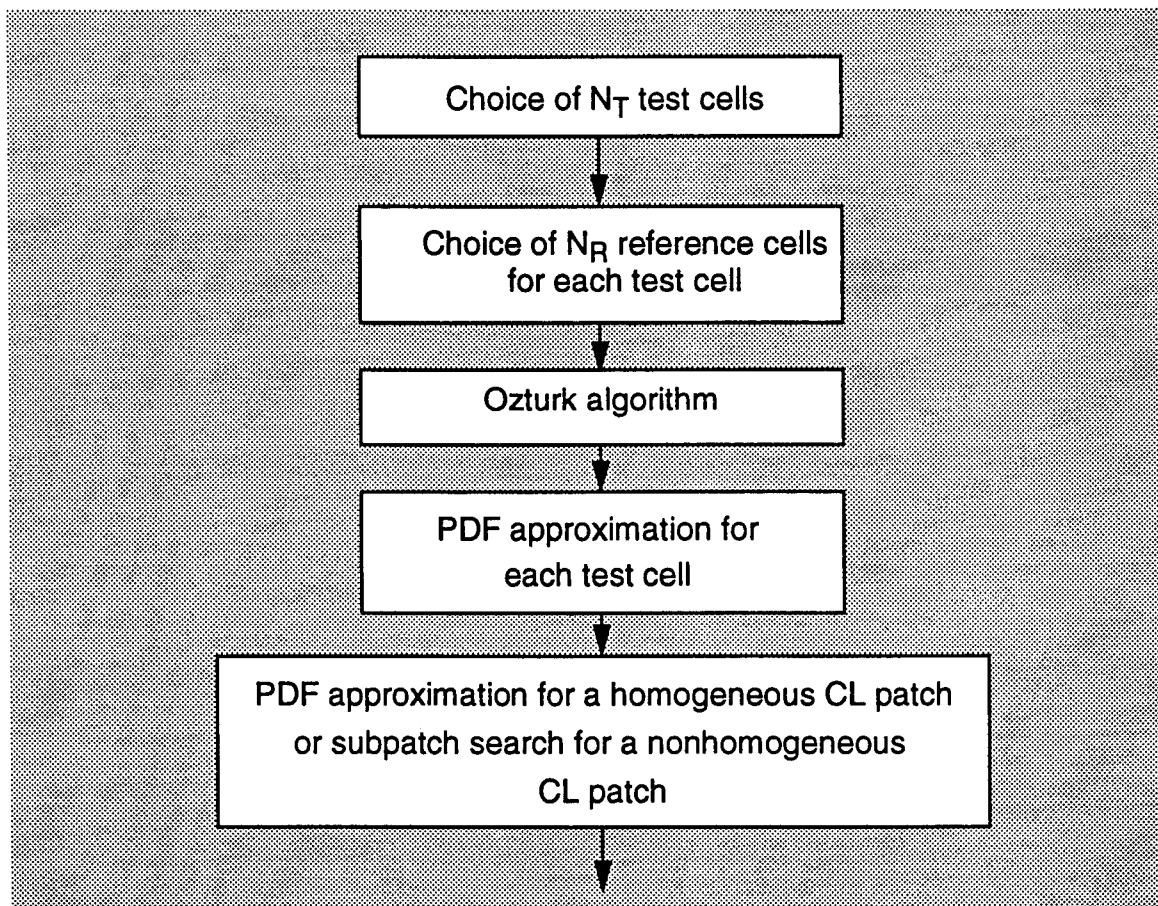


*Figure VII.4.3 - PDF Approximation Stage*

#### **VII.4.4.3 - Resolution of Discrepancies**

In this section, rules are developed to enable resolution of discrepancies that may occur during the PDF approximation stage. Discrepancies may arise during two different phases of this stage: (1) during the PDF approximation for each test cell and (2) during PDF approximation for a homogeneous CL patch or subpatch search for a nonhomogeneous CL patch. These phases are viewed as two substages and are investigated next.

- 1 - PDF approximation for each test cell: In order to approximate the PDF(s) of a test cell, steps 1 through 5 of the PDF approximation stage are implemented, as presented in Section VI.4.5. As shown in the examples of section VI.5, the outcome of the Ozturk algorithm phase is rejected whenever none of the allowable distributions (i.e., W, L, K) is found to be a suitable approximation. This decision is based on the fact that the data are known to be generated from either W, L, or K. When the data cannot be approximated by one of the allowable PDFs, a violation type of discrepancy is detected. At this point, the diagnosis process hypothesizes that the presence of outliers may be the source for the distortion causing the discrepancy. The first row of Table VII.4.15 summarizes resolution of the discrepancy that may occur in the PDF approximation of a test cell.

Even though the data are known to be generated from the W, L, and K distributions, they may not be representative. As a result, the allowable distributions may not provide suitable approximations even after removal of the outliers. Because the data have been identified as belonging to WSC, the Gaussian receiver is likely to produce false alarms. Consequently, the discrepancy is resolved by discarding the data. The second row of Table VII.4.15 summarizes resolution of this discrepancy.

Discrepancy (Violation Type)	Diagnosis (Source of Distortion)	Reprocessing
None of the allowable distributions is found to be a suitable approximation for the test cell	Presence of outliers	Remove outliers
After removal of outliers none of the allowable distributions is found to be a suitable approximation for the test cell	Data is not representative	Discard data

Table VII.4.15 - Discrepancies in the PDF Approximation of a Test Cell Stage

- 2 - PDF approximation for a CL patch: In order to approximate the PDF of a CL patch, step 6 of the PDF approximation stage is implemented. As discussed in Section VII.4.4.1, the decision that there exists a suitable approximating PDF for a CL patch is based on the outcome of the exclusion table. As stated previously, a discrepancy is detected when one or more **X**'s occur in the exclusion table.

When this happens, two cases are possible:

- 2.a - The CL patch is homogeneous. In this case, the discrepancy is of the conflict type because the expectation that only 's should be encountered in the exclusion table has not materialized. However, the full length minor axis criterion has yet to be applied to the PDF that would be obtained by averaging over the parameters of all the test cells for the best approximating PDF kind. This is necessary because an **X** which appears in the exclusion table due to two test cells having widely separated (U,V) coordinates may disappear when the (U,V) coordinates of each test cell are compared to those of the average PDF. Should this fail, an exclusion table is generated for the next best ranked PDF kind. If only ✓'s appear in the exclusion table, the parameters for this PDF kind are averaged over all the test cells and the average PDF is used to approximate the homogeneous CL patch. If one or more **X**'s appear in the exclusion table, phase

-2.a- is repeated until all possible PDF kinds have been exhausted. Should all possibilities fail, it is assumed that the CL patch is not homogeneous and the process initiates phase -2.b-.

- 2.b - The CL patch is not homogeneous. In this case, the discrepancy is of the violation type because none of the allowable PDF kinds is able to model the entire CL patch. Therefore, it should be modeled by two or more approximating PDFs. By using the exclusion table to identify groupings and by introducing new test cells between the groupings to generate even larger exclusion tables, the system attempts to determine a suitable number of PDFs for modeling the nonhomogeneous CL patch. This is achieved by examining the patterns of X's and ✓'s which appear, as discussed below.

For example, five test cells numbered a, b, c, d, and e might yield the exclusion table shown in Table VII.4.16. By interchanging rows and columns b and c, Table VII.4.17 results. From this table, there are seen to be two groupings: cells a, c and cells b, d, e. To determine whether the CL patch may consist of more than two groupings, new test cells, numbered f, g, h, which are located between the groupings are introduced. After rearranging rows and columns, the exclusion table given by Table VII.4.18 may result. By inspection, it is concluded that cells f, g, h are not common to the previous two groupings. It is concluded that the CL patch is likely to be composed of at least three groupings. On the other hand, the introduction of cells f, g, h might result in the exclusion table shown in Table VII.4.19. Here, cells f, g, and h are seen to be common to both of the original groupings. Cells f, g, and h can be classified as "border" test cells (i.e., cells having reference cells extending into more than one homogeneous subregion of the CL patch). It is concluded that two subregions are likely to exist within the CL patch. Further refinements can be made by introducing additional new test cells and studying the resulting exclusion tables.

In general, additional groupings are identified when new test cells cannot be associated with existing groupings. Otherwise, new test cells will either be as-

Cell No.	a	b	c	d	e
a	✓	✗	✓	✗	✗
b	✗	✓	✗	✓	✓
c	✓	✗	✓	✗	✗
d	✗	✓	✗	✓	✓
e	✗	✓	✗	✓	✓

Table VII.4.16 - Exclusion Table for Cells a, b, c, d, and e

Cell No.	a	c	b	d	e
a	✓	✓	✗	✗	✗
c	✓	✓	✗	✗	✗
b	✗	✗	✓	✓	✓
d	✗	✗	✓	✓	✓
e	✗	✗	✓	✓	✓

Table VII.4.17 - Exclusion Table When b and c are Interchanged

Cell No.	a	c	f	g	h	b	d	e
a	✓	✓	✗	✗	✗	✗	✗	✗
c	✓	✓	✗	✗	✗	✗	✗	✗
f	✗	✗	✓	✓	✓	✗	✗	✗
g	✗	✗	✓	✓	✓	✗	✗	✗
h	✗	✗	✓	✓	✓	✗	✗	✗
b	✗	✗	✗	✗	✗	✓	✓	✓
d	✗	✗	✗	✗	✗	✓	✓	✓
e	✗	✗	✗	✗	✗	✓	✓	✓

Table VII.4.18 - Exclusion Table When f, g, and h are Added

Cell No.	a	c	f	g	h	b	d	e
a	✓	✓	✓	✓	✓	✗	✗	✗
c	✓	✓	✓	✓	✓	✗	✗	✗
f	✓	✓	✓	✓	✓	✓	✓	✓
g	✓	✓	✓	✓	✓	✓	✓	✓
h	✓	✓	✓	✓	✓	✓	✓	✓
b	✗	✗	✓	✓	✓	✓	✓	✓
d	✗	✗	✓	✓	✓	✓	✓	✓
e	✗	✗	✓	✓	✓	✓	✓	✓

Table VII.4.19 - Exclusion Table When f, g, and h Are Added

sociated with existing groupings or be classified as border cells. When all cells of the CL patch have been used as either test cells or reference cells and when new test cells result only in border cells, the refinement procedure stops and the system assumes that additional groupings do not exist.

- 2.c - The next step in the procedure is to identify those cells in the various homogeneous subregions of the CL patch. In general, each test cell in a grouping has associated with it  $N_R$  reference cells. It is assumed that all  $N_R$  reference cells belong to the same subregion as the corresponding test cell. All the cells identified for a particular subregion are assigned the same number. For example, all the cells in the  $k$ th subregion are assigned the number  $k$ . At this point each cell in the CL patch will have one or more numbers assigned to it. Those cells with a single assigned number are assumed to belong to the numbered subregion. Those cells with more than one assigned number are assumed to belong to a border region bordering the numbered subregions. For example, a cell with the assigned numbers  $j$  and  $k$  is assumed to be in a border region bordering the  $j$ th and  $k$ th subregions. Similarly, a cell with the assigned numbers  $j$ ,  $k$ , and  $m$  is assumed to be in a border region bordering the  $j$ th,  $k$ th, and  $m$ th subregions.

- 2.d - Once the subregions have been identified, the PDF associated with each subregion is approximated. This is accomplished by following the procedure previously outlined in substeps 6.1-6.3 of step 6 for the PDF approximation strategy. Depending upon the application, the data from the border regions can either be discarded or approximated by one of the PDFs from the bordering subregions.

In summary, two types of discrepancies can arise during the PDF approximation of a CL patch, as shown in Table VII.4.20. When the CL patch may be homogeneous but cannot be approximated by the best average PDF, a conflict type of discrepancy is noted and the diagnosis suggests that the next best average PDF be tried. On the other hand, when it is concluded from the exclusion table that not all cells in a CL patch can be approximated by the same PDF, a violation type of discrepancy is detected indicating that the CL patch is not homogeneous. The diagnosis recommends that the CL patch data should be reprocessed to search for subpatches within the CL patch. Once the subregions have been identified, their PDFs are approximated.

Discrepancy	Diagnosis (Source of Distortion)	Reprocessing
Not all test cells can be approximated by the best average PDF (conflict type)	CL patch may be homogeneous but cannot be approximated by the best average PDF	Try the next best average PDF
Not all test cells can be approximated by any of the average PDF(s) (violation type)	CL patch is not homogeneous	Separate subpatches and approximate their corresponding PDF(s)

Table VII.4.20 - Discrepancies in the PDF Approximation of a CL Patch

Examples are now presented to illustrate control by IPUS of the PDF approximation stage.

## **VII.5 - Examples**

The IPUS concepts presented in Section VII.4 are now illustrated by continuing the examples treated previously in Sections VI.5.1, VI.5.2, and VI.5.3. In this section, the possible kinds of approximating PDFs are ranked as explained in Section VII.4.4. For each approximating kind of PDF, the corresponding exclusion table is then built. Conclusions from examination of the exclusion tables are indicated with either an “All pass” or a “Not all pass” label. A “Not all pass” label indicates that the corresponding exclusion table includes at least one **X** and that the full length minor axis criterion fails with the average PDF for one or more test cells. On the other hand, an “All pass” label indicates that the corresponding exclusion table does not include any **X**’s. Hence, all test cells may be approximated by the corresponding kind of PDF. For the kinds of PDFs that can approximate the distribution of the CL patch the scale, shape, and location parameters are averaged over all of the test cells in the CL patch to obtain an average PDF. PDFs that cannot approximate a particular CL patch either because of failure to pass the half length criterion or a “Not all pass” label are labeled N/A to indicate not applicable.

In order to evaluate the effectiveness of the proposed approach for the partitioning of the surveillance volume, results obtained for the number of CL patches, number of cells in each CL patch, and estimated CNR for each CL patch are compared to the generated ones. On the other hand, because the CL patch cells contain additive BN data, the PDF underlying a CL patch is not the PDF of the generated CL data alone. In general, analytical expressions for the PDF of the sum of BN and CL data are difficult to obtain. However, by using the Ozturk algorithm on 1000 BN plus CL data points, a very accurate approximation is obtained for the underlying PDF of the CL patch.

### **VII.5.1 - Example 1**

Consider Tables VI.5.7-VI.5.10 which summarize the results of steps 1 through 5 of the PDF approximation strategy for the example of Section VI.5.1. Note that CL patches 1, 2, and 3 can be approximated by any one of the three PDF kinds, whereas, as indicated in Table VI.5.10, CL patch 4 can be approximated only by the Weibull PDF. Tables VII.5.1-VII.5.4 summarize the results for step 6 of the PDF approximation strategy for the four CL patches identified thus far. An exclusion table was generated for the allowable PDF kinds in each CL patch. As shown in Tables VII.5.1-VII.5.4, all of the PDF kinds are labeled "All pass" indicating that none of the exclusion tables contained an **X** mark. Consequently, average values for the parameters of all the allowable PDF kinds are also tabulated in Tables VII.5.1-VII.5.4.

Average PDF	Rank	Exclusion Table	Shape	Scale	Location
W	1	All pass	2.05	3.14	0.64
L	3	All pass	0.19	7.27	-4.00
K	2	All pass	50.0	0.43	0.73

Table VII.5.1 - Average PDF(s) for CL Patch 1

Table VII.5.5 uses the results presented in Tables VI.5.6 and VII.5.1-VII.5.4 to list the best average PDF for each CL patch. Comparing the results in Tables VII.5.5 and VI.5.1 note that (1) regions for all four of the CL patches have been estimated, (2) the sample CNRs for CL patches A, C, and D, as evaluated according to Section VI.2.2, are within 1 dB of the generated values while that for CL patch B is within 3.31 dB, (3) the number of cells included in CL patches A, B, C, and D are close to the number of cells generated. In fact, a separate evaluation indicates that 96.5%, 98.3%, 97.2%, and 99.3% of the generated cells have been correctly classified for CL patches A, B, C, and D, respectively.

Average PDF	Rank	Exclusion Table	Shape	Scale	Location
W	2	All pass	2.56	1.29	31.38
L	1	All pass	0.13	4.32	28.17
K	3	All pass	50.0	0.15	31.62

Table VII.5.2 - Average PDF(s) for CL Patch 2

Average PDF	Rank	Exclusion Table	Shape	Scale	Location
W	2	All pass	1.96	15.52	-0.04
L	1	All pass	0.25	20.09	-30.09
K	3	All pass	33.28	2.96	0.08

Table VII.5.3 - Average PDF(s) for CL Patch 3

Average PDF	Rank	Exclusion Table	Shape	Scale	Location
W	1	All pass	4.51	90.82	14.97
L			N/A		
K			N/A		

Table VII.5.4 - Average PDF(s) for CL Patch 4

Clutter Patch (No.)	CNR (dB)	Number of cells	PDF (best)	Shape parameter	Scale parameter	Location parameter
A (1)	9.04	113	W	2.05	3.14	0.64
B (3)	23.31	1444	L	0.25	20.09	-30.09
C (2)	30.63	151	L	0.13	4.32	28.17
D (4)	40.56	146	W	4.51	90.82	14.97

Table VII.5.5 - Assessment Parameters of the Mapping and Indexing Stages

With regard to the goodness of the PDF approximations, Figures VII.5.1, VII.5.3, VII.5.5, and VII.5.7 show the location in the approximation chart, indicated by o, for the accurate approximation of the underlying CL patch PDF (i.e., PDF corresponding to the sum of CL and BN in the patch). These were obtained by generating 1000 points for each CL patch. The results are summarized in Table VII.5.6. Figures VII.5.2, VII.5.4, VII.5.6, and VII.5.8 show the PDFs from Table VII.5.5 (solid lines) obtained by the mapping and indexing stages, superimposed on the corresponding PDFs from Table VII.5.6 (dashed lines).

The comparison for CL patch A is given in Figure VII.5.2. Although the best approximating PDF is Weibull while the underlying PDF is Lognormal, the curves are reasonably close except for a small offset in their location. Figure VII.5.4 shows the comparison for CL patch B. Here the best approximating and underlying PDFs are both Lognormal with shape parameters 0.25 and 0.27, respectively. However, the scale and location parameters are not as closely matched. This accounts for the discrepancy between the two curves. The results for CL patch C are shown in Figure VII.5.6. As with CL patch A, the best approximating PDF is Weibull while the underlying PDF is Lognormal. In this case, the two curves differ substantially and a poor approximation has been made. Finally, the comparison for CL patch D is shown in Figure VII.5.8. Although the best approximating PDF is Weibull while the underlying PDF is SU-Johnson, note that the curves are reasonably close except for a small offset in their height and location.

The best approximating PDFs from Table VII.5.5 are superimposed on the histograms for CL patches A, B, C, and D in Figures VII.5.9-VII.5.12, respectively. Whether or not the best approximating PDFs are close to the underlying PDFs, note that the best approximating PDFs nicely overlay the corresponding histograms. Relative to CL patch C, it is seen that the large amount of data with values above 33 are not representative of the underlying PDF shown in Figure VII.5.6. This may be due to inclusion in CL patch C of cells originating in CL patch D.

CL Patch	PDF	Distance	Shape	Scale	Location	(U,V)
A	L	$0.61 \times 10^{-2}$	0.16	9.33	-5.65	(-0.0213, 0.3225)
B	L	$0.35 \times 10^{-2}$	0.27	26.25	-13.43	(-0.0416, 0.3282)
C	W	$0.22 \times 10^{-2}$	2.17	0.87	31.56	(-0.0296, 0.3382)
D	SU-Johnson	$0.79 \times 10^{-2}$	(40.0, 40.0)	54.19	164.51	(0.0223, 0.3379)

*Table VII.5.6 - Accurate Approximation of Underlying CL patch PDFs*

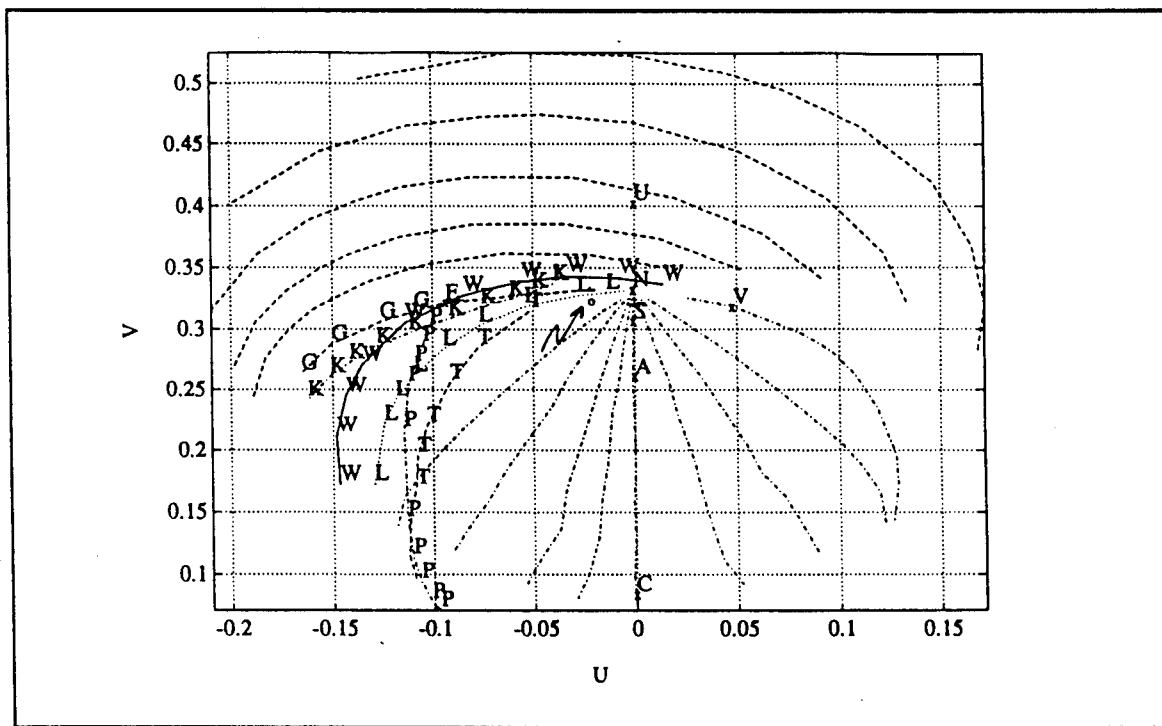


*Figure VII.5.1 - Location of the Locus End Point for CL Patch A*

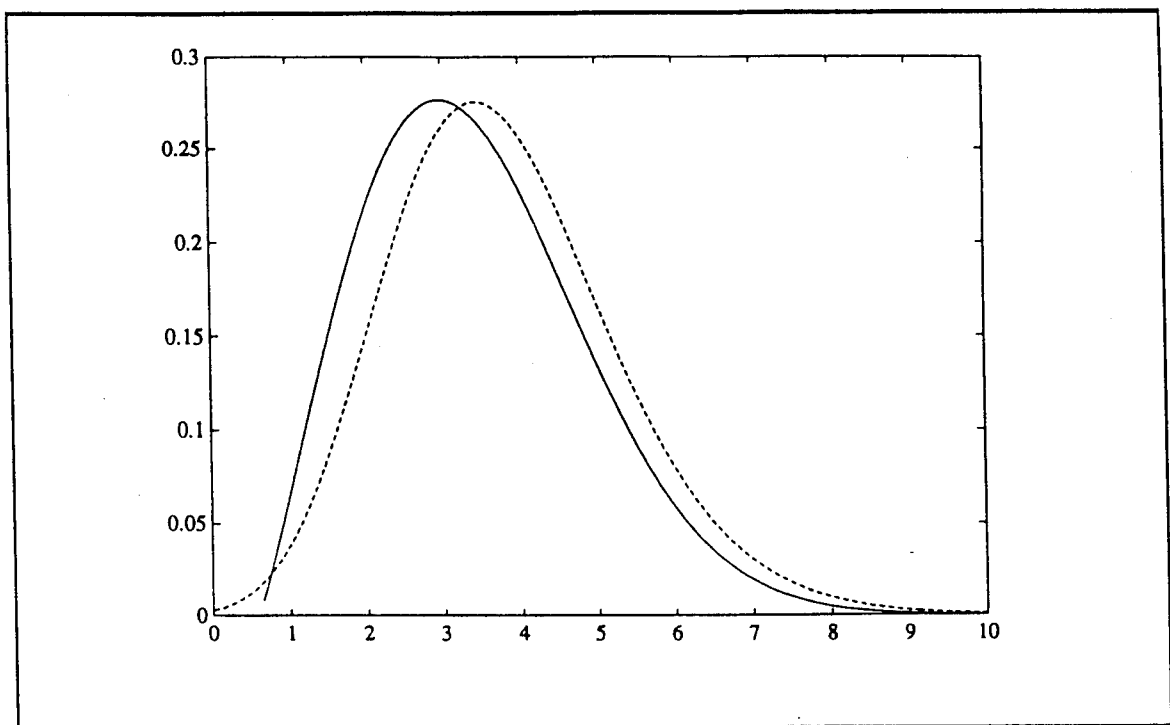


*Figure VII.5.2 - PDF Comparison for CL patch A*

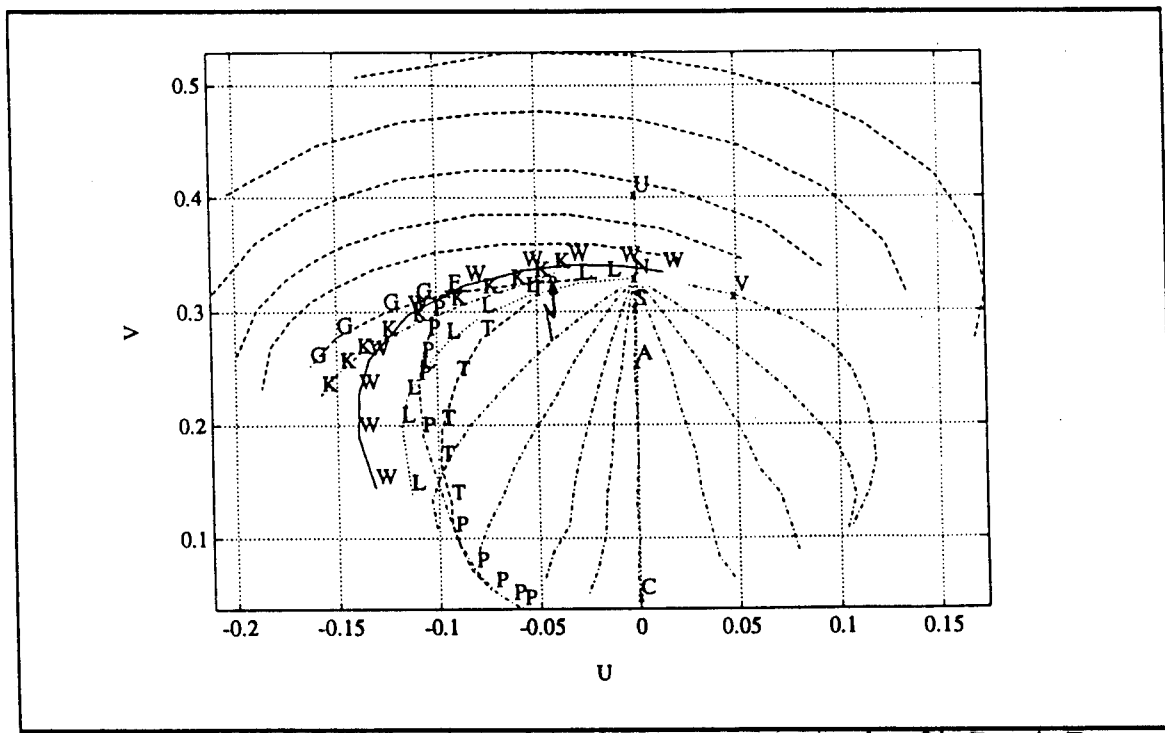


*Figure VII.5.3 - Location of the Locus End Point for CL Patch B*

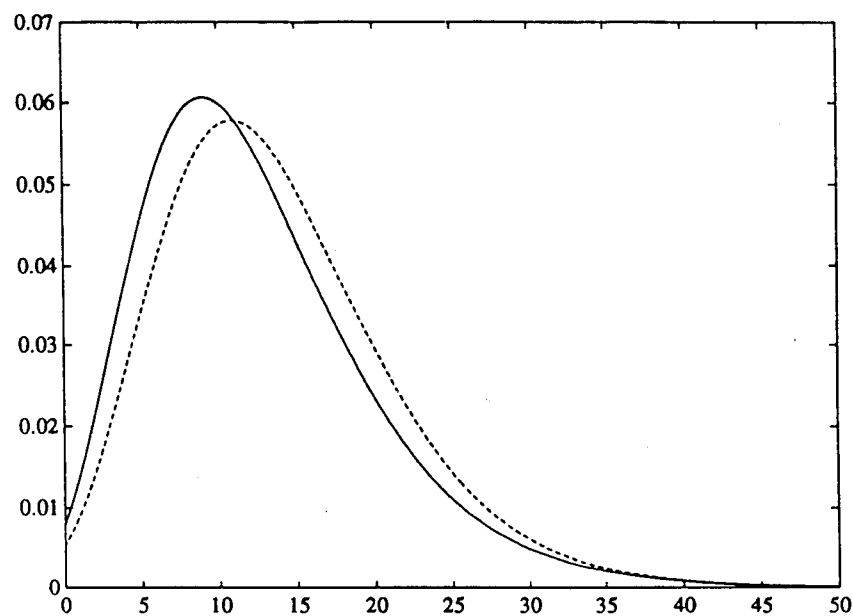


Figure VII.5.4 - PDF Comparison for CL patch B

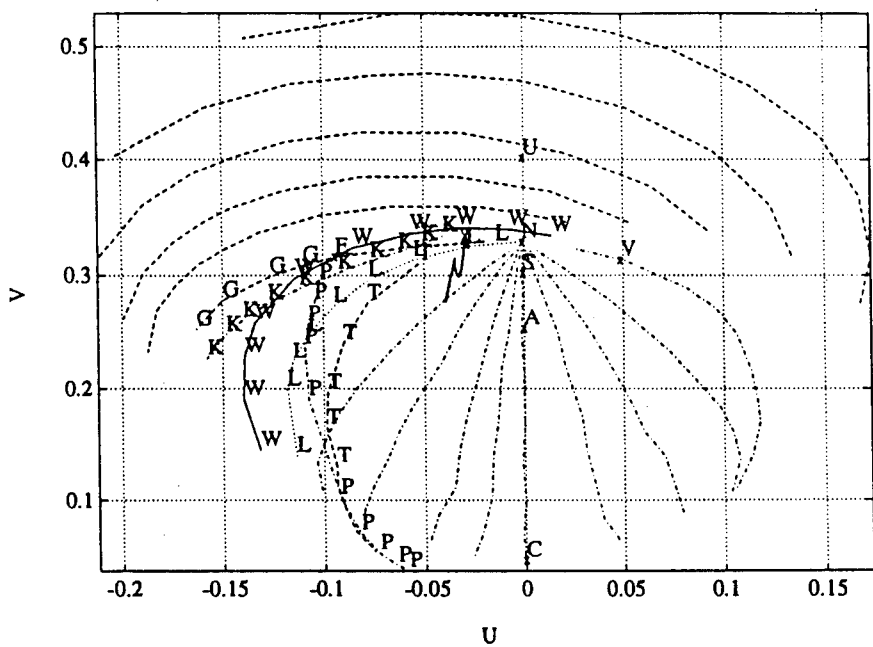


Figure VII.5.5 - Location of the Locus End Point for CL Patch C

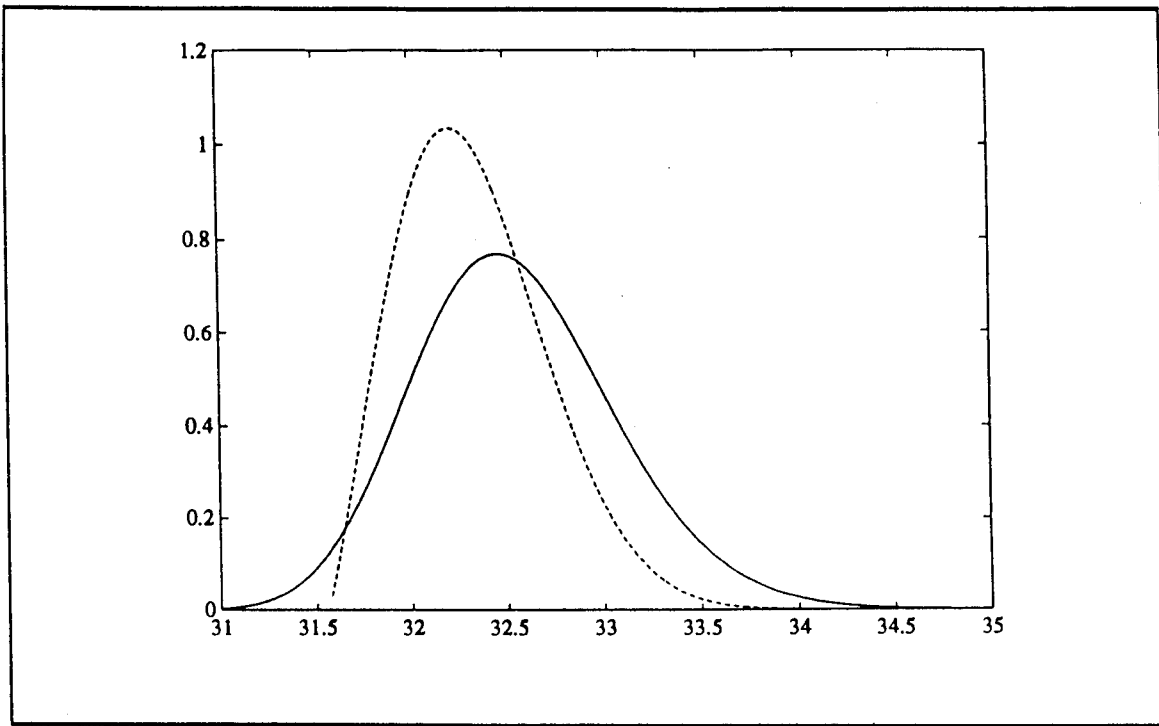


Figure VII.5.6 - PDF Comparison for CL patch C

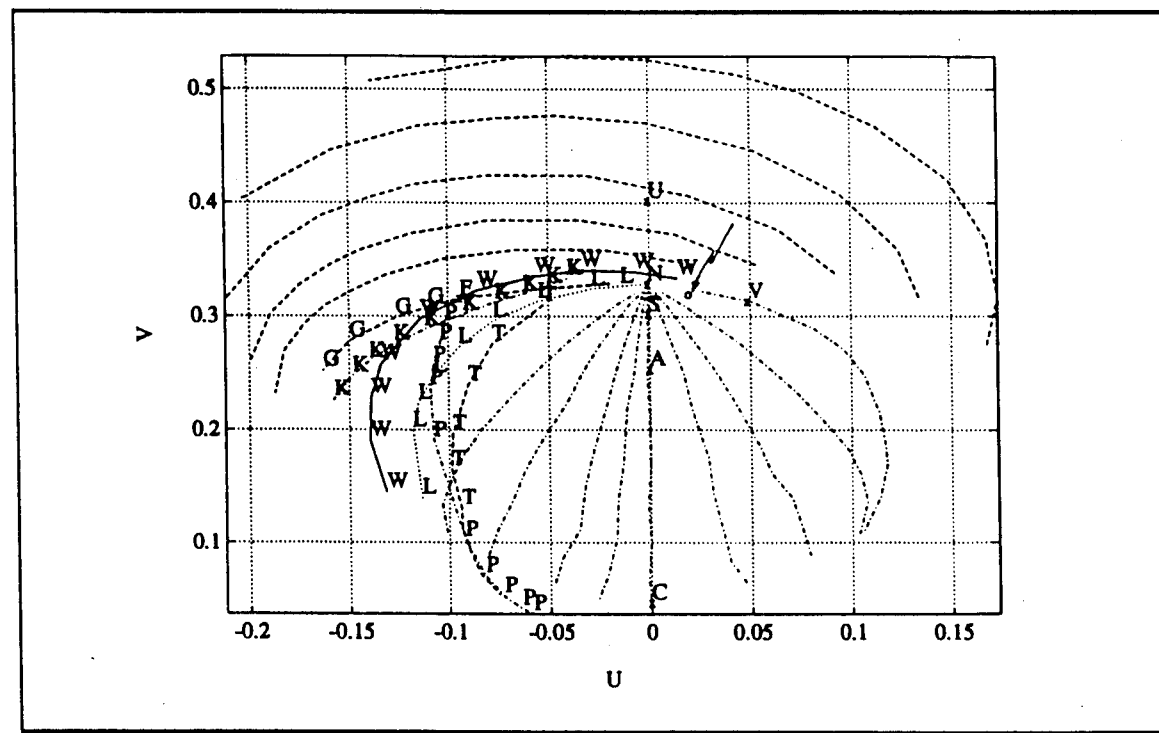


Figure VII.5.7 - Location of the Locus End Point for CL Patch D

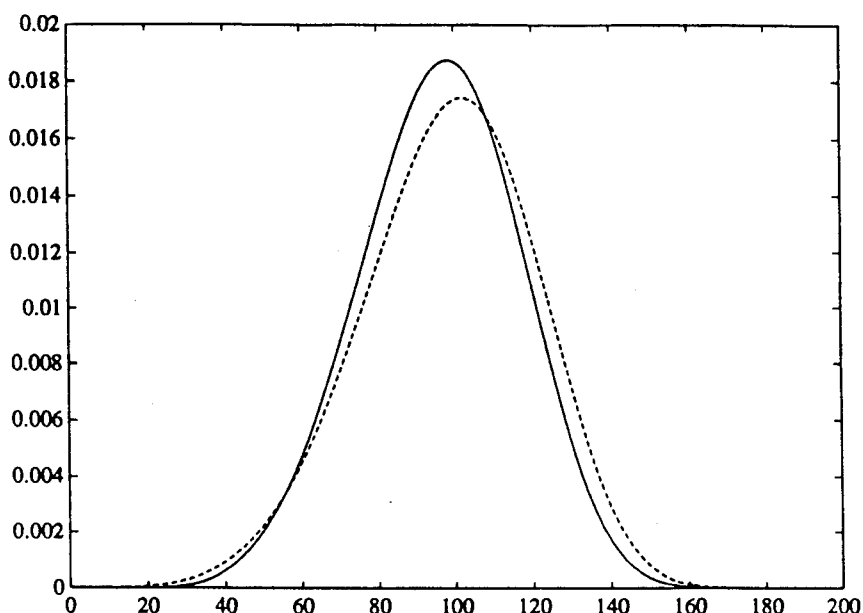


Figure VII.5.8 - PDF Comparison for CL patch D

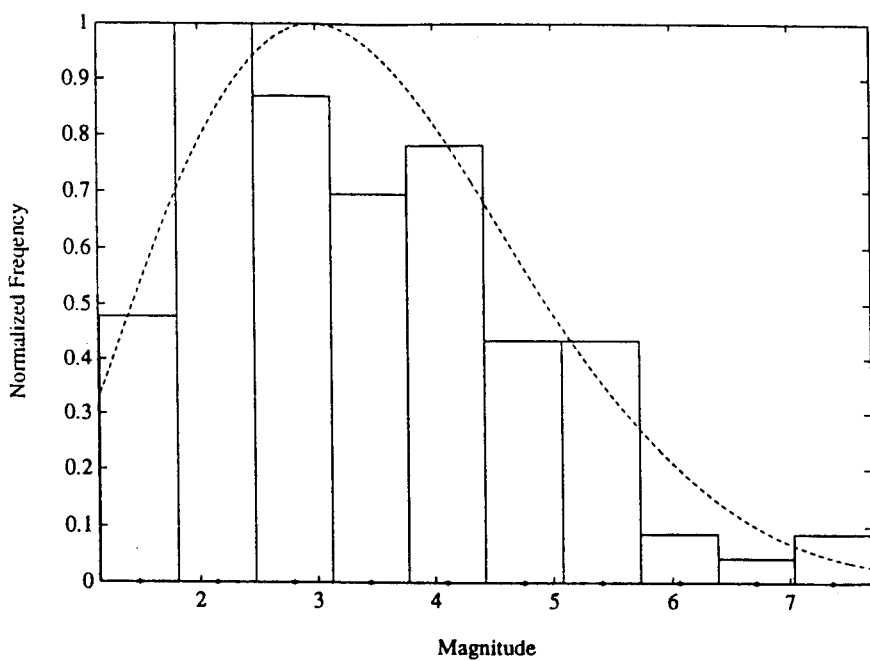


Figure VII.5.9 - Histogram and Best Approximating PDF for CL patch A

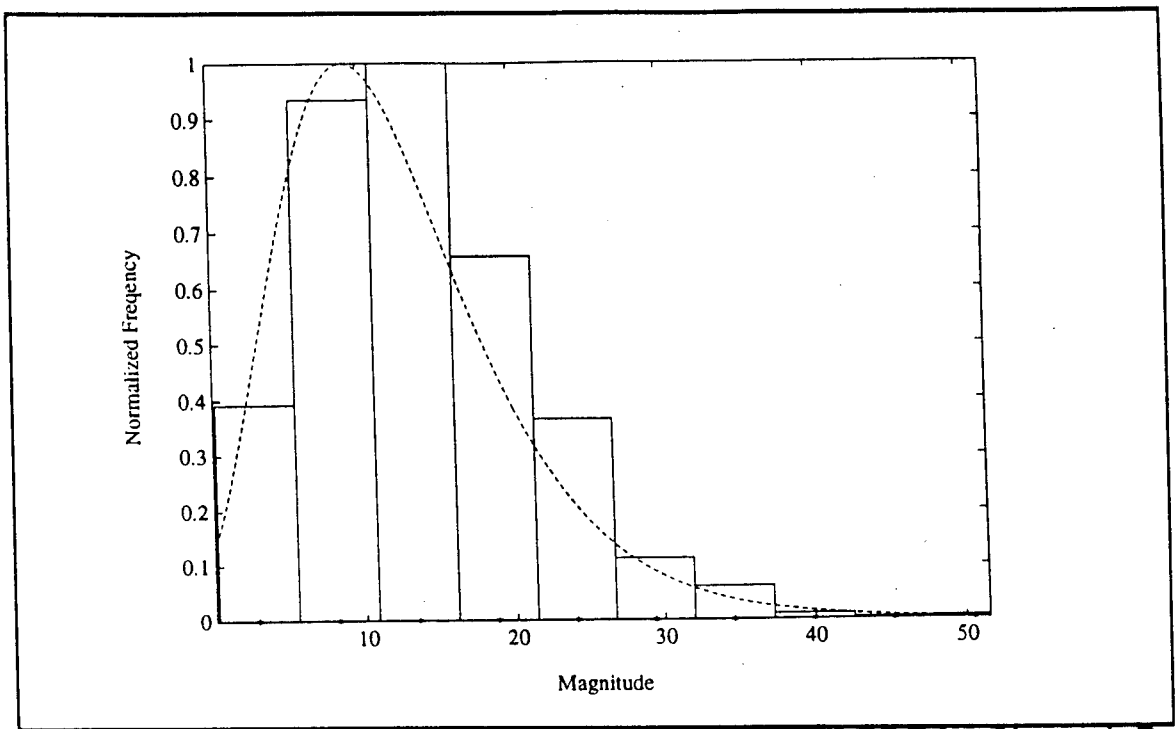


Figure VII.5.10 - Histogram and Best Approximating PDF for CL patch B

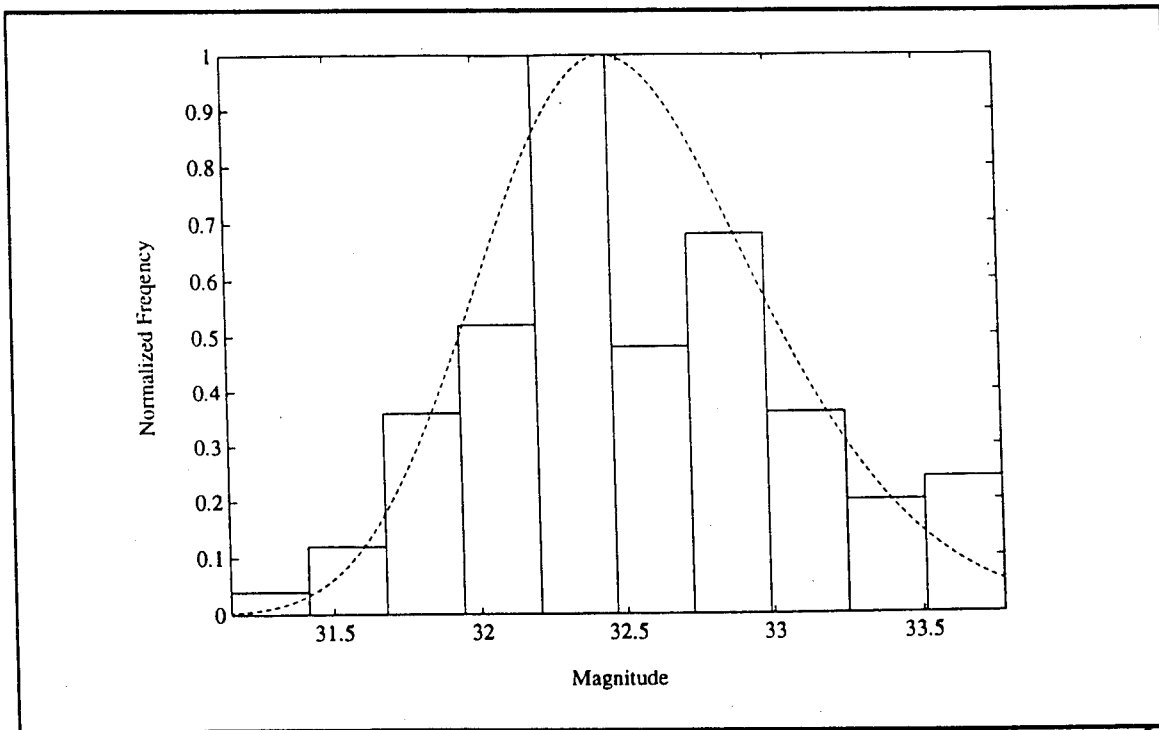


Figure VII.5.11 - Histogram and Best Approximating PDF for CL patch C

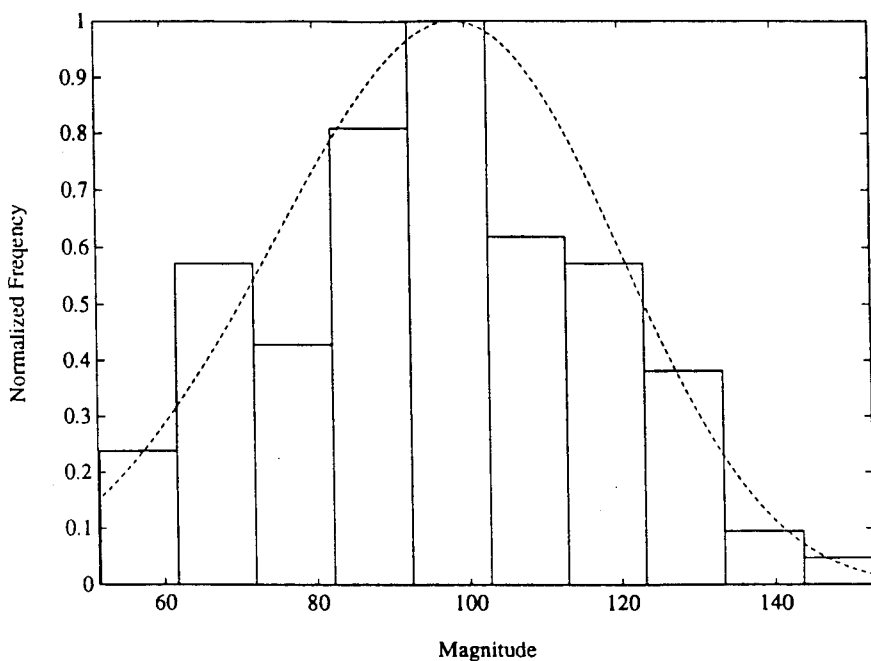


Figure VII.5.12 - Histogram and Best Approximating PDF for CL patch D

### VII.5.2 - Example 2

Consider now Tables VI.5.16-VI.5.18 which summarize the results of steps 1 through 5 of the PDF approximation strategy for the example of Section VI.5.2. Note that CL patches 1 and 3 can be approximated by any one of the three PDF kinds, whereas, as indicated in Table VI.5.17, CL patch 2 can be approximated only by the Lognormal PDF. Tables VII.5.7-VII.5.9 summarize the results for step 6 of the PDF approximation strategy for the three CL patches identified thus far. An exclusion table was generated for the allowable PDF kinds in each CL patch. As shown in Tables VII.5.8-VII.5.9, the Lognormal and K PDF kinds are labeled "Not all pass" for CL patches 2 and 3, respectively, indicating that the corresponding exclusion tables contained one or more X's and that the full length minor axis criterion has failed when applied to the average PDFs obtained by averaging over the parameters of all the test cells for the corresponding PDF kinds. Consequently, a N/A label is posted for each of the Lognormal and K PDF kinds in Tables

VII.5.8-VII.5.9, respectively. Average values for the parameters of all the allowable PDF kinds labeled with an "All pass" are also tabulated in Tables VII.5.7-VII.5.9.

Average PDF	Rank	Exclusion Table	Shape	Scale	Location
W	3	All pass	1.34	4.22	0.46
L	1	All pass	0.43	5.94	-2.20
K	1	All pass	8.11	2.06	-0.82

Table VII.5.7 - Average PDF(s) for CL Patch 1

Average PDF	Rank	Exclusion Table	Shape	Scale	Location
W			N/A		
L	1	Not all pass		N/A	
K			N/A		

Table VII.5.8 - Average PDF(s) for CL Patch 2

Average PDF	Rank	Exclusion Table	Shape	Scale	Location
W	2	All pass	1.03	2.49	0.90
L	3	All pass	0.61	3.15	-0.42
K	1	Not all pass		N/A	

Table VII.5.9 - Average PDF(s) for CL Patch 3

The exclusion table, corresponding to the Lognormal entries in Table VI.5.17 for CL patch 2, is shown in Table VII.5.10. The patterns of X's and ✓'s in the table clearly defines two different regions. One region consists of test cells numbered 1 and 77. The other region consists of the remaining test cells numbered 154, 231, and 308. This suggests the presence of at least two homoge-

neous subpatches in CL patch 2. In order to investigate whether more than two subpatches exist, three more test cells are considered which are located in between the two cited regions. The additional test cells are numbered 96, 115, and 134. Steps 1 through 5 of the PDF approximation strategy for these cells are summarized in Table VII.5.11. The new exclusion table, shown in Table VII.5.12 suggests that only two subpatches exist in the CL patch. The overlapping that exists between the two regions is due to the test cells located near the edges separating the two subpatches and whose reference cells extend to both regions. The conclusion that CL patch 2 consists of two subpatches is recognized by the IPUS program as a discrepancy.

Cell No.	1	77	154	231	308
1	✓	✓	✗	✗	✗
77	✓	✓	✗	✗	✗
154	✗	✗	✓	✓	✓
231	✗	✗	✓	✓	✓
308	✗	✗	✓	✓	✓

*Table VII.5.10- Exclusion Table for the Example of Table VI.5.17*

Test Cell No.	PDF	Rank	Distance	Shape	Scale	Location	(U,V)
96	W	2	$0.57 \times 10^{-2}$ ✓	0.91	1.56	1.29	(-0.0992, 0.3091)
	L	6	$0.21 \times 10^{-1}$ ✓	0.68	1.87	0.52	
	K	1	$0.41 \times 10^{-2}$ ✓	1.75	2.15	0.42	
115	W	3	$0.16 \times 10^{-1}$ ✓	1.00	1.83	1.25	(-0.1045, 0.3327)
	L	7	$0.40 \times 10^{-1}$ ✓	0.60	2.34	0.24	
	K	5	$0.27 \times 10^{-1}$ ✓	2.17	2.10	0.37	
134	W	2	$0.16 \times 10^{-2}$ ✓	1.04	1.97	1.28	(-0.0888, 0.3224)
	L	5	$0.23 \times 10^{-1}$ ✓	0.59	2.45	0.27	
	K	4	$0.10 \times 10^{-1}$ ✓	3.08	1.86	0.31	

*Table VII.5.11 - PDF approximation for Test Cells No. 96, 115, and 134 of the Example of Section VI.5.2, CL Patch 2*

Cell No.	1	77	96	115	134	154	231	308
1	✓	✓	✓	✓	✓	✗	✗	✗
77	✓	✓	✓	✓	✓	✗	✗	✗
96	✓	✓	✓	✓	✓	✓	✓	✓
115	✓	✓	✓	✓	✓	✓	✓	✓
134	✓	✓	✓	✓	✓	✓	✓	✓
154	✗	✗	✓	✓	✓	✓	✓	✓
231	✗	✗	✓	✓	✓	✓	✓	✓
308	✗	✗	✓	✓	✓	✓	✓	✓

*Table VII.5.12 - Exclusion Table for the Example of  
Tables VI.5.17 and VII.5.11*

Having detected the discrepancy, the diagnosis process in the IPUS control initiates a search for the subpatches. Specifically, (1) test cells numbered 1 and 77 have their reference cells numbered 1, while test cells numbered 154, 231, 308 have their reference cells numbered 2, (2) all reference cells numbered with 1 and 2 at the same time are declared as cells close to the boundary separating the CL subpatches. Their reference cells defines the boundary region where a test cell in one region has some of its reference cells extending to the other region. When this step is completed, the subpatches and the boundary region are defined as shown in Figure VII.5.13. Note that the CL patch now consists of three different regions. The lower portion of the CL patch includes part of generated CL patch C while the upper portion includes part of generated CL patch D. The in-between region contains cells from both CL patches C and D. The subpatches are relabeled 2 and 4, as shown in Figure VII.5.13. It is found that CL patch 2 contains 99 cells, CL patch 4 contains 183 cells, and the boundary region contains 26 cells. Also, based on the 99 cells of CL patch 2 and the 183 cells of CL patch 4, the CNRs for CL patches 2 and 4 are equal to 10.10 dB and 8.47 dB, respectively.

The PDF(s) of the CL subpatch regions are next approximated by considering the average PDF(s) for test cells 1 and 77 for CL patch 2 and 154, 231, and 308 for CL patch 4. In absence of additional information, the test cells located in the boundary region are approximated either by the PDF of CL patch 2 or the PDF of CL patch 4. Tables VII.5.13 and VII.5.14 summarize the results for step 6 of the PDF approximation for the subpatches numbered 2 and 4.

Average PDF	Rank	Exclusion Table	Shape	Scale	Location
W	N/A				
L	1	All pass	0.84	1.27	0.96
K	N/A				

Table VII.5.13 - Average PDF(s) for CL Patch 2 Using Test Cells Numbered 1 and 77

Average PDF	Rank	Exclusion Table	Shape	Scale	Location
W	1	All pass	1.80	3.54	0.47
L	3	All pass	0.27	7.24	-3.85
K	2	All pass	33.97	0.76	0.26

Table VII.5.14 - Average PDF(s) for CL Patch 4 Using Cells Numbered 154, 231, and 308

Table VII.5.15 uses the results presented in Tables VI.5.12, VII.5.7, VII.5.9, VII.5.13, and VII.5.14 to list the best average PDF for each CL patch. Note that both the L and K distributions are listed as the best approximating PDFs for CL patch A because their rankings were identical. Comparing the results in Tables VII.5.15 and VI.5.11 note that (1) regions for all four of the CL patches have been estimated, (2) the sample CNRs for CL patches B, C, and D, as evaluated according to Section VI.2.2, are within 1.5 dB of the generated values while that for CL patch A is within 2.03 dB, (3) the number of cells included in CL patches A, and B are close to the number of cells generated.

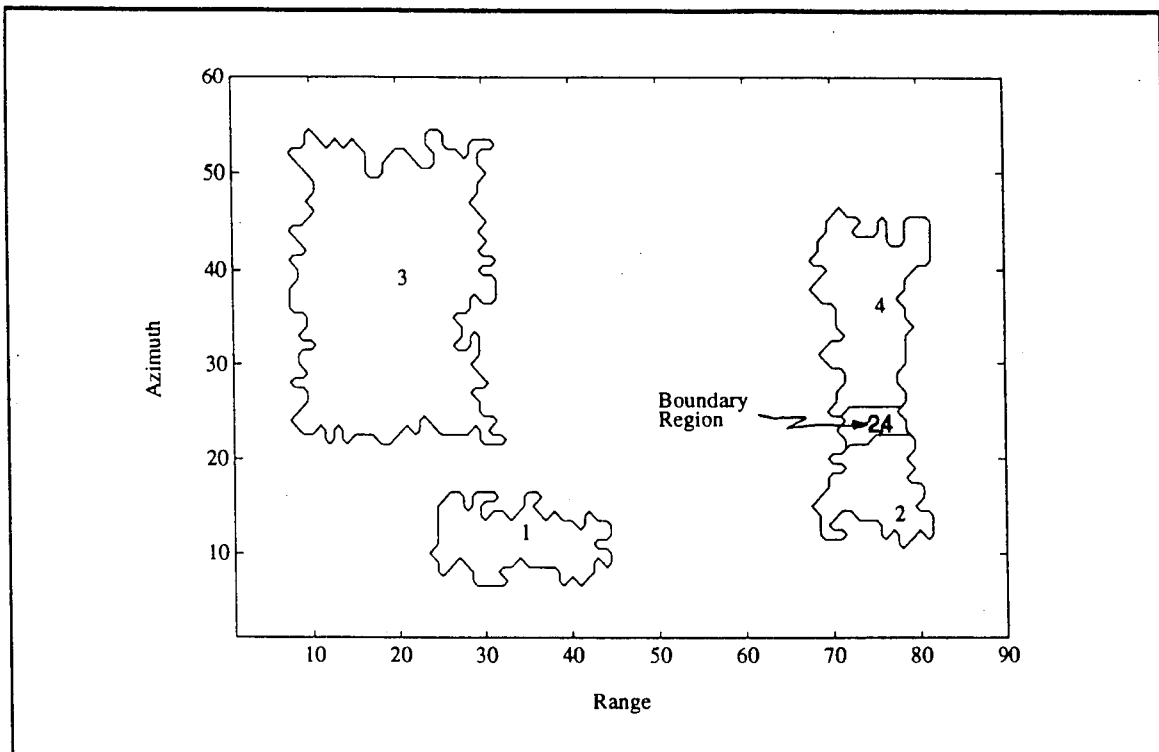


Figure VII.5.13 - Boundaries of the Scene Resulting from Step 6 of the PDF Approximation Stage

In fact, a separate evaluation indicates that 98.7%, and 92.5% of the generated cells have been correctly classified for CL patches A, and B, respectively. Also, 63.3%, and 99.1% of the generated cells have been correctly classified for CL patches C, and D, respectively.

Clutter Patch (No.)	CNR (dB)	Number of cells	PDF (best)	Shape parameter	Scale parameter	Location parameter
A (1)	12.03	133	L K	0.43 8.11	5.94 2.06	-2.20 -0.82
B (3)	8.65	622	W	1.03	2.49	0.90
C (2)	10.10	99	L	0.84	1.27	0.96
D (4)	8.47	183	W	1.80	3.54	0.47

Table VII.5.15 - Assessment Parameters of the Mapping and Indexing Stages

With regard to the goodness of the PDF approximations, Figures VII.5.14, VII.5.16, VII.5.18, and VII.5.20 show the location in the approximation chart, indicated by o, for the accurate approximation of the underlying CL patch PDF (i.e., PDF corresponding to the sum of CL and BN in the patch). These were obtained by generating 1000 points for each CL patch. The results are summarized in Table VII.5.16. Figures VII.5.15, VII.5.17, VII.5.19, and VII.5.21 show the PDFs from Table VII.5.15 (solid lines) obtained by the mapping and indexing stages, superimposed on the corresponding PDFs from Table VII.5.16 (dashed lines).

The comparison for CL patch A is given in Figure VII.5.15. Although the best approximating PDF is Lognormal while the underlying PDF is Weibull, the curves are reasonably close except for a difference in their heights. Figure VII.5.17 shows the comparison for CL patch B. In contrast to CL patch A, the best approximating PDF is Weibull while the underlying PDF is Lognormal. Note that the curves are reasonably close. However a small offset in location is used to compensate for a slight mismatch in shape. The results for CL patch C are shown in Figure VII.5.19. The best approximating PDF is Lognormal while the underlying PDF is SU-Johnson. In this case, the two curves differ substantially and a poor approximation has been made. Had the SU-Johnson been included in the library of allowable PDF kinds, a better approximating PDF would have been obtained. Finally, the comparison for CL patch D is shown in Figure VII.5.21. Here the best approximating and underlying PDFs are both Weibull with scale parameters 3.54 and 3.43, respectively. However, the shape and location parameters are not close. This accounts for the discrepancy between the two curves.

The best approximating PDFs from Table VII.5.15 are superimposed on the histograms for CL patches A, B, C, and D in Figures VII.5.22-VII.5.25, respectively. Whether or not the best approximating PDFs are close to the underlying PDFs, note that the best approximating PDFs nicely overlay the corresponding histograms. Relative to CL patch D, it is seen that the large amount of data with values below 2.5 are not representative of the underlying PDF shown in Figure

VII.5.21. This may be due to inclusion in CL patch D of cells originating in CL patch C, as seen in Figure VII.5.13.

CL Patch	PDF	Distance	Shape	Scale	Location	(U,V)
A	W	$0.73 \times 10^{-2}$	1.31	3.98	1.12	(-0.0733, 0.3364)
B	L	$0.30 \times 10^{-1}$	0.49	3.67	-1.13	(-0.0840, 0.3297)
C	SU-Johnson	$0.11 \times 10^{-3}$	(1.31, -0.7)	0.69	2.94	(-0.0555, 0.2590)
D	W	$0.33 \times 10^{-2}$	2.24	3.43	2.48	(-0.0278, 0.3345)

Table VII.5.16 - Accurate Approximation of Underlying CL patch PDFs

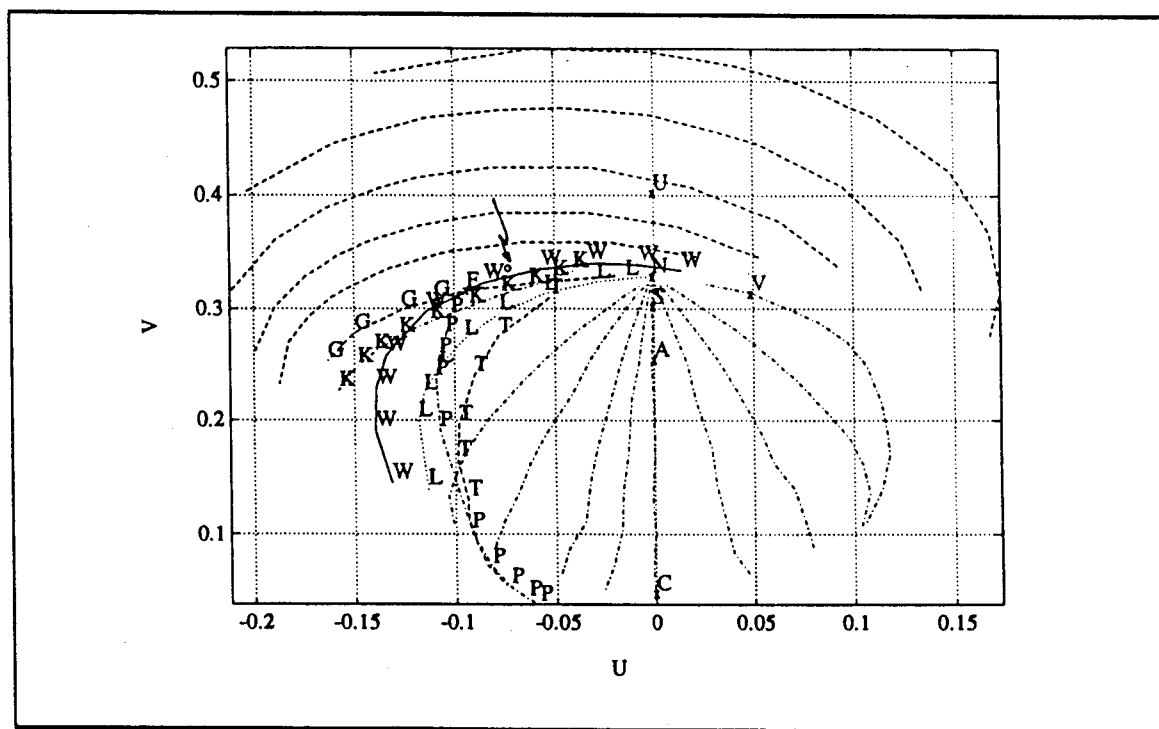


Figure VII.5.14 - Location of the Locus End Point for CL Patch A

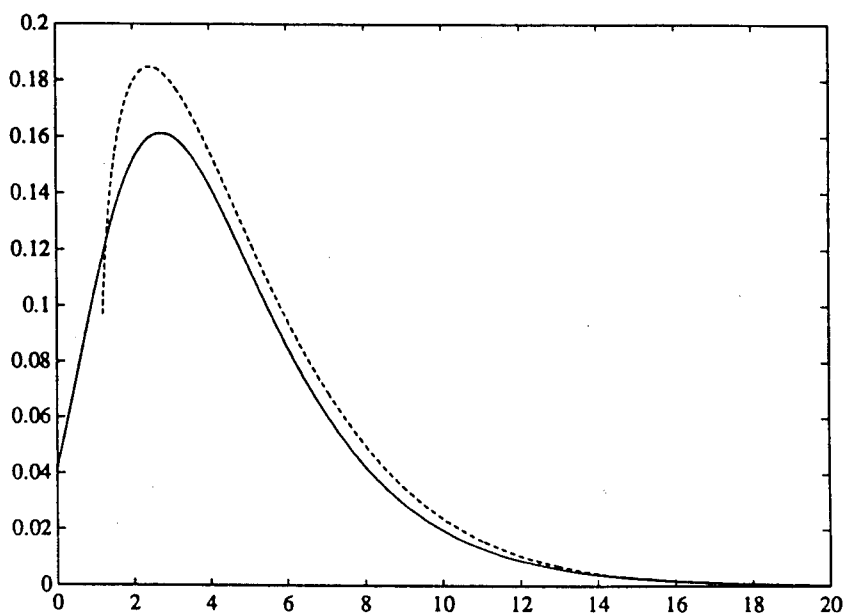


Figure VII.5.15 - PDF Comparison for CL patch A

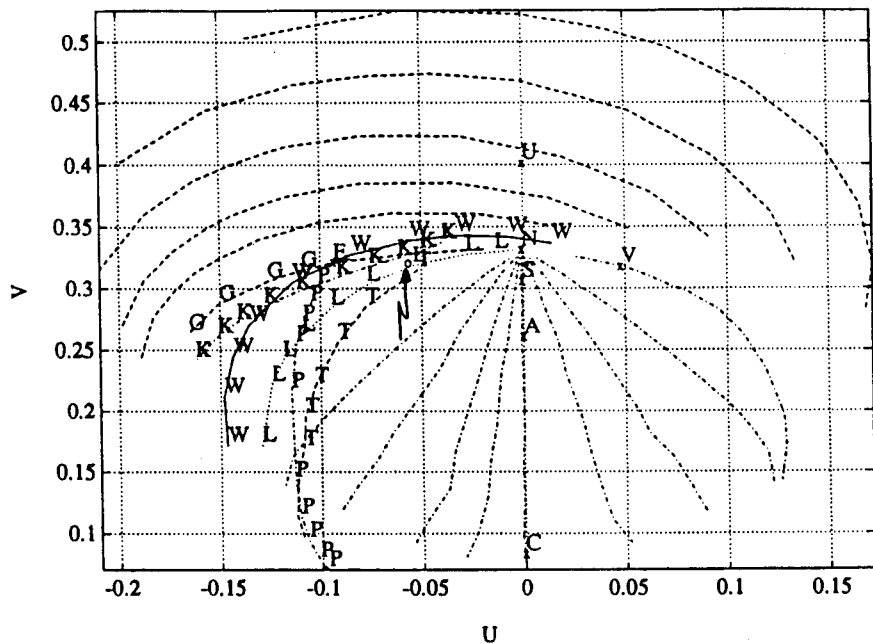


Figure VII.5.16 - Location of the Locus End Point for CL Patch B

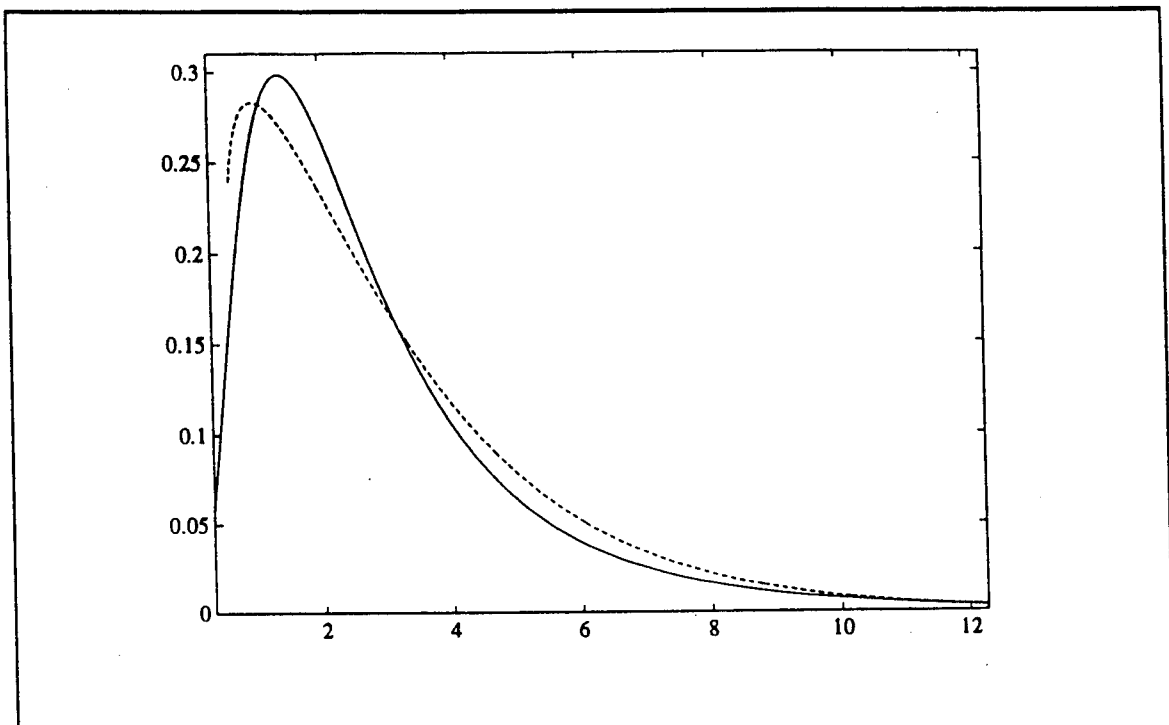


Figure VII.5.17 - PDF Comparison for CL patch B

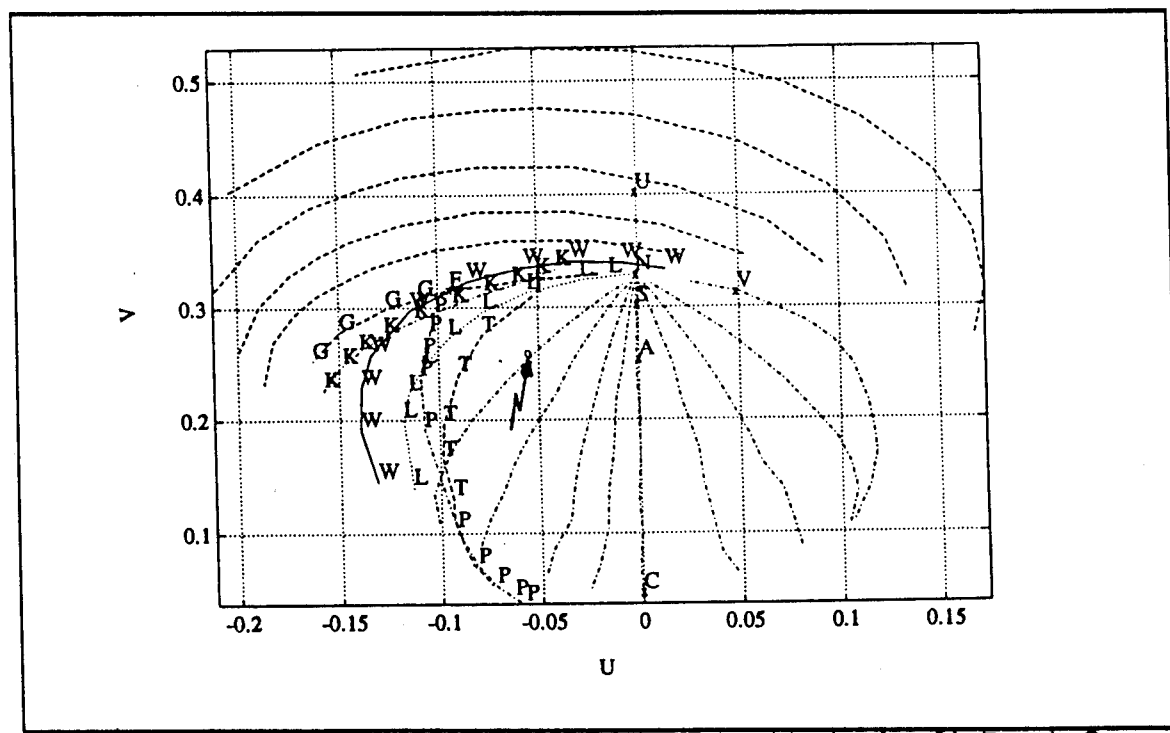


Figure VII.5.18 - Location of the Locus End Point for CL Patch C

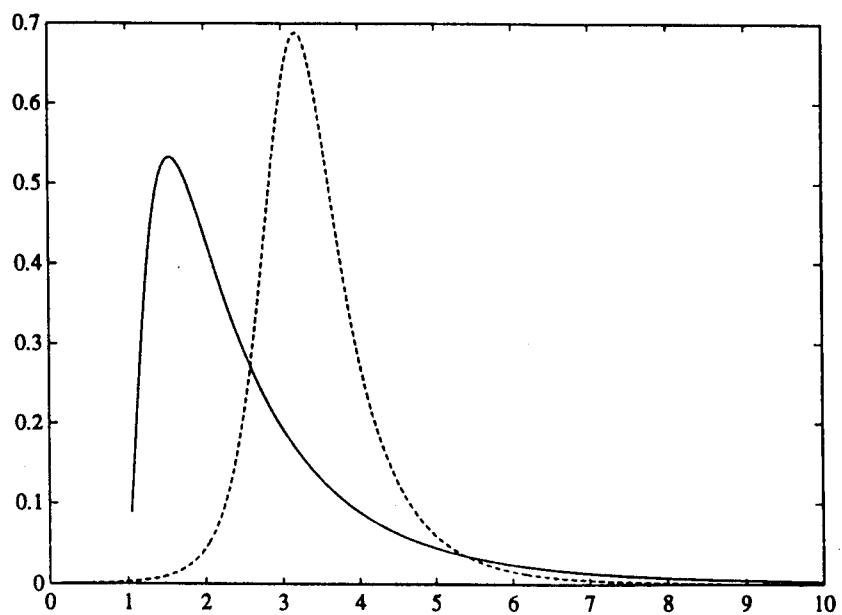


Figure VII.5.19 - PDF Comparison for CL patch C

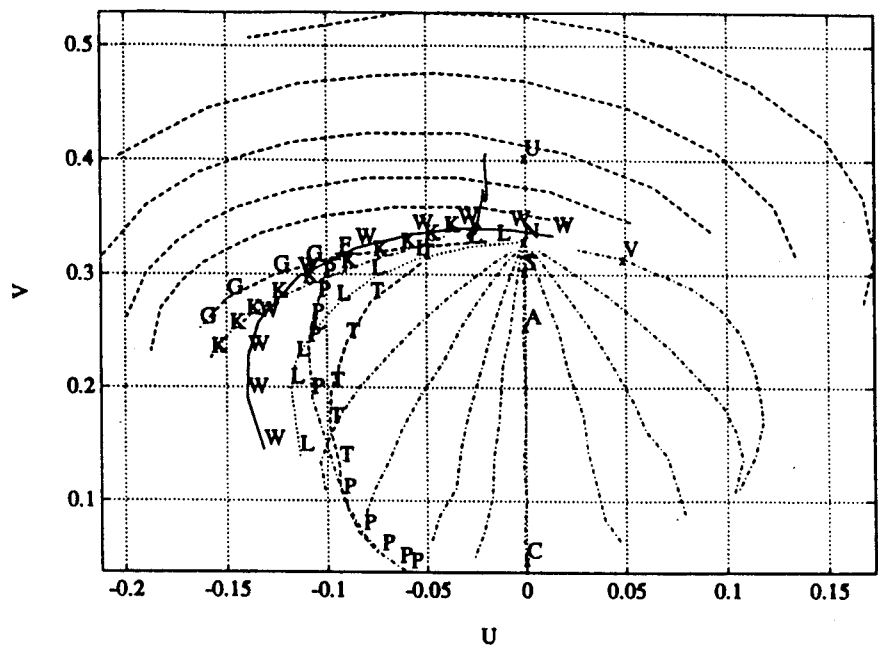


Figure VII.5.20 - Location of the Locus End Point for CL Patch D

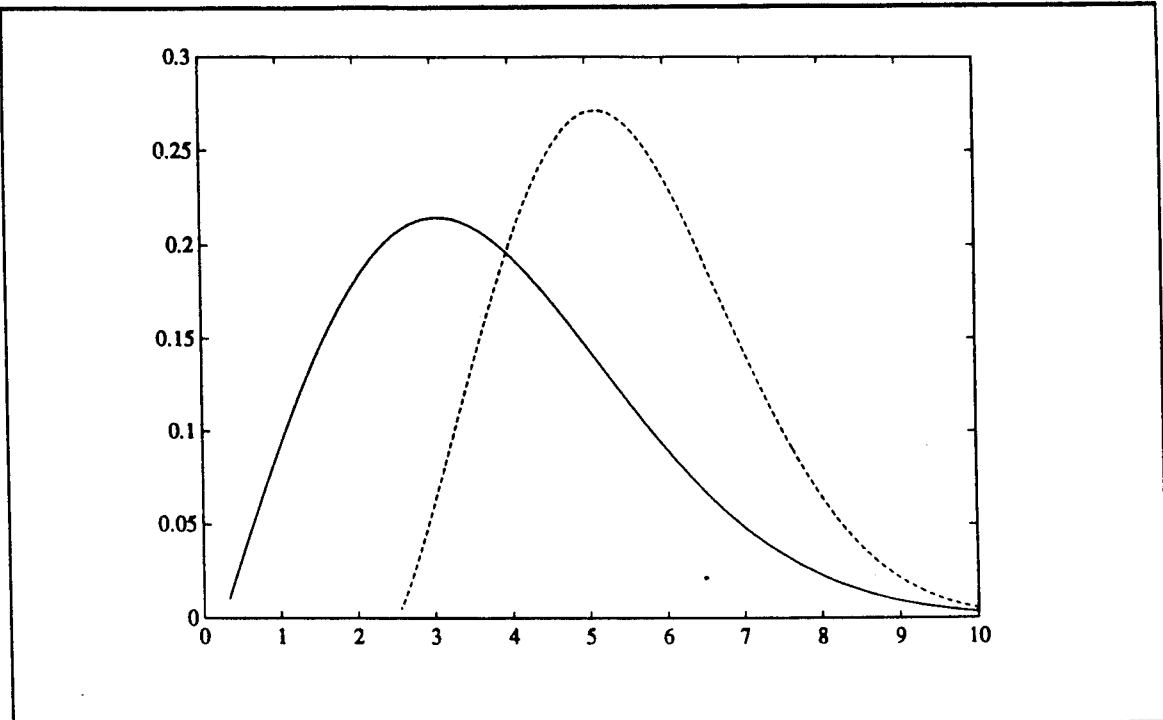


Figure VII.5.21 - PDF Comparison for CL patch D

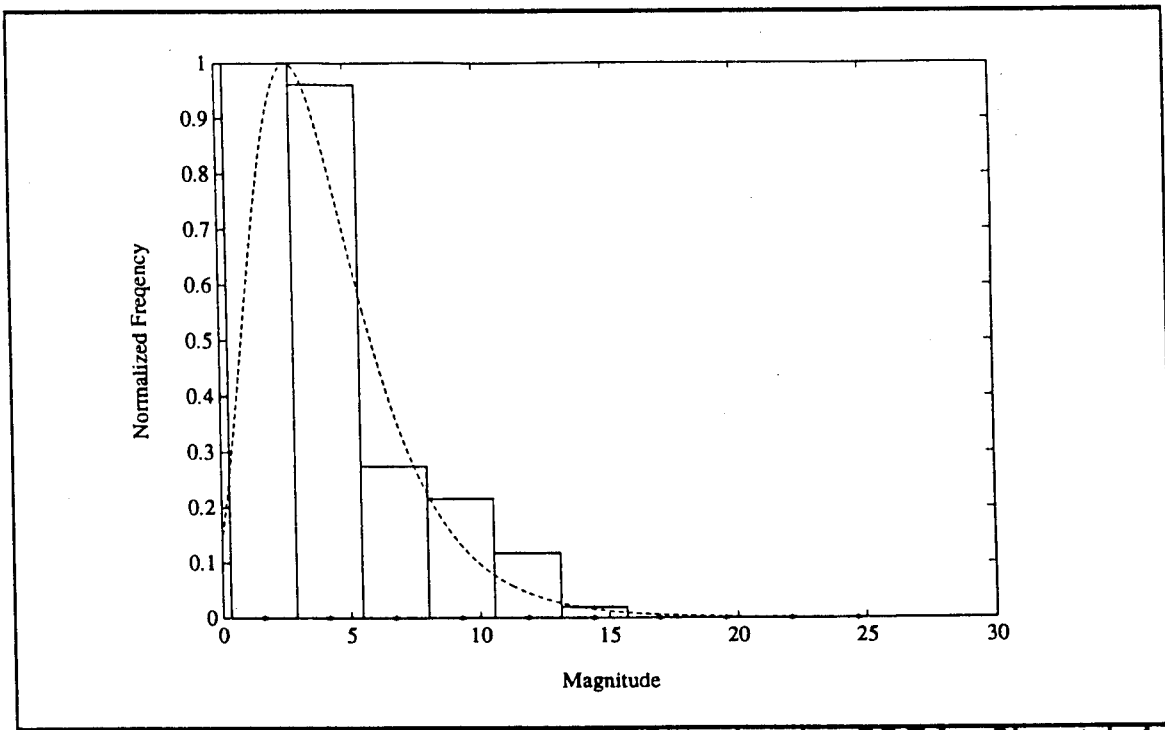


Figure VII.5.22 - Histogram and Best Approximating PDF for CL patch A

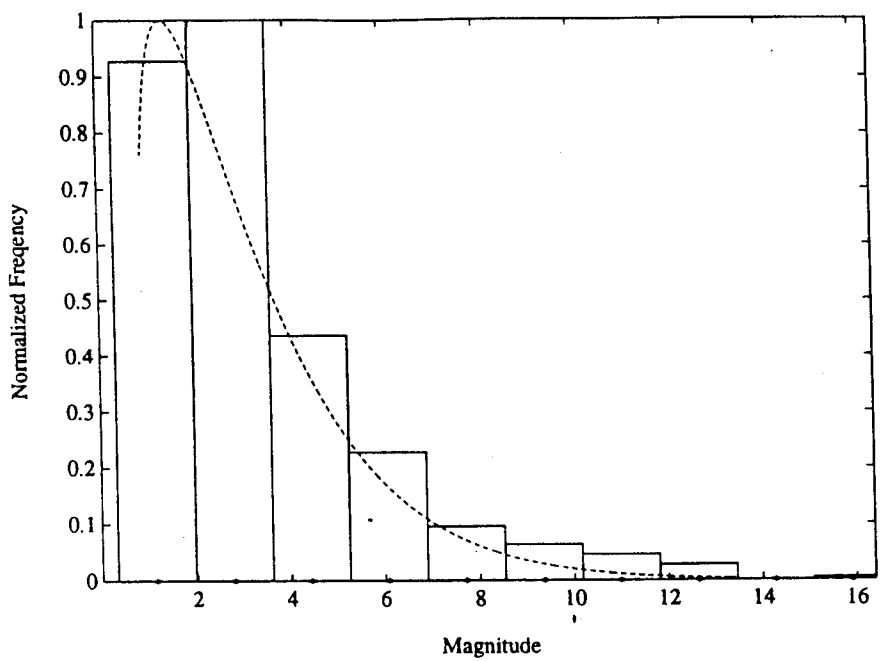


Figure VII.5.23 - Histogram and Best Approximating PDF for CL patch B

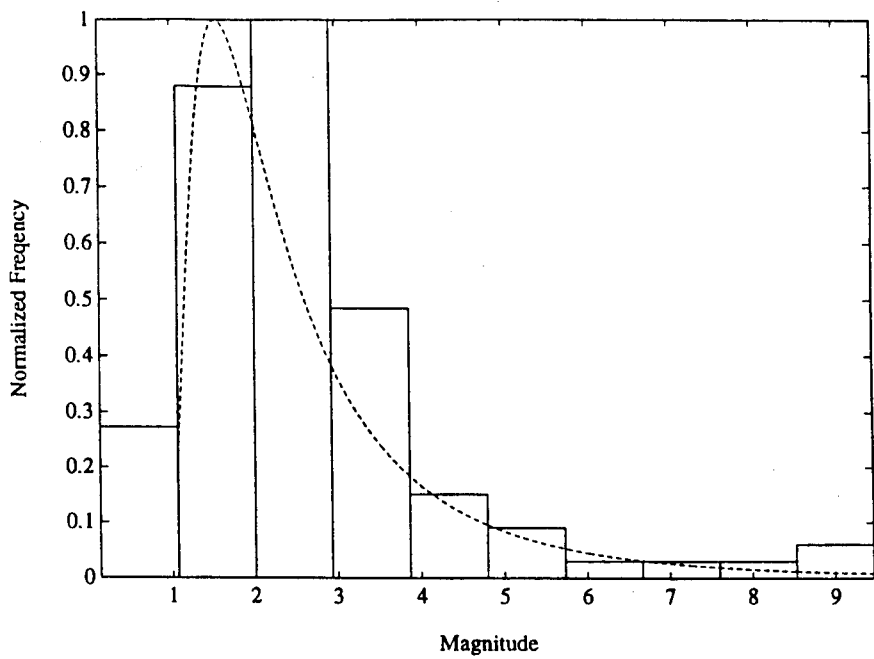


Figure VII.5.24 - Histogram and Best Approximating PDF for CL patch C

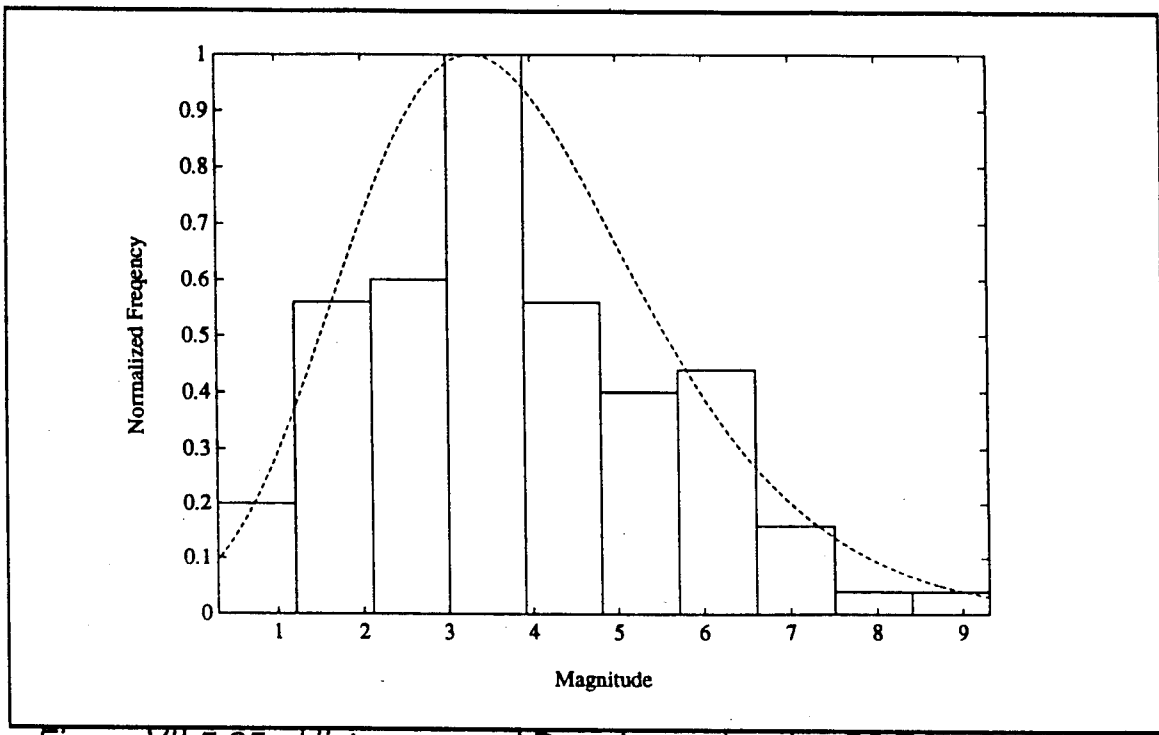


Figure VII.5.25 - Histogram and Best Approximating PDF for CL patch D

### **VII.5.3 - Example 3**

Finally, consider Tables VI.5.24-VI.5.26 which summarize the results of steps 1 through 5 of the PDF approximation strategy for the example of Section VI.5.3. Note that CL patch 2 can be approximated by any one of the three PDF kinds, whereas, as indicated in Tables VI.5.24 and VI.5.26, CL patches 1 and 3 can be approximated only by the Weibull and K PDFs. Tables VII.5.17-VII.5.19 summarize the results for step 6 of the PDF approximation strategy for the three CL patches identified thus far. An exclusion table was generated for the allowable PDF kinds in each CL patch. As shown in Tables VII.5.17-VII.5.19, all of the PDF kinds are labeled "All pass" indicating that none of the exclusion tables contained an **X** mark. Consequently, average values for the parameters of all the allowable PDF kinds are also tabulated in Tables VII.5.17-VII.5.19.

Table VII.5.20 uses the results presented in Tables VI.5.20 and VII.5.17-VII.5.19 to list the best average PDF for each CL patch. Comparing the results in

Tables VII.5.20 and VI.5.19 note that (1) regions for CL patches A and B have been estimated, whereas the regions for the contiguous CL patches C and D have been approximated as a single region, (2) the sample CNRs for CL patch A, as evaluated according to Section VI.2.2, is within 1 dB of the generated values while that for CL patch B is within 3.47 dB, (3) the number of cells included in CL patches A and B are close to the number of cells generated. In fact, a separate evaluation indicates that 97.8% and 98.3% of the generated cells have been correctly classified for CL patches A and B, respectively.

For this particular example, the PDF approximation strategy is not able to recognize that more than one subpatch exists in CL patch 2. In order to evaluate the severity of this result, we analyze the PDFs of CL patches C and D. As shown in Figures V.4.26.(d) and (e), even though the data amplitude histograms of CL patches C and D are different (CL patch C data amplitudes extend only from 3.1 to 3.25 whereas CL patch D data amplitudes extend from 2 to 3.75), they have the same maximum located around 3.15. When BN is added to both CL patches C and D, their histograms become as shown in Figures VII.5.26.(a) and (b), respectively. When BN data is added, the data amplitudes of both CL patches C and D extend over longer intervals ranging from 3.1 to 5.4. Note, also, that the shapes of both histograms are very similar. Thus, when BN data is added both CL patches C and D can be approximated by the same PDF. It is, therefore, concluded for this example that it is reasonable to approximate both CL patches C and D as a single CL patch (numbered 2).

Average PDF	Rank	Exclusion Table	Shape	Scale	Location
W	1	All pass	2.16	3.86	-0.07
L	N/A				
K	2	All pass	50.0	0.49	0.43

Table VII.5.17 - Average PDF(s) for CL Patch 1

Average PDF	Rank	Exclusion Table	Shape	Scale	Location
W	2	All pass	2.32	1.15	3.02
L	1	All pass	0.17	2.72	1.29
K	3	All pass	48.76	0.14	3.17

*Table VII.5.18 - Average PDF(s) for CL Patch 2*

Average PDF	Rank	Exclusion Table	Shape	Scale	Location
W	2	All pass	1.74	4.53	0.84
L	N/A				
K	1	All pass	31.16	1.03	0.39

*Table VII.5.19 - Average PDF(s) for CL Patch 3*

Clutter Patch (No.)	CNR (dB)	Number of cells	PDF (best)	Shape parameter	Scale parameter	Location parameter
A (1)	9.34	124	W	2.16	3.86	-0.07
B (3)	13.47	306	K	31.16	1.03	0.39
C + D (2)	10.63	341	L	0.17	2.72	1.29

*Table VII.5.20 - Assessment Parameters of the Mapping and Indexing Stages*

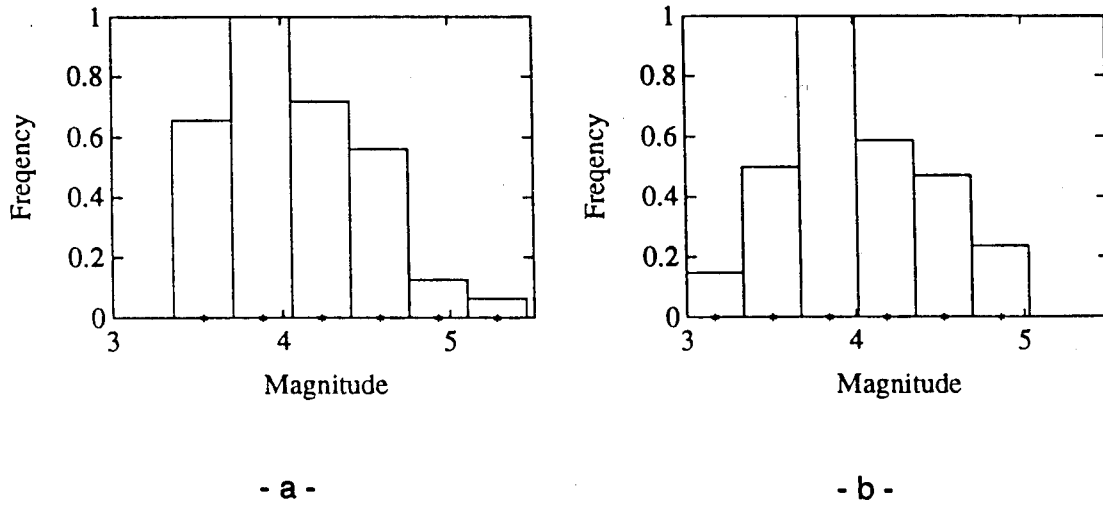


Figure VII.5.26 - Data Amplitude Histograms Including Additive BN Data for (a) CL Patch C and (b) CL Patch D

With regard to the goodness of the PDF approximations, Figures VII.5.27, VII.5.29, VII.5.31, and VII.5.33 show the location in the approximation chart, indicated by o, for the accurate approximation of the underlying CL patch PDF (i.e., PDF corresponding to the sum of CL and BN in the patch). These were obtained by generating 1000 points for each CL patch. The results are summarized in Table VII.5.21. Figures VII.5.28, VII.5.30, VII.5.32, and VII.5.34 show the PDFs from Table VII.5.20 (solid lines) obtained by the mapping and indexing stages, superimposed on the corresponding PDFs from Table VII.5.21 (dashed lines).

The comparison for CL patch A is given in Figure VII.5.28. Here the best approximating and underlying PDFs are both Weibull with shape parameters 2.16 and 2.24 and scale parameters 3.86 and 3.43, respectively. However, location parameters are not as closely matched. This accounts for the discrepancy between the two curves. Figure VII.5.30 shows the comparison for CL patch B. Although

the best approximating PDF is K while the underlying PDF is Weibull, the curves are reasonably close. The results for CL patch C, defined as part of CL patch 2, are shown in Figure VII.5.32. The best approximating PDF is Lognormal while the underlying PDF is Weibull. In this case, the two curves are reasonably close except for a small offset in their location and height. Finally, the comparison for CL patch D, defined as part of CL patch 2, is shown in Figure VII.5.34. The best approximating PDF is Lognomal while the underlying PDF is SU-Johnson. the two curves differ substantially and a poor approximation has been made. As was the case in Example 2, had the SU-Johnson been included in the library of allowable PDF kinds, a better approximating PDF would have been obtained.

The best approximating PDFs from Table VII.5.20 are superimposed on the histograms for CL patches A, B, C, and D in Figures VII.5.35-VII.5.38, respectively. Whether or not the best approximating PDFs are close to the underlying PDFs, note that the best approximating PDFs nicely overlay the corresponding histograms.

CL Patch	PDF	Distance	Shape	Scale	Location	(U,V)
A	W	$0.33 \times 10^{-2}$	2.24	3.43	2.48	(-0.0278, 0.3345)
B	W	$0.80 \times 10^{-2}$	2.0	5.11	0.53	(-0.0353, 0.3485)
C	W	$0.19 \times 10^{-2}$	2.18	1.02	2.93	(-0.0292, 0.3384)
D	SU-Johnson	$0.17 \times 10^{-2}$	(2.97, -0.0094)	1.53	5.74	(-0.0098, 0.3156)

Table VII.5.21 - Accurate Approximation of Underlying CL patch PDFs

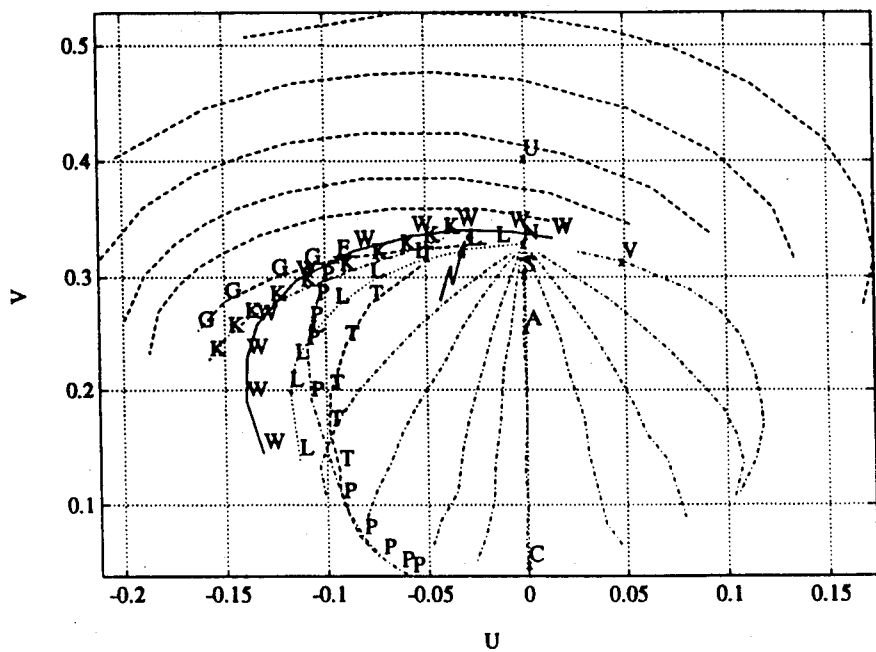


Figure VII.5.27 - Location of the Locus End Point for CL Patch A

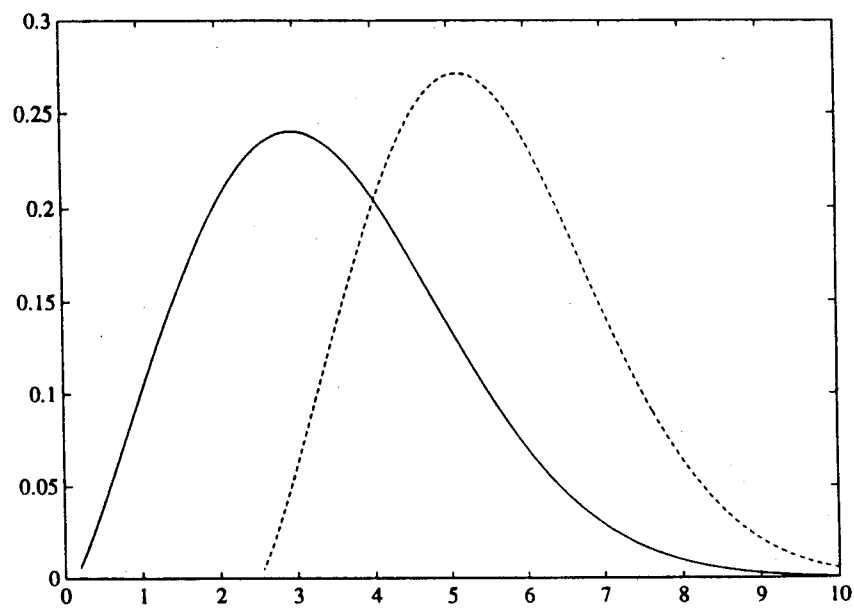


Figure VII.5.28 - PDF Comparison for CL patch A

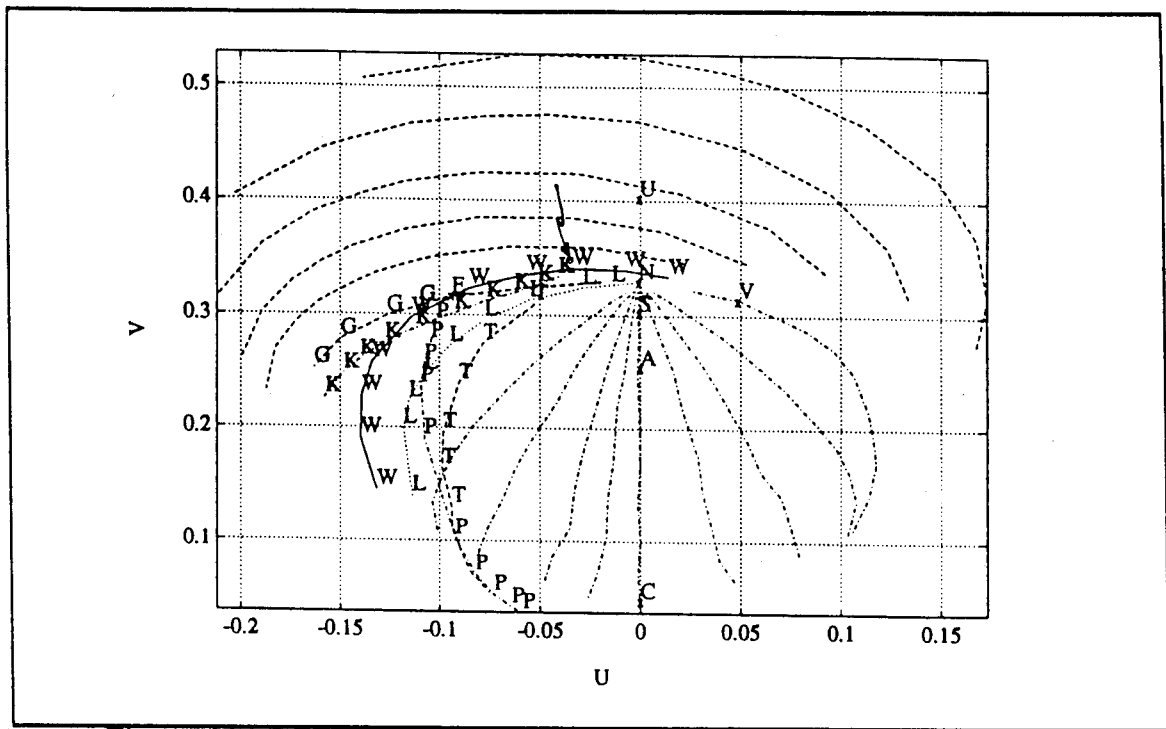


Figure VII.5.29 - Location of the Locus End Point for CL Patch B

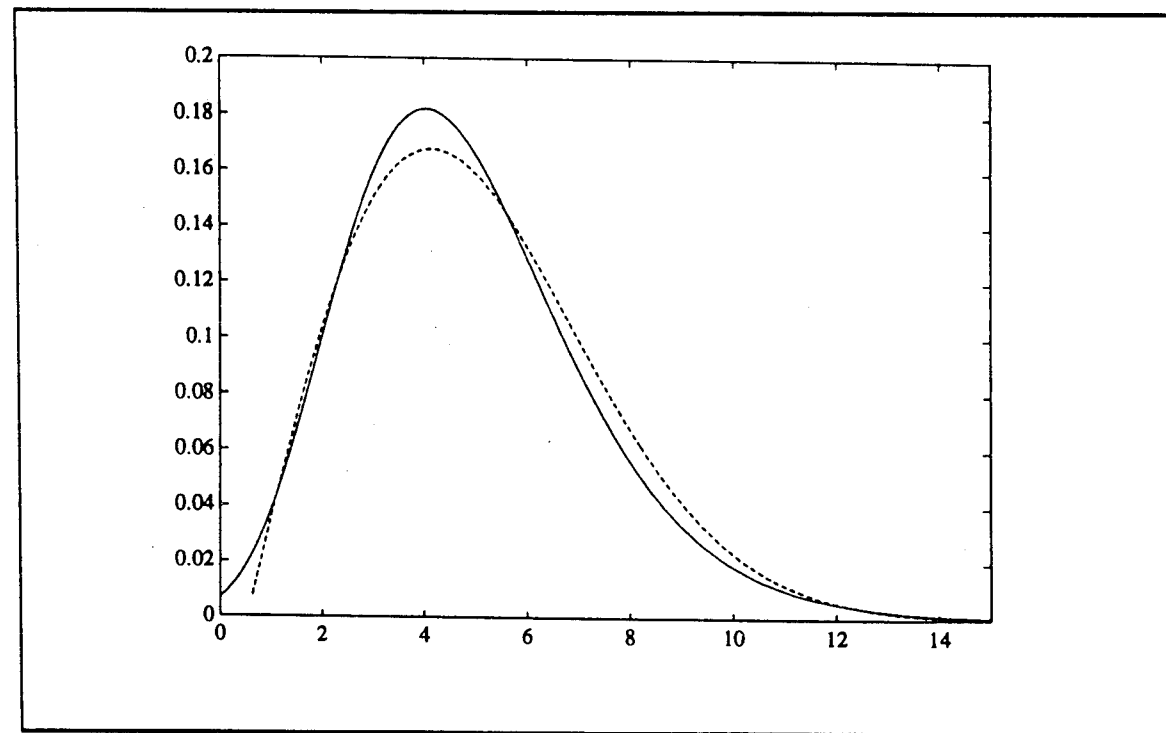


Figure VII.5.30 - PDF Comparison for CL patch B

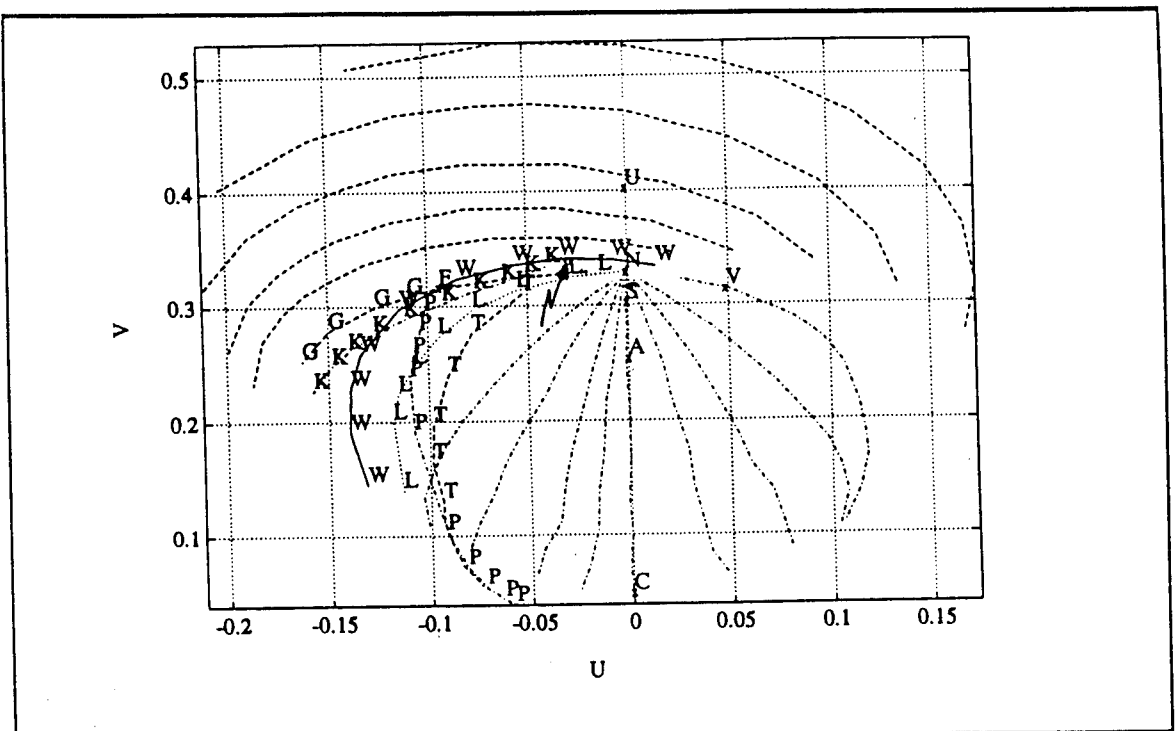


Figure VII.5.31 - Location of the Locus End Point for CL Patch C

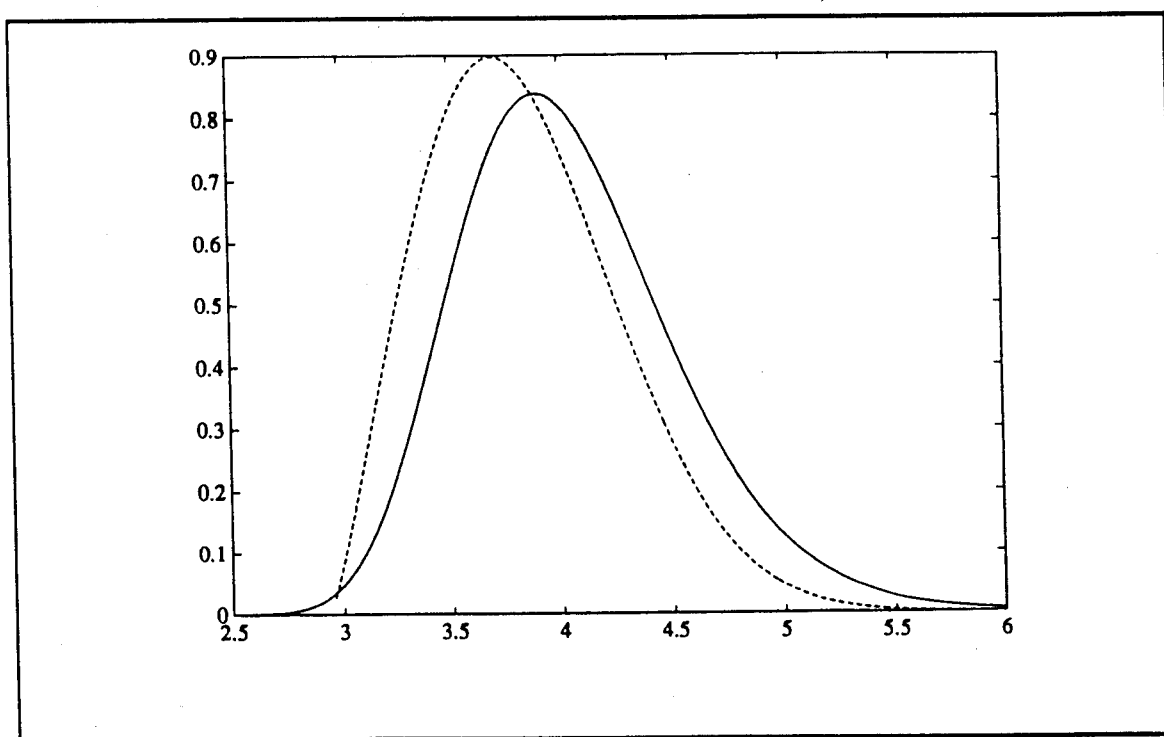


Figure VII.5.32 - PDF Comparison for CL patch C

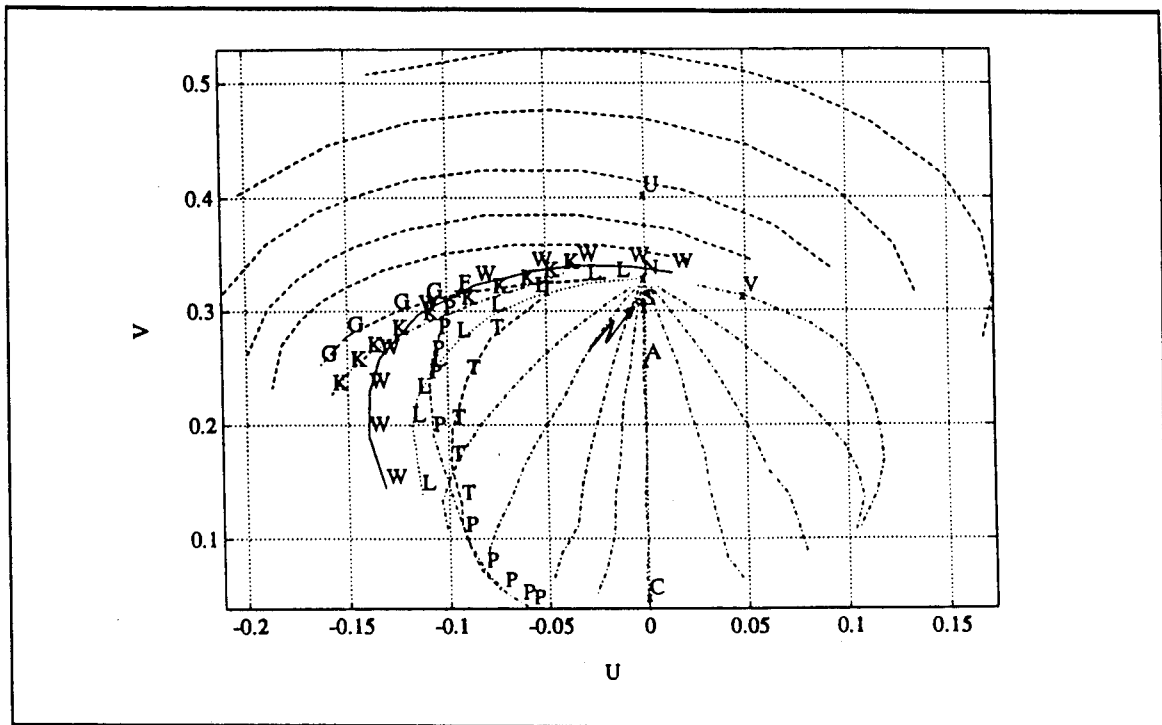


Figure VII.5.33 - Location of the Locus End Point for CL Patch D

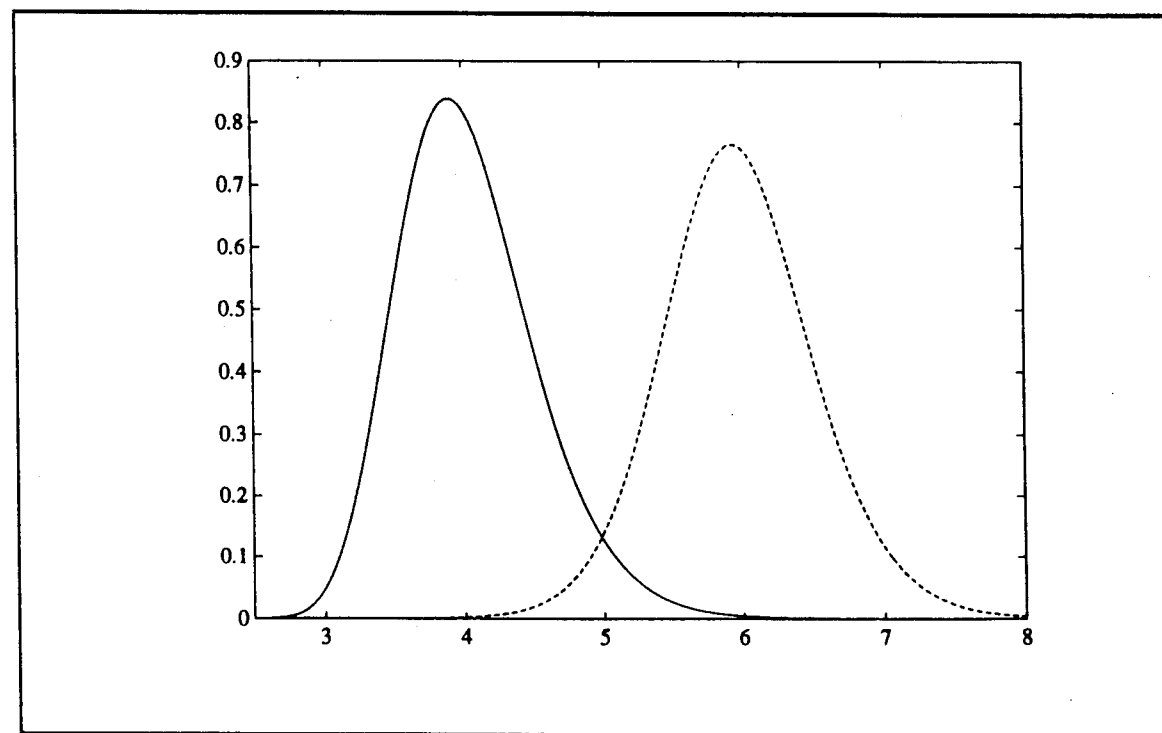


Figure VII.5.34 - PDF Comparison for CL patch D

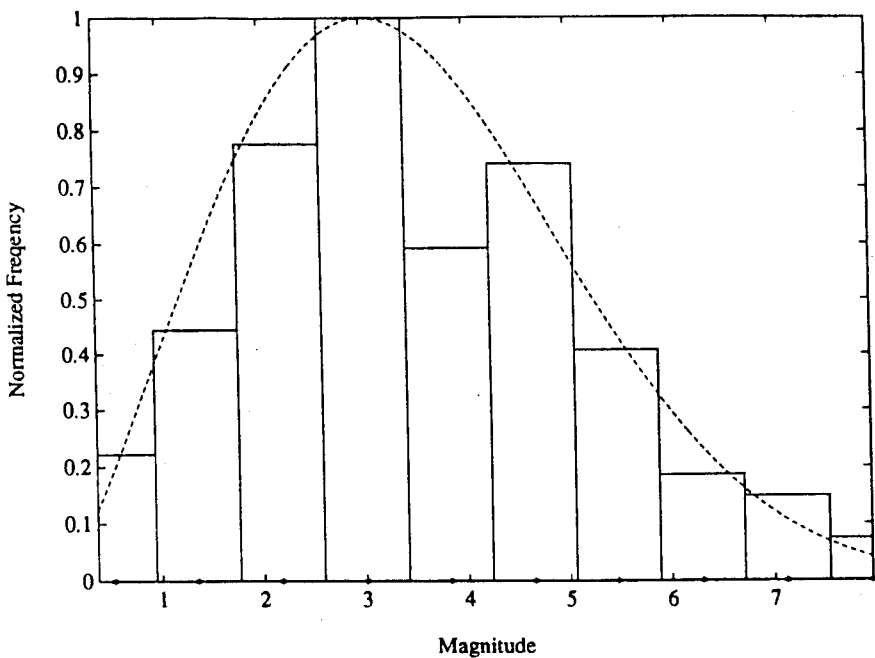


Figure VII.5.35 - Histogram and Best Approximating PDF for CL patch A

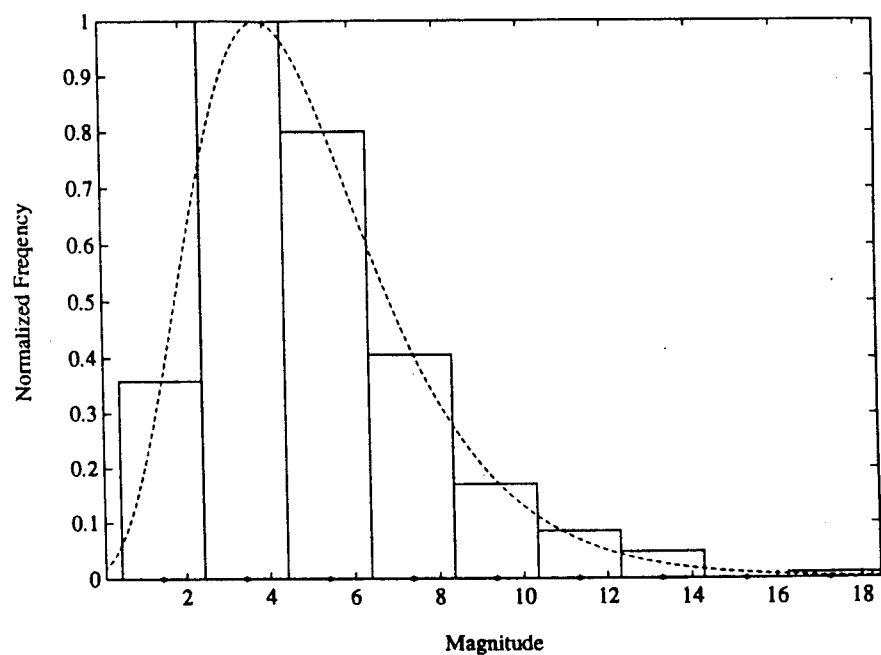


Figure VII.5.36 - Histogram and Best Approximating PDF for CL patch B

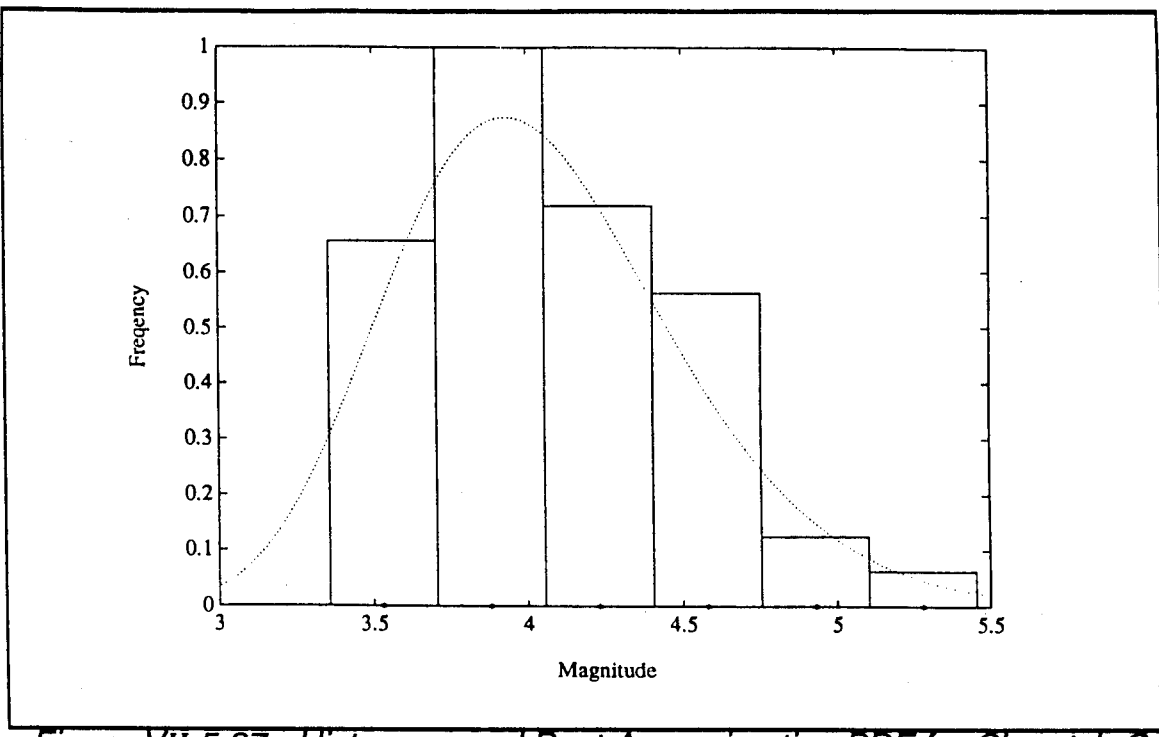


Figure VII.5.37 - Histogram and Best Approximating PDF for CL patch C

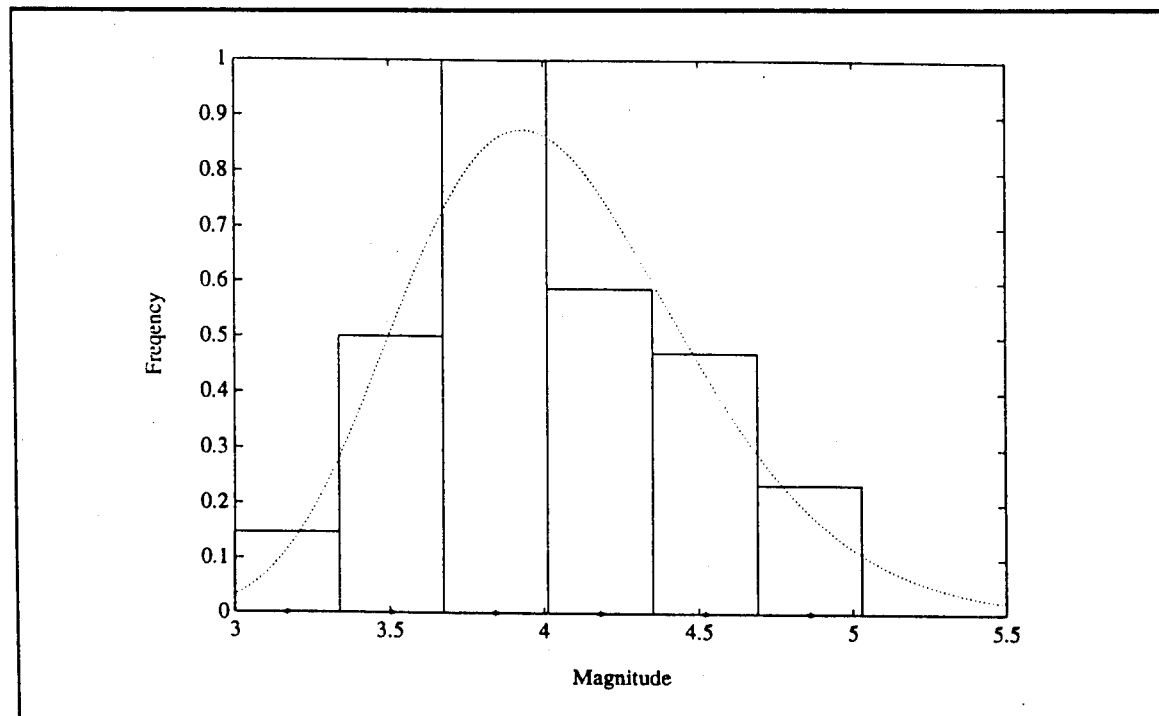


Figure VII.5.38 - Histogram and Best Approximating PDF for CL patch D

## **VII.6 - Conclusion**

In this chapter, expert system rules were developed to control the decisions needed for operation of the mapping and indexing stages. Discrepancies were determined which enable identification of the sources of distortions which in turn enables reprocessing.

Using the results developed in this chapter the three examples begun in Section V.4 were completed. For Example 1, in which the CNRs for CL patches A, B, C, and D were 10, 20, 30, and 40dB, respectively, it was possible to identify and approximate all four clutter regions. This was possible because of the significant difference in amplitudes between the CL patches and the BN. Example 2 had added complexity because the CNRs of the contiguous CL patches C and D were identical. Even so, the indexing procedure was able to recognize that CL patch 2 consisted of two CL subpatches. In addition, the poor PDF approximation that can result with a limited library of PDFs was demonstrated. Finally, Example 3 investigated the situation where, even though the underlying PDFs of CL patches C and D were noticeably different, the addition of BN resulted in similar histograms. As a result, CL patches C and D were modeled as a single homogeneous CL patch. This example illustrates one of the pitfalls that can arise with small amounts of random data.

## Chapter VIII

### Conclusion

#### **VIII.1 - Conclusion**

Current radars are typically designed on the assumption that the clutter and background noise are both Gaussian random processes. Such receivers are matched filters which maximize signal-to-noise ratio by filtering to the extent possible the desired target returns from the disturbance. When it is not possible to separate the clutter from the target by means of spatial and/or temporal filtering, the optimal Gaussian receiver performs poorly.

However, it is known that an optimal non-Gaussian receiver in a non-Gaussian environment can perform significantly better than the Gaussian receiver in situations where the disturbance and target spectra completely overlap. The major problem is that there are an infinity of different non-Gaussian probability distributions and, in a practical situation, the environment is unknown.

This dissertation demonstrates, in conjunction with an expert system, that it is possible to partition a surveillance volume into clutter and background noise regions and to approximate the underlying probability distribution of each region. This is highly significant because real data is likely to be nonhomogeneous and nonstationary. It is for this reason that optimal processors may not work well on real data. The results obtained in this research provide an innovative approach to analyzing and characterizing real data. Several computer generated examples are used to demonstrate the proposed methods.

#### **VIII.2 - Future Research**

In this dissertation it was shown that the mapping and indexing stages

have potential for being able to successfully monitor a random environment. The following problems were suggested by this research and remain to be addressed in the future:

- Measures should be developed to enable a qualitative performance analysis of the proposed mapping and indexing procedures and the rules to be used by IPUS.
- Criteria to guarantee convergence of the iteration process in the mapping procedure should be developed.
- The IPUS control should be able not only to control individually the mapping and indexing stages but also to interact backward between these stages. Recall from Section VI.4.4 that outliers may exist in a set of reference cells that may arise due to (1) misclassified BN cells in a CL patch or misclassified CL cells in the BN, (2) cells having data values of low probability of occurrence, and (3) cells containing signals from strong targets. Feedback between the indexing and mapping stages should be introduced to account and correct for outliers.
- A strategy should be developed to enable handling of the next set of data from the same environment to update the information of the mapping and indexing stages without processing all the data but rather by doing a series of checks.
- A detection strategy and expert system rules need to be developed for the target detection stage presented in Chapter II.
- Following the detection stage, a target tracking strategy needs also to be developed. Note, for example, that when a target is present in a given cell, its presence in subsequent cells should be consistent with a reasonable track.
- Environmental models based on collected real data and physical considerations should be verified using the Ozturk algorithm in order to gain confidence in these models.

- The Ozturk algorithm currently analyzes univariate random data. It is proposed to extend the Ozturk algorithm to the multivariate random data case.
- The trade off in computational complexity for generating an average approximating PDF for each CL patch or subpatch versus using the Ozturk algorithm once for all cells in a region should be investigated.
- The effectiveness of using various image processing procedures found in the literature [24] and [25] for the mapping and indexing procedures should be investigated.

## References

- [1] Harry L. Van Trees, Detection, Estimation, and Modulation Theory. Part I, John Wiley & Sons. New York, 1968.
- [2] M. Rangaswamy, D. Weiner, A. Ozturk, "Spherically Invariant Random Processes for Modeling and Distribution Identification of Non-Gaussian Random Vectors." IEEE Trans. on AES, vol 3, July 1992.
- [3] P. Chakravathi, "Subclutter Visibility: The Problem of Weak Signal Detection." Ph.D. Dissertation, Syracuse University, 1993.
- [4] M. Sekine, T. Musha, et al., "On Weibull Distributed Weather Clutter." IEEE Trans. on AES, 1979, AES-15, pp. 824-828.
- [5] E. Jakeman, "On the Statistics of K-distributed Noise", J. Phys. A, 1980, 13, pp. 31-48.
- [6] S. Watts and K.D. Ward, "Spatial Correlation in K-distributed Sea Clutter", IEE proc. F, Comun., Radar & Signal Process., 1987, 134, (6), pp. 526-532.
- [7] C.W. Hawkes, S.S. Haykin, "Modeling of Clutter for Coherent Pulsed Radar." IEEE Trans., 1975, IT-21, pp. 703-707.
- [8] A. Farina, A. Russo, F.A. Studer, "Coherent Radar Detection in Log-normal Clutter." IEE Proc. F, Commun, Radar & Signal Process., 1986, 133, (1), pp. 39-54.
- [9] E. Conte, M. Longo, "On a Coherent Model For Log-normal Clutter." IEE Proc. F, Commun., Radar & Signal Process., 1987, 134, (2), pp. 198-201.
- [10] S. Watts, "Radar Detection Prediction in K-distributed Sea Clutter and Thermal Noise." IEEE Trans. on AES, 1987, AES-23, pp. 40-45.
- [11] M. Rangaswamy, "Spherically Invariant Random Processes for Modeling,

Simulation and Distribution Identification of Correlated Non-Gaussian Radar Clutter." Ph.D. Dissertation, Syracuse University, 1992.

- [12] J.F.C. Kingman, "Random Walks with Spherical Symmetry." *Acta Math.*, Stockholm 109, 1963, pp. 11-53.
- [13] K. Yao, "A Representation Theorem and Its Applications to Spherically Invariant Random Processes." *IEEE Trans. on IT*, 1973, IT-19, pp. 600-608.
- [14] J. Goldman, "Detection in the Presence of Spherically Symmetric Random Processes." *IEEE Trans. on IT*, 1976, IT-22, pp. 52-58.
- [15] H. Brehm, "Description of Spherically Invariant Random Processes by Means of G-functions." *Springer Lecture Notes*, 1982, 969, pp. 39-73.
- [16] E. Conte, M. Longo, "Characterization of Radar Clutter as a Spherically Invariant Random Process." *IEE Proc. F, Commun., Radar & Signal Process.*, 1987, 134, (2), pp. 191-197.
- [17] Saleem A. Kassam, Signal Detection in Non-Gaussian Noise. Springer-Verlag, New York.
- [18] P. Chakravathi, D. Weiner, A. Ozturk, "On Determination of Radar Thresholds for Non-Gaussian Pulses from Experimental Data." *IEEE Trans. on AES* (Submitted).
- [19] H. Wang, L. Cai, "On Adaptive Multiband Signal Detection with GLR algorithm." *IEEE Trans. on AES*, AES-27, no. 2, March 1991.
- [20] V. Lesser, H. Nawab, et al., "Integrated Signal Processing and Signal Understanding." *Umass. Tech. Report*, 91-34, December 1991.
- [21] H. Nawab, V. Lesser, Integrated Processing and Understanding of Signals in Symbolic and Knowledge-Based Signal Processing. Edited by A.V. Oppenheim and H. Nawab, Prentice Hal, Englewood Cliffs, N.J., 1991.

- [22] H. Nawab, V. Lesser, "High-Level Adaptive Signal Processing." NAIC Final Report, vol. 17, October 1989.
- [23] P. Chakravathi, D. Weiner, "Performance of the Locally Optimum Detector in a Correlated Non-Gaussian Disturbance." Submitted to the 35th Midwest Symposium on Circuits & Systems, Washington D.C.
- [24] R. Gonzalez, P. Wintz, "Digital Image Processing." 2nd edition, Addison-Wesley Publishing Company, Nov. 1987.
- [25] E. Hall, Computer Image Processing and Recognition. Academic Press, 1979.
- [26] R. R. Shah, "A New Technique for Distribution Approximation of Random Data." Master's thesis, Syracuse university, December 1993.
- [27] A. Ozturk, "A New Method for Distribution Identification." Submitted for publication to JASA.
- [28] A. Ozturk, "A General Algorithm for Univariate and Multivariate Goodness of Fit Tests Based on Graphical Representation." Communication in Statistics, 1991.
- [29] A. Ozturk and E. J. Dudewicz, "A New Statistical Goodness of Fit Test Based on Graphical Representation." The Biometrical Journal, 1991.
- [30] L. K. Slaski, "An Introduction to Dr. Ozturk's Algorithm for PDF Approximation." Rome Laboratory Internal Report, USAF, March 1993.
- [31] Z. Chair and P. K. Varshney, "Optimal Data Fusion in Multiple Sensor Detection Systems." IEEE Trans. T-AES, Vol. AES-22, pp 98-101, January 1986.

## VITA

[PII Redacted]

**NAME OF AUTHOR:** Mohamed Adel Slamani

[REDACTED]

[REDACTED]

### **GRADUATE AND UNDERGRADUATE STUDIES:**

Ecole National Polytechnique, Algiers  
Syracuse University, Syracuse

### **DEGREES AWARDED:**

Ingenieur d'etat, Ecole National Polytechnique, 1986,Algiers  
M.S., Syracuse University, Syracuse, 1991.

### **AWARDS AND HONORS:**

Best overall student, Ecole Nationale Polytechnique, Algiers, June 1986  
Best senior project, Ecole Nationale Polytechnique, Algiers, June 1986  
Full scholarship from the Ministry of Education of Algeria, 1987-1989  
Graduate Scholarship, Syracuse University, September 1989-1994  
Who's Who Among Students in American Universities and Colleges, 1993

### **PROFESSIONAL EXPERIENCE:**

Research Assistant, Department of Electrical and Computer Engineering,  
Syracuse University

Rome Laboratory  
Customer Satisfaction Survey

RL-TR-\_\_\_\_\_

Please complete this survey, and mail to RL/IMPS,  
26 Electronic Pky, Griffiss AFB NY 13441-4514. Your assessment and  
feedback regarding this technical report will allow Rome Laboratory  
to have a vehicle to continuously improve our methods of research,  
publication, and customer satisfaction. Your assistance is greatly  
appreciated.

Thank You

---

---

Organization Name: \_\_\_\_\_ (Optional)

Organization POC: \_\_\_\_\_ (Optional)

Address: \_\_\_\_\_

1. On a scale of 1 to 5 how would you rate the technology  
developed under this research?

5-Extremely Useful 1-Not Useful/Wasteful

Rating \_\_\_\_\_

Please use the space below to comment on your rating. Please  
suggest improvements. Use the back of this sheet if necessary.

2. Do any specific areas of the report stand out as exceptional?

Yes \_\_\_\_\_ No \_\_\_\_\_

If yes, please identify the area(s), and comment on what  
aspects make them "stand out."

3. Do any specific areas of the report stand out as inferior?

Yes        No       

If yes, please identify the area(s), and comment on what aspects make them "stand out."

4. Please utilize the space below to comment on any other aspects of the report. Comments on both technical content and reporting format are desired.

***MISSION  
OF  
ROME LABORATORY***

**Mission.** The mission of Rome Laboratory is to advance the science and technologies of command, control, communications and intelligence and to transition them into systems to meet customer needs. To achieve this, Rome Lab:

- a. Conducts vigorous research, development and test programs in all applicable technologies;
- b. Transitions technology to current and future systems to improve operational capability, readiness, and supportability;
- c. Provides a full range of technical support to Air Force Materiel Command product centers and other Air Force organizations;
- d. Promotes transfer of technology to the private sector;
- e. Maintains leading edge technological expertise in the areas of surveillance, communications, command and control, intelligence, reliability science, electro-magnetic technology, photonics, signal processing, and computational science.

The thrust areas of technical competence include: Surveillance, Communications, Command and Control, Intelligence, Signal Processing, Computer Science and Technology, Electromagnetic Technology, Photonics and Reliability Sciences.